Metabolic assessment of perfused livers using magnetic resonance imaging and spectroscopy



Liam A. J. Young
Somerville College

A thesis submitted for the degree of
Doctor of Philosophy

Radcliffe Department of Medicine
University of Oxford

Michaelmas Term, 2021

Metabolic assessment of perfused livers using magnetic resonance imaging and spectroscopy

Liam A. J. Young
Somerville College, Michaelmas Term 2021
A thesis submitted for the degree of Doctor of Philosophy

Abstract

Liver transplantation is the only definitive treatment for end-stage liver disease. However, a shortage of suitable donor organs means that currently up to 30% of patients become too ill or die before ever receiving a transplant. Normothermic machine perfusion (NMP) offers a potential solution by reducing preservation injury which might enable the safe transplantation of higher-risk livers, thereby expanding the donor pool and reducing waiting list mortality. To achieve the full potential of machine perfusion in transplantation, a set of sensitive and specific biomarkers are needed to enable accurate prediction of a donated livers ability to survive the transplantation process and function in the recipient. Unfortunately, such a set of biomarkers is not yet established.

This thesis explores the potential of magnetic resonance (MR) imaging and spectroscopy to provide novel biomarkers for the prediction of transplantability in ex vivo livers. Deceased donor transplantation necessarily subjects livers to a metabolic and physiological insult during death of the donor. I quantified this using magnetic resonance in porcine models. Then I assessed the ability of temperature-corrected MR techniques to assess organ viability in ex vivo human liver during the traditional preservation of static cold storage. I then demonstrated non-invasive assessment of porcine livers during prolonged perfusion on a novel MR-compatible normothermic machine perfusion (NMP) system. Finally, I showed the proof-of-principle for performing MR assessment of ex vivo human livers during NMP.

Transplantation is currently undergoing a dramatic transformation with the incorporation of machine perfusion technologies and this thesis suggests that MR techniques hold immense potential for providing non-invasive assessment of transplantability in ex vivo livers.

Acknowledgements

Firstly, I would like to thank my supervisors Professors Christopher Rodgers, Constantin Coussios, and Peter Friend for their unending patience, guidance, help and support throughout my studies. Chris' enthusiasm for all of my mad ideas, Constantin's reminders to always look at the big picture and Peter's crash courses in clinical practice have really helped me develop as both a scientist and an individual. It has been a privilege to be given the freedom to explore every idea whilst in the comforting knowledge that there was always a safety net to catch me if things went wrong.

I would also like to give thanks to Professor Rutger Ploeg and Dr Aaron Hess for helping to shape this thesis, being on my thesis committee, and always being available to give helpful advice.

Without the many colleagues and friends who kindly helped me at all times of day and night, the work detailed in this thesis would simply not have been possible. I would like to thank all of the surgeons who have retrieved and prepared organs for me: Dr Annemarie Weissenbacher, Dr Etohan Ogbemudia, Dr Fungai Dengu, and especially Dr Carlo Ceresa who was ever present.

My thanks also go to all of the team at the Oxford Centre for Clinical Magnetic Resonance Research (OCMR), especially the physics group for their constant insights and the radiographers for accommodating my last-minute request for 30+ hours of scanner time – particular thanks must go to Jane Francis for enabling this. All of the team at OrganOx Ltd, especially Daniel Voyce, have also provided invaluable support. Connor Scott and Dr Richard Colling's assistance with histological processing and assessment was greatly appreciated.

In Denmark, Professor Christoffer Laustsen, Dr Esben Hanssen, and their team made me incredibly welcome and I would like to thank them for always saying 'yes' whenever I thought up another experiment we could do.

Special thanks must go to Dr Ladislav Valkovic, Dr Jane Ellis, Dr Justin Lau, Dr Jack Miller, and Dr Ferenc Mozes for being 'on-call' to scan ex vivo organs with me and for keeping me sane whilst scanning at 2 AM.

I am dedicating this thesis to my loving fiancée, Rhiannon. You have been endlessly patient and understanding as I have discussed everything or disappeared at all times of the day and night. You have provided incredible amounts of love and cake to carry me through every low or celebrate every high.

I would like to thank my family for all the love, friendship, teasing and support you have given me through the years. A special thanks must go to my parents, Helen and Matthew, and my sister, Alice, who are a constant source of encouragement and who seemingly never tire of hearing me ramble on about a new, 'interesting' thing I have learnt. Without all of you, I would not have been able to have undertaken this degree.

Finally, I would like to give my warmest thanks to all of the donors and their families. Without their kind gift, this research would not have been possible.

Research outcomes

Journal articles

[1] **L. A. J. Young**, C. D. L. Ceresa, F. E. Mózes, J. Ellis, L. Valkovic, R. Colling, C.-C. Coussios, P. J. Friend, and C. T. Rodgers, "Noninvasive assessment of steatosis and viability of cold-stored human liver grafts by MRI," *Magnetic Resonance in Medicine*, vol. 86, no. 6, pp. 3246–3258, 2021.

[2] T. Prudhomme, J. F. Mulvey, **L. A. J. Young**, B. Mesnard, M. L. Lo Faro, A. E. Ogbemudia, F. Dengu, P. J. Friend, R. Ploeg, J. P. Hunter, and J. Branchereau, "Ischemia-reperfusion injuries assessment during pancreas preservation," *International Journal of Molecular Sciences*, vol. 22, p. 5172, Feb 2021.

[3] E. A. Selvaraj, F. E. Mózes, A. Jayaswal, M. H. Zafarmand, Y. Vali, J. A. Lee, C. K. Levick, **L. A. J. Young**, N. Palaniyappan, C. H. Liu, G. P. Aithal, M. Romero-Gómez, M. J. Brosnan, T. A. Tuthill, Q. M. Anstee, S. Neubauer, S. A. Harrison, P. M. Bossuyt, M. Pavlides, and the LITMUS Investigators, "Diagnostic accuracy of elastography and magnetic resonance imaging in patients with NAFLD: A systematic review and meta-analysis.," *Journal of Hepatology*, vol. 75, pp. 770–785, Feb 2021.

[4] A. Apps, J. Lau, J. Miller, A. Tyler, **L. A. J. Young**, A. J. M. Lewis, G. Barnes, C. Trumper, S. Neubauer, O. J. Rider, and D. J. Tyler, "Proof-of-principle demonstration of direct metabolic imaging following myocardial infarction using hyperpolarized ^{13}C CMR," *JACC: Cardiovascular Imaging*, vol. 14, no. 6, pp. 1285–1288, 2021.

Conference abstracts

[1] **L. A. J. Young**, C. D. L. Ceresa, J. J. J. J. Miller, L. Valkovic, D. Voyce, E. M. Tunnicliffe, J. Ellis, D. J. Tyler, P. J. Friend, C. C. Coussios, and C. T. Rodgers, "Assessing metabolism and function of normothermically perfused ex vivo livers by multinuclear MR imaging and spectroscopy," in *Proc. Intl. Soc. Mag. Reson. Med. 26*, p. 440, 2018.

[2] **L. A. J. Young**, J. J. J. Miller, L. Valkovic, E. S. S. Hansen, M. A. McLean, F. A. Gallagher, C. Laustsen, D. J. Tyler, C. T. Rodgers, and J. Y. C. Lau, "ROKET: a robust keto enol tautomerisation phantom for multi-site, multi-vendor hyperpolarized ^{13}C studies," in *Proc. Intl. Soc. Mag. Reson. Med. 28*, p. 3028, 2020.

[3] J. Y. Lau, A. Apps, J. J. J. J. Miller, A. Tyler, **L. A. J. Young**, A. J. Lewis, G. Barnes, C. Trumper, S. Neubauer, O. J. Rider, and D. J. Tyler, "Human ^{13}C hybrid-shot spiral (HYSS) imaging of pathological cardiac metabolism following myocardial infarction," in *Proc. Intl. Soc. Mag. Reson. Med. 28*, p. 1194, 2020.

[4] C. Hill, F. E. Mozes, **L. A. J. Young**, L. Biasiolli, M. D. Robson, and V. Grau, "Deep learning based multi-organ detection: a step closer to liver T_1 map quality assurance," in *Proc. Intl. Soc. Mag. Reson. Med. 28*, p. 2598, 2020.

[5] **L. A. J. Young**, C. D. L. Ceresa, F. E. Mozes, J. Ellis, L. Valkovic, C. C. Coussios, P. J. Friend, , and C. T. Rodgers, "Temperature sensitivities of T_1, fat fraction and water resonance frequency characterized in ex vivo human livers," in *Proc. Intl. Soc. Mag. Reson. Med. 27*, p. 1756, 2019.

[6] J. Y. C. Lau, **L. A. J. Young**, T. Zhou, A. Tyler, J. J. J. J. Miller, and D. J. Tyler, "HyperMaple: Maple syrup as a glassing agent for dnp sample preparation," in *Proc. Intl. Soc. Mag. Reson. Med. 27*, p. 4276, 2019.

[7] J. Y. C. Lau, **L. A. J. Young**, J. J. J. Miller, C. T. Rodgers, and D. J. Tyler, "Pyruvate keto-enol tautomerization and its potential impact on apparent pyruvate T_1," in *Proc. Intl. Soc. Mag. Reson. Med. 27*, p. 4277, 2019.

[8] **L. A. J. Young**, C. D. L. Ceresa, D. Voyce, J. Ellis, F. E. Mozes, J. Lau, J. J. J. J. Miller, L. Valkovic, D. J. Tyler, P. J. Friend, C. C. Coussios, and R. C. T, "Metabolic assessment

of perfused ex vivo human livers by MRS and MRI," in *Proc. Magnetic Resonance Spectroscopy Workshop*, 2018.

[9] C. D. L. Ceresa, D. Nasralla, T. Cornfield, A. Clark, P. Hook, **L. A. J. Young**, C. C. Coussios, L. Hodson, and P. J. Friend, "Exploring the structural and functional effects of normothermic machine perfusion and defatting interventions on human steatotic livers," in *Hepatology*, vol. 68, p. 2A, 2018.

[10] **L. A. J. Young**, C. D. L. Ceresa, D. Voyce, J. Ellis, F. E. Mozes, J. Lau, J. J. J. J. Miller, L. Valkovic, D. J. Tyler, P. J. Friend, C. C. Coussios, and R. C. T, "Assessment of perfused ex vivo human livers by MRS and MRI," in *Proc. British Chapter Intl. Soc. Mag. Reson. Med.*, 2018.

[11] **L. A. J. Young**, C. D. L. Ceresa, J. J. J. J. Miller, L. Valkovic, D. Voyce, J. Lau, A. Weissenbacher, J. Ellis, F. E. Mozes, D. J. Tyler, P. J. Friend, C. C. Coussios, and C. T. Rodgers, "Metabolic assessment of normothermically perfused ex vivo livers by multi-nuclear magnetic resonance imaging and spectroscopy," in *Proc. Post-graduate Meeting British Chapter Intl. Soc. Mag. Reson. Med.*, 2018.

Awards and prizes

- Winner of **best presentation prize** at the 2018 international Magnetic Resonance Spectroscopy Workshop in Utrecht, the Netherlands, for a presentation demonstrating the proof-of-concept for MRS assessment of human livers during ex vivo normothermic machine perfusion.
- Awarded **Magna Cum Laude Merit award** at the 2018 annual meeting of the International Society for Magnetic Resonance in Medicine (ISMRM) for my abstract describing an MR-compatible normothermic machine perfusion system.
- Winner of **best presentation prize** at the post-graduate meeting of the British Chapter of ISMRM for a presentation exploring MRI assessment of ex vivo livers during normothermic machine perfusion.

Table of contents

Table of contents ix

List of figures xii

List of tables xiv

List of abbreviations xv

1 Introduction 1
- 1.1 Motivation 1
- 1.2 Objectives 2
- 1.3 Outline of chapters 3

2 Transplantation and Normothermic machine Perfusion 5
- 2.1 Liver Transplantation 5
  - 2.1.1 Indications for Transplantation 5
  - 2.1.2 Donor organ shortage 7
  - 2.1.3 A traditional view of marginal organs 8
- 2.2 Preservation strategies 12
  - 2.2.1 Static cold storage 13
  - 2.2.2 Normothermic machine perfusion 14
  - 2.2.3 Viability assessment of donated organs 15

3 Magnetic Resonance Imaging and Spectroscopy of the Liver 17
- 3.1 Physical basis 17
  - 3.1.1 Excitation and relaxation 19
  - 3.1.2 Acquiring an MR image or spectrum 20
- 3.2 MRI and MRS in the liver 23
  - 3.2.1 Relaxometry 23
  - 3.2.2 Quantification of steatosis 29
  - 3.2.3 Measuring diffusion and perfusion 33
  - 3.2.4 Metabolic imaging and spectroscopy 36
- 3.3 Summary 42

4 Investigating the effect of death on liver metabolism and structure in a porcine model 44
- 4.1 Background 44
- 4.2 Aims 47
- 4.3 Methods 47
  - 4.3.1 Multi-site validation of MR protocol 47
  - 4.3.2 Porcine Study Protocol 49
  - 4.3.3 Donor animal preparation 51
  - 4.3.4 Donation after circulatory death model 52
  - 4.3.5 Donation after brain-stem death model 53
  - 4.3.6 MR Protocol 55

4.3.7 Planned biochemical and histological analysis 58
4.3.8 Statistical analysis 59
4.4 Results 59
4.4.1 Validation and optimisation of MR methods 59
4.4.2 Normal Ranges of MR parameters 63
4.4.3 Structural and metabolic changes in the liver during donation after circulatory death 65
4.4.4 Structural and metabolic changes for donation after brain-stem death 70
4.5 Discussion 71
4.6 Conclusion 78

5 Examination of cold stored human livers with magnetic resonance 79
5.1 Background 79
5.2 Aims 80
5.3 Methods 81
5.3.1 Study protocol 81
5.3.2 Liver specimens and preparation for MRI 81
5.3.3 MR Examination 83
5.3.4 Functional assessment of livers during normothermic machine preservation 86
5.3.5 Histological assessment 87
5.3.6 Statistical analysis 88
5.4 Results 89
5.4.1 Liver function during normothermic machine perfusion 89
5.4.2 Non-invasive temperature measurement 89
5.4.3 Relaxometry 91
5.4.4 Quantification of Steatosis 93
5.4.5 Correlation of imaging parameters with histology and liver function 96
5.5 Discussion 97
5.6 Conclusion 102

6 Exploring metabolic and structural effects of normothermic machine perfusion in ex vivo porcine livers 104
6.1 Background 104
6.2 Aims 107
6.3 Methods 108
6.3.1 Study design and animal models 108
6.3.2 Donor procedure 108
6.3.3 Preservation phase 109
6.3.4 MR assessment 113
6.3.5 Histological assessment 115
6.3.6 Biochemical assessment 116
6.3.7 Functional assessment of livers during NMP 117
6.3.8 Statistical analysis 118
6.4 Results 118
6.4.1 Clinical assessment 118

6.4.2 Haemodynamic and tissue perfusion assessment 119
6.4.3 Perfusate biochemistry 125
6.4.4 Tissue assessment 129
6.4.5 Metabolic assessment 131
6.5 Discussion 137
6.5.1 Impact of changes to clinical perfusion system 137
6.5.2 Replication of physiological conditions 138
6.5.3 Is donor history or functional assessment more valuable? 140
6.5.4 Timing of viability assessment 141
6.5.5 Limitations 142
6.6 Conclusion 143

7 Assessment of perfused human livers by MRI and MRS: a feasibility study 144
7.1 Background 144
7.2 Aims 146
7.3 Methods 146
7.3.1 Liver procurement and perfusion protocol 146
7.3.2 MR examination 147
7.3.3 Haemodynamic and biochemical analysis of liver function 147
7.3.4 Statistical analysis 148
7.4 Results 148
7.4.1 Clinical data 148
7.4.2 Haemodynamic and perfusion characteristics 149
7.4.3 Metabolic assessment 151
7.4.4 Tissue characterisation 154
7.5 Discussion 155
7.5.1 Perfusion quality 155
7.5.2 Liver function 157
7.5.3 Tissue assessment by relaxometry 158
7.5.4 Hepatic steatosis 159
7.5.5 Energy metabolism 159
7.5.6 Clinical implications 160
7.5.7 Limitations 162
7.6 Conclusion 163

8 Summary and outlook 164
8.1 Conclusions 164
8.2 Future outlook 168
8.2.1 Other impacts 169

Bibliography 171

List of figures

2.1 Indications for transplantation 6
2.2 Organ donation and transplantation statistics 8

3.1 Spectral density function and dependence of relaxation times on correlation time 21
3.2 An inversion recovery pulse sequence diagram 24
3.3 A variable flip angle T_1 mapping pulse sequence diagram 25
3.4 The shMOLLI pulse sequence diagram 26
3.5 Summary of a single voxel STEAM spectroscopy sequence 30
3.6 Typical proton spectrum of steatotic human livers 30
3.7 The spin echo diffusion weighted imaging pulse sequence diagram 33
3.8 Summary of hepatic metabolism 37
3.9 Pulse-acquire spectroscopy and 1-D ISIS pulse sequences 38

4.1 In vivo porcine study protocol 51
4.2 Representative T_1 maps from a phantom and liver of a healthy human volunteer. 60
4.3 Comparison of shMOLLI and VFA T_1 measurements 61
4.4 IVIM models fitted to DWI data from porcine livers 62
4.5 RF excitation profile for a ^{31}P ISIS sequence 64
4.6 Representative B_1, T_1, and T_2 parametric maps of healthy in vivo porcine livers 64
4.7 Physiological changes following WLST 67
4.8 Localisation of ^{31}P-MRS acquisitions in an in vivo porcine model. 68
4.9 Changes in hepatic energy metabolism during warm ischaemia 69
4.10 Changes in ATP signal intensity during warm ischaemia 69
4.11 T_{2w} image of porcine brain with a balloon inside the cranium 71
4.12 Haemodynamic and biochemical changes during brain-stem death 72
4.13 Changes in MR biomarkers following brain-stem death 73

5.1 MR assessment of cold stored liver study protocol 82
5.2 Temperature changes in livers during SCS 91
5.3 Temperature sensitivity of T_1 92
5.4 Temperature sensitivity of T_2 and $T_2^\star$ 94
5.5 Temporal variation of liver temperature, T_1 and PDFF during SCS 95
5.6 Temperature sensitivity of PDFF 96
5.7 Correlation of PDFF with histological and functional biomarkers 97
5.8 Correlation of T_1 with histological and functional biomarkers 98

6.1 Porcine NMP MRI study protocol 108
6.2 Schematic of MR-compatible NMP system 111
6.3 Collagen proportionate area calculation 116
6.4 VITTAL assessment of livers during NMP 120
6.5 Haemodynamic in ex vivo livers during NMP 124
6.6 IVIM measurements of diffusion and perfusion in ex vivo livers during NMP 126

6.7 Changes in PaO_2 and $PaCO_2$ in ex vivo livers during NMP..... 127
6.8 Arterial blood gas assessment of ex vivo livers during NMP 128
6.9 Collagen proportionate area assessed in ex vivo porcine livers during NMP. 130
6.10 Liver T_1 in ex vivo porcine livers during NMP..... 130
6.11 Example ShMOLLI T_1 maps for 6 porcine livers during NMP 132
6.12 Comparison of perfusate lactate and T_1 for determination of liver function . 133
6.13 Changes in ATP content in ex vivo porcine livers during NMP and SCS ... 134
6.14 Representative ^{31}P spectra from ex vivo porcine livers during NMP and SCS 135
6.15 Hyperpolarized MRS assessment of ex vivo porcine livers during NMP 136
6.16 Spatial variation of hyperpolarized pyruvate and lactate signal 136

7.1 Haemodynamic changes in ex vivo human liver during NMP..... 150
7.2 Changes in perfusion and diffusion in ex vivo human livers during NMP... 151
7.3 Arterial blood gas analysis of ex vivo human livers during NMP 152
7.4 Changes in ATP/Pi ratio in ex vivo human livers during NMP 153
7.5 Hyperpolarised MRS assessment of ex vivo human livers during NMP 154
7.6 shMOLLI T_1 maps measured in ex vivo human livers during NMP 155
7.7 Changes in liver T_1, T_2 and PDFF during ex vivo NMP 156

List of tables

2.1 Donor risk scores 12
2.2 Transplantability criteria applied in clinical trials 15
2.3 Perfusate lactate viability criteria used in clinical trials 16

4.1 Chemical composition of a relaxometry phantom 48
4.2 Summary of MR sequence parameters 50
4.3 Summary of initial values and constraints on IVIM models 56
4.4 Fit statistics for bi- and tri-exponential IVIM models 63
4.5 IVIM parameters in healthy in vivo porcine liver 63
4.6 Normative ranges of biochemical and MR biomarkers in healthy porcine liver 65
4.7 Changes in hepatic perfusion and relaxivities during warm ischaemia 66

5.1 Prior knowledge parameters for fat and water spectra 86
5.2 Donor demographics and liver function parameters during NMP 90
5.3 Temperature sensitivities of T_1, T_2, and $T_2^\star$ in human livers during SCS 93
5.4 Temperature sensitivities of fat fraction measurements 94
5.5 Cut-off values of T_1 and PDFF for determining liver function 99

6.1 Comparison of ex vivo livers during NMP to normal ranges for in vivo liver 122
6.2 Temporal changes in liver biochemical and MR parameters during NMP .. 123

7.1 Donor demographics 149

List of abbreviations

ADP Adenosine diphosphate.

AIC Akaike's information criterion.

AMARES Advanced Method for Accurate, Robust and Efficient Spectral fitting of MRS data with use of prior knowledge.

AMP Adenosine monophosphate.

ATP Adenosine triphosphate.

bSSFP Balanced steady state free precession.

BW Bandwidth.

CPA Collagen proportionate area.

DBD Donation after brain-stem death.

DCD Donation after circulatory death.

DNP Dynamic nuclear polarisation.

DWI Diffusion weighted imaging.

ECD Extended criteria donor.

FA Flip angle.

FID Free induction decay.

FoV Field of view.

FWIT Functional warm ischaemia time.

GRAPPA Generalized auto-calibrating partially parallel acquisition.

GRE Spoiled gradient recalled echo.

H&E Hematoxylin and eosin.

HBD Heart beating donor.

HIC Hepatic iron content.

HTK Histidine tryptophan ketoglutarate.

ICP Intracranial pressure.

IDEAL Iterative decomposition of water and fat with asymmetric echo times and least-squares estimate.

ISIS Image selected in vivo spectroscopy.

IVC Inferior vena cava.

IVIM Intra-voxel incoherent motion.

MAP Mean arterial pressure.

MELD Model for end-stage liver disease.

MOLLI Modified Look Locker inversion.

MR Magnetic resonance.

MRI Magnetic resonance imaging.

MRS Magnetic resonance spectroscopy.

NAFLD Non-alcoholic fatty liver disease.

NAS Non-alcoholic fatty liver disease activity score.

NHBD Non-heart beating donor.

NMP Normothermic machine perfusion.

NMR Nuclear magnetic resonance.

$PaCO_2$ Partial pressure of carbon dioxide in arterial blood.

PaO_2 Partial pressure of oxygen in arterial blood.

PAS Periodic acid-Schiff.

PDE Phosphodiester.

PDFF Proton density fat fraction.

Pi Inorganic phosphate.

PME Phosphomonoester.

PNF Primary non-function.

RF Radio frequency.

ROI Region of interest.

SCS Static cold storage.

shMOLLI Shortened modified Look Locker inversion.

SNR Signal to noise ratio.

STEAM Stimulated echo acquisition mode.

T_1 Longitudinal relaxation time.

T_2 Transverse relaxation time.

TE Echo time.

TI Inversion time.

TR Repetition time.

UW University of Wisconsin.

VFA Variable flip angle.

WLST Withdrawal of life sustaining treatment.

1

Introduction

1.1 Motivation

Liver transplantation is the only definitive treatment for end-stage liver disease. However, a shortage of suitable donor organs means that currently 15-30% of patients will become too ill or die before ever receiving a transplant.[161,115] The shortfall in the number of suitable donors, combined with the increasing prevalence of liver diseases, has driven the transplantation of increasingly high risk organs.[210]

However, transplanting a liver which is too severely damaged may lead to graft failure, which is fatal for the recipient unless they can rapidly have another liver transplant.[97] Therefore, it is essential that there is an accurate assessment of a donated livers' ability to survive the transplantation process prior to implanting the graft into a patient. Unfortunately, the current procedure for determining whether to transplant a liver relies rely on crude measures of liver health such as visual inspection of the graft, age of the donor and duration of any ischaemic periods.[74,51,24] There is a clinical need for a more accurate selection process. My thesis explores whether magnetic resonance imaging (MRI) and spectroscopy (MRS) could provide sensitive and specific biomarkers to guide such a process.

Normothermic machine perfusion (NMP) is a modern approach to organ preservation that can reduce post-transplant graft injury by 50%.[150] In addition to reducing the insult to

the donated liver, NMP also provides an opportunity to assess function during preservation while the ex situ liver remains in a functional state with a supply of oxygenated blood and nutrients at 37°C. This provides an excellent opportunity to significantly expand the donor pool without compromising patient outcomes. This promise was demonstrated in a recent study by Mergental et al. which demonstrated that using NMP and viability testing it was safe to transplant >70% of livers deemed non-transplantable by all UK transplant centres.[139] Although this study demonstrated the paradigm shift possible through the addition of these techniques, a lack of sensitive and specific biomarkers of organ viability meant that 18% of the patients required re-transplantation.[139] Additionally to reduce the risk to the patients, conservative limits were applied to the viability assessment and hence some donated grafts may have been unnecessarily discarded. Therefore, there is a pressing need for a set of sensitive and specific biomarkers to predict viability for transplantation during either traditional preservation methods, such as static cold storage, or enhance preservation methods including NMP.

MRI and MRS are non-invasive and non-ionising techniques to measure metabolism and phsyiology in vivo. In the liver, they have shown great promise at diagnosing patients with conditions such as non-alcoholic fatty liver disease and cirrhosis.[11,170] Therefore, MRI and MRS may make excellent techniques to assess a donated livers viability for transplantation.

1.2 Objectives

This thesis explores the use of magnetic resonance (MR - i.e. MRI and MRS) biomarkers to assess the metabolic and physiological state of donated livers. My specific aims were:

1. To characterise the effects of death, determined by neurological and circulatory criteria, on hepatic metabolism and physiology.

2. To examine the potential of MR biomarkers to predict liver function during preservation via static cold storage.

3. To use MR biomarkers to explore metabolic and physiological changes in ex vivo livers during an extended period of preservation by NMP.

4. To demonstrate the feasibility of performing MR assessments of ex vivo human livers during NMP.

This work intends to identify possible biomarkers for viability that can be tested as hypotheses in future prospective clinical trials. However, the experiments needed to achieve these aims are necessarily very interdisciplinary in nature and required the input of many people in addition to myself. A list of all major contributions in contained in the acknowledgements but in the work that follows I led the design of and ran all experiments, optimised the MR protocols, performed the MR scanning, collected the blood and tissue samples, and created analysis pipelines to analyse all the resulting data. However, while I did gain some basic surgical skills to enable me to prepare livers for ex vivo perfusion, all of the in vivo surgery and liver retrievals detailed in this thesis were completed by an excellent team of qualified surgeons.

1.3 Outline of chapters

I begin with a brief introduction of liver transplantation in Chapter 2. I also explain the clinical importance of developing a set of effective and validated biomarkers to predict a donated organs viability for transplantation.

In Chapter 3 I present the fundamental principles of magnetic resonance physics and how MRI/MRS methods are applied to study the liver.

In Chapter 4, I establish baseline values from which all deceased donor liver transplantation must start. This is achieved by using MRI and MRS to examine changes in metabolism and physiology in the liver using a large animal model of a donor after circulatory death and a donor after brain-stem death.

In Chapter 5, I examine the temperature sensitivity of MR metrics and propose a temperature correction algorithm in order to enable MR assessment of ex vivo human livers during preservation by static cold storage. Then using a set of clinically applied definition of

viability, I investigate the promise of MR biomarkers for the prediction of viability in ex vivo static cold stored livers.

In Chapter 6, I move from traditional techniques of organ preservation to novel enhanced methods and investigate the metabolic and physical changes occurring in ex vivo livers during preservation by NMP. I examine two different large animal models with varying duration of warm and cold ischaemia to demonstrate the importance of performing a liver specific viability assessment rather than relying solely on donor history.

In Chapter 7, I demonstrate the feasibility of performing MR examinations on ex vivo human livers during NMP, to show the potential clinical applications.

I conclude in Chapter 8 by summarising the main conclusions from my research and highlighting its key implications for future studies. In particular, I summarise my findings regarding the biomarkers which appear to have the most promise in the prediction of donor liver viability for transplantation and hence may be deserving of further study.

2

Transplantation and Normothermic machine Perfusion

2.1 Liver Transplantation

For patients with liver failure, interventions to support or replace liver function only provide temporary, limited relief and transplantation is the only effective treatment.[192] Since Starzl et al. performed the first successful clinical liver transplant in 1967,[198] the procedure has evolved into a mainstay of clinical practice with excellent patient survival rates of over 94% at one year and 84% at five years routinely seen.[160] Therefore, liver transplantation has become the treatment of choice for an increasing spectrum of patients with a wide range of metabolic, chronic, and acute liver diseases as well as some types of cancer.

2.1.1 Indications for Transplantation

Liver transplantation is offered to all patients with end-stage liver disease, where the projected life expectancy following a transplant exceeds that of the underlying condition, generally <1 year, or where the patient's liver disease is causing an unacceptable quailty of life.[71] The most common indication for liver transplantation is cirrhosis, with patients refered when major complications of cirrhosis such as variceal haemorrhage, ascites, or encephalopathy occur.[71]

Acute liver failure is an urgent indication for transplantation, most commonly associated with hepatitis A and B or paracetamol overdoses. A summary of the range of indications for the 150,000 liver transplants performed in Europe between 1988 - 2020 is presented in Figure 2.1.

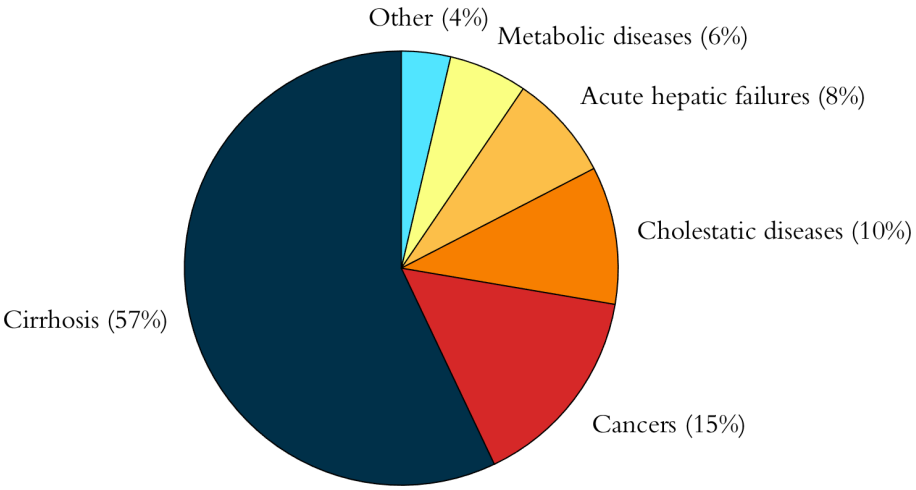


Figure 2.1: The main diseases which lead to liver transplantation in Europe.[72] Other indications include: benign liver tumours or polycystic diseases (0.015%), Budd-Chiari (0.008%), parasitic diseases (0.001%) as well as many less common diseases.

With an ever increasing number of indications for transplantation, it becomes progressively more difficult to ensure that the optimal patient receives a transplant at the right time in order to secure the best outcomes - a task which is not aided by a global shortage of suitable donor organs available. A range of different objective scores have been developed to prioritise patients on the waiting list and ensure equitable access to transplantation. In the US and Europe, the model for end-stage liver disease (MELD) score or, a derivative of MELD that also accounts of sodium levels (MELD-Na), are used to stratify patient using objective measures such as bilirubin, creatinine, and international normalised ratio (INR) to predict higher and lower risk patients and hence ensure that the patients with the greatest need receive a transplant first.[107,17] Recently, the United Kingdom took a step further and implemented an allocation policy based on the transplant benefit score which uses 21 recipient and 7 donor criteria to maximise the predicted post-transplant survival benefit achievable with the specific type of donor liver on offer compared to survival on the waiting list over a 5-year period.[81,188]

2.1.2 Donor organ shortage

In recent years, liver transplantation has become a victim of its own success. As improvements in organ preservation, surgical techniques, immunosuppression and post-operative management have greatly improved patients outcomes, demand for liver transplantation has also greatly increased. Indeed, the number of patients listed for a liver transplant in the UK has doubled over the last 15 years. However, the ability of liver transplantation to save the lives of patients with end-stage liver disease is limited by a shortage of suitable donor organs. Unfortunately, the imbalance between waiting list demands and suitable donor organs available results in between 15 and 30% of patients dying or becoming too ill to survive the procedure before they receive a life-saving transplant.[161,115]

In some cases, living donation can help to mitigate differences between donor organ supply and demand. However, this is not available in all countries, not all patients have a suitable donor and there are serious ethical concerns surrounding the serious complications and donor mortality associated with the donor procedure.[129,211] Given these issues, living donation has had very little impact on the number of liver transplants in the UK.[160]

Instead many countries have focused on increasing utilisation of deceased donor livers by extending liver acceptance criteria.[210] As Figure 2.2 shows, by considering a greater number of high risk or marginal livers for transplant, the number of donors available have been increased by 2/3rd over the last 15 years. However, by definition, marginal livers carry a higher risk of primary graft dysfunction or primary non-function (PNF) which increases the risk of morbidity and mortality for the recipient.[140] Therefore, extreme care must be taken when considering marginal or extended criteria donors and any donor organs that are unlikely to function after transplantation discarded. Differentiating organs that present an unacceptable risk is very challenging though. Hence even with the extreme demand for donor organs, the need for caution combined with the lack of sensitive and specific tests that can determine viability for transplantation has led to over 6000 livers, which were offered for donation and met the initial screening criteria, not being transplanted over the last 15 years in the UK alone (Figure 2.2).

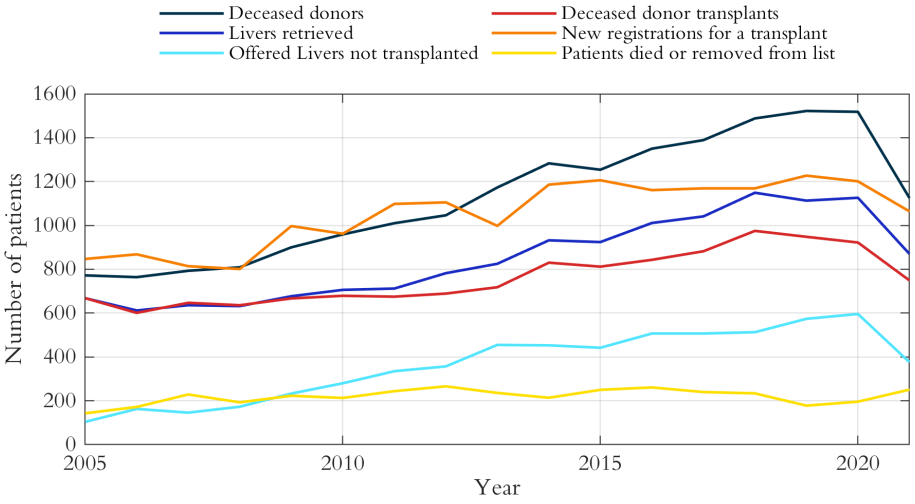


Figure 2.2: Summary of the changes in the utilisation of livers from deceased donors and demands for liver transplantation in the UK since 2005.[161] Note: The significant deviation of the 2020-2021 data compared to previous trends is a result of interruptions of transplant programmes by the global SARS-COV2 pandemic.

2.1.3 A traditional view of marginal organs

A liver will be deemed marginal if it possesses certain donor or preservation characteristics that are known to increase the risk of post-transplant complications such as graft failure. Livers with these characteristics are more sensitive to hypoxia and so suffer from a more severe ischaemia reperfusion injury.[238] By the nature of the transplant process, donor organs go through severe physiological and metabolic trauma during death of the donor, organ procurement, preservation, transportation, and implantation and marginal organs are less able to recover from these insults. Unfortunately, in addition to an increased risk of PNF, marginal grafts also carry an increased risk of rejection, early allograft dysfunction, and biliary complications such as ischaemic cholangiopathy.[97,76] Several factors have been identified as independent predictors of increased risk such as: increasing donor age, donation following circulatory death, and the presence of steatosis.

2.1.3.1 Donor age

Given the liver's ability to re-generate, ageing tends to have a minor effect on liver function in vivo. However, as the liver ages it shrinks by between 20 and 40%, sees reduced liver blood flow due to thicker arteriolar walls, and metabolic changes which reduce gluconeogenic

capacity which leads to increased lipid accumulation.[65] These changes, plus increased levels of pro-inflammatory cytokines, reduce the liver's ability to recover from an insult and the sensitivity to diseases increases.[108] The average number of co-morbidities also increases as a patient becomes older. Therefore, repeated studies have shown older livers are less likely to survive the transplantation process and hence have significantly worse post-transplant outcomes.[66,163,74,24]

2.1.3.2 Type of donor

In the United Kingdom, the vast majority of liver transplants are performed using organs donated from deceased donors.[161] Therefore, most livers that are considered for transplantation have sustained a severe insult during the death of the donor. Traditionally, the death of organ donors was confirmed by neurological criteria, i.e. the absence of brain-stem reflexes, in a pathway termed donation after brain-stem death (DBD). However, more recently donors have had death confirmed by circulatory criteria, i.e. the loss of cardiac output and electrical activity. This second pathway for organ donation - donation after circulatory death (DCD)- inevitably exposes the organs to a period of hypoxia at physiological temperature (warm ischaemia).

Following brain-stem death, the liver remains perfused but the donor will become haemodynamically unstable. The Cushing's reflex (hypertension and badycardia) seen immediately following brain death will quickly transition into a period of tachycardia and intense vasoconstriction as a result of a surge in catecholamines. Following the catecholamine storm, periods of vasodilation and severe hypotension often occur. This process creases a pro-inflammatory and intermittently partial ischaemic environment for the liver, which if not properly managed can lead to increased rates of post-transplant complications.

However, the impact of brain-stem death on the liver is much smaller than the impact of circulatory death with repeated studies showing that livers donated following circulatory death carry a significantly higher risk of post-transplant graft loss and recipient mortality.[32] This difference is driven by the inevitable period of warm ischaemia that the liver experiences in-between circulatory arrest and the cooling in situ flush in a DCD retrieval. In a DBD

retrieval the liver will remain perfused and oxygenated until the moment that the aorta is cross-clamped and cold in situ perfusion in started, creating a minimal amount of functional warm ischaemia time (FWIT). In contrast during a DCD retrieval, the liver will experience an uncontrollable period of FWIT from when the donors systolic blood pressure falls below 50 mmHg through circulatory arrest and stand-off period until the onset of cold in situ perfusion.[26] Increasing the duration of FWIT drastically increases the risk of post-transplant complications (specifically acute rejection, graft failure, and ischaemic cholangiopathy)[206] and hence it is recommended to only use livers that have suffered <20 minutes FWIT.[59,26]

However, the exact cut-off time is arbitrary and the decision whether it is safe to proceed is made on the basis of many factors. Therefore, many DCD livers are retrieved and later declined for transplantation. Indeed over the last 10 years the number of DCD donors has drastically increased but due to a poor rate of utilisation the number of DCD liver transplants remains comparatively small.[160] In 2021, DCD livers represented 43% of the donor pool but only 18% of liver transplants in the UK.[152,160] Better assessment and preservation methods are needed to enable safe transplantation of more DCD livers.

2.1.3.3 Hepatic steatosis

Although, steatotic livers may exhibit near-normal biochemical function prior to retrieval, they are particularly sensitivty to ischaemia reperfusion injury and hence are a high risk for post-transplant complications. For this reason, an estimated 1000 donated steatotic livers are discarded in the US every year and as the donor population becomes increasingly obese, this situation is only going to get worse.[153] Many studies have demonstrated that the presence of severe macrovesicular steatosis can decrease graft survival by up to 70% and so steatotic livers are not discarded without reason.[196] However, in the effort to expand the donor pool utilisation of steatotic livers could make a huge difference and hence a range of enhanced preservation techniques are being developed specifically for steatotic livers.[21,38]

Currently the level of steatosis is assessed primarily by visual inspection of the graft with yellowing of the parenchyma, rounded edges and a firm texture taken as evidence of severe steatosis[232]. This is not a reliable method of assessment however, with studies

suggesting that up to 1 in 6 livers that are discarded for being severely steatotic have been incorrectly categorised and could have been transplanted.[183] The gold-standard assessment of steatosis is histological assessment of a biopsy sample. However, this suffers from significant inter-observer and sampling variability.[68] In addition to the technical issues, the unpredictable nature of organ donation timing leads to significant logistical requirements to provide a rapid on-call pathology service and hence pre-transplant biopsies are not available at many transplant centres. Therefore, in order to better utilise steatotic livers, more accurate methods of steatosis quantification will be needed.

2.1.3.4 Donor Risk Indexes

Although each factor discussed above has been identified as an independent predictor of post-transplant complications, the decision whether to transplant a donated liver is by necessity multi-factorial. Therefore, a variety of population-based scoring systems have been developed which attempt to combine a variety of independent risk factors to to predict the overall risk for a specific donated liver (Table 2.1). All risk indices take into account a mix of parameters to account for donor characteristics, the cause of death, and logistics of the transplant process with varying philosophies determining which parameters are included. For example, although cold ischaemia time is a major risk factor for post-transplant graft survival, the Eurotransplant-, UK- and French-derived risk scores do not include it as it is not known at the time of offering.

All of the risk scores have been shown to be predictive of outcomes in a large cohorts.[74,24,51,228] However, there remains a large degree of uncertainty of whether a given organ is suitable for transplantation. Indeed, in a recent international survey of expert transplant surgeons that asked whether they would transplant a set of donated livers, having been given all of the information that was available to the surgeon who actually handled the case, the coefficient of agreement was just 0.11 across all cases and dropped to -0.01 and 0.02 for older and steatotic donors respectively.[168] Concerningly, none of these coefficients of agreement are significantly different to random chance. Therefore, the current donor risk indices are clearly not sufficient to accurately identify viable organs for transplantation.

Table 2.1: Summary of parameters used in four population-based risk score for predicting liver viability for transplantation.

	Risk score	DRI[74]	ET-DRI[24]	DLI[51]	DQI[228]
	Study population size	20,023	5,939	7,929	3961
	Study location	US	Europe	UK	France
Donor or preservation characteristic	**Increased Risk**				
Donor characteristics					
Age	Older	✔	✔	✔	✔
Race	African-American	✔	-	-	-
Sex	Female	-	-	✔	-
Height	Shorter	✔	-	✔	-
Smoking history	Smoker	-	-	✔	-
Type of donor					
Cause of death	Cerebrovascular accident	✔	✔	-	✔
DBD or DCD	DCD	✔	✔	✔	-
Whole or Split graft	Split	✔	✔	✔	✔
ICU stay duration	Longer	-	-	-	✔
Logistics of offer					
Cold ischaemia time	Longer	✔	-	-	-
Geographical allocation	Greater distance	✔	✔	-	-
Type of offer	Rescue offer	-	✔	-	-
Donor biochemistry					
GGT	Elevated	-	✔	-	-
Bilirubin	Elevated	-	-	✔	-
MDRD Creatine clearance (eGFR)	Lower	-	-	-	✔

Abbreviations: *donor liver index, DLI; donor quality index, DQI; donor risk index, DRI; estimated glomerular filtration rate, eGFR; Eurotransplant, ET; gamma glutamyltransferase, GGT; intensive care unit, ICU; modification of diet in renal disease, MDRD.*

Hence, additional assessments are needed to enable safe utilisation of more donated livers and improved post-transplant outcomes.

2.2 Preservation strategies

The nature of transplantation means that the donor liver needs to be outside of the body for a period of time between being removed from the donor and implanted into the recipient. Due to logistical reasons, this process is commonly several hours as the organ is moved from the donor's hospital to the recipients which can be in different regions or even different countries.[160,72] Therefore, the organ must be preserved while outside of the body in order to ensure optimal function for the recipient.

2.2.1 Static cold storage

Static cold storage (SCS) has remained the standard of care preservation method in solid organ transplantation since the 1980's. The technique aims to replace blood with an isosmotic, buffered preservation solution and suppress metabolism through hypothermia.[15] During SCS, the lack of blood flow through the liver prevents the supply of oxygen, nutrients and co-factors to the liver or the removal of waste products. Therefore, as anaerobic metabolism continues (at 10% of the usual metabolic rate while at 4 °C) a build up of waste products occurs and adenosine triphosphate (ATP) is degraded.[50] This in turn causes cell swelling and lysis which leads to a loss of transcellular electrolyte gradients and the activation of phospholipases.[34] Unfortunately, all of the cellular damage and metabolite imbalances cause secondary injury during re-perfusion when metabolism re-starts at a normal rate. During this time a large efflux of toxic molecules is formed and a severe inflammatory response ensues through both direct and in-direct cytotoxic mechanisms. This combination of damage from the prolonged ischaemia and the rapid reperfusion is known as ischaemia reperfusion injury and is the cause of most post-transplant complications.[238]

Preservation solutions contain large molecular weight anions in an attempt to reduce the amount of cell swelling by being osmotically balanced and chelating many of the calcium and ferric irons that are released during ischaemia.[15] The addition of adenosine and other key metabolites is designed to aid the re-starting of aerobic metabolism during re-perfusion. University of Wisconsin (UW) solution is the most commonly used preservation solution but there are many others, such as histidine tryptophan ketoglutarate (HTK) solution, which have been shown to be equivalent.[164]

SCS is cheap, easy, and has proven to be an effective method of preservation for healthy donor organs for over 40 years with >75% 5-year survival rates commonly seen.[160] However, given the level of insult it subjects the organs too, the more marginal organs, which have already sustained a level of injury, are not able to survive the transplant process. For these organs a different preservation method is needed.

2.2.2 Normothermic machine perfusion

Although only included in the National Institute for Health and Care Excellence (NICE) guidelines in 2019,[151] preserving livers using normothermic machine perfusion (NMP) is not a new concept. Indeed, Carell and Lindbergh showed that organs could be held viable for several days when perfused with normothermic oxygenated serum in a chamber they constructed in 1935.[36] However, technical issues and the complexity of the system prevented its widespread use. Over 80 years later, technology has progressed and the demand to expand the donor pool is sufficiently urgent that transplantation has renewed its enthusiasm for machine perfusion.

NMP provides the liver with oxygen and nutrients at 37 °C in order to maintain it ex situ in a functional state. Many different systems have been developed to perform this task but all include a circuit comprising of a blood reservoir, an oxygenator, a heat exchanger and either one or two pumps to provide both the arterial and venous input to the liver. The system can be designed to give supply at constant pressure or flow, have pulsatile or non-pulsatile flow, and use a blood based perfusate or acellular oxygen carrier.[178,70,116] However, all of the systems are designed to mimic physiological conditions, to lesser and greater extents and minimise ischaemia re-perfusion injury by maintaining normal metabolism. This has enabled longer preservation of organs and preservation of organs that were too severely damaged for preservation with SCS, with pre-clinical large animal studies demonstrating 100% graft survival after either 72 h of preservation or in a model with 1 h warm ischaemia.[218,190] Indeed, Eshmuminov et al. have recently demonstrated that a liver can be maintained with physiological function seen during NMP for up to 1 week.[70]

In a clinical setting, NMP has been shown to reduce graft injury, measured by hepatocellular enzyme release, by 50% compared to SCS in a large multi-centre randomised controlled trial.[150] The exact mechanisms generating these beneficial effects have not yet been determined. However, it is likely that maintaining more physiological metabolism replenishes ATP, prevents the build-up of the ischaemic milieu, and maintains a healthy endothelium. The direct link between increased hepatic ATP and good post-transplant outcome has

Table 2.2: Summary of the biomarkers used in viability criteria in all clinical trials that have reported assessing organ viability during normothermic machine perfusion

Study	op den Dries et al. [2013]	Sutton et al. [2014]	Mergental et al. [2016]	Ravikumar et al. [2016]	Watson et al. [2017]	Nasralla et al. [2018]	Mergental et al. [2018]	Watson et al. [2018]	de Vries et al. [2019]	van Leeuwen et al. [2019]	Matton et al. [2019]	Pavel et al. [2019]	Ciria et al. [2019]	Bral et al. [2019]	Ceresa et al. [2019]	Mergental et al. [2020]	Reiling et al. [2020]	Zhang et al. [2020]	Cardini et al. [2020]
Number of livers perfused	4	12	6	20	12	137	12	47	7	16	29	5	4	46	34	31	20	4	34
Number considered for transplantation	0	0	6	20	12	137	0	47	7	16	6	0	0	46	34	31	10	4	34
Number of livers transplanted	–	–	5	20	12	121	–	22	5	11	4	–	–	43	31	22	10	4	25
DBD:DCD	0:4	2:10	2:4	16:4	3:9	91:46	4:8	35:12	0:7	0:16	5:24	0:5	4:0	33:10	24:10	12:10	7:13	1:3	30:4
Assessment criteria																			
Perfusate lactate clearance	✔	–	✔	✔	✔	✔	✔	✔	✔	✔	✔	✔	✔	✔	✔	✔	✔	✔	✔
Maintenance of physiological pH	✔	–	✔	✔	✔	✔	✔	✔	✔	✔		✔	–	✔	✔	✔	✔	✔	✔
Evidence of glucose metabolism	✔	–	–	–	✔	✔	–	✔	–	–	–	–	–	✔	✔	–	✔	–	–
Evidence of bile production	✔	✔	✔	✔	–	✔	✔	–	✔	✔	✔	✔	–	✔	✔	✔	✔	✔	✔
Low ALT or AST concentrations	✔	–	–	–	✔	–	–	✔	–	–	✔	✔	–	✔	✔	–	–	–	–
Stable haemodynamic flow rates	–	–	✔	✔	–	–	✔	–	–	–	–	✔	✔	✔	✔	✔	✔	–	–
Homogeneous perfusion	–	–	✔	–	–	–	✔	–	–	–	–	–	–	–	–	✔	✔	–	–
Stable haemodynamic pressures	–	–	–	–	–	–	–	–	–	–	–	–	✔	–	–	–	–	–	–
Bile composition	–	–	–	–	–	–	–	✔	✔	✔	✔	–	–	–	–	–	–	–	✔

Abbreviations: *alanine aminotransferase, ALT; aspartate aminotransferase, AST; donation after brain-stem death, DBD; donation after circulatory death, DCD*

been shown previously in clinical studies while pre-clinical models have demonstrated regeneration of ATP during NMP.[118,231] Further studies are needed to continue to explore the mechanism of action of NMP to enable further exploitation of the effects to improve outcomes.

2.2.3 Viability assessment of donated organs

In addition to the uncertainty over viability for transplantation that is present when using donor risk indices for livers preserved using SCS, Mergental et al. have recently shown that these traditional concepts of what constitutes a non-viable organ are not applicable to livers preserved by NMP. In fact, the VITTAL study demonstrated that it is possible to safely transplant over 70% of the organs currently deemed non-viable with 100% 90-day survival.[139] This is only possible due to an additional benefit of NMP - the potential to perform organ-specific viability testing.

As livers are held in a metabolically active state during NMP, one could in theory monitor the metabolic and physiological state of the liver and use these readouts to determine when a liver is viable. Indeed this is what was performed in the VITTAL study. However, the

Table 2.3: Summary of the cut-off values applied in all clinical trials that have reported using perfusate lactate concentration as a biomarker to predict a liver's viability for transplantation during normothermic machine perfusion.

Study	op den Dries et al. [2013]	Mergental et al. [2016]	Ravikumar et al. [2016]	Watson et al. [2017]	Nasralla et al. [2018]	Mergental et al. [2018]	Watson et al. [2018]	de Vries et al. [2019]	van Leeuwen et al. [2019]	Matton et al. [2019]	Pavel et al. [2019]	Ciria et al. [2019]	Bral et al. [2019]	Ceresa et al. [2019]	Mergental et al. [2020]	Reiling et al. [2020]	Zhang et al. [2020]	Cardini et al. [2020]
Acceptable perfusate lactate concentration or change																		
≤4.4 mmol/L	-	-	-	-	-	-	-	-	-	-	✔	-	-	-	-	-	-	-
≤2.5 mmol/L	-	✔	-	-	-	✔	-	-	-	✔	-	-	-	-	✔	-	✔	-
≤2.0 mmol/L	-	-	-	-	-	-	-	-	-		-	-	-	-	-	✔	-	-
≤1.7 mmol/L	-	-	-	-	-	-	-	✔	✔	-	-	-	-	-	-	-	-	-
Peak fall ≥4.4 mmol/L/kg/h	-	-	-	-	-	-	✔	-	-	-	-	-	-	-	-	-	-	-
No threshold defined	✔	-	✔	✔	✔	-	-	-	-	-	-	✔	✔	✔	-	-	-	✔

optimum biomarkers to use for this assessment and the appropriate cut-off values to apply remain elusive. Table 2.2 details all of the clinical trials that have suggested or used biomarkers to assess a livers viability for transplantation during NMP. What becomes strikingly apparent is the lack of consensus on the appropriate biomarkers to include and as Table 2.3 highlights, even within a biomarker many studies agree is useful, the appropriate thresholds to apply are not known.

The VITTAL criteria are the most widely used viability test to date and require the liver to clear perfusate lactate to below 2.5 mmol/L within 4 h and maintain it below this level. Then additionally the liver must meet two of the secondary criteria which include: metabolism of glucose, production of bile, stable flow rates down the hepatic artery and portal vein of >150 mL/min and 500 mL/min respectively, and a visibly homogeneous perfusion with a soft parenchyma.[117] These criteria accurately predicted the short-term post-transplant function with 100% graft and patient survival to 90-days. However, this failed to identify the 18% of grafts that required re-transplantation within the first 2-years due to biliary strictures.[139] Therefore, new biomarkers are needed to improve the sensitivity and specificity of viability prediction in order to move to a truly organ-specific assessment which ensures maximum organ utilisation is combined with maximum safety for the recipient.

3

Magnetic Resonance Imaging and Spectroscopy of the Liver

Magnetic resonance imaging (MRI) and spectroscopy (MRS) are versatile, non-invasive and non-ionising methods that probe biological, physical and chemical states in vitro and in vivo. The techniques are underpinned by the phenomenon of nuclear magnetic resonance (NMR), which describes the interaction of the quantum mechanical phenomenon of nuclear spin with electric and magnetic fields. In this chapter, I explain the salient aspects of NMR and MRI theory that are specifically relevant to this thesis. I also highlight how MR techniques have been utilised in the clinical assessment of the liver disease and in the field of solid organ transplantation. A more comprehensive description of the quantum mechanical underpinnings and technical details of MRI are excellently described by Hore's textbook "Nuclear Magnetic Resonance",[96] Haacke et al.'s "Magnetic Resonance Imaging",[29] and de Graaf's "In Vivo NMR Spectroscopy",[58] which served as a references for much of this chapter.

3.1 Physical basis

At the centre of every atom is an atomic nucleus. Each nucleus has intrinsic properties such as mass, electric charge and, crucially for MRI, nuclear spin. The magnetic behaviour

of a nucleus is predominantly determined by its nuclear spin quantum number (I) and its gyromagnetic ratio (γ). I depends on the relative number of nucleons (protons and neutrons) within the nucleus. For known chemical elements, I varies between 0 and 9/2 in half integer steps. However, this thesis will considers only nuclei with $I = 1/2$ (specifically ^{1}H, ^{13}C, and ^{31}P). In the absence of an external magnetic field, a nucleus has $2I + 1$ degenerate energy levels. Application of an external magnetic field breaks the degeneracy of these states yielding two energy levels (for nuclei with $I = 1/2$) through Zeeman splitting. Fundamentally, all MR techniques probe these energy levels in different ways.

The interaction of a particle in a magnetic field can be explained through the magnetic moment vector, which is dependent on the intrinsic nuclear angular momentum $\hat{\boldsymbol{J}}$ of the particle via Wigner Eckart theorem:

$$\hat{\boldsymbol{\mu}} = \gamma\hat{\boldsymbol{J}} = \gamma\hbar\hat{\boldsymbol{I}} \tag{3.1}$$

given $\hat{\boldsymbol{J}}$ is itself determined by $\hat{\boldsymbol{I}}$ ($\hat{\boldsymbol{J}} = \hbar\hat{\boldsymbol{I}}$).

From a classical interpretation, one can then understand why this property is termed 'spin' even though it involves no physical movement. A magnetic moment μ in a magnetic field $\boldsymbol{B}$ will experience a torque $\boldsymbol{\tau}$:

$$\boldsymbol{\tau} = \boldsymbol{\mu} \times \boldsymbol{B} \tag{3.2}$$

Given, torque is the derivative of angular momentum with respect to time, Equations 3.1 and 3.2 can be combined to give:

$$\frac{d\boldsymbol{\mu}}{dt} = \gamma\boldsymbol{\mu} \times \boldsymbol{B} \tag{3.3}$$

Thus showing that the magnetic moment precesses around the external magnetic field, i.e. the magnetic moment has constant magnitude but continually rotates around the $\boldsymbol{B}$ field direction. The Larmor equation, which calculates the angular frequency of this precession, ω, can be deduced from 3.3 and a consideration of the system's geometry to yield:

$$\omega = -\gamma B. \tag{3.4}$$

When a macroscopic object is studied, MR techniques detect the net response of an *ensemble* of a great many individual nuclear spins. When the ensemble of spins is in an

external magnetic field ($\boldsymbol{B_0}$), on average more spins will align with the field than oppose it as this is the lower energy state. This polarisation of the sample results in a net magnetisation ($\boldsymbol{M_0}$). The difference in energy levels is usually small in comparison to thermal energy and hence the difference between the number of spins aligned with $\boldsymbol{B_0}$ ($N_\uparrow$) and opposed to $\boldsymbol{B_0}$ ($N_\downarrow$) is very small. Indeed the polarisation at a temperature (T) is determined by the Boltzmann distribution:

$$\frac{N_\uparrow}{N_\downarrow} = e^{-\frac{\Delta E}{k_b T}} = e^{-\frac{\hbar \gamma B_0}{k_b T}}. \tag{3.5}$$

Equation 3.5 predicts a net polarisation of 0.0005%, 0.0008% and 0.002%, for ^{13}C, ^{31}P, and ^{1}H at a clinical magnetic field strength of 3T. This corresponds to a difference of $\sim$1 in 100,000 nuclei and is what makes MR an inherently insensitive compared to other forms of spectroscopy. However, when a sufficiently large number of nuclei are considered these differences are detectable.

3.1.1 Excitation and relaxation

At thermal equilibrium in a static field, each individual spin has a random phase. Hence the ensemble has no overall net phase and so the net magnetisation vector $\boldsymbol{M_0}$ lies parallel to $\boldsymbol{B_0}$. Application of a radio frequency (RF) pulse oscillating at the Larmor-frequency of the nucleus examined, generates an orthogonal second magnetic field $\boldsymbol{B_1}$. This perturbs the system and induces phase coherence amongst the processing spins thus rotating $\boldsymbol{M_0}$ away from $\boldsymbol{B_0}$. The degree of rotation θ, termed the flip angle, is determined by the magnitude and duration of the RF pulse and is given by Equation 3.6.

$$\theta = \gamma \int_0^t |\boldsymbol{B_1}|\, dt \tag{3.6}$$

As $\boldsymbol{M_0}$ precesses, its oscillating transverse component induces a voltage in receiver coils placed orthogonal to $\boldsymbol{B_0}$. This is the signal detected in MR experiments and is called a free induction decay (FID).

The detected MR signal is termed a decay, because $\boldsymbol{M_0}$ relaxes back to align with $\boldsymbol{B_0}$. This occurs through spin-lattice (T_1) and spin-spin (T_2) relaxation. T_1 relaxation is driven by fluctuations in the local magnetic fields, which when they occur at the Larmor frequency

enable the nuclei to change energy levels via stimulated emission. In solutions, fluctuations in the dipolar-coupling between spins due to molecular tumbling are the most common source of T_1 relaxation. The rate of recovery of the z-component of $\boldsymbol{M_0}$, ie. the component parallel to $\boldsymbol{B_0}$, is parametrised by a time constant T_1 such that:

$$M_z(t) = M_{z(0)}e^{-\frac{t}{T_1}} + M_0\left(1 - e^{-\frac{t}{T_1}}\right) \tag{3.7}$$

Additional signal decay occurs as the spins lose phase coherence through spin-spin relaxation and reduce the transverse magnetisation component during data sampling. This T_2 relaxation occurs due to two mechanisms. Firstly, local fluctuations in the magnetic field cause dephasing of the spins as well as the energy transitions for T_1 relaxation. In addition to this, dipolar transitions see two spins exchange their longitudinal angular momentum in zero energy processes. The net effect of these two mechanisms is parametrised by T_2 according to Equation 3.8.

$$M_{xy}(t) = M_{xy(0)}e^{-\frac{t}{T_2}} \tag{3.8}$$

A third reversible dephasing effect occurs due to inhomogeneities in the $\boldsymbol{B_0}$ field and is parametrised by T_2'. This parameter combines with T_2 to give the overall transverse decay constant $T_2^\star$ (Equation 3.9).

$$\frac{1}{T_2^*} = \frac{1}{T_2} + \frac{1}{T_2'} \tag{3.9}$$

Given the sensitivity to the rate of molecular tumbling, T_1, T_2 and $T_2^\star$ are sensitive to the local molecular environment of nuclei (Figure 3.1). This allows discrimination between water in different environments (e.g. water bound to large immobile proteins, restricted within tissue, or free to move in blood). It also enables sensitisation to disease such as fibrosis, inflammation and oedema, as these conditions change the tissue micro-structure and create either increasingly bound or free water.

3.1.2 Acquiring an MR image or spectrum

Through the application of a variety of excitation pulses, and appropriate spatial-temporal variation of magnetic field gradients additional frequency and phase data can be encoded into the FID signal(s). This enables more accurate spatial localisation of signals, as is performed in

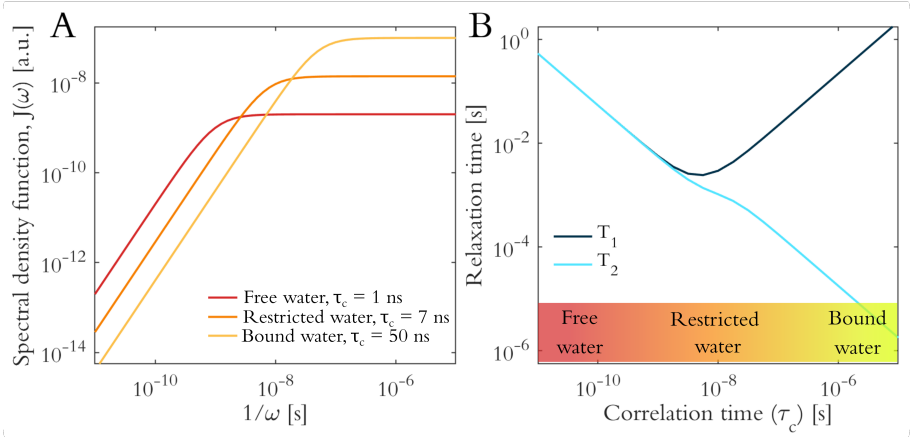


Figure 3.1: Spectral density as a function of resonance frequency for three different water pools (A) and the effect of correlation time (τ_c) on relaxation times of water at 3T (B). τ_c is a measure of the rate of molecular tumbling. The dominant water pool at a given τ_c is also highlighted. The figure was generated using the Solomon-Bloembergen equations.[195,20,30]

imaging methods, or more accurate information about the chemical composition of the material for spectroscopic techniques.

Three main methods are used to provide spatial encoding in MRI:

1. *Slice selection*

   A linear magnetic field gradient is applied perpendicular to the desired slice to generate spatial variation in the resonance frequency of the nuclei. Simultaneously, a shaped RF pulse (ie. one with a defined bandwidth) is used to selectively excite spins in the chosen imaging plane by matching the RF pulse frequency to the local resonance frequency.

2. *Frequency encoding*

   Often termed the 'readout gradient', a strong gradient is applied perpendicular to the slice select gradient to dephase the transverse magnetisation in a spatially dependent manner. A second smaller gradient of opposite amplitude is then applied to rephase the magnetisation. When the areas of the two gradient waveforms are equal at a given spatial position, spins will be back in phase and signal will be detected in a

gradient-recalled echo (GRE).

3. *Phase encoding*

   To obtain an additional dimension of localisation, a phase encoding gradient is applied in the third axis which makes spins to accrue a spatially dependent phase. When this gradient is turned off, spins will have a known phase shift as a function of distance in the third axis. Repeating acquisitions with different phase encoding will enable full sampling of the third axis. Combining this phase shift with the phase variation generated by the frequency encoding and the selective localised excitation from the slice selection, this allows 3D localisation of the detected FID signal.

The FID data acquired using these methods is in the spatial frequency domain, called k-space. Complex image space data ρ can be obtained from the FID k-space data s with a two-dimensional Fourier-transform:

$$\rho\left(xy\right) = \int_x \int_y s\left(x,y\right) e^{+2\pi i\left(k_x(t)x + k_y(t)y\right)} dxdy \tag{3.10}$$

Alternatively if no magnetic field gradients are applied during readout and any signal localisation is achieved purely during excitation, a range of spectral information can be acquired instead of the spatial information. Variation in chemical composition and relative abundance can be obtained by this and it forms the basis of magnetic resonance spectroscopy. Equation 3.4 is strictly only true for a bare nucleus. In an atom or molecule, variations in the distribution of electrons around the nuclei provides a variable amount of shielding from the magnetic field which causes differences in the resonance frequency of different nuclei according to their local chemical environment. Therefore, the resonance frequency of species i in a molecular environment in is better characterised by Equation 3.11 where the extent of shielding of species i is parametrised by σ_{i}.

$$\omega_{\mathrm{i}} = -\gamma B_0 \left(1 - \sigma_{\mathrm{i}}\right) \tag{3.11}$$

This enables the differentiation of different chemical species through changes in frequency and is usually reported as a chemical shift δ_{i} relative to a reference standard ω_{ref} to ensure

measurements are independent of the magnetic field strength used:

$$\delta_{\mathrm{i}} = \left(\frac{\omega_{\mathrm{i}} - \omega_{\mathrm{ref}}}{\omega_{\mathrm{ref}}} \right) \times 10^6. \tag{3.12}$$

Similarly to imaging, the NMR spectrum can be obtained from the FID via a Fourier-transform, which in this case converts between the time domain and the spectral frequency domain.

3.2 MRI and MRS in the liver

Application of the physical phenomenon described above have proven an effective method for non-invasive assessment of liver health and disease.

3.2.1 Relaxometry

As described in Section 3.1.1, the T_1, T_2, and $T_2^\star$ relaxation rates are acutely sensitive to the micro-environment of nuclei. Therefore, mapping variation of the relaxation rates across the liver has proven to be an effective method to monitor physiology changes both on a global scale, as is seen in conditions such as non-alcoholic fatty liver disease (NAFLD) or haemochromatosis, or locally to detect tumours. [106,89,143]

3.2.1.1 T_1 mapping

Traditionally, T_1 has been measured using an inversion recovery sequence (Figure 3.2) where longitudinal magnetisation is inverted before a spin-echo readout is performed following a range of different inversion times (TI). Fitting the signal recovery following inversion as a function of TI, as described in Equation3.13, allows a calculated T_1 value to be obtained.

$$S(\mathrm{TI}) = S_0 \left(1 - 2e^{-\frac{TI}{T_1}} \right) \tag{3.13}$$

However, this is a very slow measurement requiring repeated acquisitions with very long repetition times (typically $>5 \times T_1$), which is not practical in most clinical scans. Therefore, a range of fast T_1mapping techniques have been proposed to speed up acquisition albeit at the cost of additional biases or uncertainty in the measurement.

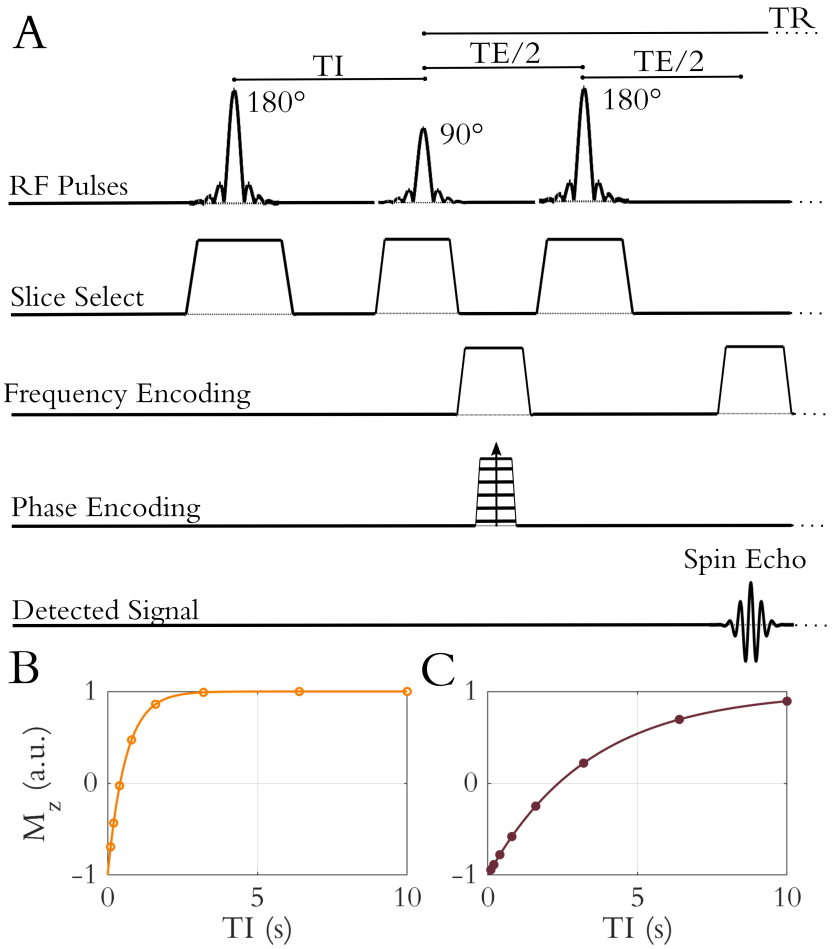


Figure 3.2: Summary of an inversion recovery spin echo T_1 mapping sequence. An inversion pulse is applied before a spin echo readout block to acquire an image at a given inversion time (TI). The evolution of M_Z for species with a short (600 ms, orange) and long (3400 ms, red) T_1 relaxation rates as a function of TI are presented (B and C). A very long TR is used (typically $>5 \times T_1$) to ensure ensure complete relaxation between measurements. Abbreviations: *echo time, TE; inversion time, TI; radio frequency, RF; repetition time, TR.*

Variable flip angle (VFA) T_1 mapping

VFA T_1 mapping, also termed driven-equilibrium single-pulse observation of T_1 (DESPOT1),[95] is a rapid T_1 measurement technique that uses multiple spoiled gradient echo acquisitions with different flip angles θ_n to calculate T_1 maps (Figure 3.3). A very short repetition time is used to hold the magnetisation in a partially saturated steady state during the image acquisition, which adds both a T_1 and flip angle dependence to the detected signal. Therefore if the detected signal intensity across a range of flip angles is fit to Equation 3.14, an estimate

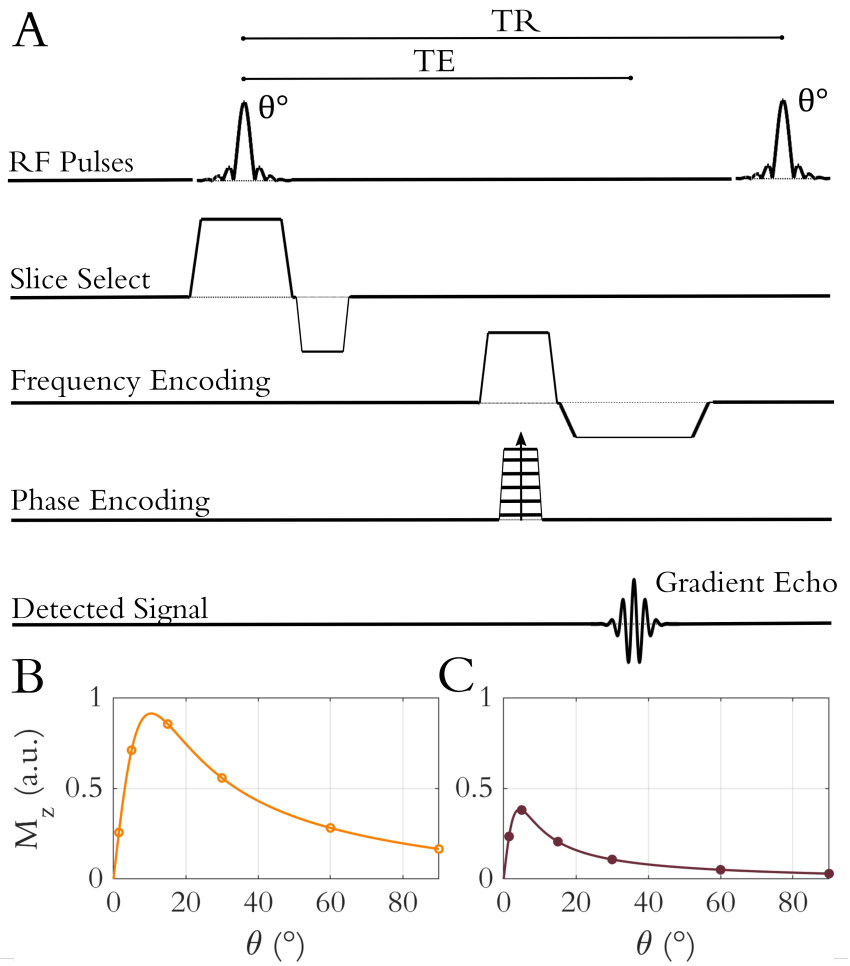


Figure 3.3: Summary of a variable flip angle T_1 mapping sequence. A gradient recalled echo sequence is used with flip angle θ and a short TR to acquire an image with magnetisation in a steady state. By iterating over a range of θ, T_1 can be calculated as the saturation of the steady state signal is dependent on T_1. The sensitivity of the detected signal to increasing flip angles is demonstrated for species with a short (600 ms, orange) and long (3400 ms, red) T_1 relaxation rates (B and C respectively). Abbreviations: *echo time, TE; radio frequency, RF; repetition time, TR*

of T_1 in each pixel.

$$S(\theta_n) = S_0 \left[\frac{1 - \exp\left(-\frac{TR}{T_1}\right)}{1 - \cos(\theta_n) \exp\left(-\frac{TR}{T_1}\right)} \right] \sin(\theta_n) \tag{3.14}$$

In practice, the actual flip angle achieved is variable across an image and hence the calculated VFA T_1 can show spatial variation.[122] To remove this confounding effect a map of the transmit RF amplitude (B_1) is commonly measured as part of a VFA T_1 mapping experiment, using methods such as Bloch-Siegert B_1 mapping,[189] DREAM,[155] or the double angle method,[102] and the calculated VFA T_1 map corrected for any variation in B_1

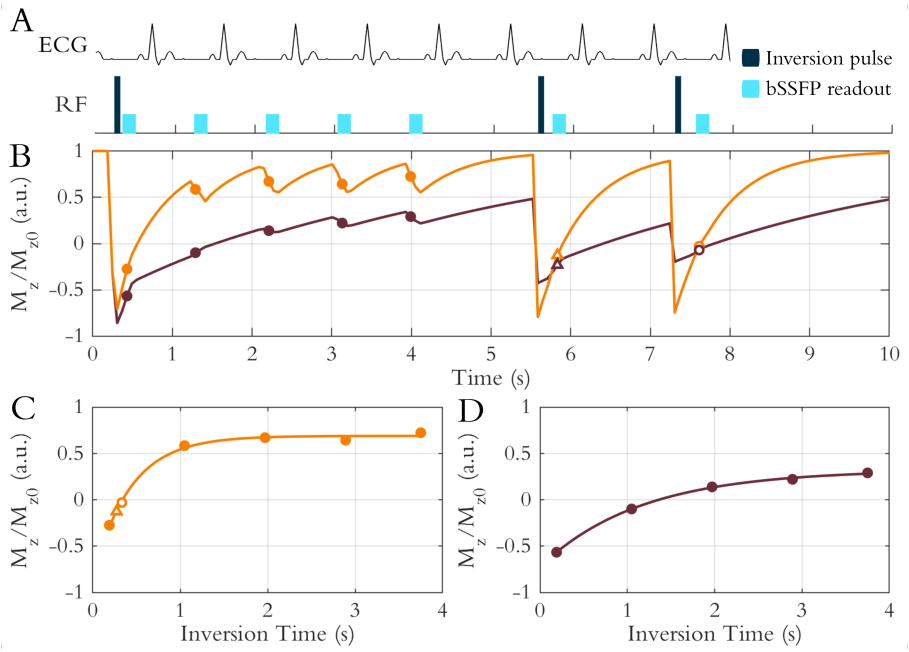


Figure 3.4: Summary of the shMOLLI T_1 mapping sequence. Adiabatic inversion pulses are applied before a series of balanced SSFP readout block to acquire an image at diastole of the cardiac cycle (A). The evolution of M_Z for species with a short (600 ms, orange) and long (3400 ms, red) T_1 relaxation rates (B). The signal recovery as a function of inversion time are shown according to the conditional fitting algorithm which uses 5 points for the long T_1 estimation and all seven data points for the short T_1 species. This figure is based upon Figure 2.19 by Mozes et al.[145]

detected.[122]

Shortened modified Look-Locker inversion recovery T_1 mapping

A popular family of rapid T_1 mapping methods are based on a modified Look-Locker inversion sequence (MOLLI)[141] or a shortened variant of MOLLI (shMOLLI).[173] These sequences have become a mainstay of cardiac MRI and are increasingly used to examine abdominal organs such as the liver. The Look-Locker inversion sequence makes repeated measurements of magnetisation following one inversion, removing the requirements for repeated measurements. Then MOLLI replaces the spin echo readout traditionally used in inversion recovery experiments with a balanced steady state free precession (bSSFP) readout and synchronises the acquisition to the patient's cardiac cycle using an electrocardiogram (ECG).[173] The bSSFP readouts create high SNR images in a short time by utilising rapidly repeated RF pulses to generate a steady state in longitudinal and transverse magnetisation. However, this means that MOLLI T_1 measurements are not purely sensitive to T_1 and instead

are confounded by factors such as T_2, B0 inhomogeneity, fat contamination, tissue iron concentration, and off-resonance effects.[146,212,147] Additionally, variation in the timing of the bSSFP readout due to changes in a patient's heart rate can also impact the calculated MOLLI T_1.[173] Where the variation due to the cardiac cycle can be assumed to be minimal (e.g. in phantoms or organs with smaller pulsatility), using a simulated physiological trigger can minimise the effect of changes in heart rate but the calculated MOLLI T_1 will still depended upon the frequency of the simulated heart rate.

As some patients find a prolonged breath-hold uncomfortable, a shortened version of MOLLI (shMOLLI) was developed to enable acquisition of a T_1 map in a shorter breath-hold. As is apparent in Figure 3.4, the application of repeated imaging readouts within one inversion recovery curve perturbs the magnetisation recovery. Therefore, the recovery signal must be fitted to Equation 3.15 first to obtain an apparent T_1 relaxation time $T_1^\star$.

$$S(TI) = A - Be^{-\frac{TI}{T_1^*}} \tag{3.15}$$

Then this value is corrected to the actual T_1 using the Deichmann-Haase formula (Equation 3.16).[61]

$$T_1 = T_1^* \left(\frac{B}{A} - 1 \right) \tag{3.16}$$

A conditional fitting algorithm, based upon an initial estimation from the first 5 measurements and the R-R interval, is used to obtain an optimal fit.[173]

Clinical utility of T_1 mapping

T_1 has been used to characterise a range of fibro-inflammatory liver diseases under the assumption that liver T_1 will increase as the extracelluar fluid increases (as seen in fibrosis) and following water accumulation within swelling cells (as seen in inflammation). Indeed, Banerjee et al. demonstrated that in patients with chronic liver disease T_1 could detect advanced fibrosis and cirrhosis (AUROC = 0.81 and 0.92 respectively).[11] T_1 has also been shown to be predictive of portal hypertension with a correlation between T_1 and invasive hepatic venous pressure gradient (HVPG) of r = 0.85.[166] Beyond these correlations with

specific histological or invasive markers, liver T_1 has also been shown to be predictive of mortality across a range of chronic liver conditions such as viral hepatitis, NAFLD, alcoholic steatohepatitis, and a range of biliary conditions.[106]

Application of T_1 mapping in transplantation has been limited to date. However, post-transplant in vivo cardiac T_1 measurements have shown promise for prediction of rejection in cardiac patients.[101] In the kidney, post-transplant T_1 measurements correlated with kidney function.[5] Application of T_1 mapping to the liver transplants, whether in vivo or ex vivo, is yet to be reported. There is a growing interest in this topic with studies running to examine the ability of post-transplant T_1 measurements to predict graft rejection and to examine the correlation between ex vivo T_1 measurements with relevant pathological findings with long-term aspirations to use MR relaxometry to predict donor organ viability for transplantation.[1,41]

However, care needs to be taken with fast T_1 mapping methods as a sacrifice for speed is additional confounding factors. For example, shMOLLI T_1 has been shown to be confounded by hepatic iron concentration (HIC), inhomogeneities in the magnetic field and the level of steatosis.[80,146,147] These confounding effects can have varied impacts on the calculated T_1, with increasing hepatic iron content reducing the shMOLLI T_1 due to faster T_2 relaxation occurring but increasing steatosis usually increasing the calculated shMOLLI T_1. The exact dependence of shMOLLI T_1 on the concentration of fat is dependent on the acquisition parameters used but under standard conditions is driven by the fat and water signals being exactly out of phase during the bSSFP readout which results in the detected signal recovery being the weighted difference of the fat and water signals.[146] For in vivo acquisitions, algorithms have been developed to correct MOLLI T_1 for these effects.[212,147] However, to date none of these algorithms have been validated for ex vivo applications.

3.2.1.2 T_2 and T_2^* mapping

Liver T_2 and $T_2^\star$ have proven to be excellent non-invasive measures of HIC. For T_2 measurements, a multi-echo spin echo acquisition is typically used with data fitted to a bi-exponential model which accounts for both slow and fast T_2 components.[197] In

comparison, T_2^* measurements usually use a multi-echo spoiled gradient echo (GRE) acquisition and fit the data to a mono-exponential model which is sometimes extended to include a constant term to account for baseline noise.[207] Conversion of T_2 or T_2^* to HIC are then performed using biopsy derived calibration curves. Good inter-scanner and inter-centre reproducibility of the measurements have been reported.[207] This has enabled MRI-based HIC measurements to be useful in the monitoring of a wide range of conditions from transfussion-dependent thalassaemia to haemochromatosis covering a range of HIC of between 0.3 to over 50 mg Fe/g dry tissue.[197] Whether T_2 and T_2^* measurements are useful in the field of solid organ transplantation remains an unanswered question.

3.2.2 Quantification of steatosis

As discussed in Section 2.1.3.3, the level of hepatic steatosis is an important predictor of graft function from donated livers. However, high levels of steatosis (usually defined using the Dallas Heart Study threshold of fat fractions >5.56%[204]) are also seen in a wide range of liver diseases as well as being risk factors for other conditions including Type-2 diabetes.[227,204] Liver biopsy has been the traditional gold-standard for steatosis assessment in the liver but high inter-measurement and inter-reader variability and risks associated with the procedure mean that in recent years MR spectroscopy- and imaging-based proton density fat fraction measurements have been quantify to assess hepatic steatosis.[68,227]

3.2.2.1 ^{1}H-MRS

Single voxel ^{1}H-MRS, commonly measured using either multi-echo, T_2-corrected stimulated echo acquisition mode (STEAM)[78] or point-resolved spectroscopy (PRESS),[22] has been shown to provide an accurate measurement of hepatic steatosis when compared to histological references. This has made ^{1}H-MRS the gold-standard method for non-invasive measurement of hepatic fat concentration.

STEAM combines three slice-selective 90°-pulses with three orthogonal gradients to generate a stimulated echo from protons located within a cuboid-shaped voxel at the intersection of the three orthogonal planes (Figure 3.5). The timing of the stimulated echo is

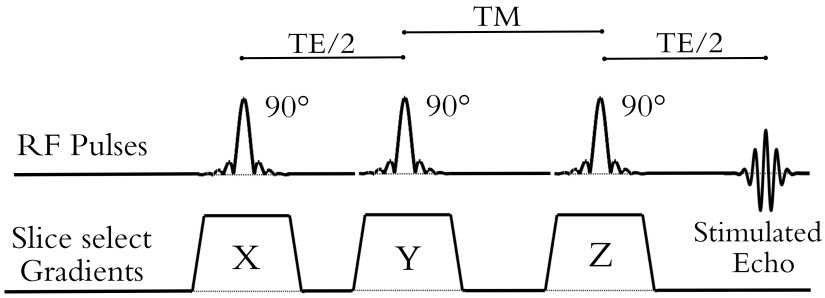


Figure 3.5: Summary of a single voxel stimulated echo acquisition mode (STEAM) spectroscopy sequence. Abbreviations: *echo time, TE; mixing time, TM, radio frequency, RF.*

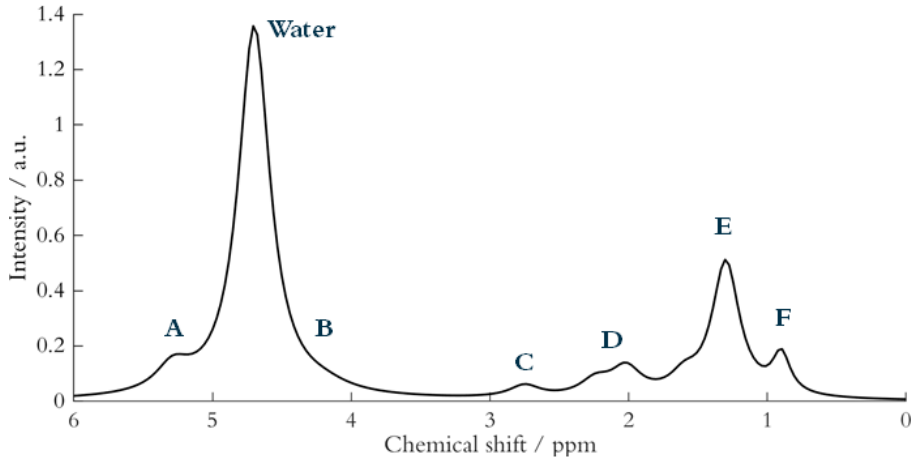


Figure 3.6: Typical ^{1}H-MRS spectrum of a steatotic human liver. The fat peaks are assigned as described by Hamilton et al.: A, -C**H**=C**H**- and C**H**-O-CO-; B, -C$\mathbf{H}_2$-O-CO-; C, -CH=CH-C$\mathbf{H}_2$-CH=CH-; D, -CO-C$\mathbf{H}_2$-CH_2- and -C$\mathbf{H}_2$-CH=CH-C$\mathbf{H}_2$-; E, -CO-CH_2-C$\mathbf{H}_2$- and -$(C\mathbf{H}_2)_n$-; and F, -$(CH_2)_n$-C$\mathbf{H}_3$. For in vivo spectra acquired at 3T, unless water suppression is applied peaks A and B are typically hidden within the water peak and peak C is often too small to detect.

determined by the spacing of the three RF-pulses. The spacing between the first two pulses determines the echo time. Meanwhile, the interval between the second and third pulses is a mixing time during which the signal is stored along the z-axis, preventing T_2 decay. Therefore, STEAM is able to have shorter echo times (typically ~7 ms) than PRESS. For PRESS the echo time is determined by the spacing of all three pulses. Additionally, the use of 90° pulses (rather than the 180° pulses used in PRESS) allows STEAM to have sharper slice profiles, a higher bandwidth and lower deposition of energy into the tissue than PRESS. The main disadvantage of STEAM is that at a matched repetition time and echo time, the detected signal is limited to half that of PRESS. However for steatosis quantification within

the liver in vivo, the better localisation, lower energy deposition, and shorter echo time are more beneficial than the theoretical additional signal that PRESS could offer and hence STEAM remains the main spectroscopic technique used.

A typical ^{1}H spectrum of a steatotic human liver is shown in Figure 3.6. Hamilton et al. characterised this spectrum, showing that a typical in vivo liver spectrum consists of 6 visible fat peaks in addition to the water signal and that the relative amplitude of the different fat species is a function of the saturation of the lipid molecules (i.e. how many double bonds are present).[85] Using this prior knowledge, the amplitudes of the peaks can be obtained through spectral fitting, whereby a combination of Lorentzian functions at the expected frequencies of the chemical species present are fit to the measured spectrum, using software packages such as LCModel or the OXSA toolbox in the frequency-domain with a non-linear least squares algorithm or time-domain with the AMARES algorithm respectively.[174,175] After these peak amplitudes are corrected for signal losses due to different relaxation rates of each chemical species, using either previously published or measured T_1 and T_2 values, proton density fat fraction (PDFF) can be calculated according to:

$$PDFF = \frac{\rho_F}{(\rho_W + \rho_F)} \tag{3.17}$$

where ρ_F and ρ_W are the sums of the T_1- and T_2-corrected amplitudes for all of the fat and water peaks respectively.[86]

3.2.2.2 Proton density fat fraction mapping

Although ^{1}H-MRS provides a detailed and accurate assessment of the hepatic fat content, it is slow and only provides information about one small region of liver (typically $2\times2\times2$ mm^3). Therefore, Dixon et al. and later Reeder et al. developed imaging techniques to rapidly generate maps of hepatic fat concentration. Based upon multi-echo spoiled GRE sequences, these techniques fit the signal variation across different echo times to a model which accounts for the frequency offset between fat and water's resonance frequencies. This then enables high resolution fat fraction, or if T_1 and $T_2^{\star}$ are accounted for, PDFF images to be generated from data that was acquired in <10 seconds. If the $T_2^{\star}$ of fat and water are

considered equal, as is commonly done,[236] the signal evolution as a function of echo time TE can be modelled by:

$$S(TE) = e^{-TE/T_2^*} K \left((1 - PDFF) + PDFF \sum_{\mathrm{p}=1}^{P} \alpha_{\mathrm{p}} e^{2\pi i f_{\mathrm{p}} TE} \right) e^{-2\pi i \Phi TE}, \qquad (3.18)$$

where the fat spectrum is modelled as a series of P peaks with chemical shifts f_{p} relative to water and amplitudes α_{p}, such that $\sum_{\mathrm{p}=1}^{P} \alpha_{\mathrm{p}} = 1$, Φ is the phase shift due to field inhomogeneities, ρ_{W} and ρ_{F} are the proton densities of water and fat, and $K = \rho_{\mathrm{W}} + \rho_{\mathrm{F}}$. Using Equation 3.18, the $T_2^\star$-iterative decomposition of water and fat with asymmetric echo times and least-squares estimate ($T_2^\star$-IDEAL) algorithm can be applied to obtain parametric maps of PDFF, $T_2^\star$, and B_0.[180,236]

Initially, Dixon et al. proposed using 2 echo times to capture the fat and water signals when directly out of phase and in phase (1.1 ms and 2.3 ms at 3T or 2.3 ms and 4.6 ms at 1.5T).[64] However, it is now recommended to acquire additional echoes (typically 6 - 12) at shorter echo spacings (typically 1 ms) as this is more robust in situations where the $T_2^\star$ becomes very short (e.g. in haemochromatosis) and allows changes in the chemical composition of the fat to be accounted for through spectral modelling.[236]

This technique has rapidly increased in popularity due to the ease of acquisition and wide availability on clinical systems. It has been validated against MRS PDFF and has shown strong reproducibility between different sites, scanners, and field strengths.[93] However, care must be taken to account for confounding factors such as: noise bias, inter-subject spectral variations, and frequency shifts of water due to changes of temperature or pH. The last of these points are especially important when considering ex vivo organs where homoeostasis of pH and temperature are not guaranteed.

Bannas et al. have demonstrated that both spectroscopic- and imaging-based PDFF measurements correlate strongly with the triglyceride content of wedge biopsies taken from ex vivo livers in room temperature phosphate buffered saline.[13] This suggests that these techniques could provide a non-invasive method to assess the level of steatosis in donor organs. However, the resonance frequency of lipids and water have different sensitivities to temperature.[172] Given PDFF measures rely on the resonance frequency difference between

fat and water species to separate the signals, PDFF is inherently confounded by temperature.[92] Therefore, additional studies are needed to assess the techniques accuracy both at lower temperatures experienced during SCS and during ex vivo normothermia in order to show whether they are truly suitable for use in transplantation.

3.2.3 Measuring diffusion and perfusion

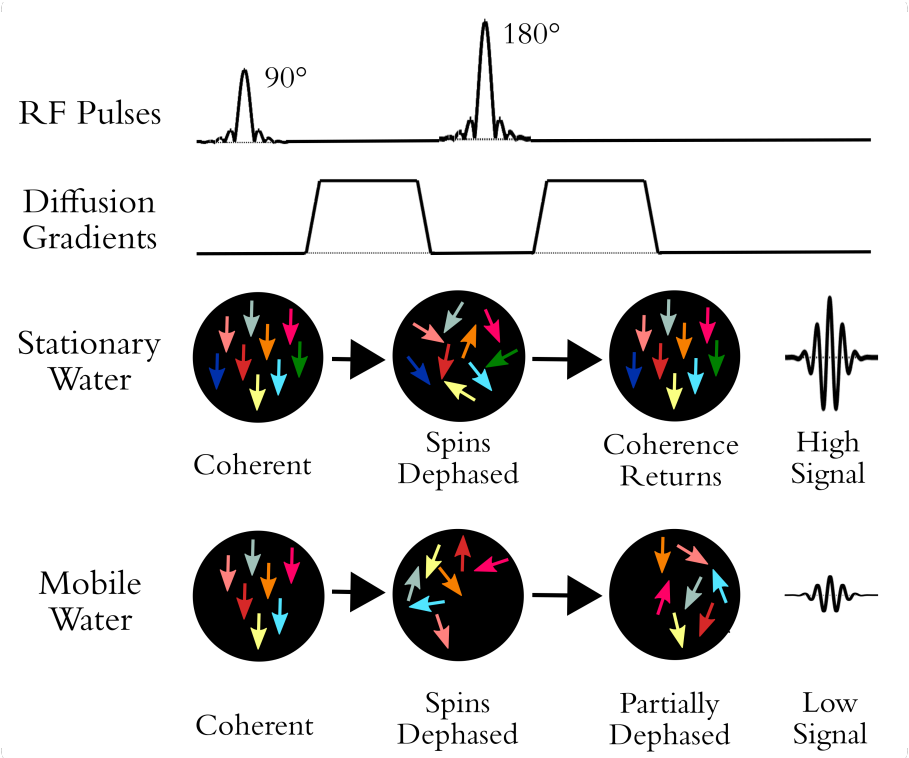


Figure 3.7: Summary of a spin-echo diffusion weighted imaging sequence (A). The effect of the diffusion gradients on spins in stationary (B) and mobile (C) water are shown with their resulting signal intensity.

Diffusion weighted imaging (DWI) is a staple of modern clinical MRI and has proved effective at detecting regions of ischaemic injury following a stroke as well as identifying tumours. By applying equal and opposite magnetic field gradients before and after a refocusing pulse during a spin-echo pulse sequence, any stationary spins see the effect of the gradients cancelled out but any spins which have moved between the two gradient pulses will have a reduction in the net magnetisation (Figure 3.7). Thereby, the addition of the gradients adds a diffusion weighting to an image with areas of low diffusivity retaining high signal and areas with high diffusivity yielding very little signal.

In a solution where molecules have completely free diffusion, the amount of signal decay observed depends on the diffusivity (D), the strength of the gradient pulse (G), the duration of the gradient pulse (δ), and the time between the two gradient pulses (Δ) according to:

$$\frac{S_i}{S_0} = \exp\left(-\gamma^2 G^2 \delta^2 \left(\Delta - \frac{\delta}{3}\right) D\right). \tag{3.19}$$

All of the terms defining the diffusion gradients, and hence the diffusion weighting of the image, are commonly combined into a b-value such that $b = -\gamma^2 G^2 \delta^2 \left(\Delta - \frac{\delta}{3}\right)$.

3.2.3.1 Intra-voxel incoherent motion

In 1988, Le Bihan et al. showed that in the case of restricted diffusion, as is found in tissue, additional diffusion compartments are present and hence suggested using a intra-voxel incoherent motion (IVIM) model to characterise these compartments.[120] By making multiple measurements at a range of b-values, one can fit the resulting changes in signal to obtain the diffusion coefficients and relative contribution of each compartment to the signal. Traditionally, this model has assumed that there are two components which contribute to signal decay in diffusion weighted imaging: 1) a slow-decaying component which is due to the passive diffusion of the tissue and 2) a fast-decaying component which is caused by the perfusion of the tissue. Using this model, the signal decay of DWI data is fitted according to a bi-exponential model:[120]

$$\frac{S_\mathrm{b}}{S_0} = (1 - f_\mathrm{P}) \cdot \exp\left(-b \cdot D\right) + f_\mathrm{P} \cdot \exp\left(-b \cdot [D + D^*]\right), \tag{3.20}$$

where $\frac{S_\mathrm{b}}{S_0}$ is the normalise signal intensity at b-value b, D is the pure diffusion coefficient of passive molecular diffusion, D^* is the pseudo-diffusion coefficient representing the incoherent micro-circulation (i.e. the perfusion-related diffusion), and f_P is the perfusion fraction determining the relative contributions of the two compartments.

However, achieving reproducible measurements of the pseudo-diffusion coefficient and perfusion fraction is very challenging and has been shown to depend on the number and spacing of b-values used, the field strength of the scanner used,[187] and the fitting method. Even within the same study, with a completely matched protocol and fitting parameters, the

reported reproducibility of the perfusion fraction and psuedo-diffusion coefficient are poor with 95% limits of agreements allowing changes of up to 25% and 59% respectively.[7]

One proposed method for improving the stability and reproducibility of the fit is to perform a segmented fitting. This method relies on the contribution of signal decay due to the micro-vasculature becoming negligible at high b-values (typically $\geq$200 s/mm^2).[45] Therefore by only considering the high b-values initially, the model can be simplified to a single mono-exponential one:

$$S_{\mathrm{b}} = S_{\mathrm{int}} \cdot \exp\left(-b \cdot D\right), \tag{3.21}$$

where S_{int} is the $b = 0$ intercept of the exponential fit with only $b \geq$200 s/mm^2. The fitted value of the pure diffusion coefficient can then be substituted into Equation 3.20 to reduce the number of parameters included in the fit of the bi-exponential model.

Even with improved fitting methods, recent studies have reported poor agreement of the bi-exponential model with measured data in human livers and have suggested the presence of additional diffusion compartments. For example, Hayashi et al. proposed an additional very slow compartment observable at very high b-values (>1000 s/mm^2), which may be useful in cirrhotic livers.[88] However, for studies with b-values <1000 s/mm^2 the most common third compartment is an additional intermediate diffusion compartment between the slow passive diffusion and very fast micro-perfusion.[45,187,37] Given the unique dual arterial and venous blood supply to the liver and the wide range of vessels present, it would not be surprising if there were an additional set of compartments between the pure molecular diffusion and very fast perfusion in the micro-vasculature. Wurnig et al. take this hypothesis further and proposed that the three observed diffusion compartments represent the passive water diffusion in hepatocytes and extracellular space, the portal venous flow, and arterial perfusion respectively.[230]

Regardless of the biological causes of the compartments, the extended three component IVIM model can be modelled by:

$$\frac{S_{\mathrm{b}}}{S_0} = (1 - f_1 - f_2) \cdot \exp\left(-b \cdot D\right) + f_1 \cdot \exp\left(-b \cdot D_1^*\right) + f_2 \cdot \exp\left(-b \cdot D_2^*\right), \tag{3.22}$$

where now f_1 and f_2 are the perfusion fractions of the intermediate and fast perfusion components, D is still the passive diffusion coefficient, and D_1^* and D_2^* are the psuedo-diffusion coefficients for the intermediate and fast diffusion compartments respectively.

More validation is needed to ascertain the optimum model to fit DWI data. However, multiple studies have suggested that IVIM models may be predictive of hepatic fibrosis,[48] steatosis,[124] and cirrhosis.[167] Therefore, application of a suitable IVIM model may aid the viability assessment of donor livers.

3.2.4 Metabolic imaging and spectroscopy

The liver is a very dynamic organ which is capable of altering its metabolism in order to maintain metabolic haemostasis within both the liver and circulating blood.[79] Figure 3.8 highlights some of the key metabolic pathways that are modulated within the liver to control the concentration of metabolites such as glucose, lactate, fatty acids, and triglycerides. Given the wide range of metabolites from these pathways that MRS techniques are able to measure, MRS has been shown to provide a detailed non-invasive assessment of hepatic metabolism in a range of clinical settings.[112,44,43]

^{1}H-MRS is the most commonly used and, as described in Section 3.2.2.1, can provide an accurate assessment of intra-hepatic triglyceride content through the proton density fat fraction. More advanced techniques have shown that other metabolites, such as choline, lactate, and succinate may also be measured in the liver.[131] Although, the significantly lower concentrations of the additional metabolites makes the acquisitions longer and more complex and may even limit the detection of the metabolites to cases of severe disease (e.g. detection of succinate by ^{1}H-MRS has only been reported within liver tumours and not healthy tissue).[131]

Examinations of different nuclei by MRS techniques including phosphorus (^{31}P) or carbon (^{13}C) can allow additional pathways such as oxidative phosphorylation and glycolysis to be probed. In the absence of exogenous tracers, these techniques are limited by the relatively low concentrations of the metabolites studies and hence have inherently lower signal to noise (SNR) than ^{1}H-MRS.

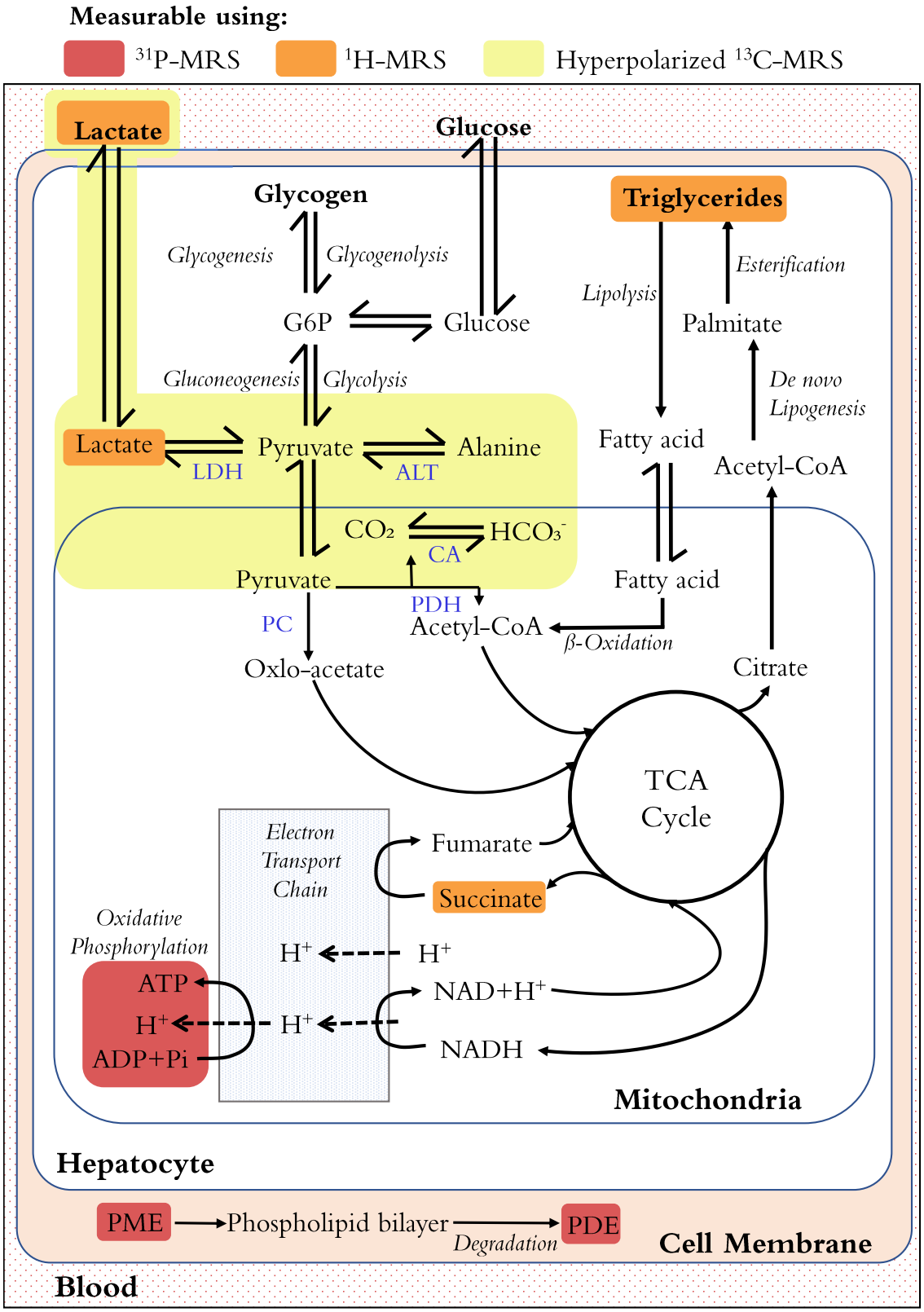


Figure 3.8: Summary of key metabolic pathways in the liver. Names of the pathways are given in italics, while enzymes are blue. The wide range of metabolites measurable by ^{31}P-, ^{1}H, and ^{13}C-MRS are highlighted. Abbreviations: adenosine biphosphate, ADP; adenosine triphosphate, ATP; alanine transaminase, ALT; carbonic anhydrase, CA; coenzyme-A, CoA; inorganic phosphate, Pi; lactate dehydrogenase, LDH; pyruvate carboxylase, PC; phosphodiester, PDE; pyruvate dehydrogenase, PDH; phosphomonoester, PME; nicotinamide adenine dinucleotide, NAD

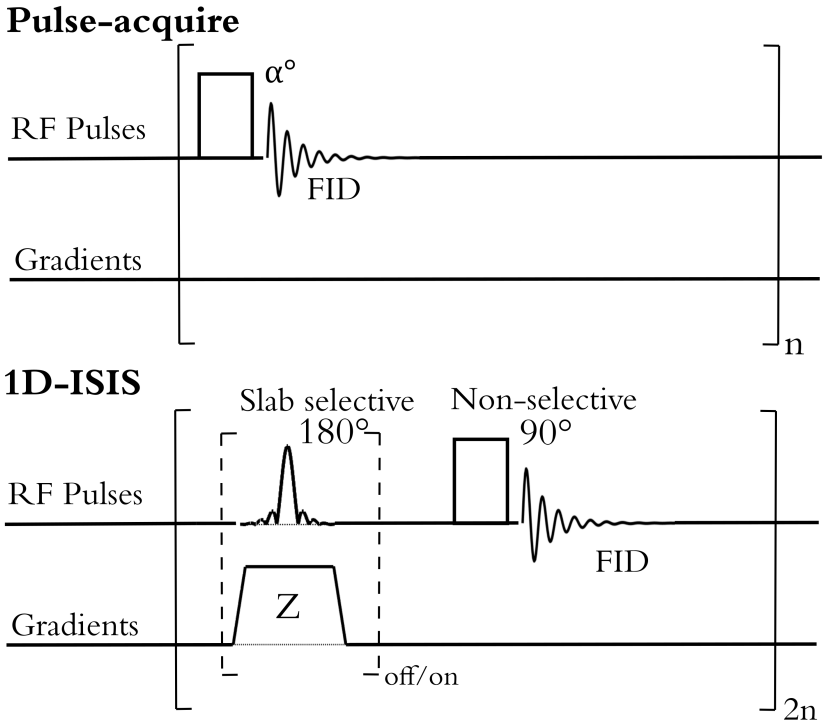


Figure 3.9: Summary of a non-localised pulse-acquire spectroscopy sequence and a slab-selective 1-D ISIS pulse sequence. In the ISIS sequence, the slab-selective inversion pulse is turned on and off in alternate acquisitions and the resulting pair of spectra subtracted to retain signal solely from the desired slice.Abbreviations: *free induction decay, FID; Image-selected In Vivo, ISIS.*

Because of the significantly lower SNR of x-nuclei spectroscopy (i.e. nuclei other than ^{1}H), acquisition sequences generally perform less localisation and hence cover a larger voxel than ^{1}H-MRS sequences. The simplest spectroscopy sequence is non-localised pulse-acquire spectroscopy, where a single RF pulse is used to excite signals before the FID is recorded (Figure 3.9). Using this sequence the only signal localisation achieved is a result of the sensitivity profile of the RF coil, which for x-nuclei spectroscopy is generally a hemisphere with a radius of a few centimetres (given that small surface loop coils are usually used). If additional localisation is required in 1 dimension, the pulse-acquire sequence can be converted to an Image-selected in vivo spectroscopy (ISIS) sequence through the addition of a slice-selective inversion pulse before the pulse-acquire acquisition (Figure 3.9). Repeating the acquisition with the inversion pulse turned off and subtracting the two resulting spectra allows selection of signal only from within the desired slice. In many cases, this 1-dimensional localisation, combined with the effects of the coil sensitivity, can enable

effective 3-dimensional signal localisation for x-nuclei spectroscopy without a significant penalty in the spectral SNR.

3.2.4.1 Phosphorus MRS

Given the importance of phosphate groups in the production of adenosine triphosphate (ATP), ^{31}P-MRS can assess the state of oxidative energy metabolic within the mitochondria. Despite being inherently a low SNR technique, with signal limited by a low gyromagnetic ratio and low concentrations of the observed metabolites, the 100% natural abundance of the NMR active isotope of phosphorus and high biological importance of the metabolites measured mean that ^{31}P-MRS has given unique insights into the metabolic dysfunction present in a range of clinical conditions from heart failure to liver cirrhosis.[23,158,136]

Given the low SNR of the technique, highly sensitive small surface coils are predominantly used in ^{31}P-MRS with signal localisation either provided purely by the coil sensitivity profile or by slab-selective techniques such as 1-dimensional image selected in vivo spectroscopy (ISIS). This, combined with averaging of multiple acquisitions, provides sufficient signal to detect a range of ^{31}P metabolites.

By measuring the amplitude and chemical shift of the three ATP resonances and the resonance of ATP's degradation product, inorganic phosphate (Pi), one can obtain an assessment of bioenergetic state of the liver and hence monitor oxidative phosphorylation. Additionally, the relative abundance of phosphomonoester (PME) and phosphodiesters (PDE) enables assessments of the cell membranes as PMEs are metabolic pre-cursors for lipid bi-layer production and PDEs are degradation products of the cell wall. The PDE peak in the liver has also been shown to contain signal from phosphatidylcholine, a constituent of bile, which holds promise in the monitoring of biliary diseases. Finally using the relative chemical shift difference between the α-ATP and Pi resonances or the α-ATP and β-ATP resonances, intra-cellular pH and free magnesium concentration can be obtained.

Given the important metabolic pathways examined by ^{31}P-MRS and the importance of ATP content on transplant outcomes, it is unsurprising that several studies have used ^{31}P-MRS to examine ex vivo transplant organs to compare the effect of preservation method

on energetic metabolism. Because of the lack of aerobic metabolism, ATP is rapidly degraded during static cold storage. Therefore, very little or no ATP signal has been detected by ^{31}P-MRS in either livers, pancreata, or kidneys during SCS limiting the predictive power of ^{31}P-MRS in cold stored organs. Indeed, Wolf et al. scanned 25 human livers transplant grafts during SCS and concluded that ^{31}P-MRS derived ATP content was not predictive of post-transplant graft function when performed in cold stored organs.[229] However, the authors did suggest that levels of PME and PDE could be useful indicators of graft viability by assessing the potential to rapidly regenerate ATP from adenosine monophosphate (AMP) and the extent of damage to the cell membrane during cold ischaemia respectively.[229] Further studies of ex vivo porcine livers during either SCS or hypothermic machine perfusion, found similar effects but none reported sufficient predictive power to cause the introduction of this measurement into a clinical pipeline.[56]

However, when enhanced preservation methods were used, such as hypothermic machine perfusion in the liver or the two-layer method in pancreata, significant regeneration of ATP could be detected by ^{31}P-MRS. In pre-clinical models this correlated with both the level of damage to that the organ was subjected to and post-transplant outcome.[114,42,233] This work failed to move through to clinical utility however as the experiments were performed in the late 1990's in a period of time when transplantation was still almost exclusively using SCS for organ preservation. As described in Section 2.2.2, improvements in technology and increased demand for transplant organs means that machine perfusion is now increasingly utilised in transplantation. Additionally, the technological improvements have enabled preservation by machine perfusion at normothermic temperatures rather than hypothermic temperatures that were the focus of the previous studies. It is therefore timely to re-assess the utility of ^{31}P-MRS for assessment of transplantability of liver grafts preserved via NMP.

3.2.4.2 Carbon MRS

Given the abundance of carbon-based molecules in metabolic processes, carbon MRS could provide a non-invasive method to monitor metabolic flux in a wide range of pathways from

glycolysis to fatty acid oxidation. However, the only naturally occurring isotope of carbon that is magnetically active (i.e. has a spin quantum number $I > 0$) is ^{13}C, which is only 1.1% abundant naturally. This combined with the very low gyromagnetic ratio of carbon compared to protons or phosphorus, means that ^{13}C MRS is intrinsically a very insensitive technique.

Several methods have been attempted to improve the SNR of the measured spectra, for example increasing the number of averages, N_{averages}, in the experiment as SNR $\propto \sqrt{N_{\text{averages}}}$ or increasing the magnetic field strength, B_0, as SNR $\propto B_0$. The addition of a ^{13}C-labelled tracer has also been utilised to temporarily increased the relative abundance of ^{13}C and hence the signal detected. Combinations of these methods can have enabled rates of glycogenolysis and gluconeogenesis to be measured over a few hours.[112] However, these studies require a large amount of tracer to be administered[200] and the SNR improvements are not sufficient to enable a rapid measurement of metabolic flux.

Hyperpolarization

Hyperpolarization is the umbrella term for an array of techniques that offer a solution to these issues by temporarily increasing the polarisation of a ^{13}C-labelled tracer which can briefly offer a 10,000-fold increase in SNR. As described in Section 3.1, under normal conditions the net polarisation of ^{13}C nuclei in a 3T magnetic field is only around 0.0005%. However, this can be increased using dynamic nuclear polarisation (DNP). DNP exploits the high polarisation of unpaired electron spins at low temperatures (typically <1 K) and 'transfers' the electron polarisation to the nuclei by irradiating the sample with microwaves of frequency equal to the difference between the electron Lamor frequency (ω_e) and the nuclei Lamor frequency (ω_n). This irradiation triggers double and zero quantum transitions between the dipolar coupled nuclear and electron energy states, so called 'flip-flip' and 'flip-flop' transitions, and increases nuclear polarisation.[4] Additional polarisation is gained through the cross effect, where inhomogeneous line-broadening and dipolar coupling of electrons promote electron-electron-nuclear 'flip-flop-flip' transitions, and thermal mixing, which is a two step process. Briefly, the microwave irradiation causes a reduction in effective

magnetic field seen by the electrons and so a cooling of spin temperature. This then triggers a 'flip-flop' transition between two coupled electrons and releases a quantum of energy which excites the nuclear transition.[4] The net effect of these processes is a net polarisation of ∼40% (>×80,000 higher than normal).

However, the polarisation occurs at ∼1 K in a solid, or glass, state and hence the sample needs to be rapidly re-warmed and melted in order to enable injection into tissue. Ardenkjaer-Larsen et al. demonstrated that by performing a fast-dissolution with pressurised super-heated water, the sample could be rapidly and repeatability prepared for injection and that the resulting solution would enable a ×10,000 increase in SNR.[9]

Clinical application of hyperpolarized ^{13}C-MRS

Given its central location to glycolytic metabolism, favourable T_1 relaxation time, and chemical stability, [1-^{13}C]pyruvic acid has been the focus of most clinical hyperpolarized studies to date. It has been used to examine changes in glycolytic metabolism in a range of conditions, showing promise in detection of regions of ischaemic tissue in patients with myocardial infarction as well as the effect of treatment on tumour metabolism in patients with liver cancer.[8,44]

Recently, Mariager et al. showed that glycolytic metabolism could be assessed and regional differences observed in ex vivo pig kidneys that were preserved using NMP. The authors suggest that this could improve the understanding of the metabolism present in a kidney graft prior to transplantation and hence could form a useful assessment of transplantability.[133] No studies have reported application of hyperpolarized methods for viability assessment of ex vivo livers. However, the promising work by Mariager et al. in the kidney suggest that this should be explored.

3.3 Summary

This chapter has provided a brief overview of the theoretical under-pinning and application of MRI and MRS for the assessment of liver disease and assessment of transplant grafts. All

of the following studies aim to build upon this previous understanding and examine new applications of the most promising MR techniques.

4

Investigating the effect of death on liver metabolism and structure in a porcine model

4.1 Background

It is well known that organs donated following circulatory death have worse post-transplant outcomes than those from donors following brain-stem death, whose outcomes are in turn worse than whole-organ living donors in organs where this is ethical to perform (e.g. in kidney transplantation).[176 53 156] The underlying cause of these differences is believed to be variable rates of injury to the tissue caused by differences in the amount of inflammation, a-typical metabolism, and warm ischaemia between the different donor types.[238]

In the UK, donation after circulatory death is primarily employed for candidate donors who do not meet the exact criteria for brain-stem death but have irrecoverable neurological injury, with both the patient's next of kin and medical team in agreement that further treatment is futile. These donors, termed Maastrict category III, have a controlled donation following the withdrawal of life sustaining treatment (WLST).[208 111]

Although organ procurement from Maastrict category III donors is termed 'controlled',

large physiological changes have been observed following the WLST both on a systematic and liver-specific level.[225 184] These periods of increased inflammation, decreased blood flow and lack of adequate oxygenation, all while still at 37°C, are thought to drive the increased ischaemia re-perfusion injury observed in DCD livers. The duration of these unstable periods can vary from 5 minutes to several days.[201] Further, following confirmation of circulatory arrest different countries require a further stand-off period of up to 20 minutes before death can be declared. Therefore, it is important to understand the effect of extended warm ischaemia on the liver when donated following WLST.

In contrast, blood flow continues following brain-stem death. However, the increased ischaemia of the brain-stem, cerebrum, and spinal chord triggers a sympathetic response of catecholamine release. This in turn triggers vasoconstriction with reduced blood flow to the abdominal organs and a systematic inflammatory response which impairs organ function. Recent work using small animal models has demonstrated profound organ specific changes in metabolism of the kidneys and liver during the first 4 hrs following brain-steam death.[214 213] Although difficult to measure accurately in clinical situations, due to the exact start of brain-stem death being unknown, the duration of brain-stem death prior to organ procurement is usually longer with median durations of up to 24 hrs and maximum durations of over 100 hrs.[162] However, increased waiting time seems to not have deleterious impact on outcomes post-transplant and may even have protective effects in some organs.[105 104 162] To put these stochastic clinical observations on a firm footing, it is important to characterise both metabolic and structural changes in the liver over an extended period of time following brain-stem death.

In Chapters 5-7 of this thesis, I examine the effect of different preservation techniques on liver metabolism and physiology using MR. However, to put those measurements in context, we must first understand both what the normal range of each parameter is and also what impact the metabolic and physiological injuries to the liver caused during death of the donor have on these MR parameters. There is a paucity of literature detailing normal ranges for MR parameters in the livers of large animal models and even fever studies have examined the effects of circulatory or brain-stem death on MR parameters. It is especially difficult

to find comparable values given the sensitivity of MR parameters to factors such as field strength, acquisition technique, and scanner manufacturer.[54 93 209] Therefore, this chapter describes my preparatory work to establish normal ranges for the key MR parameters used throughout this thesis in a healthy large animal model and to characterise any deviations from the normal range which occur in the liver during and following death, confirmed by circulatory or brain-stem criteria.

Logistical considerations beyond my control and the COVID-19 pandemic dictated that the in vivo experiments from this chapter and ex vivo experiments from Chapter 6 were performed at different sites. At present, Oxford University is unable to perform in vivo porcine imaging using a clinical MRI scanner. Therefore, I travelled to Aarhus University, Denmark, to perform all of the in vivo porcine imaging studies at a site with the facilities to enable this. In contrast, development of novel ex vivo machine perfusion systems has been a significant area of research in Oxford University for almost 20 years whereas Aarhus University has no pre-existing research programs in this area. Hence all ex vivo work detailed in this thesis was performed at Oxford University. Unfortunately, the different research focuses mean that the two universities have different 3T MRI scanners with different contracts with the manufacturers to enable different pulse sequences to be used. Therefore, I performed a brief multi-site standardisation study as described in this chapter. During this work, the COVID-19 pandemic hit, which forced me to twice leave Denmark earlier than planned and hence limited the scope of the multi-site standardisation study and the numbers of experiments that could be performed.

As detailed above, one of the key changes that occurs following both circulatory arrest and brain-stem death is variation in haemodynamic parameters. This change in blood supply to, and perfusion of, the liver is likely a key factor driving metabolic changes and determining the extent of injury to the liver. To assess these changes non-invasively, I applied intra-voxel incoherent motion (IVIM), which is a diffusion weighted imaging (DWI) technique that has previously been shown to characterise perfusion and diffusion with-in the liver. Given the uncertainty around the optimum diffusion model to apply (see Section 3.2.3), I additionally tested a range of IVIM models and fitting techniques in order to

obtain the optimum measures of perfusion and diffusion within the liver in healthy pigs and following confirmation of death.

4.2 Aims

In this chapter I aim to:

- Standardise an MR protocol between two different 3T MRI scanners(Siemens TIM-Trio and Skyra models).
- Validate analysis pipelines for techniques where there is not yet a consensus of the optimum method.
- Characterise the normal range for magnetic resonance (MR) parameters in healthy Landrace pigs.
- Assess structural and physiological changes occurring in the liver during organ donation following circulatory death and following brain-stem death using porcine models.
- Examine the effect of increasing time after declaration of death on liver metabolism and physiology.

4.3 Methods

4.3.1 Multi-site validation of MR protocol

In order to enable a comparison between in vivo and ex vivo porcine data, which is reported in Chapter 6, I performed a multi-centre validation study was performed between the 3T MRI scanner at Oxford (TIM-Trio, Siemens, Erlangen, Germany) on which all ex vivo perfusion experiments reported in Chapter 6 were performed and the 3T MRI scanner at Aarhus (Skyra, Siemens, Erlangen, Germany) on which all in vivo porcine acquisitions reported in this chapter were performed.

A summary of the acquisition protocols for the two scanners is shown in Table 4.2. For most sequences protocols were exactly matched on the two scanners. However, due to differences in software versions (VB17A for the TIM-trio scanner and VD13C for the Skyra scanner), licenses, and hardware performance of the systems, it was not possible to perfectly match T_1 mapping sequences. Consistency of relaxometry measurements was assessed using a previously validated QA phantom, which was used in a large multi-centre registry study and has been shown to be stable over time and following transportation.[239] The phantom has nine compartments filled with agar, carrageenan, and $NiCl_2$ in varying concentrations in order to obtain a range of T_1 and T_2 relaxation times (Table 4.1).

Table 4.1: Relaxometry phantom chemical composition with the T_1 and T_2 relaxation rates measured at 21.0±0.5°C within one month of manufacture as reported by Zhang et al.[239]

Compartment	Chemical composition			Reported relaxation rates at 21.0°C (ms)	
	Agar (%)	Carrageenan (%)	$NiCl_2$ (mM)	$T_{1\ shMOLLI}$	$T_{2\ SE}$
A	0.5	0.33	0.11	275.8 ±2.1	265.9 ±4.8
B	0.5	0.00	0.63	266.2 ±4.6	259.0 ±2.2
C	0.0	0.00	0.00	2373.4 ±184.3	2383.1 ±153.9
D	1.9	0.00	1.20	72.2 ±0.7	71.4 ±0.4
E	2.0	0.00	0.77	69.6 ±1.2	70.7 ±0.8
F	2.0	0.00	0.52	80.2 ±1.4	78.4 ±2.8
G	1.5	0.10	4.50	72.4 ±0.7	68.5 ±1.1
H	3.0	0.00	0.46	56.9 ±0.4	56.5 ±2.6
I	1.8	0.00	2.00	74.0 ±0.7	72.5 ±1.5

Phantom T_1 measurements were performed on each scanner and the associated data reconstructions performed. The phantoms were left in the same room as the MRI scanner for at least 12 hours prior to acquisition to ensure thermal equilibrium and the surface temperature of the relaxometry phantom was recorded using an MR-safe thermometer strip (14-40 Dual Scale LCD, 1 °C resolution, Good Life Innovations Ltd, East Sussex, UK).

Given the significant differences in dependence on T_2 between the T_1 mapping techniques used at the two sites and the large variation in T_2 of the phantom samples (50 - 300 ms), a T_2-corrected shMOLLI T_1 measurement was calculated for phantom measurements using the empirically determined equations derived from 1004 measurements

of 50 QA phantoms by Zhang et al.:[239]

$$T_{1,\mathrm{T_2corrected}} = T_1\left(-5.50\times(T_2)^{-0.94}+1.005+Residual_{\mathrm{T_1}}\right), \tag{4.1}$$

where $T_{1,\mathrm{T_2corrected}}$ is the T_2- corrected shMOLLI T_1, T_1 is the raw shMOLLI T_1 value, and $Residual_{\mathrm{T_1}}$ is:

$$Residual_{\mathrm{T_1}} = -8.21\times10^{-12}\times T_1^3+4.44\times10^{-8}\times T_1^2-6.78\times10^{-5}\times T_1+2.75\times10^{-2}. \tag{4.2}$$

All porcine livers in this work are scanned in or retrieved from healthy, lean pigs. Therefore, the variation in T_2 and fat fraction should be minimal. Therefore, no T_2 correction was applied to the phantom vials within twice the normal range of liver T_2 values to examine if the two T_1 mapping techniques could be directly comparable over the small range of T_2 expected in this study. To assess the applicability of this assumption in vivo, four shMOLLI T_1 measurements were performed on a healthy, lean human participant (male, 23 years old, BMI = 17.2 kg/m^2) in repeated scans over 3 weeks on the 3T TIM-Trio scanner before four variable flip angle (VFA) T_1 measurements were performed on the Skyra scanner. Normal physiological variation was assessed through the repeated scans. Results from the VFA and shMOLLI T_1 measurements were compared.

4.3.2 Porcine Study Protocol

Figure 4.1 shows an outline of the study protocol. Briefly, eight non-fasted female Landrace pigs (41 kg, range = 38 - 46 kg) were included in this study with four assigned to each arm (DCD or DBD). Baseline scans (^{31}P MRS and ^{1}H MRI) were acquired to both act as a paired control for later measurements and establish normal ranges of the MR parameters.

The study has two arms, with 4 pigs in each. In the DCD arm, life sustaining treatment was withdrawn to induce circulatory arrest. In the DBD arm, fluid was infused into a balloon in the cranial epidural space to increase intra-cranial pressure until brain-stem death was confirmed. In both arms, repeated measures of ^{31}P MRS and ^{1}H MRI measurements were made with needle biopsies and blood samples taken at regular intervals. The DCD group were followed up for 2.5 hrs as to-date 90-minutes is the longest period of warm ischaemia

Table 4.2: Summary of the MR sequence parameters used on each MRI scanner.

Contrast	**shMOLLI T_1**	**VFA T_1**	**B_1^+**	**T_2^*/PDFF**	**DWI†**	**T_2MRS**	**T_2MRI**
MRI Scanner	TIM-Trio	Skyra	Skyra	Both	Both	Skyra	Skyra
Sequence	shMOLLI WIP	VIBE	'tfl_b1map'	multi-echo GRE	SE-EPI	Single voxel STEAM	multi-echo SE
TR (ms)	2.52	7.15	10,000	15	3300	150 - 2000‡	6000
TE (ms)	1.05	3.66	1.41	1.1 to 12.1	65	15 - 110‡	12 to 200
Δ TE (ms)	-	-	-	1.0	-	Variable	12
Flip angle (°)	35	3, 19	80 (pre-SAT) 8 (readout)	3	90	90	180
Field of view (mm^2)	288 × 384	300 × 244	450 × 450	440 × 398	380 × 285	-	300 × 262.5
Resolution (mm^3)	1.0 × 1.0 × 8.0	0.9 × 0.9 × 4.0	7.0 × 7.0 × 16.0	1.7 × 1.7 × 8.0	1.4 × 1.4 × 8.0	2.0 × 2.0 × 2.0	1.2 × 1.2 × 8.0
Bandwidth (Hz/px)	898	445	1565	1560	2040	4000	890
Parrallel imaging	GRAPPA, R = 2	GRAPPA, R = 2	-	-	GRAPPA, R = 2	-	GRAPPA, R = 2
Number of Slices	1	30	10	10	19	-	1
Additional parameters	6/8 partial Fourier simulated heart rate = 75 bpm				b = 0, 10, 20, 40, 60, 80, 100, 200, 400, 800 mm^2/s, 3 diffusion directions, 6 NEX, Respiratory gated*, Perpendicular diffusion directions on TIM Trio; 3-scan TRACE use on Skyra.		6/8 partial Fourier Respiratory gated*

†Only acquired in vivo

‡TR and TE combinations used for multi-TR multi-TE MRS were: 150, 175, 200, 225, 250, 275, 300, 325, 350, 400, 450, 500, 600, 700, 800, 900, 1000, 1250, 1500, 2000 ms with a fixed TE of 15 ms; before eight additional spectra with TR = 1000 ms and TE = 20, 25, 30, 35, 50, 70, 90, 110 ms.

*Respiratory gating only used during in vivo acquisitions and for sequences with acquisition times longer than it is safe to pause ventilation in an anaesthetised porcine subject.

Abbreviations: DWI, diffusion weighted imaging; EPI, echo-planar imaging; GRAPPA, generalized auto-calibrating partial parallel acquisition; GRE, gradient re-called echo; mc-SE, multi-contrast spin echo; NEX, number of excitations; PDFF, proton density fat fraction; SE, spin echo;VFA, variable flip angle;VIBE, volume interpolated breath-hold examination.

that has been shown to be a survivable injury following transplantation using all preservation techniques in porcine models and hence by 2.5 hrs the liver will be definitely non-viable for transplantation.[77]

For the DBD arm, MR parameters were recorded and biopsy and blood samples obtained for 12 hrs following confirmation of brain-stem death.

All experiments were approved by the Danish Animal Experiments Inspectorate under the Danish Veterinary and Food Administration.

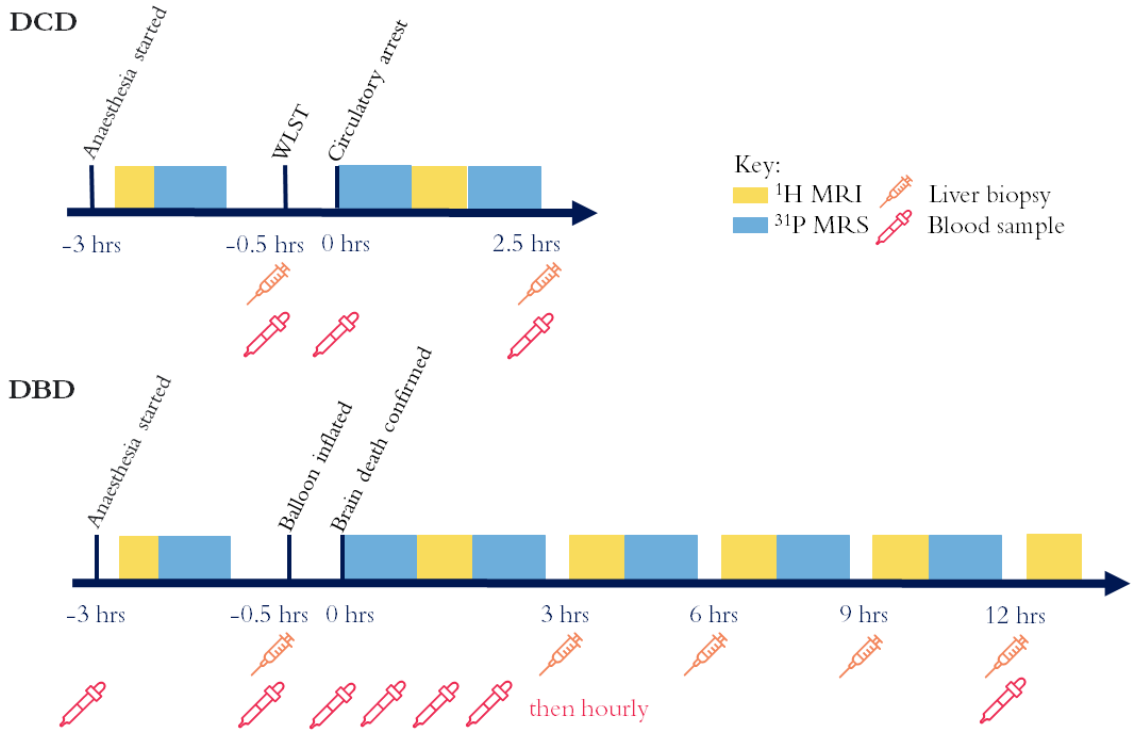


Figure 4.1: Overview of the study protocol.

4.3.3 Donor animal preparation

Immediately upon arrival to the surgical facilities the animals were sedated with midazolam (0.5 mg/kg) and azaperone (0.5 mg/kg) to enable establishment of intravenous access. Propofol (3 mg/kg) was administered intravenously to allow endotracheal intubation and connection to a ventilator. 10,000 units of unfractionated heparin was administered to prevent clotting. Continuous anaesthesia and analgesia was maintained with propofol (3.5 mg/kg/h) and fentanyl (2.5 μ/kg/h) infusions. Mechanical ventilation was performed with

a mixture of atmospheric air and medical oxygen. A tidal volume was set at 8-10 mL/kg and the respiratory rate adjusted to maintain a partial pressure of carbon dioxide in arterial blood ($PaCO_2$) between 5.5 and 6.5 kPa and a partial pressure of oxygen in arterial blood (PaO_2) >12.0 kPa. Positive end-expiratory pressure was set to 5 cm H_2O and the fraction of inspired oxygen (FiO_2) was set between 0.25-0.4. Ventilation of animals was adjusted if the pH moved out of the acceptable range (7.37 - 7.45). Body temperature was measured with a rectal temperature probe and was maintained above 36 °C.

4.3.3.1 Exclusion Criteria

Exclusion criteria defined before the study were as follows:

- The animal shows signs of being clinically ill (e.g. diarrhoea).
- Mean arterial pressure (MAP) was < 60 mmHg for any 15 minute period (excluding any time following circulatory death).
- Blood lactate concentration became ≥9 mmol/L.
- Intracranial pressure failed to exceed MAP (brain death model only).
- SaO_2 < 90% with FiO_2 = 0.30 during the period following the induction of brain death (brain death model only).

4.3.4 Donation after circulatory death model

Prior to induction of circulatory death the fraction of inspired oxygen was reduced to 25% and 20 mL boluses of propofol and fentanyl were administered. Mechanical ventilation was then withdrawn and the intubation tube clamped. The arterial pressure tracing was monitored and circulatory arrest declared when no pulsatility was evident. Heart rate and blood pressure were recorded every 30 seconds until circulatory arrest was declared. In two pigs, 1 mL blood samples were collected every minute from the cessation of mechanical ventilation until the declaration of circulatory arrest. A stand-off period of 10 minutes was then observed.

Animals were then moved back to the MRI scanner for post-mortem examination.

4.3.5 Donation after brain-stem death model

4.3.5.1 Induction of brain death

During induction of brain death, the level of anaesthesia and analgesia was increased to 31 mL/h for propofol and 12 mL/h of fentanyl. Two holes were drilled in the cranium and a 20 Fr Foley catheter was inserted into the anterior hole with the balloon of the catheter placed in the epidural space. Intracranial pressure (ICP) was measured through a steel introducer needle from a 22 G Venflon (Becton Dickinson, NJ, USA) inserted subdurally into the posterior hole.

The balloon was slowly inflated at a rate of 30 mL/hr with saline solution. Once the cerebral perfusion pressure became negative (i.e. MAP < ICP) and remained negative, brain-stem death was declared as blood flow to the brain had ceased.[226] The saline infusion then continued for an additional 15 minutes. The balloon remained inflated for the remainder of the experiment.

4.3.5.2 Donor management following confirmation of brain death

Following confirmation of brain death, an organ management protocol was implemented to maintain the donors in a stable state. The protocol was based on standard clinical practice and is detailed below.[82 159]

Cardiovascular management

The MAP was maintained >70 mmHg by fluid administration in the first instance. A maximum of two 250 mL fluid boluses were administered if MAP fell below the threshold to examine the physiological response. If the MAP showed response, defined as an increase of at least 5 mmHg following fluid administration, further fluid up to a maximum of 2 L was administered to stabilise MAP. If the MAP continued to fall <60 mmHg, noradrenaline was titrated (0 - 0.5 μg/kg/min to prevent functional warm ischaemia. After the first 30 minutes following confirmation of brain death, hypertension (MAP > 110 mmHg) was treated with

2-5 mL boluses of labetalol (5 mg/mL). Bradycardia, defined as a heart rate < 30 beats/min, was treated with intravenous administration of 1 mg atropine. Sinus Tachycardia (heart rate > 120 beats/min with a variable rate and normal p waves on ECG) was initially treated with a 1 - 5 mg bolus of metoprolol, followed by a continuous infusion of 83-166 μg/kg/hr if necessary. Meanwhile, Supraventricular tachycardia, which was defined as a regular heart rate > 120 beats/min with abnormal p waves, was corrected with a 1 - 2 L fluid bolus in the first instance and then metoprolol as per the treatment of sinus tachycardia from then on.

Fluid management

Fluid homeostasis was maintained by continuous infusion of 200 - 500 mL/hr saline. This was titrated to ensure a central venous pressure of between 6 and 10 mmHg and a haematocrit >30%. If the donor developed diabetes insipidus (urinary output > 12 mL/kg/hr and a serum sodium concentration > 150 mmol/L) 1 - 2 μg of desmopressin was administered.

Biochemical management

Parenteral nutrition (SmofKabiven, Fresenius Kabi AB, Sweden) was infused at 20 mL/hr following confirmation of brain death. Regular arterial blood gas samples were collected and analysed. Serum potassium concentration was maintained between 3.0 and 6.0 mmol/L through administration of insulin, glucose, and potassium. 5 - 10 mmol of calcium chloride was administered to treat hypocalcemia (serum calcium < 1.1 mmol/L). Additional glucose boluses were administered to maintain blood glucose levels between 5 and 15 mmol/L.

Mobilisation

To prevent the collection of fluid within the pig, the pig was rotated 90° along the long axis every three hours.

4.3.6 MR Protocol

4.3.6.1 MRI Acquisition

All in vivo porcine experiments were performed on a 3T MRI system (Skyra, Siemens, Erlangen, Germany). ^{1}H imaging and spectroscopy was performed using a posterior spine array and flexible 18-channel anterior array. The protocol consisted of: $B_1{}^+$ mapping performed using a vendor supplied pre-saturation turboFLASH sequence; T_2 mapping using a multiple echo spin echo sequence, T_1 mapping using a variable flip angle protocol; $T_2{}^\star$ and PDFF mapping with a multi-echo GRE sequence, and diffusion weighted imaging using a spin-echo echo planar imaging sequence. Full details of the acquisition parameters used are shown in Table 4.2. The two flip angles used (3 and 19 ms) in the VFA acquisition were chosen automatically by the vendor supplied reconstruction software (MapIT, Siemens Healthcare, Erlangen, Germany) to optimise the acquisition for an expected T_1 value of 700 ms (i.e. an approximate T_1 value of health liver in vivo).

4.3.6.2 Image analysis of in vivo data

Unless otherwise stated, all analysis of imaging biomarkers was performed using 3 regions of interest (ROI) placed in the liver parenchyma away from any obvious vasculature.

Relaxometry

T_1 and T_2 maps were generated on the scanner using the vendor supplied processing pipeline (MapIT, Siemens Healthcare, Erlangen, Germany). The T_1 pipeline is based on a driven equilibrium single pulse observation of T_1(DESPOT)[219 63] with $B_1{}^+$ correction to account for flip angle inhomogeneity across each slice. While the T_2 analysis used a pixel-wise, mono-exponential non-negative least-squares (NNLS) method. $T_2{}^\star$ and fat fraction were quantified using a complex, multi-peak mono-exponential model in the MRQuantif toolbox.[55] Liver iron content ($LIC_{T_2^*}$) in mg/g was then calculated using the empirically derived equation and unit conversion factor:[55 89]

$$LIC_{T_2^*} = \left(\frac{0.314s}{T_2^*} - 0.96\right) \div 18. \tag{4.3}$$

Table 4.3: Summary of initial values and constraints placed on IVIM fitting models based on the parameters described by Riexinger *et al.*[187]

Bi-exponential model			
Parameter	**f**	**D ($\times 10^{-3}$ s/mm^2)**	**D* ($\times 10^{-3}$ s/mm^2)**
Initial value	10	1	80
Lower bound	0	0.01	10
Upper bound	100	Inf	Inf

Tri-exponential model					
Parameter	**f_1 (%)**	**f_2 (%)**	**D ($\times 10^{-3}$ s/mm^2)**	**D$^*_1$ ($\times 10^{-3}$ s/mm^2)**	**D$^*_2$ ($\times 10^{-3}$ s/mm^2)**
Initial value	10	10	1	80	1000
Lower bound	0	0	0.01	10	10
Upper bound	100	100	Inf	Inf	Inf

Diffusion and perfusion quantification

First, using the $b = 0$ s/mm^2, a series of three 15 mm^2 regions of interest were drawn on the the three central slices of the liver parenchyma with care taken to avoid any obvious vasculature. The mean signal intensity from all ROIs was then calculated for each b-value. All signal intensities were then normalised to the signal intensity at $b = 0$ s/mm^2. The variation in normalised signal intensity with increasing b-value was fitted to either the bi-exponenital model (Equation 3.20) or the tri-exponential model (Equation 3.22 using a non-linear least squares algorithm (lsqcurvefit) in MATLAB (MathWorks, Natwick, MA). Table 4.3 shows the initial values and constraints placed upon the fitting, which are based on the constraints reported by Riexinger et al..[187]

The 'multistart' option in MATLAB was used to generate 1000 random starting points within the specified limits to reduce the chance of finding a local minimum. The fit result with the minimal residual was taken.

For segmented fitting, first data from b > 200 s/mm^2 were fitted to Equation 3.21. Then the rest of the parameters for the bi-exponential or tri-exponential model were fitted in a second stage.

4.3.6.3 MRS acquisition and analysis

A ^{31}P-MRS examination was performed using a ^{31}P 10 cm loop coil (PulseTeq, Surrey, UK) for the circulatory death group and a dual-tuned ^{1}H/^{31}P 12 cm flex coil (Rapid

Biomedical, Rimpar, Germany) for the brain-stem death group. A change in coils between the two groups was necessary because the 10 cm loop coil was damaged beyond repair by during an enforced pause in experiments caused by COVID-19 lockdowns following the completion of the circulatory death experiments. However, the two coils used have previously been shown to have comparable excitation profiles and give equivalent results.[69] Localised free induction decays were acquired using a slab-selective one dimensional version of the image-selective in vivo spectroscopy (ISIS) sequence. Localisation used a gradient offset independent (GOIA) adiabatic inversion, with wideband uniform rate and smooth truncation (WURST) RF modulation. A WURST-16 pulse was used for the RF field and WURST-4 for the gradient modulations, termed "GOIA-WURST(16,4)". The sensitivity profile of the coil provided localisation within the slice. Excitation pulse power was scaled to generate a 90°flip angle 4-9 cm from the coil. In vivo scans were performed with free breathing due to the difficulties performing repeated breath-holds in animal models. MRS scans were performed without respiratory gating. Spectra were acquired with: TR/TE = 3000/0.7 ms, bandwidth = 5 kHz, averages = 300, and 2048 complex points.

Pre-processing of spectra was performed in using the FID-A toolbox,[193] with individual spectra aligned using time-domain spectral registration[154] prior to averaging and then undergoing a two-fold zero-filling to reduce the appearance of noise in the spectrum. Spectral quantification was performed using the OXSA toolbox[175] implementation of the AMARES algorithm[216] in MATLAB (Mathworks, Natwick, USA). Changes in energy metabolism were investigated through the ratio of signal intensity from ATP and Pi peaks as well as the proportion of the normalised α, β, and γ peaks present at each time point.

The frequency profile of the RF pulses was characterised using a 33 mM di-potassium hydrogen phosphate K_2HPO_4 phantom which was placed within a head loader (GE Healthcare, Chicago, USA). Spectra were acquired with 12 averages and the excitation frequency was adjusted in steps of 2.5 ppm between -20 and 20 ppm relative to on-resonance excitation. A smoothing spline was fit to the peak integrals to generate a correction function.

4.3.7 Planned biochemical and histological analysis

During all experiments, two arterial blood gas samples were collected at baseline and at regular intervals following circulatory death (2 h post-mortem) or brain-stem death (15 min, 30 min, 1 h and then hourly). At each time point, one sample was immediately tested using a clinical blood gas analyser (ALB90 Flex, Radiometer, Crawley, UK) for: PaO_2, $PaCO_2$, pH, haematocrit, and concentrations of sodium, potassium, calcium, lactate and glucose. A second sample was centrifuged at 3000 rpm for 15 min at 4 °C. Supernatant was pipetted into 500 μL aliquots and stored at -80 °C.

Liver biopsies were performed at baseline and 2 h following circulatory arrest or at baseline and every 3 h following confirmation of brain-stem death. A small incision ($\sim$5 cm) into the abdomen enabled visualisation of the liver for the needle biopsies and any resultant bleeding to be stopped prior to closing of the incision and resumption of scanning. Biopsy samples were fixed in formalin and stored at 4 °C prior to paraffin-embedding and subsequent analysis.

The COVID-19 pandemic delayed processing of the frozen blood and fixed tissue samples. Nevertheless, the frozen blood samples will be thawed, vortexed, and analysed on a clinical biochemistry analyser via spectrophotometry (Abbott Architect c8000, Abbott diagnostics, IL, USA) to assess the concentrations of: alanine aminotransferase (ALT), aspartate aminotransferase (AST), gamma glutamyl transferase (GGT), total bilirubin, alkaline phosphatase (ALP), lactate dehydrogenase (LDH), and urea. The haemolysis index will also be calculated. Meanwhile, the fixed tissue samples will be sectioned at 4 μm thickness and stained with haematoxylin and eosin (H& E) to identify changes in basic tissue structures. Periodic acid-Schiff (PAS) staining will be performed to asses changes in tissue glycogen concentration and picrosirius red red staining will be performed to monitor changes in fibrosis.

4.3.8 Statistical analysis

Unless otherwise stated, all data are presented as a inter-pig mean ±standard deviation and all fitting parameters are presented as the mean followed by 95% confidence intervals. Inter-subject variation was assessed using the coefficient of variation ($CoV = \left(\frac{\text{standard deviation}}{\text{mean}}\right) \times 100\%$).

Performance of diffusion models was assessed through calculation of adjusted $R^2$and the second-order Akaike's Information Criterion (AICc)[144]:

$$AdjustedR^2 = 1 - \frac{RSS}{TSS} \times \frac{n-1}{n-k-1} \tag{4.4}$$

$$AICc = n \times ln\left(\frac{RSS}{n}\right) + \frac{2K\left(K+1\right)}{N-K-1} \tag{4.5}$$

where RSS is the sum of squares of the residuals, TSS is the total sum of squares, n is the number of *b*-values, k is the number of parameters in the model, and $K = k + 1$. A decrease in AICc of >2 was considered to represent a significantly improved model.[31] To aid interpretation of the AICc values, the evidence ratio was calculated according to:

$$P(\text{model 1 better than model 2}) = \frac{\exp\left(-0.5\Delta AICc\right)}{1 + \exp\left(-0.5\Delta AICc\right)} \tag{4.6}$$

[144] where $\Delta AICc = AICc_{\text{model 2}} - AICc_{\text{model 1}}$.

The effect of cardiac death on each parameter was assessed using a paired Student's t-test. A correction for multiple comparisons was performed using Holm's method. All statistical hypothesis testing was performed at significance level $\alpha = 0.05$.

4.4 Results

4.4.1 Validation and optimisation of MR methods

4.4.1.1 Validation of T_1 measurements

A strong linear correlation was observed between VFA and shMOLLI T_1measurements (ρ= 0.995, R^2= 0.988, $P < .001$, Figure 4.3). Applying a T_2 correction to the shMOLLI

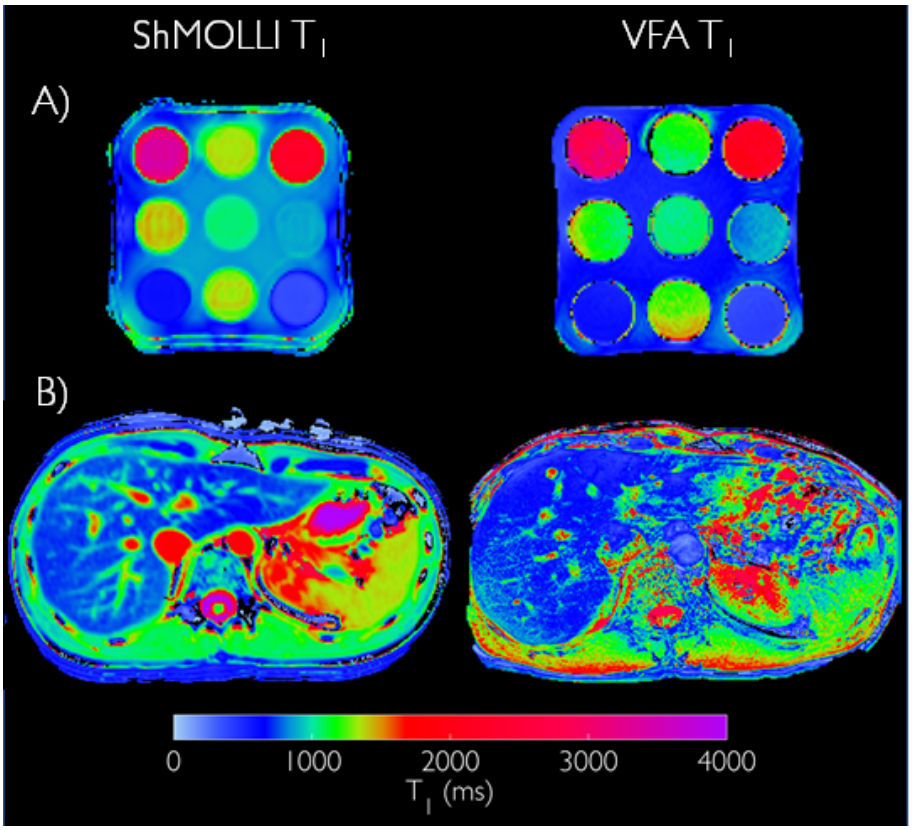


Figure 4.2: Example shMOLLI and VFA T_1 maps of a phantom (A) and the liver a healthy human volunteer (B).

T_1 values reduced the sum of the residuals from a unity plot from 6.5 $\times 10^4$ ms^2 to 1.7 $\times 10^4$ ms^2. As shown in Figure 4.3, no significant bias or offset was observed between VFA and shMOLLI T_1 measurements (slope = 1.03 [0.92 - 1.15] and intercept = -31 [-171 - 109] ms, AIC_C (linear fit) = 65.6 vs AIC_C (equivalence) = 65.5). No significant differences were observed between the repeated in vivo human measurements between VFA or raw shMOLLI T_1 values (768 $\pm$41 ms and 786 $\pm$34 ms for VFA and shMOLLI T_1 respectively, P = 0.50).

4.4.1.2 Optimisation of IVIM model

Figure 4.4 shows fits of the averaged normalised signal decay from all baseline in vivo porcine measurements. Remaining structure in the residuals from the bi-exponential model fitting results is presented which appears to be removed by extension to the tri-exponential model. Table 4.4 presents a statistical comparison of the bi-exponential and tri-exponential models.

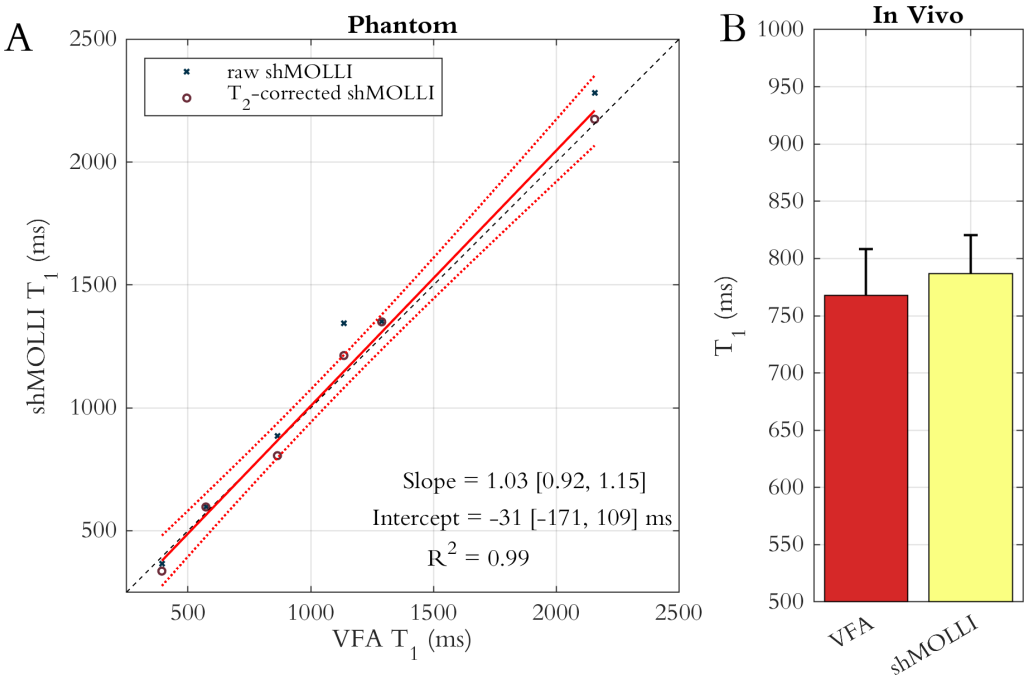


Figure 4.3: Comparison of shMOLLI and VFA T_1 measurements in a phantom (A) and in repeated measures of one in vivo human participant (B). A linear fit of the shMOLLI and VFA T_1 phantom measurements is presented. The in vivo human measurements are shown as the mean and standard deviation of 4 repeated measurements on different days. Each individual in vivo measurement was calculated as the mean of 3 ROIs placed in the parenchyma of the right lobe of the liver with care taken to avoid any obvious vasculature.

The tri-exponential model provided improved R^2 and second-order Akaike's Information Criterion (AICc) in comparison to the bi-exponential model. The tri-exponential model was 50,000 times more likely to be a better fit according to the evidence ratio (2.20/0.04 = 50,000). A slight preference for the full fitting algorithm was observed for the bi-exponential model (mean evidence ratio of segmented vs full fitting = 0.04). No significant differences were observed in the fitting statistics of the tri-exponential model between the full and segmented fitting algorithms. For the bi-exponential model all parameters had comparable coefficients of variation regardless of fitting method. The fitted $D^\star$ was higher in the full fitting ($120.0 \pm 16.6 \times 10^{-3}$ mm^2/s compared to $97.8 \pm 15.4 \times 10^{-3}$ mm^2/s, $P = 0.02$) but all other parameters were independent of fitting method ($P > 0.24$). However, for the tri-exponential model improved the stability of the fitting, demonstrated through a reduced coefficient of variation in the calculated diffusion coefficients (Table 4.5). Fits of the fast diffusion coefficient ($D^\star_2$) were very unstable in the full fitting model with a coefficient

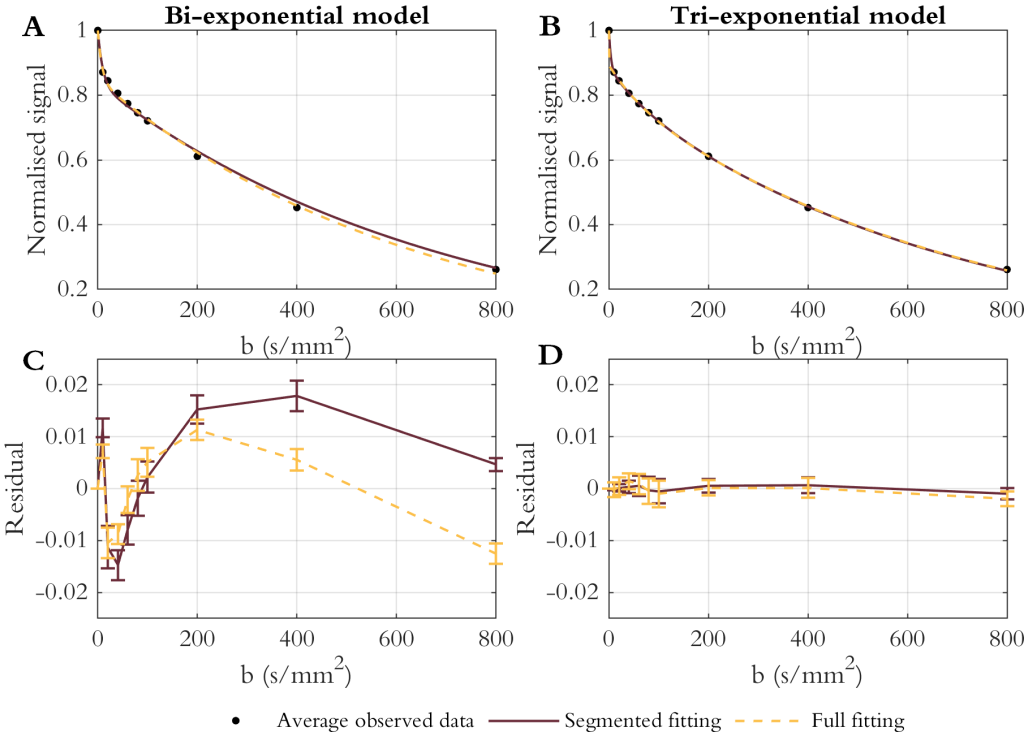


Figure 4.4: Example fits of diffusion weighted imaging data from eight in vivo porcine livers. (A) and (B) are fits of the average data from all livers while (C) and (D) show the mean and standard deviation of the residuals from a fit of each individual liver.

of variation of 63% across the eight pigs and a significantly higher estimated value (2289.7 $\pm$1444.0 $\times 10^{-3}$ mm^2/s compared to 268.8 $\pm$44.4 $\times 10^{-3}$ mm^2/s, $P = 0.001$). Given the improved fit of the tri-exponential model and improved stability of the segmented fitting method, all further IVIM fitting was performed using a segmented fit of the tri-exponential model.

4.4.1.3 Off-resonance correction of ^{31}P MRS

Figure 4.5 shows the excitation profile of the pulses in the 1-D ISIS sequence. The pulse excites between -7.5 and 7.5 ppm efficiently (> 75 % of the value with no frequency offset). However, there is a minimum in the excitation profile near to the expected resonance frequency of β-ATP. Performing a frequency-offset correction by normalising based upon a fitted spline of the excitation profile reduced the coefficient of variation in the measurements in a phantom from 62.7% to just 8.4% within the frequency range of $\pm$20 ppm. Therefore, frequency offset correction was applied to all in vivo porcine measurements.

Table 4.4: A summary of the fitting statistics obtained from bi- and tri-exponential IVIM models to diffusion weighted imaging data of eight in vivo porcine livers. Parameters are represented as mean followed by 95% confidence limits in brackets. Abbreviations: *second-order Akaike's Information Criterion, AICc.*

Model	Adjusted R^2	AICc	Evidence Ratio	
			Segmented Vs Full fitting	Bi- vs Tri-exponential fitting
Bi-exponential				
Segmented	0.994 [0.991 0.996]	-58.7 [-64.0 -55.8]	0.04 [0.03 0.08]	0.03×10^{-5} [0.00 0.19×10^{-5}]
Full fitting	0.997 [0.995 0.998]	-65.1 [-70.7 -61.9]	1.00	0.19×10^{-4} [0.00 0.96×10^{-4}]
Tri-exponential				
Segmented	1.000 [0.999 1.000]	-91.0 [-102 86.7]	2.20 [0.08 8.91]	—
Full fitting	1.000 [0.999 1.000]	-91.0 [-107 -82.3]	1.00	—

Table 4.5: Summary of the effect of fitting model and technique on IVIM parameters. All data are presented as mean ±standard deviation of the fitting results from scans in eight anaesthetised pig livers. The coefficient of variation of each parameter is presented in brackets. Any significant differences between the segmented and full fitting techniques are highlighted with $*$ for $P \leq .05$ and $***$ for $P \leq .001$.

Model	**Fitting method**	**f (%)**	**f_1 (%)**	**f_1 (%)**
Bi-exponential	Segmented	16.6 ±3.7 (22.1)	-	-
	Full	15.4 ±3.6 (23.4)	-	-
Tri-exponential	Segmented	-	7.8 ±1.0 (13.4)	11.6 ±3.1 (26.4)
	Full	-	8.8 ±1.1 (12.7)	11.1 ±2.8 (24.7)

Model	**Fitting method**	**D ($\times 10^{-3}$ mm^2/s)**	**D* ($\times 10^{-3}$ mm^2/s)**		**D$^*_1$ ($\times 10^{-3}$ mm^2/s)**	**D$^*_2$ ($\times 10^{-3}$ mm^2/s)**	
Bi-exponential	Segmented	1.44 ±0.12 (8.7)	97.8 ±15.4 (15.7)	$*$	-	-	
	Full	1.54 ±0.14 (9.1)	120.0 ±16.6 (13.8)		-	-	
Tri-exponential	Segmented	1.44 ±0.12 (8.7)	-		13.6 ±2.1 (15.4)	268.8 ±44.4 (16.5)	$***$
	Full	1.42 ±0.14 (9.9)	-		13.7 ±4.1 (29.7)	2289.7 ±1444.0 (63.1)	

4.4.2 Normal Ranges of MR parameters

Table 4.6 presents the ranges of relaxometry and diffusion MR biomarkers measured in the liver of eight nominally healthy anaesthetised pigs. Example T_1, B_1, and T_2 parametric maps acquired in the healthy anaesthetised pigs are shown in Figure 4.6. IVIM parametric maps were not generated as the fitting required a higher SNR than was available in a single pixel and hence averaging of all pixels within an ROI was required. Intra-subject variability of all of the MR biomarkers was small with coefficients of variation <20% for all biomarkers apart from $T_2^\star$, fat fraction, and f_2. $T_2^\star$ and fat fraction are both very small in lean, healthy porcine

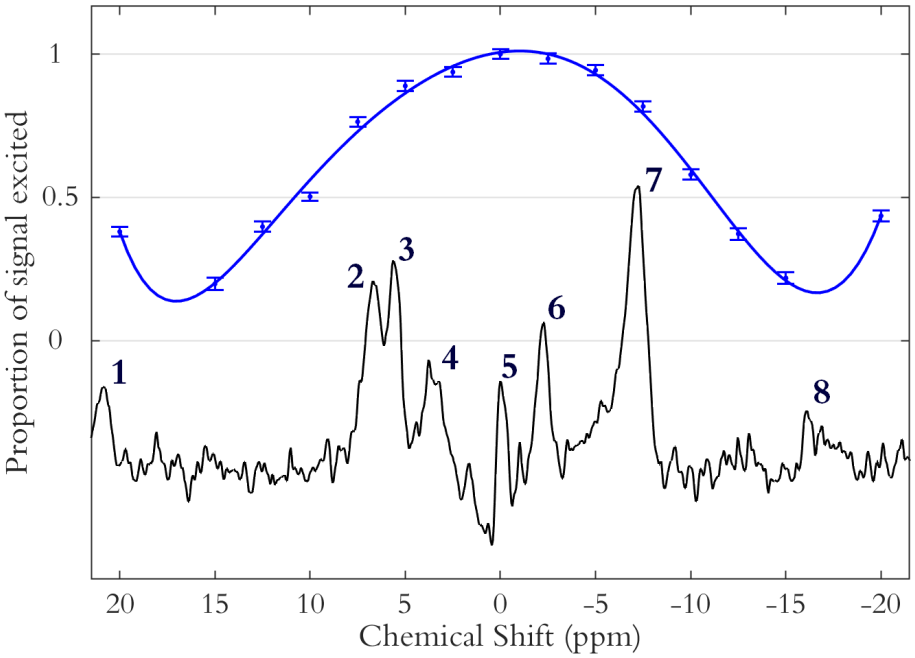


Figure 4.5: RF pulse excitation profile as a function of frequency offset measured using a 33 mM inorganic phosphate phantom (blue bars). The blue line shows a fitted spline that was used to perform a frequency correction. An example in vivo porcine liver ^{31}P spectrum (black line) centered on phosphocreatine (PCr) is presented below with peaks assigned as: 1 - PPA fiducial; 2 - phosphodiesters; 3 - inorganic phosphate; 4 - phosphomonesters; 5 - PCr; and 6, 7, and 8 - γ, α, and β-ATP respectively.

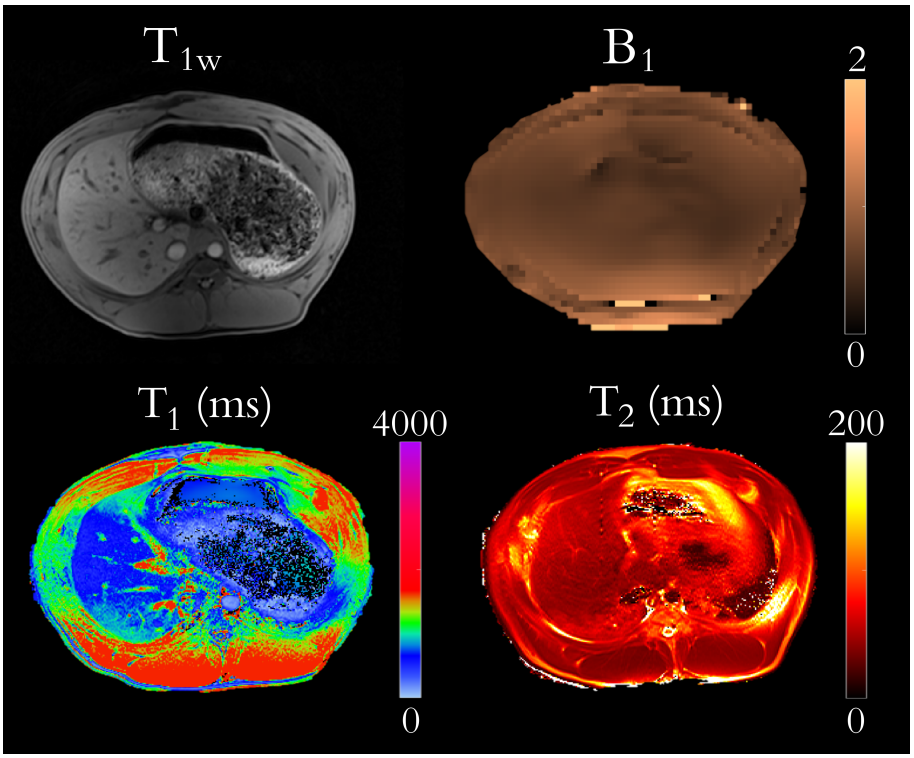


Figure 4.6: Example B_1, T_1, and T_2 parametric maps of healthy in vivo porcine livers. A T_{1w} image is also shown to aid anatomical referencing.

Table 4.6: Normal ranges of biochemical and MR biomarkers in an anaesthetised porcine model.

Measurement technique	Variable	Mean ±standard deviation	Coefficient of variation (%)	Reference range
Arterial blood gas				
	Lactate (mmol/L)	1.19 ±0.57	47.9	0.37 – 3.13
	Glucose (mmol/L)	6.29 ±1.22	19.4	3.82 – 9.97
	pH	7.49 ±0.05	0.67	7.37 – 7.61
	PaO_2 (kPa)	24.7 ±10.3	41.7	9.43 – 56.6
	$PaCO_2$ (kPa)	5.5 ±0.6	10.9	4.1 – 7.0
	Haematocrit (%)	30.8 ±1.5	4.9	27.1 – 34.6
Intravoxel incoherent motion				
	f_1 (%)	7.75 ±1.04	13.4	5.15 – 10.35
	f_2 (%)	11.56 ±3.05	26.4	5.79 – 21.74
	D ($\times 10^{-3}$ mm^2/s)	1.44 ±0.13	9.0	1.12 – 1.75
	D^*_1 ($\times 10^{-3}$ mm^2/s)	13.64 ±2.10	15.4	8.38 – 18.91
	D^*_2 ($\times 10^{-3}$ mm^2/s)	268.75 ±44.38	16.5	157.44 – 380.07
Variable flip angle				
	T_1 (ms)	794 ±58	7.3	649 – 940
Multi-echo spin echo				
	T_2 (ms)	45.0 ±4.0	8.9	34.8 – 55.1
Multi-echo gradient echo				
	T_2^* (ms)	22.4 ±5.0	22.3	12.8 - 37.4
	Fat fraction (%)	1.03 ±0.27	26.2	0.52 - 1.92
	LIC (mg/g)	1.2 ±0.2	16.7	0.9 - 1.6

Abbreviations: *perfusion fraction of fast compartment, f_2; perfusion fraction of intermediate compartment, f_1; liver iron content, LIC; partial pressure of carbon dioxide in arterial blood, $PaCO_2$; partial pressure of oxygen in arterial blood, PaO_2; passive diffusion coefficent, D; pseudo-diffusion coefficient of fast compartment, D^*_2; pseudo-diffusion coefficient of intermediate compartment, D^*_1.*

liver meaning even the small variation that is seen causes a large coefficient of variation, while uncertainty in the fit of the fast perfusion fraction likely accounts for the variation observed in f_2.

4.4.3 Structural and metabolic changes in the liver during donation after circulatory death

Figure 4.7 shows the strong systematic physiological response observed immediately following the withdrawal of lift-sustaining treatment. The five physiological phases, previously described by White et al.[225], were seen as described below:

1. Pulmonary vasoconstriction (0 - 1.5 min). A decline in systematic oxygen delivery characterised by falling PaO_2 and MAP.

2. Hyperdynamic phase (1.5 - 4.5 min). This phase was characterised by continued decline in PaO_2 levels combined with a significant increase in MAP (62.5 ±4.6

Table 4.7: Changes in tissue perfusion and relaxometry biomarkers following 60 minutes of warm ischaemia.

	Baseline	**60-min warm ischaemia**	**Percentage change (%)**	***P*-value**
f_1 (%)	7.4 ±1.0	5.5 ±0.1	-26	0.04
f_2 (%)	9.9 ±2.1	1.1 ±0.2	-89	0.003
D	1.37 ±0.08	1.06 ±0.08	-23	0.01
$D^{\star}_1$ ($\times 10^{-3}$ mm^2/s)	13.3 ±2.3	8.5 ±0.3	-36	0.02
$D^{\star}_2$ ($\times 10^{-3}$ mm^2/s)	260.2 ±60.6	1432 ±2059	+450.3	0.35
$T_{1\,VFA}$ (ms)	820 ±29	1028 ±260	+25.4	<0.001
$T_{2\,MRI}$ (ms)	42.2 ±2.3	36.1 ±3.3	-14.5	0.02
$T_2^{\star}$ (ms)	20.6 ±4.0	8.15 ±1.2	-60.4	0.02
FF (%)	1.1 ±0.3	3.8 ±0.4	+236.6	0.004
LIC (mg/g)	1.3 ±0.2	2.6 ±0.3	+106.4	0.01

mmHg to 153.9 ±60.6 mmHg,P = 0.02) and an increased instability in the heart rate (65.6 ±3.7 bpm to 92.0 ±49.6 bpm, P = 0.32).

3. Agonal phase (4.5 - 8 min). Progressive acidosis was observed with a trend of decreasing pH, rising lactate and $PaCO_2$ levels (Figure 4.7 D - F). This combined with persistent low PaO_2 levels, caused a fall in cardiac output characterised through falling MAP and further instability in heart rate.

4. Circulatory arrest (8 - 14 min). No tracing was visible on the pulse pressure monitor 11 ±3 min following WLST. Cessation of antegrade circulation was confirmed at this point by central venous pressure being grater than or equal to mean arterial pressure in all animals.

5. Stand off phase (14 - 20 min). No further cardiac activity was observed for at least 6 minutes following arrest and circulatory death was confirmed.

Table 4.7 summarises the changes in ^{1}H-MR parameters following 60 minutes of warm ischaemia. All parameters showed significant changes apart from the very fast pseudo-diffusion coefficient ($D^{\star}_2$) which had significant fitting noise due to the very small contribution to the signal (f_2 = 1.09 ±0.24 %).

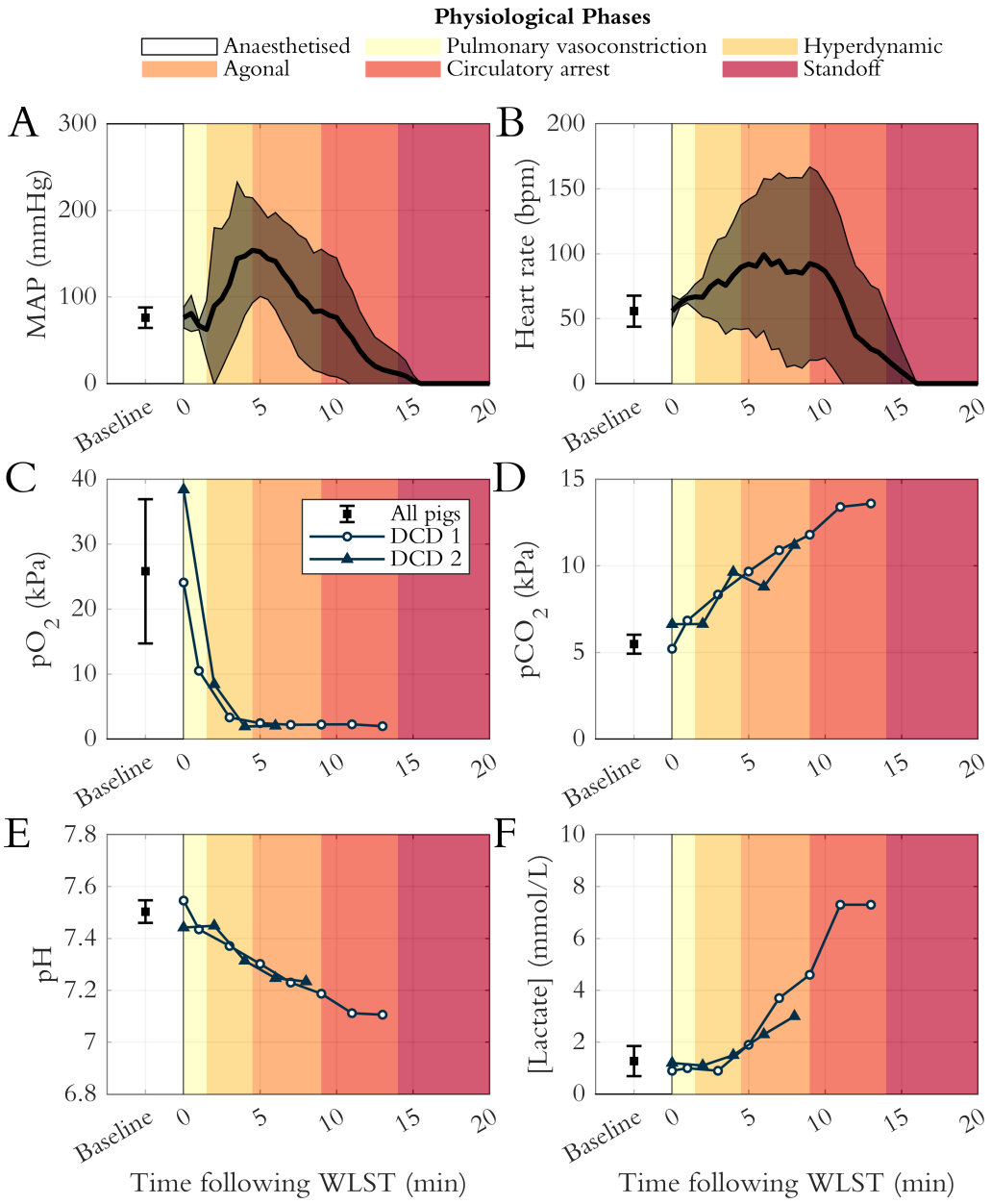


Figure 4.7: A summary of physiological changes observed following withdrawal of life-sustaining treatment (WLST). The physiological stages shown follow the model of White et al..[225] Arterial blood gas samples were only taken from 2 pigs.

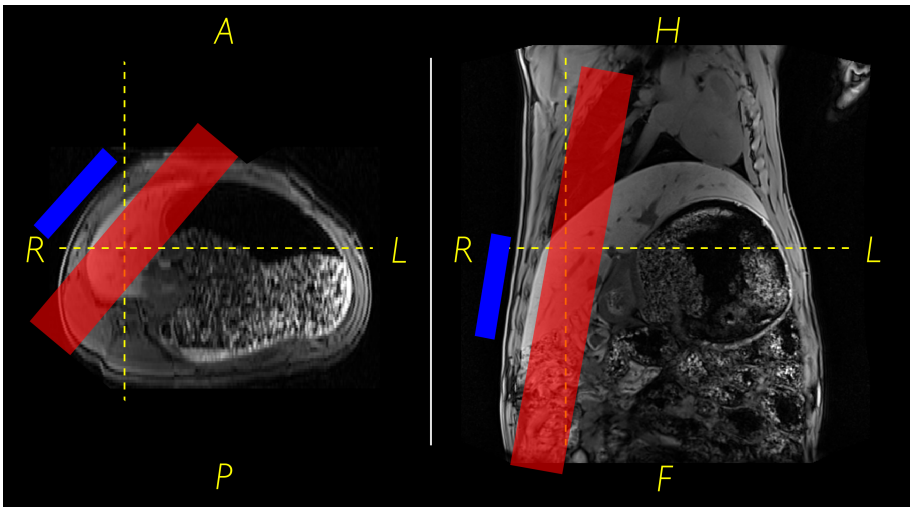


Figure 4.8: T_{1W} localiser images showing porcine anatomy in axial and coronal planes. Overlaid is an example setup used for ^{31}P-MRS acquisitions with the position of the ^{31}P loop coil shown in blue and the inversion slice used for ISIS acquisitions shown in red.

4.4.3.1 Changes in oxidative metabolism

Figure 4.9 shows example spectra from a porcine liver at baseline and following 120 mins of warm ischaemia. A significant decrease in the ATP:Pi ratio was observed with prolonged warm ischaemia (1.09 $\pm$0.22 vs 0.30 $\pm$0.05 and 0.17 $\pm$0.01, P = 0.04 and 0.02, for baseline measurements and those performed after 45 minutes and 120 minutes of warm ischaemia respectively). A trend of increasing reduction of the ATP:Pi ratio was can been seen between measurements after 45 minutes and 120 minutes of warm ischaemia although this was not significant (P = 0.06). An example of the coil and slice positioning used to acquire the ^{31}P-MRS data is shown in Figure 4.8.

The signal intensity of the β-ATP peak decayed more rapidly than α-ATP with 4.4 $\pm$8.6 % β-ATP signal remaining after 120 mins of warm ischaemia compared to 55.3 $\pm$27.5 % of α-ATP signal (P = 0.04). Figure 4.10 shows how γ-ATP signal appeared to decay at an intermediate rate between those of α-ATP and β-ATP, although this was not statistically significant ($P > 0.28$).

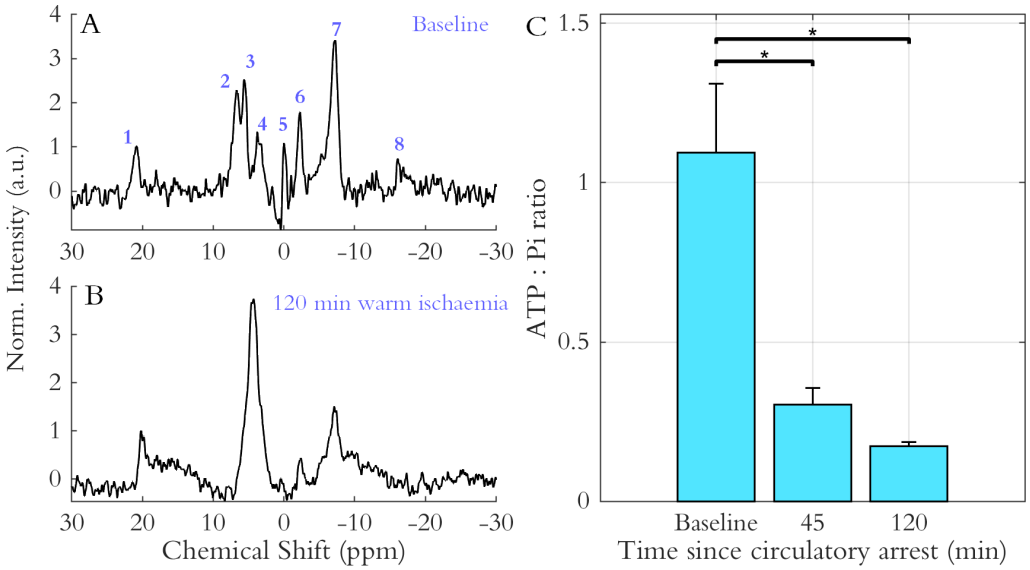


Figure 4.9: A summary of the changes in hepatic ^{31}P spectra following circulatory arrest. Example spectra at baseline (A) and at 120 minutes post-mortem (B) are presented. The numbered peaks were assigned to: 1 - fiducial marker; 2 - phosphodiesters (PDE); 3 - inorganic phosphate (Pi); 4 - phosphomonoesters (PME), 5 - phosphocreatine (PCr), and 6, 7, and 8 to γ, α, and β-ATP respectively. Quantitative changes in the ATP:Pi ratio with increasing warm ischaemia duration are also shown (C).

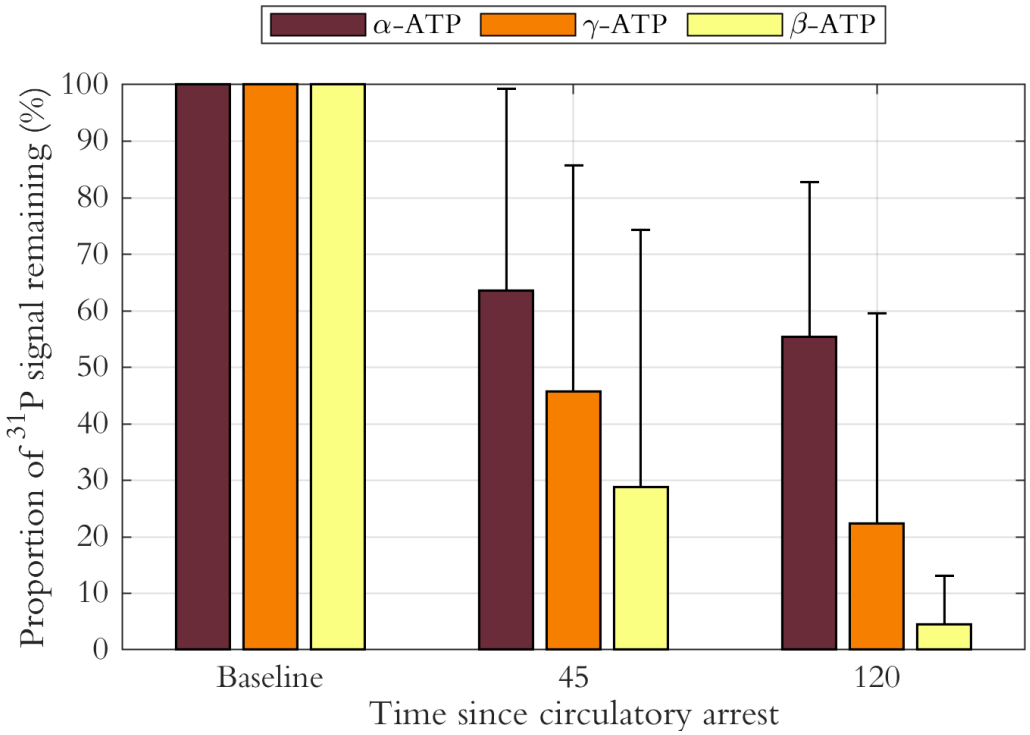


Figure 4.10: Changes in signal intensity of the three ATP peaks at increasing durations of warm ischaemia relative to their initial levels in the baseline scan.

4.4.4 Structural and metabolic changes for donation after brain-stem death

All four baseline scans were successfully completed for the brain death study arm. The first experiment in the study arm completed the study without any deviation to the protocol. However while anaesthetised, the following three pigs had extended periods of arrhythmia with unstable heart rates. In all cases, inflation of the balloon in the cranium, as shown in Figure 4.11, increased ICP and caused brain death in 18 $\pm$6 min. During induction of brain-stem death in the first two of the cases where arrhythmia had been observed, ICP increased as anticipated and triggered the Cushing's response where blood pressure increased to attempt to exceed ICP. Once MAP exceeded 100 mmHg and 200 mmHg respectively, both animals went into cardiac arrest. Cardiopulmonary resuscitation was performed for 5 minutes but spontaneous circulation could not be restarted. In order to prevent this in the forth experiment an ECG was performed following identification of periods of arrhythmia. From this, and in consultation with a cardiologist, the animal was diagnosed with atrial fibrillation and atrioventricular heart block. To treat these conditions, isoprenalin was administered intravenously and a DC cardioversion was performed. This resulted in normal sinus rhythm. 0.1 mg of atropine was administered intramuscular to assist in maintenance of this rhythm. No further periods of arrhythmia or atrial fibrillation were detected in the next hour prior to induction of brain-stem death. Both animals that did not arrest during the induction of brain-stem death (#1 and #4) continued to maintain spontaneous sinus rhythm until the end of the experiment.

Figure 4.12 summarises the changes seen in systematic parameters with extended periods of brain-stem death. Briefly, severe changes are seen during induction and immediately following confirmation of brain-stem death, with significant acidosis, high lactate content and unstable haemodynamic parameters. All of these factors return to within the normal range seen in the baseline scans within 4 hours of brain-stem death and remained within the normal range until the end of the experiment.

A different story is seen in relaxometry parameters (Figure 4.13). Liver T_1 initially increased before returning to normal values of $T_1$by 12 hrs of brain-stem death. Liver



Figure 4.11: T_{2w} image of porcine brain following inflation of a balloon within the cranium.

T_2 continually increased and remained elevated. ATP content increased in the immediate period following induction of brain-stem death before remaining stable for the rest of the experiment at slightly reduced levels compared to baseline measurements. Diffusion and perfusion parameters within the liver appeared to become more unstable following brain-stem death but remained close to or within the normal physiological range throughout the experiment.

4.5 Discussion

In Chapters 5 - 7, I assess the effect of different preservation methods on ex vivo liver grafts and investigate the promise of MR biomarkers to determine an organ's viability for transplantation. However, in order to evaluate these effects properly, it is first important to

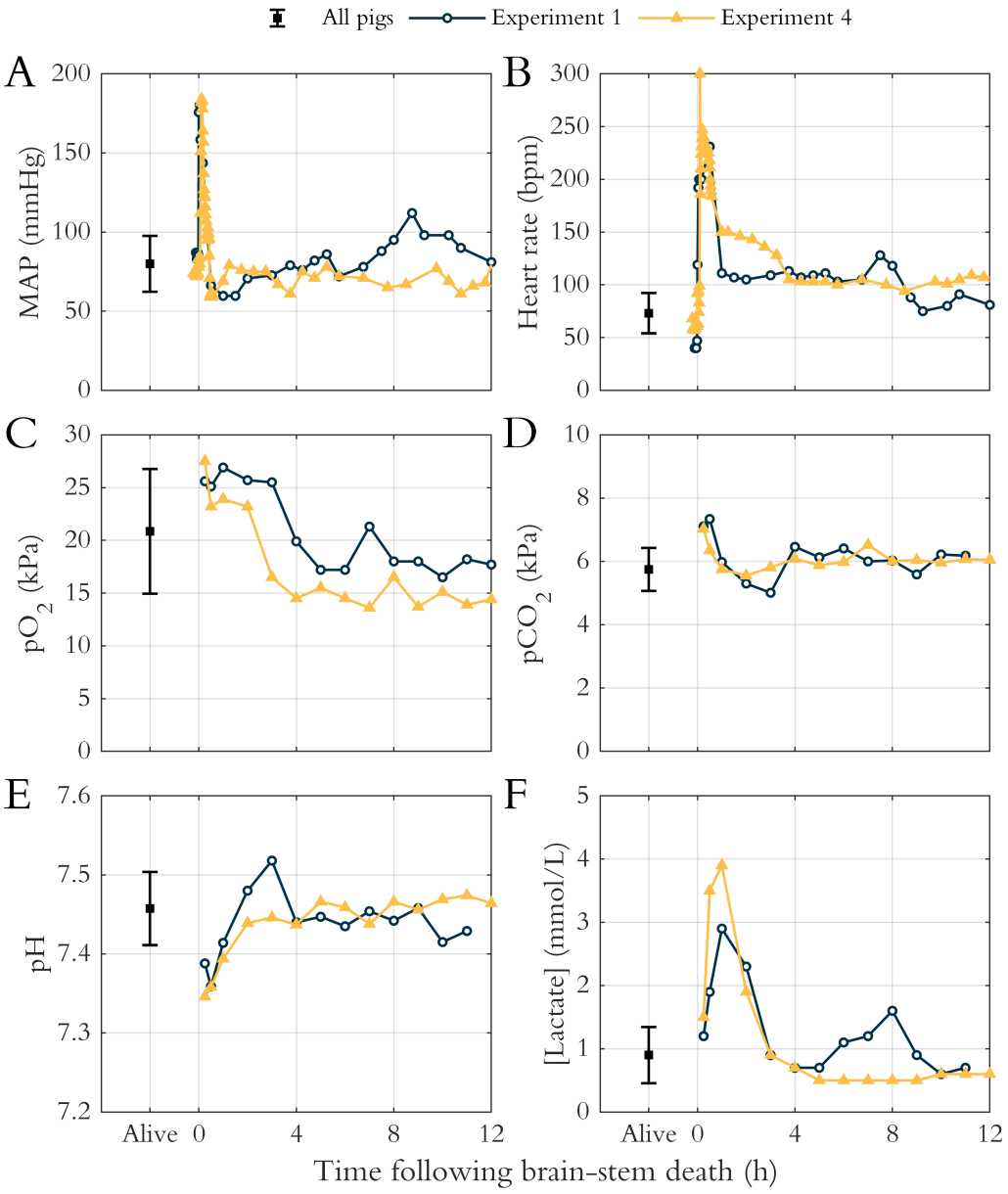


Figure 4.12: A summary of haemodynamic and biochemical changes during and after induction of brain-stem death in a porcine model.

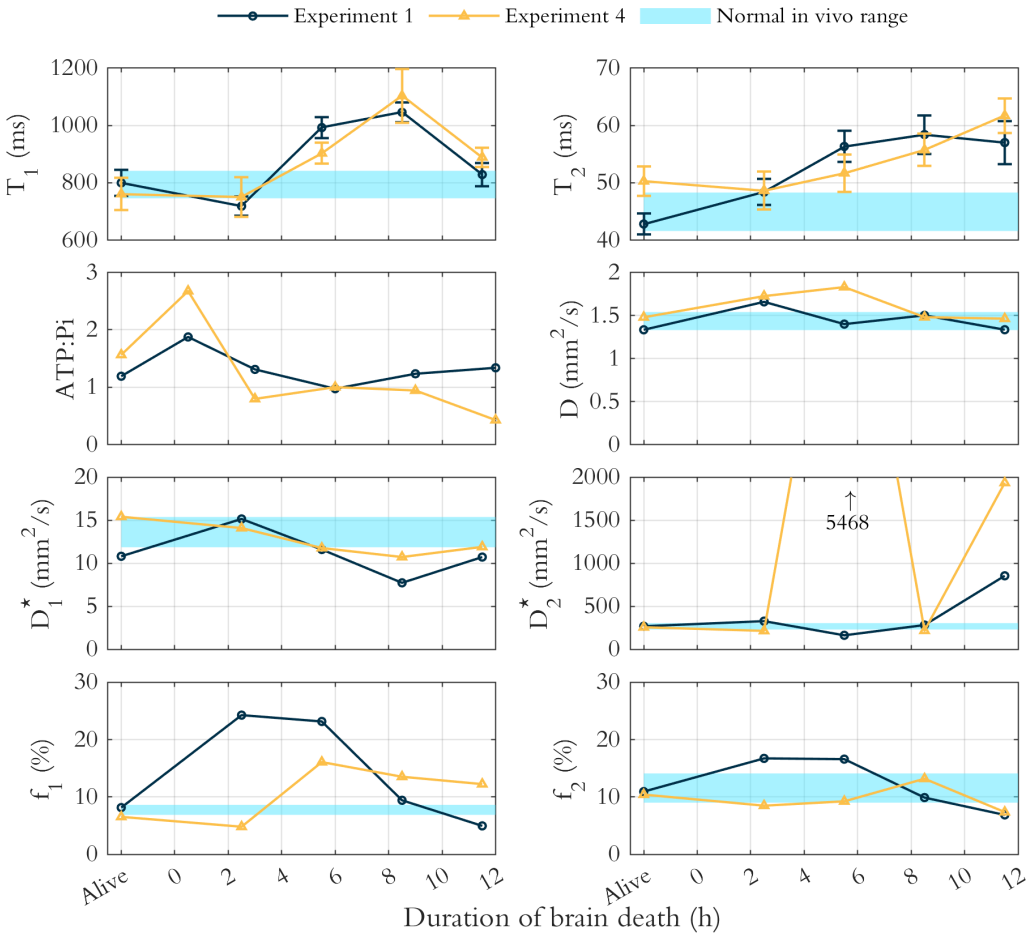


Figure 4.13: A summary of changes in MR biomarkers following brain-stem death in a porcine model.

understand what physiological baseline any preservation methods are working from given the large insults that could have occurred in livers during organ donation from a deceased donor. Therefore in this chapter, I have validated a T_1 mapping protocol at two sites using two models of 3T MRI scanner, and examined the impact of death by circulatory and brain-stem criteria on hepatic metabolism and physiology through a range of MR biomarkers.

In the first section of the work, I showed comparable measurements of relaxometry parameters between two different Siemens 3T scanners. Most acquisitions used closely matched acquisition sequences and protocols, so agreement is unsurprising. However, due to hardware and contractual constraints at different sites, two different T_1 mapping techniques needed to be used for this study. This raised potential issues as shMOLLI T_1 measurements are known to be confounded by changes in T_2 relaxation rates and hepatic fat content more severely than VFA T_1 measurements due to the balanced steady-state free precession

readout used in the shMOLLI sequence. The phantom used to validate the measurements had samples with a very wide range of T_2 values (ranging from 50 - 2000 ms) and hence a bias was seen in the raw shMOLLI T_1 values in comparison to the VFA T_1 measurements in samples with very high T_2 values. Application of a T_2 correction proposed by Zhang et al. to the samples with very long T_2 values reduced the bias seen in these measurements.[239] In comparison to the phantom however, liver T_2 values are typically <40 ms at 3T and all porcine livers are scanned in or retrieved from healthy, lean pigs which were shown to have very low fat content and low iron deposition. Therefore, the effect of T_2 and hepatic fat content on shMOLLI measurements will be negligible for in vivo measurements. A set of in vivo repeatability measurements confirmed that the variability between the measurement techniques is smaller than physiological noise in the measurements as has been found in previous larger reproducibility studies.[209 46] Therefore, VFA and shMOLLI were deemed comparable in this work.

A lack of clear consensus in the literature as to the optimum model to fit DWI data in the liver prompted an investigation of the modelling of perfusion and diffusion in porcine liver. Both bi- and tri-exponential IVIM models provided a good fit of the data with adjusted R^2 values of >0.994 but a significant amount of remaining structure was visible in the residuals of the bi-exponential fits suggesting that the model was not fully characterising the diffusion and perfusion present in the liver. Adding a third diffusion compartment removed any visible structure in the residuals of the fit and significantly improved the modelling of the data and hence the tri-exponential model was chosen as the optimum model for porcine livers.

Fitting of bi- and tri-exponential models is notoriously difficult and unstable. Therefore, I also applied a segmented fitting method which first fits the passive molecular diffusion coefficient using data with long b-values ($\geq$200 s/mm^2) where it can be assumed that signal contribution from microvascular perfusion is negligible, and then uses this result to fit the full model to all of the data. This gave more stable results with reduced inter-subject variability and no significant differences in the predictions for all parameters apart from the fast pseudo-diffusion coefficient (D^*_2). D^*_2 appeared to be very unstable when fitted

using the full model - evidenced by a 144% coefficient of variation between scans and erratic predicted values - which may explain why there is a significant difference in only this parameter between the two fitting methods. The instability of the fastest diffusion compartment may also have been driven by a limited number of b-values short enough to characterise the compartment. Indeed there are only 3 b-values <20 s/mm^2 used in this study, which may not be sufficient for a compartment with very high rates of diffusion.

All of the relaxometry, fat fraction and perfusion biomarkers appeared to be tightly controlled and reproducible with coefficients of variation of less than 20% between the eight pigs scanned.

Significant changes were observed in all relaxometry and perfusion parameters following 60 minutes of warm ischaemia in the DCD model, which clearly demonstrates the huge impact of 60 minutes of warm ischaemia. The large increase in liver T_1 following 60 minutes of warm ischaemia is likely to indicate increasing levels of oedema since T_1 has been shown previously to be very sensitive to changes in oedema in tissue.[75] This effect will be enhanced as increasing levels of necrosis cause cell swelling and lysis, which in turn will result in more oedema as the duration of warm ischaemia increases.[83] Although generally less sensitive than T_1, one would expect T_2 and $T_2^\star$ to also increase with increasing oedema. However the opposite trend was observed. This is likely explained by the stagnation of blood within the liver causing an apparent increase in hepatic iron content. Haemoglobin becomes paramagnetic once de-oxygenated and the perturbations caused by the deoxyhaemoglobin will promote faster T_2 relaxation, without having a large impact on T_1 as the paramagnetic iron is sequestered away inside the erythrocytes.[28] Additionally with increasing duration of ischaemia, the haemoglobin will form into methaemoglobin which is very strongly paramagnetic and will further decrease T_2 and $T_2^\star$.[127]

Re-assuringly following the cessation of circulation and hence the termination of perfusion of blood in the liver, a 10-fold decrease in the contribution of the fast micro-perfusion component (f_2) was seen. Both $D^\star_1$ and D also reduced following circulatory arrest but D showed only a small decrease, which is to be expected if this component does represent pure passive diffusion as this should continue even if perfusion is stopped. The increased predicted

pseudo-diffusion coefficient of the fast compartment and very large variability seen in $D^{\star}_2$ are likely due to the high uncertainty in the fit of this parameter given the exceedingly small contribution it makes to the signal.

The length of any warm ischaemic periods is very closely monitored during DCD transplantation with current guidelines limiting the total functional warm ischaemia time (FWIT) to <30 minutes. Recent advances in preservation methods have enabled the safe transplantation of livers with longer FWIT, up to 90 minutes, in pre-clinical models.[77] However, the data in this study emphasise the need for enhanced preservation methods following warm ischaemia as the rate of ATP depletion appears to be rapid (ATP:Pi ratio showed a >3-fold decreased within the first 45 minutes and continued to decrease to 120 minutes). Interestingly, the decrease in the ATP:Pi was only significant relative to baseline rather than between post-mortem time points. This suggests that the vast majority of the damage to oxidative metabolism occurs very rapidly following circulatory death and that prolonged periods may have progressively smaller effects, which may help to explain why post-transplant outcomes from DCD donors remain higher risk even with short warm ischaemia times.[205]

I observed significant differences between the rates of decay of the $\alpha-$, $\beta-$, and $\gamma-$ATP resonances. Although commonly termed ATP resonances, these peaks actually represent a wide array of high energy phosphate based metabolites (eg. guanosine triphosphate, cytidine triphosphate, thymidine triphosphate, uridine triphosphate).[123] The metabolites have in common a terminal phosphate structure with the α peak representing the first phosphate group attached to the cyclic carbon ring, γ the second and β representing the highest energy third phosphate group. Assuming the decay is exponential (i.e. a first order kinetic model) and that the resonances correspond to: $\beta = ATP$, $\gamma = ATP + ADP$, $\alpha = ATP + ADP + AMP$, one can estimate the decay rates for ATP, ADP and AMP during warm ischaemia. This gives estimated decay rates of -2.2 $\times 10^{-2}$ min^{-1} for ATP, -1.0 $\times 10^{-2}$ min^{-1} for ADP and an increase of 3.4 $\times 10^{-4}$ min^{-1} for AMP. These rates are consistent with an initial degradation of the highest energy phosphate, ATP, to ADP. Then as the liver become devoid of ATP, the hepatocytes switch to hydrolysing ADP to AMP and

only being hydrolysing AMP as a final resource, as has been observed in a range of other tissues through HPLC analysis.[148 128] The estimated slight increase in AMP suggests that the rate of degradation of ATP and ADP, and hence the rate of production of AMP being slightly greater than the rate of hydrolysis of AMP itself.

The two case studies examining the effect of brain-stem death on porcine livers, show a trend of a severe initial insult to haemodynamic and biochemical parameters during induction of and immediately following brain-stem death followed by a metabolic recovery. The increases seen in T_1 and T_2 suggest there is increasing inflammation in the tissue, likely as a results of the well characterised catecholamine storm.[135] That an amount of recovery was observed in the T_1 following 12 hrs of brain-stem death towards the normal range supports the idea that increased duration of brain-stem death could have protective effects on donor grafts or at least that it is not detrimental. This is also supported by the lack of any substantial trends in ATP:Pi ratio and diffusion and perfusion parameters for the duration of brain-stem death.

This study is not without limitations. Firstly, this is a hypothesis generating study which is limited by the small sample sizes used (n = 8 for assessment of normal ranges, n = 4 for DCD group, n = 2 for successful DBD group). This effect is especially profound in the DBD group where only 2 experiments have been completed successfully. Further experiments were planned to replace the lost numbers. However, travel restrictions because of the COVID-19 pandemic have prevented me from travelling to Denmark to complete these experiments.

Additionally in the MR optimisation study, the inter-site variability was only assessed through phantom measurements and repeated measures in one individual. In order to perform a more robust assessment, multiple participants would need to be scanned in future work. The phantom used to validate T_1 and T_2 mapping techniques was chosen as a validated phantom, which has been proven to be stable with-respect to time and transportation to multiple sites. However, the HCMR QA phantom is primarily designed for validation of cardiac MR protocols[239] and hence the T_2 values of the samples are higher than those typically found in the liver.

When assessing the optimum model for fitting DWI data, the lack of repeated measures in the same healthy individual means that it was not possible to assess the repeatability or reproducibility of the different fitting techniques and hence all measures of stability could be confounded by inter-subject variability.

4.6 Conclusion

An optimised MR protocol has been validated and used to establish the normal physiological range of a variety of MR biomarkers in a pre-clinical porcine model. This protocol was then used to examine the effect of death determined by circulatory and brain-stem criteria on the liver. Increasing durations of warm ischaemia duration had very large detrimental affects on almost all MR parameters measured in the liver, with increasing T_1, likely caused by increasing oedema, and decreasing ATP content observed. In contrast, increasing duration of brain-stem death appeared to allow for recovery of most biomarkers to levels within the normal physiological range after sustaining a period of quite severe insult immediately following brain-stem death. These results follow the traditional view that a whole liver graft from a living heart-beating donor would be the optimal, though not ethically possible, case; followed closely by a graft from a heart-beating donor declared dead by brain-stem criteria, before finally grafts from non-heart-beating donors which have sustained the greatest injury and hence need to be transplanted with caution.

Applying this cautious approach means that better diagnostic tests are required to give a higher level of confidence that an organ is viable for transplant. Therefore in the next chapter, I will assess the potential for MR biomarkers to non-invasively assess liver viability in organs donated after both brain-stem and circulatory death is assessed during static cold storage.

5

Examination of cold stored human livers with magnetic resonance

Aspects of the work detailed in this chapter have been published in the journal 'Magnetic Resonance in Medicine' in 2021.[235]

5.1 Background

Increasing demand for liver transplantation and a shortage of suitable donor organs is driving the use of more sub-optimal extended criteria donor (ECD) organs. However, these ECD organs carry a higher risk of post-transplant complications.[130] A lack of sensitive and specific biomarkers capable of predicting post-transplant liver function necessitates a cautious approach that currently limits the expansion of the donor pool. New biomarkers with strong predictive power for successful outcomes could enable an increase in the number of ECD grafts that can be safely used. As detailed in Chapter 3, magnetic resonance imaging (MRI) and magnetic resonance spectroscopy (MRS) can accurately quantify the level of steatosis in both in vivo and ex vivo human livers.[100] Meanwhile, human in vivo MRI studies have shown that tissue relaxation parameters, such as T_1, T_2, and $T_2^\star$, are capable of detecting fibrosis, inflammation, and iron concentration in human livers.[170,106] Therefore,

MR biomarkers may provide a non-invasive method of assessing the viability of donated livers for transplantation.

However, as explained in Section 3.1, the signal detected by MR methods is intrinsically a function of the net tissue magnetisation, which is described by the Boltzmann distribution, and the tissue relaxation rates, which are a function of molecular tumbling rates and the presence of nearby magnetic moieties such as ferrous particles. Therefore, both magnetisation and relaxation vary with temperature, and so do many MR parameters. It is normally assumed during in vivo scans that the body is at a constant physiological temperature of 37 °C. However, static cold storage (SCS) is the current gold-standard preservation method in liver transplantation where the liver is flushed with a cold preservation solution and placed in an ice bath to rapidly decrease its temperature. In other experiments where the specimen temperature is variable (for example in phantoms,[92] pre-clinical studies,[14] or in cadavers during post-mortem examinations[237]) large variations in tissue relaxation rates and the measured fat fraction are observed. Temperature sensitivities of relaxometry parameters have been characterised and corrected in the livers of cadavers during post-mortem examinations[237] and temperature correction of proton density fat fraction (PDFF) measurements has enabled accurate quantification of steatosis in ex vivo livers immersed in room temperature phosphate buffered saline.[13] However, little is known about the effect of temperature on tissue relaxation parameters and fat fraction measurements in donated human transplant livers within the typical temperature range encountered during static cold storage (0 - 15 °C[94]).

5.2 Aims

This chapter aims to:

- Assess the temperature sensitivity of tissue relaxation parameters in ex vivo human livers during static cold storage.
- Develop a temperature correction for any of the MR biomarkers found to have a significant temperature dependence.

- Apply these validated methods to explore whether MR biomarkers might predict viability to transplant in a study using ex vivo livers with a surrogate end point of normothermic machine perfusion.

5.3 Methods

5.3.1 Study protocol

The study protocol is outlined in Figure 5.1. In brief, human livers that had been donated but deemed unsuitable for transplantation underwent 48 hours of functional assessment during normothermic machine perfusion. This was part of a clinical trial examining the feasibility of removing fat from steatotic livers during ex vivo perfusion and has been described previously by Ceresa et al.[39] At the end of perfusion, a needle biopsy was taken from the liver for histopathology analysis. The livers were then cold flushed and placed on ice for a 10-hour period of cold storage. During this time, T_1, T_2, T_2^*, fat-water frequency offset, and PDFF were measured hourly on average resulting in a total of 10 measurement time points per liver. A subset of livers (n=2) were then re-warmed in a water bath and further relaxometry and PDFF measurements were made.

This study was approved by National Ethics Review Committee of the United Kingdom (REC reference 16/NE/0248).

5.3.2 Liver specimens and preparation for MRI

Six human livers were retrieved for transplantation as part of a standard multi-organ deceased donor organ retrieval.[27] The livers were deemed unsuitable for transplantation due to the presence of severe steatosis reported by the retrieval surgeon. The livers were cold flushed with University of Wisconsin (UW) solution (Bridge to Life, London, UK) and transported on ice as per standard practice. Once at the Oxford Transplant Centre, the livers were cannulated and perfused for 48 hours on a clinical normothermic machine perfusion device (*metra*®, OrganOx Ltd, Oxford, UK) as per the standard protocol (full

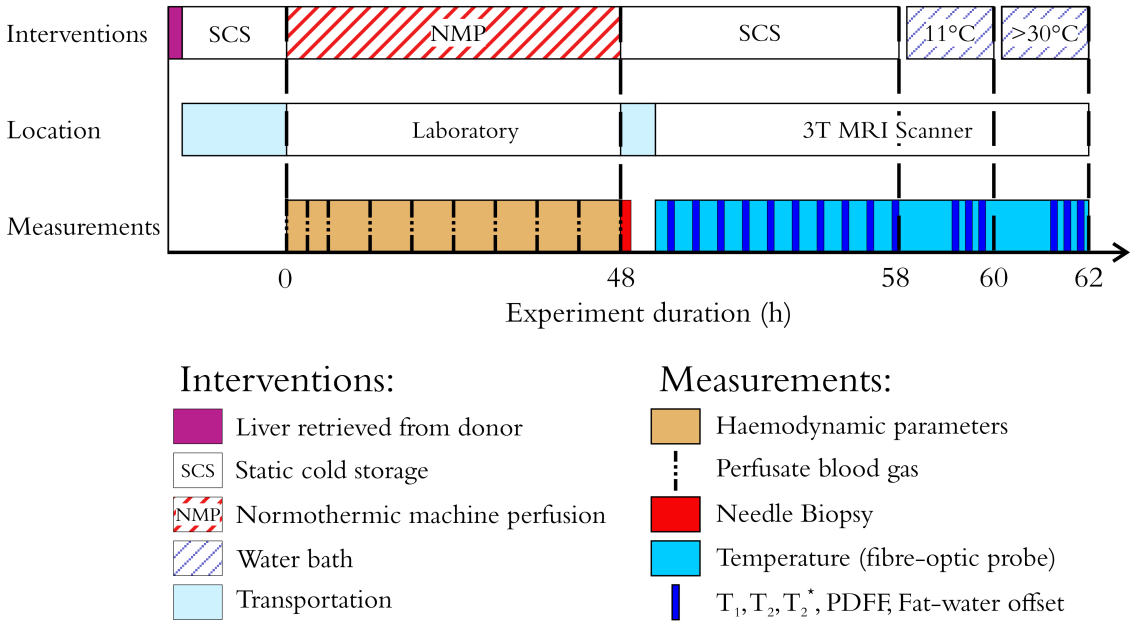


Figure 5.1: Timing of the study procedures for an ex vivo human liver. Liver function was assessed through regular arterial blood gas analysis and continuous monitoring of bile production and haemodynamic parameters as described in the study protocol. Throughout the MR examination $T_1, T_2, T_2^\star$, PDFF and fat-water offset were all measured hourly on average. Invasive temperature measurements were made using a fiber-optic temperature probe in three livers; the remaining livers remained sealed inside sterile packaging throughout the study. Two livers were re-warmed in a water bath to differentiate the impact of storage duration and temperature on relaxometry and PDFF measures.

details are provided in Section 6.3.3.1). For all perfusions, a lipoprotein apheresis filter (DALI® 500, Fresenius Medical Care (UK) Ltd, UK) was added to the perfusion circuit and additional de-fatting interventions of 1 g l-carnitine hydrochloride (Sigma-Aldrich, UK), 1 mg NKH477 hydrochloride (Cayman Chemical, USA), a reduced insulin level of 100 units (Actrapid, Novo Nordisk, UK), and a reduced perfusate glucose concentration of 5 mmol/L before infusion of total parenteral nutrition (Nutriflex Special, B Braun) were supplemented into the circuit for Livers 2 and 3. At the end of perfusion, livers were cold flushed with 3 L histidine tryptophan ketoglutarate (HTK) solution (Custodiol, Essential Pharmaceuticals LLC, USA) at 4 °C. Core biopsy samples were taken from the edge of the right lobe and fixed in 10 % formalin. All livers were then placed in excess HTK-solution within three sealed bags and stored on ice.

5.3.3 MR Examination

All livers underwent a 10-hour MRI acquisition on a clinical 3T system (Magnetom TIM-Trio, Siemens Healthineers, Erlangen, Germany) fitted with a 32 channel ^{1}H array coil (Rapid Biomedical, Rimpar, Germany) while inside an ice box. For all livers scanning started within 30 minutes after the end of perfusion. Following the 10-hours protocol, two of the livers were immersed in a water bath at 11 °C and scanned for 90 minutes before being placed into a warm water bath (at 30 °C and 35 °C respectively) and scanned for an additional 90 minutes. For the duration of the MRI protocol, all livers remained immersed in HTK solution and inside the sealed bags.

5.3.3.1 MRS Acquisition and analysis

To enable non-invasive monitoring of temperature, single voxel stimulated echo acquisition mode (STEAM)[78] spectroscopy was performed in four voxels across the liver, with and without water suppression. Three voxels were placed in the right lobe and one voxel in the left with all voxels positioned in parenchyma away from any obvious vasculature. Sequence parameters were: TE = 10 ms, TM = 7 ms, 20 × 20 × 20 mm^3 voxel size, 16 averages with water suppression and 3 without, and TR = 750 ms with water suppression and TR = 4750 ms without. All spectra were quantified using the OXSA toolbox[175] in MATLAB. Spectra acquired with water suppression were used to quantify the lipid signals that are an order of magnitude lower than the water signal. The spectra without water suppression allowed quantification of water as a reference. The temperature dependent fat-water frequency shift[172] was calculated as the difference between the main fat peak (methylene) and water. An average of all four liver voxels was calculated for global temperature assessment. To generate a linear calibration curve between fat-water frequency shift and temperature, a fibre optic temperature probe (Neoptix, Canada) was inserted into the centre of the right lobe of three livers and used to record tissue temperature throughout the study.

The longitudinal relaxation time (T_1) of water in a voxel positioned near the centre of the right lobe away from any obvious vasculature was measured using an inversion recovery

single voxel stimulated echo acquisition mode (STEAM) where a 180° inversion pulse is added prior to the previously described STEAM squence (Section 3.2.2.1).[78] Spectroscopy scans were repeated with inversion time (TI) = 50, 500, 1218, 2385, 3553, 4750, 5500, 7000 ms; repetition time (TR) = 10 s, 4 averages, 4 kHz bandwidth (BW), and 1024 complex points. Additionally, a multiple-echo time (TE), multiple-TR STEAM single-voxel sequence was used to measure the T_1 and transverse relaxation time (T_2) of water and the proton density fat fraction (PDFF) in the same voxel position.[86] This sequence repeatedly acquires STEAM spectra at varying TRs and TEs. This creates a partial saturation of the signal in each of the spectra, which is dependent on the species T_1 and T_2. Parameters used for this sequence were: TR = 150, 175, 200, 225, 250, 275, 300, 325, 350, 400, 450, 500, 600, 700, 800, 900, 1000, 1250, 1500, 2000 ms with a fixed TE of 15 ms; before eight additional spectra with TR = 1000 ms and TE = 20, 25, 30, 35, 50, 70, 90 and 110 ms. The three largest fat peaks were included in the prior knowledge and a correction for the smaller peaks was performed using a previously described standard liver spectrum.[85]

All spectra were fitted using a MATLAB implementation of advanced method for accurate, robust and efficient spectral fitting (AMARES) from the OXSA toolbox.[175] The amplitudes for the water peak from inversion recovery data were fitted to Equation 5.1:

$$S_{\mathrm{i}} = S_0 \left(1 - \exp\left(-\frac{TI_{\mathrm{i}}}{T_{1\mathrm{w}}}\right)\right), \tag{5.1}$$

where S_0 is a scaling factor proportional to proton density, S_{i} is the peak amplitude of a spectrum with inversion time TI_{i}, and $T_{1\mathrm{w}}$ is the longitudinal relaxation time constant for water. Peak amplitudes from the multiple TR and TE spectra were fitted to Equation 5.2:

$$S_{\mathrm{i}} = S_0 \left(1 - \exp\left(-\frac{\tau}{T_1}\right)\right) \exp\left(-\frac{TE}{T_2}\right), \tag{5.2}$$

where S_0 is a scaling factor proportional to proton density, τ is the time from the final pulse in the STEAM sequence to the end of the TR interval, and TE is the echo time.

The spectroscopic PDFF was defined as the ratio of corrected fat spectrum peak amplitudes to the sum of corrected water and fat spectrum peak amplitudes as shown in Equation 5.3.

$$PDFF\,[\%] = \frac{\sum_i S_{\mathrm{f_i}}}{S_{\mathrm{w}} + \sum_i S_{\mathrm{f_i}}} \times 100 \tag{5.3}$$

Here S_w is the water peak amplitude, S_{f_i} denotes the peak amplitude of the i$^{\mathrm{th}}$ fat peak. A simple spectroscopic fat fraction (FF) was calculated similarly to PDFF in Equation 5.3 using the raw peak amplitudes from the single TE, single TR STEAM spectra. Spectroscopic FF is my centre's standard measurement for steatosis quantification for in vivo human studies.[185]

5.3.3.2 MRI acquisition and analysis

Coronal T_1 maps were acquired using a shortened modified Look Locker inversion (shMOLLI) sequence with parameters based on a standardised protocol (Siemens WIP 561a, Erlangen, Germany): TR/TE = 2.52/1.05 ms, 35° readout flip angle (FA), 898 Hz/px BW, 8 mm slice thickness, seven TIs, 110 ms first TI, 80 ms TI increment, 288 × 384 field of view (FoV), 192 × 182 matrix, generalized auto-calibrating partially parallel acquisition (GRAPPA) acceleration factor R = 2, 24 reference lines, 6/8 partial Fourier in the phase encoding direction and a simulated heart rate of 75 beats/minute. The shortened modified Look Locker inversion (shMOLLI) conditional fitting algorithm was used to calculate T_1 values.[173]

Multiple echo spoiled gradient recalled echo (GRE) images were collected to obtain PDFF and $T_2^\star$ maps. Parameters for the 2D multiple-echo GRE sequence were: 6° flip angle, TR/TE = 500/ 1.25, 2.46, 3.69, 4.92, 6.15, 7.38, 8.61, 9.84 ms; 400 × 325 mm^2 field of view, 6 mm slice thickness, 128 × 128 acquisition matrix, 1090 Hz/px bandwidth, and a bipolar gradient readout scheme. PDFF was calculated using the Mixed-Magnitude/Complex method[91] initialized with the Graph Cut method[90] from the ISMRM Fat-Water Toolbox[98]. Effects of the bipolar gradients were minimised by a high bandwidth, a linear phase correction,[126] and the use of Mixed Magnitude/Complex fitting method.[91] Temperature correction of the modelled fat spectrum was performed by utilising the estimated temperature from the fat-water frequency measurements to adjust the chemical shift of the fat peaks by 0.01 ppm/°C.[92] Table 5.1 details the spectrum modelled. MRI PDFF was defined as:

$$PDFF_{\mathrm{MRI}}\,[\%] = \frac{S_{\mathrm{f}}}{S_{\mathrm{w}} + S_{\mathrm{f}}} \times 100 \tag{5.4}$$

Table 5.1: Fat and water peak parameters used prior knowledge file for spectral fitting and for fat spectral simulation during IDEAL reconstruction

Peak No.	*Species*	*Chemical Shift*† *[ppm]*	*Relative Amplitude [a.u.]*	*Linewidth*§ *[Hz]*
Fat peaks				
1	Methyl	$0.90 - \beta \times \Delta T$	0.087	20
2	Methylene	$1.30 - \beta \times \Delta T$	0.693	40
3	α-carbonyl and α-olefinic	$2.10 - \beta \times \Delta T$	0.128	40
4	Diacyl	$2.76 - \beta \times \Delta T$	0.004	20
5	Glycerol	$4.30 - \beta \times \Delta T$	0.039	40
6	Olefinic	$5.30 - \beta \times \Delta T$	0.049	30
Water peak				
	Water	4.70	1	40

†Temperature corrected chemical shifts use chemical shift values reported by Hamilton et al.[85] for human liver fat at 37°C and assume a linear temperature sensitivity (β) and difference in temperature from 37°C of ΔT.β was 0.01 ppm/°C as reported by Hernando et al..[92]

§Linewidths are only included in the prior knowledge for spectral fitting and not IDEAL spectral modelling.

where S_f and S_w are the signal intensity of the fat and water images respectively. Square regions of interest from PDFF, T_2^* and T_1 parametric maps were extracted from the same four voxel positions that the STEAM spectroscopy was acquired in. Voxels within each individual ROI were averaged to give one measurement per ROI. By assessing the spread of the four measurements, a crude assessment of spatial variation of the parameters across the liver could be achieved.

5.3.4 Functional assessment of livers during normothermic machine preservation

Throughout normothermic machine perfusion, haemodynamic parameters were continuously monitored and perfusate blood gas analysis (ALB90 Flex, Radiometer, UK) was performed at least once every six hours. At the end of perfusion, immediately before the MR examination, these parameters were used to determine functional viability of the liver according to the recently validated VITTAL criteria.[117] To be deemed functional at the end of perfusion, a liver must metabolise perfusate lactate to $\leq$2.5 mmol/L within the first 4 hours of perfusion

and maintain the perfusate lactate concentration below $\leq$2.5 mmol/L for the duration of perfusion. Additionally, the livers must also fulfil at least two out of the following criteria to be considered function:

- maintenance of stable portal vein and arterial flow rates $\geq$500 and $\geq$150 mL/min respectively
- evidence of glucose metabolism
- production of bile
- maintenance of perfusate pH $\geq$7.30
- visibly homogeneous perfusion with soft consistency of the parenchyma

All livers, whether deemed functional or non-functional during normothermic machine perfusion (NMP), were included in the MR analysis to assess whether the MR parameters are able to differentiate between them.

5.3.5 Histological assessment

Core biopsy samples were taken from the edge of the right lobe at the end of perfusion using an 18G biopsy needle (Biopince Full Core Biopsy Instrument, Argon Medical Devices, USA). Samples were immediately fixed in 10% formalin and later embedded in paraffin. Samples were then cut into 4 μm sections and stained with hematoxylin and eosin (H&E), periodic acid-Schiff (PAS), and Picosirius red. A blinded pathologist graded the sections according to the semi-quantitative non-alcoholic fatty liver disease activity score (NAS), which is a summation of levels of steatosis (graded 0-3), lobular inflammation (graded 0-3), and hepatocyte ballooning (graded 0-2).[110] Macrovesicular steatosis was quantified by digital image analysis of H&E stained sections (Visiopharm application 10119, H&E liver steatosis, Visiopharm Ltd, UK).

5.3.6 Statistical analysis

A linear mixed-effect regression analysis was performed to asses the association of the MR parameters (T_1, T_2, $T_2^\star$, and fat fraction) while accounting for underlying inter-donor variability as shown in Equation 5.5.

$$X_{\text{observed}} = \Delta_T X + X_{\text{Donor Pathology}} \tag{5.5}$$

Temperature was modelled as a fixed effect ($\Delta_T X$), assuming that the temperature sensitivity of the MR parameter (X) is consistent between livers. Then the underlying temperature independent component for the MR parameters due to variation in donor liver pathology was modelled as a random-effect ($X_{\text{Donor Pathology}}$). Temperature sensitivities were studied through the liver-independent $\Delta_T X$ component of the MR signal calculated by subtraction of the liver specific temperature-independent component from the observed value of the MR parameter. Where statistically significant temperature sensitivities were found, temperature corrected MR parameters ($X(0°\text{C})$) were calculated using Equation 5.6:

$$X(0°\text{C}) = X_{\text{observed}} - \alpha \times \Delta T, \tag{5.6}$$

where α is the temperature sensitivity of the MR parameter and ΔT is the difference in temperature from $0\,°\text{C}$.

The correlation of each MR parameter with temperature was evaluated using Pearson's correlation coefficient (ρ) and the linearity of the correlation was assessed using the coefficient of determination (R^2). For each MR parameter the overall coefficient of variation ($\overline{CV}$) was defined as the mean of the coefficients of variation calculated for each liver using:

$$CV_{\text{i}} = \frac{\sigma_{\text{i}}}{\mu_{\text{i}}} \tag{5.7}$$

where σ_{i} is the standard deviation of repeated measurements in liver i and μ_{i} is the mean value of the parameter for liver i).[19] Similarly the coefficient of repeatability ($\overline{CR}$) was defined as the mean of the coefficients of repeatability for each liver which was calculated using Equation 5.8.[18]

$$CR_{\text{i}} = 1.96 \times \sqrt{2} \times \sigma_{\text{i}} \tag{5.8}$$

All measured results are presented as mean ±standard deviation and all fitting results are presented as mean value followed by 95% confidence intervals in brackets, unless otherwise stated. Statistical significance of differences in MR parameters between functional and non-functional livers were determined using a Student's t-test. Where statistically significant differences were found, potential cut-off values for differentiation of functional and non-functional livers were proposed such that sensitivity and specificity were >80% and the Youden Index was maximised.[16] All statistical hypothesis testing was performed at significance level $\alpha = 0.05$.

5.4 Results

5.4.1 Liver function during normothermic machine perfusion

Table 5.2 details the donor characteristics and the liver's functional parameters during NMP. Five livers cleared lactate well in the first 4 hours of perfusion but only three livers maintained sufficient function to meet the functional viability criteria at the end of perfusion. Perfusion of Liver 5 was stopped after 36 hours due to visually poor perfusion of the tissue, increasing perfusate acidosis, and increasing lactate levels which did not change upon a lactate challenge. These factors meant that the liver did not meet the functional viability criteria and its function was so poor that it was deemed futile to maintain perfusion to 48 hours.

5.4.2 Non-invasive temperature measurement

Figure 5.2 presents the temperature changes observed in three livers during the first 10 hours of SCS. A strong linear dependence of fat-water frequency offset with temperature was observed ($R^2 = 0.99$, $P < 0.001$). The temperature sensitivity of fat-water frequency offset was -0.0092 ± 0.0003 ppm /°C. Using this as a conversion factor from the observed fat-water frequency offset to temperature, an average decrease in temperature of 9.2 ±4.3 °C (range = 4.5 - 15.6 °C) was non-invasively observed in all livers during the 10 hours of cold storage. Livers equilibrated to 1.4 ±1.2 °C after 10 hours of cold storage. In comparison,

Table 5.2: Donor demographics, haemodynamic and biochemical parameters characterising liver function during normothermic machine perfusion and histology results for cold stored discarded human livers. Perfusion parameters meeting the viability criteria for transplant viability are highlighted in blue.

Liver No.	*1*	*2*	*3*	*4*	*5*	*6*
Donor characteristics						
Age (years)	44	40	72	30	61	44
Sex	M	M	F	M	M	F
Donation type	DCD	DBD	DBD	DBD	DCD	DCD
Cause of death	HBI	MI	HBI	ICH	TBI	ICH
Cold ischemia time (min)	730	663	899	546	689	1122
NMP duration (hrs)	48	48	48	48	36	48
Histological steatosis (%)	24.47	35.76	22.26	6.61	39.53	14.49
Liver function during normothermic machine perfusion						
$Lactate_{4\ hrs}$ (mmol /L)	*2.4*	*2.4*	*1.0*	*2.5*	4.0	*2.3*
$Lactate_{end}$ (mmol /L)	4.2	*1.6*	*1.9*	*1.4*	14.2	*5.6*
pH_{end}	7.28	7.20	7.24	7.20	6.93	*7.34*
Hepatic artery flow rate (L/min)	*0.51* *±0.03*	*0.56* *±0.05*	*0.42* *±0.09*	*0.33* *±0.11*	*0.38* *±0.08*	*0.50* *±0.08*
Portal vein flow rate (L/min)	*1.04* *±0.03*	*1.05* *±0.06*	*1.01* *±0.03*	*1.17* *±0.06*	*1.04* *±0.08*	*1.11* *±0.06*
Total bile production (ml)	*360*	0	*80*	*400*	*320*	0
Maximum glucose metabolism (mmol/L/hr)	*-3.1*	*-3.3*	*-4.93*	*-3.1*	*-2.3*	*-3.5*
Homogenous perfusion	*Yes*	*Yes*	*Yes*	*Yes*	No	*Yes*
Viability criteria met	**No**	***Yes***	***Yes***	***Yes***	**No**	**No**

Abbreviations: NMP, normothermic machine perfusion; DBD, donation following brain-stem death; DCD, donation following circulatory death; HBI, hypoxic brain injury; MI, myocardial infarction; ICH, intracerebral haemorrhage; TBI traumatic brain injury.

after just 30 minutes of static cold storage liver temperatures were 10.6 ± 5.2 °C. Both the decreases in the average temperature and variability with increased SCS duration would be expected from thermal cooling physics.

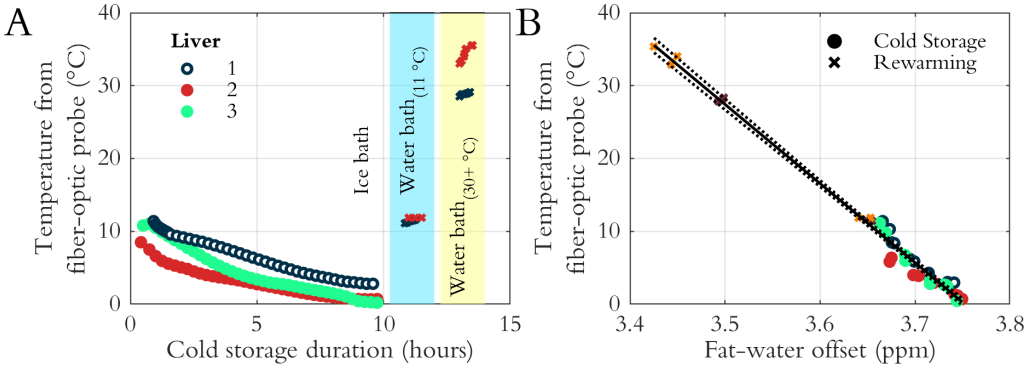


Figure 5.2: A) Temperature changes in three discarded human livers during static cold storage and re-warming (of 2 livers) in a water bath measured using a fibre optic temperature probe in the right lobe. B) Variation of chemical shift offset between the water and main fat (CH_2) peak for the same three discarded human livers as a function of temperature measured using a fibre optic temperature probe in the right lobe.

5.4.3 Relaxometry

Figure 5.3 shows the strong linear correlation ($\rho > 0.84$, $R^2 > 0.78$, $P < 0.0001$) observed between water T_1 measurements and temperature, with sensitivities of 9.79 ms / °C (7.16 – 12.43), 10.48 ms / °C (8.23 – 12.74), and 10.16 ms / °C (8.70 – 11.61) for STEAM-IR T_1, multi-TR multi-TE T_1, and shMOLLI T_1 respectively.

Calculating temperature-corrected T_1 values using these temperature sensitivities reduced the coefficient of variation from 5.25 %, 6.34 %, and 5.46 % to 2.87 %, 3.54 %, 3.68 % for the three techniques as shown in Table 5.3.

Similarly, decreases were observed in the coefficients of reproducibility following temperature correction from 110 ms, 112 ms, and 98 ms to 58 ms, 60 ms, and 63 ms for STEAM-IR T_1, multi-TR multi-TE T_1, and shMOLLI T_1 respectively. Multi-TR, multi-TE spectroscopy data were not acquired for Liver 6 and hence Liver 6 was excluded from any analysis of multi-TR multi-TE spectroscopy data. No significant correlations were observed between T_2, measured spectroscopically, or $T_2^\star$, measured using multi-echo GRE, and temperature (Figure 5.4).

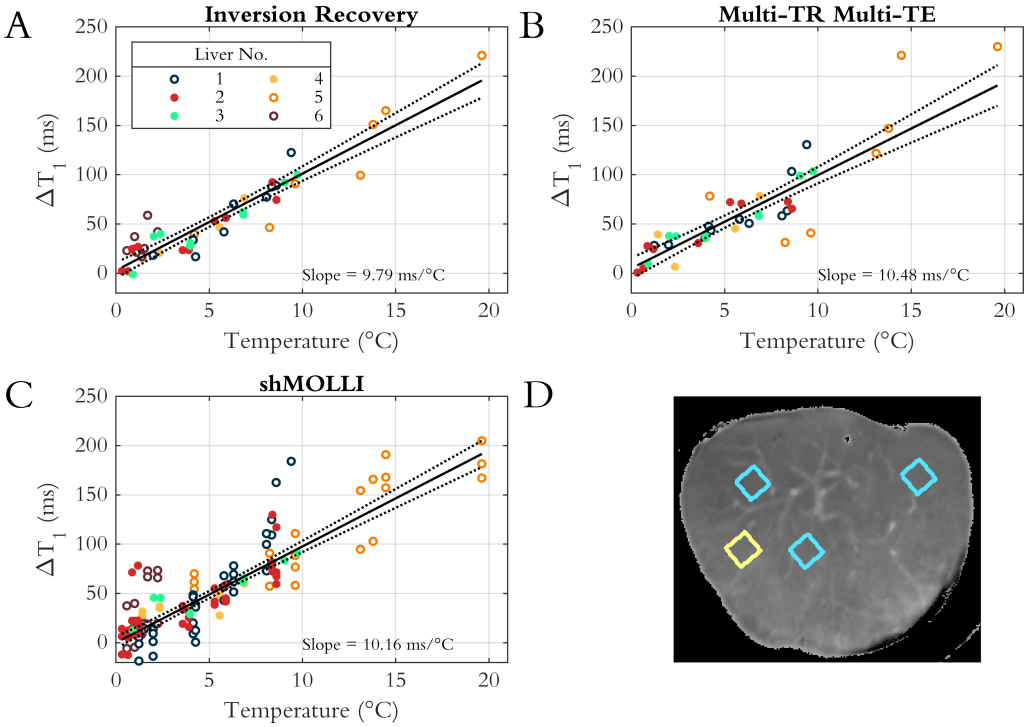


Figure 5.3: Variation of T_1 as a function of temperature during static cold storage measured using single voxel STEAM inversion recovery spectroscopy as gold standard (A) and multiple repetition time, multiple echo time single voxel STEAM spectroscopy (B) and shMOLLI (C) sequences. Three spectroscopy voxels were placed in the right lobe and one in the left lobe away from any vasculature as shown in a representative image of a cold stored liver (D). Temperature measurements were collected from fat-water offset frequency in all four voxels and averaged together. These voxels were used as regions of interest for the shMOLLI T_1 maps and the yellow voxel was used for the spectroscopic relaxometry measurements.

Repeated measurements within a liver were very reproducible with coefficients of reproducibility of 1.32 ms for T_2 measurements and 10.23 ms for T_2^* measurements. When re-warmed in a water bath to the starting temperature of 11 °C for 90 minutes, the T_1 values for Livers 1 and 2 returned to within 3% of the initial values. Upon further heating in water baths of 30 °C (Liver 1) or 35 °C (Liver 2) for 90 minutes T_1 increased further as can be seen in Figure 5.5.

The calculated T_1 and liver temperature were still increasing when the re-warming experiment was stopped, suggesting that thermal equilibrium was not reached.

Table 5.3: Temperature sensitivities of T_1, T_2, and $T_2^\star$ in ex vivo human livers during static cold storage. Additionally, the average coefficients of variation and reproducibility for repeated measurements in the livers before and, where a significant correlation with temperature is observed, after temperature correction.

	Gradient (% / C)	*P-value*	*Coefficient of variation (%)*		*Coefficient of reproducibility (ms)*	
			Raw data	*Temperature corrected*	*Raw data*	*Temperature corrected*
T_1						
IR spectroscopy	9.79 (7.16 - 12.34)	<0.0001	5.25	2.87	110	58
Multi-TR multi-TE spectroscopy	10.48 (8.23 - 12.74)	<0.001	6.34	3.54	112	60
shMOLLI	10.16 (8.70 - 11.61)	<0.0001	5.46	3.68	98	63
T_2						
Multi-TR multi-TE spectroscopy	0.00 (-0.05 - 0.05)	0.86	1.72	-	1.32	-
$T_2^\star$						
Multi-echo GRE	-0.12 (-0.35 - 0.11)	0.31	16.20	-	10.59	-

5.4.4 Quantification of Steatosis

Figure 5.6 shows the strong linear correlation between fat fraction and temperature ($\rho = 0.80$, $R^2 = 0.64$, $P < 0.0001$) and between proton density fat fraction and temperature ($\rho = 0.65$ and 0.78, $R^2 = 0.42$ and 0.61 for spectroscopic and imaging measurements respectively, $P < 0.001$). Both PDFF measures, calculated from spectroscopic and imaging data respectively, were much less dependent on temperature than a simple spectroscopic fat fraction (lipid signal / lipid + water peak amplitudes) measurement with slopes of 0.22% /°C (0.10-0.33) and 0.26% /°C (0.21-0.30) for the PDFF measures compared to 0.47% /°C (0.40-0.54) for the simple spectroscopic fat fraction.

Performing a temperature correction reduced the intra-liver measurement variation, as evidenced by a decrease in the coefficient of reproducibility from 5.19%, 2.40%, and 1.08% to 3.50%, 2.08%, and 0.64% for spectroscopic fat fraction, spectroscopic PDFF and imaging based PDFF (Table 5.4).

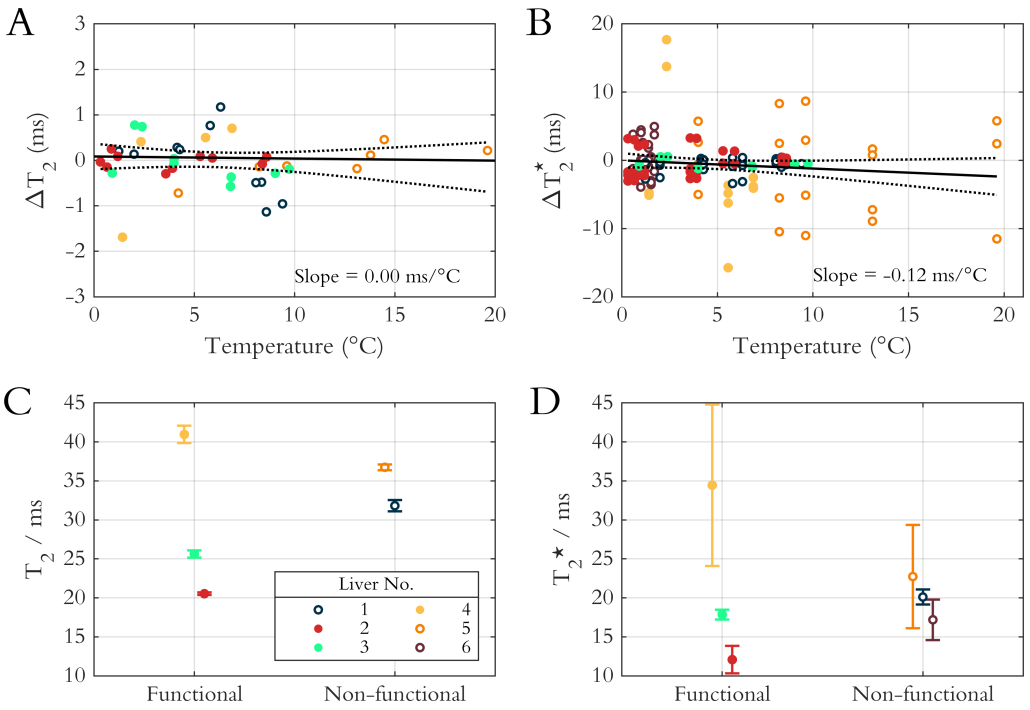


Figure 5.4: (A) Variation of T_2 as a function of temperature during static cold storage measured using a multi-repetition time, multi-echo time single voxel STEAM spectroscopy sequence. (B) Variation of $T_2^\star$ as a function of temperature in the same livers. $T_2^\star$ was measured using a multiple-echo GRE sequence and four regions of interest were assessed as previously shown in Figure 5.3 to yield four measurement per time point. (C) and (D) show the distribution of T_2 and $T_2^\star$ values in livers deemed functional and non-functional during NMP. In all plots closed data points represent livers deemed functional and open points represent livers deemed non-functional. Multi-repetition time, multi-echo time single voxel STEAM spectroscopy was not acquired for Liver 6 and hence Liver 6 is excluded from the T_2 panels.

Table 5.4: Temperature sensitivities of spectroscopic fat fraction (FF_{MRS}), spectroscopic proton density fat fraction ($PDFF_{MRS}$) and proton density fat fraction calculated from multi-echo GRE images ($PDFF_{MRI}$) in ex vivo human livers during static cold storage. Additionally, the average coefficients of variation and reproducibility for repeated measurements in the livers before and after temperature correction are presented.

	Gradient (% / C)	*P-value*	*Coefficient of variation (%)*		*Coefficient of reproducibility (%)*	
			Raw data	*Temperature corrected*	*Raw data*	*Temperature Corrected*
FF_{MRS}	0.47 (0.40 - 0.54)	<0.0001	27.22	32.78	5.19	3.50
$PDFF_{MRS}$	0.22 (0.10 - 0.33)	<0.001	27.55	36.05	2.40	2.08
$PDFF_{MRI}$	0.26 (0.21 - 0.30)	<0.0001	22.67	17.42	1.08	0.64

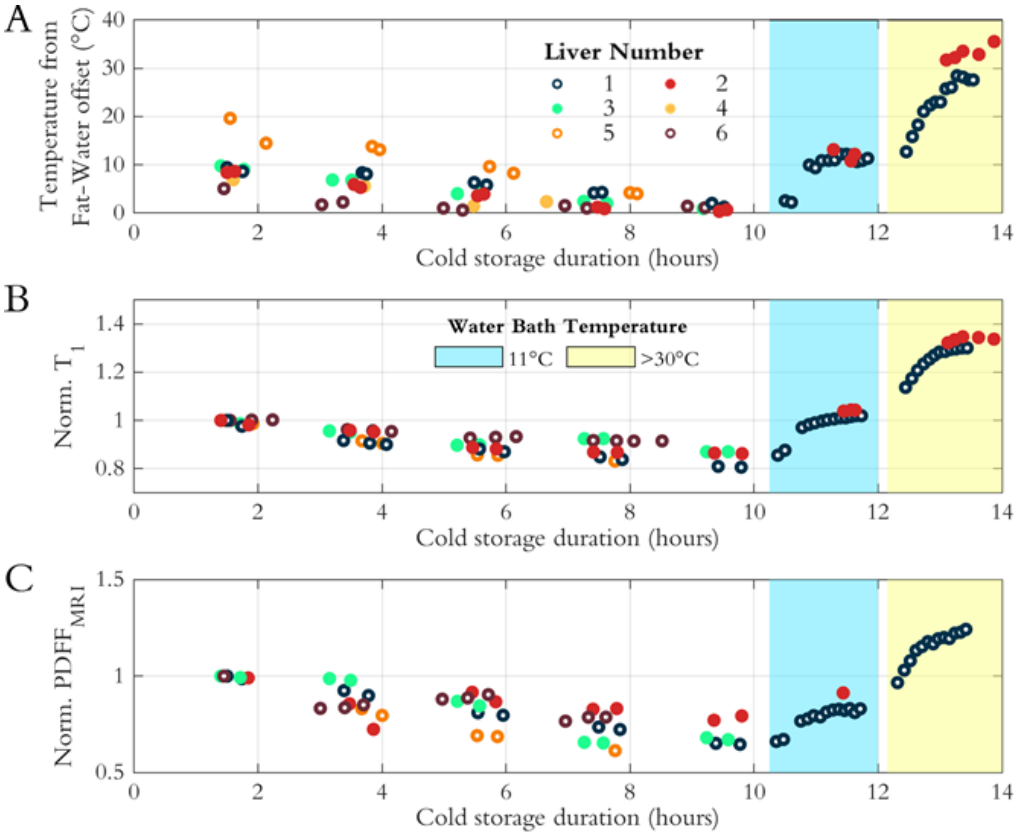


Figure 5.5: Changes in temperature (A), shMOLLI T_1 (B) and MRI-PDFF (C) as a function of time. shMOLLI T_1 and MRI-PDFF are both normalised to the initial value. Following 10 hours of static cold storage, both livers were placed into a water bath at 11 °C for 90 minutes before being placed into a water bath at 30 °C (Liver 1) or 35 °C (Liver 2) to re-warm.

A slight increase was observed in the coefficient of variation following temperature correction from 27.22% and 27.55% to 32.78% and 36.05% for spectroscopic FF and PDFF measurements respectively. This effect was driven by a decrease in the mean calculated spectroscopic FF and PDFF values following the correction. The coefficient of variation of imaging-based PDFF measurements decreased from 22.67% to 17.42% following temperature correction. When re-warmed to 11 °C, the measured fat fraction increased. However, it only recovered to 80% of the initial measurement during static cold storage (Figure 5.5C). Further increasing the water bath temperature (to 30 °C for Liver 1 and 35 °C for Liver 2) increased the measured fat fraction to a maximum of 128% of the first measurement during static cold storage. However, as with calculated temperature and T_1 values, the calculated fat fraction was still increasing when the experiment was stopped suggesting that thermal equilibrium was not reached.

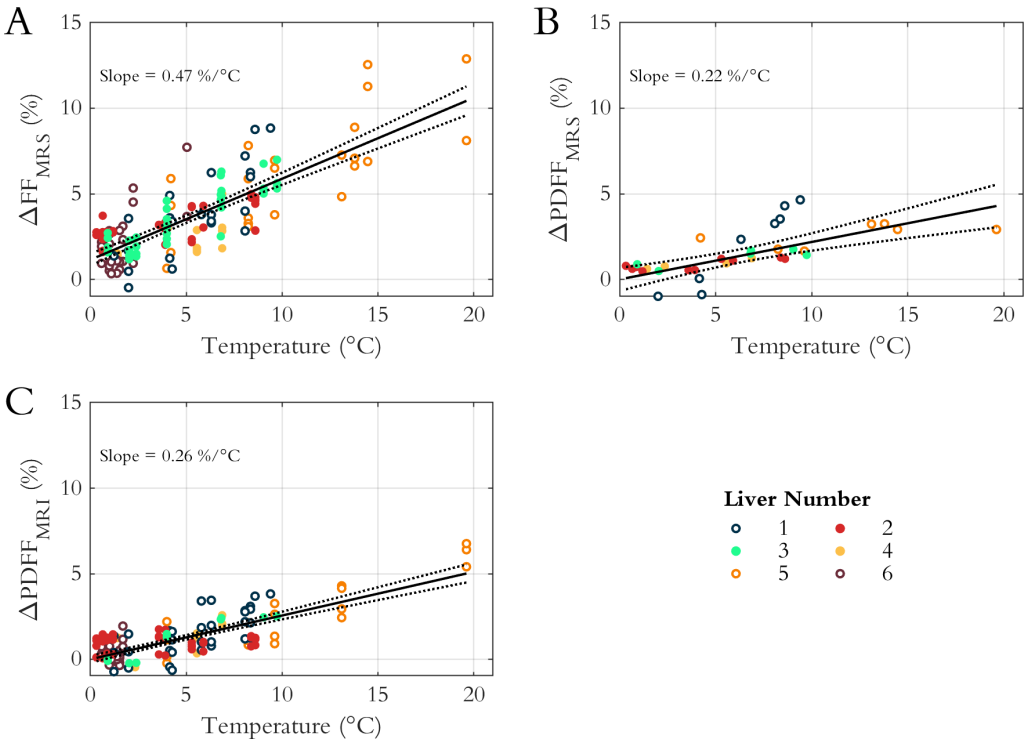


Figure 5.6: Variation of calculated fat fraction as a function of temperature for STEAM single voxel spectroscopy (A), a T_1 and T_2 corrected multi-TR multi-TE STEAM single voxel spectroscopy (B), and a multi-echo GRE imaging sequence (C).

5.4.5 Correlation of imaging parameters with histology and liver function

Figure 5.7 shows the significant correlations of temperature-corrected imaging-based PDFF and spectroscopic fat fraction with macrovesicular steatosis content measured in biopsy samples ($\rho = 0.57$ and 0.52, $R^2 = 0.33$ and 0.41, $P < 0.05$ for imaging PDFF and spectroscopic fat fraction respectively).

The correlation of spectroscopic PDFF with macrovesicular steatosis was also positive but non-significant ($\rho = 0.54$, $R^2 = 0.29$, $P = 0.34$) Correlations of shMOLLI T_1, STEAM-IR T_1, and multi-TR, multi-TE T_1 values with NAFLD activity score measured from biopsies were also positive but not statistically significant ($P = 0.99$, 0.49, and 0.69 respectively. Figure 5.8).

Significant differences were observed in shMOLLI T_1 and STEAM-IR T_1 between the livers deemed functional by the viability criteria and those deemed non-functional (520 $\pm$ 48 ms versus 676 $\pm$ 34 ms, $P = 0.01$, for shMOLLI T_1 and 636 $\pm$ 50 ms versus 762 $\pm$

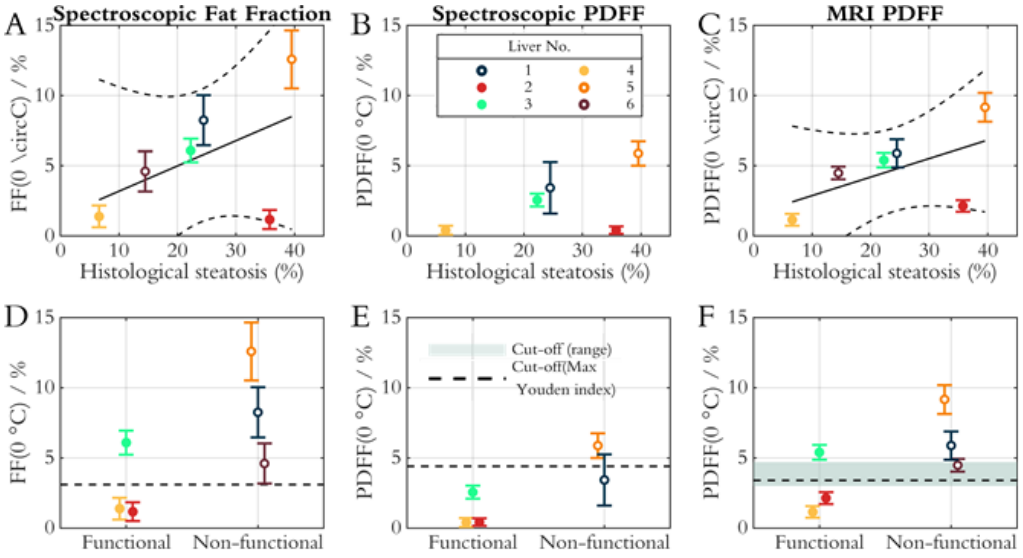


Figure 5.7: Correlations of fat fraction and proton density fat fraction measurements with histological and functional assessment biomarkers in ex vivo human livers. (A) Correlation of temperature corrected spectroscopic fat fraction, FF(0 °C), with macrovesicular steatosis measured from biopsy samples using ImageJ. (B) and (C) show the same correlations for temperature corrected proton density fat fraction, PDFF(0 °C), acquired using spectroscopy and imaging methods respectively. (D - F) show FF(0 °C) and PDFF(0 °C) values for livers deemed functional during normothermic machine perfusion using the viability criteria and those deemed non-functional. Possible cut-off values for differentiating functional and non-functional livers are presented at the maximum Yoden Index and as a range which all achieve >80% sensitivity and specificity.

25 ms, $P = 0.02$, for STEAM-IR T_1). Livers deemed functional also had a trend towards lower fat fraction and PDFF than livers deemed non-functional, but this trend was not significant (2.9 ± 2.8% in livers deemed functional versus 8.5 ± 4.0% in those deemed non-functional using spectroscopic fat fraction, $P = 0.12$, or 2.9 ± 2.2% versus 6.5 ± 2.4%, $P = 0.13$ using imaging-based PDFF). No significant differences were observed in T_2 or T_2^* between functional and non-functional livers (5.4 C and D). A range of cut-off values for T_1 and PDFF would separate functional from non-functional livers with sensitivity and specificity >80% in the small group of livers assessed in this study (see Table 5.5).

5.5 Discussion

This study demonstrates that temperature is a significant confounding factor for MRI- and MRS-based fat fraction and T_1 measurements in ex vivo human livers during static

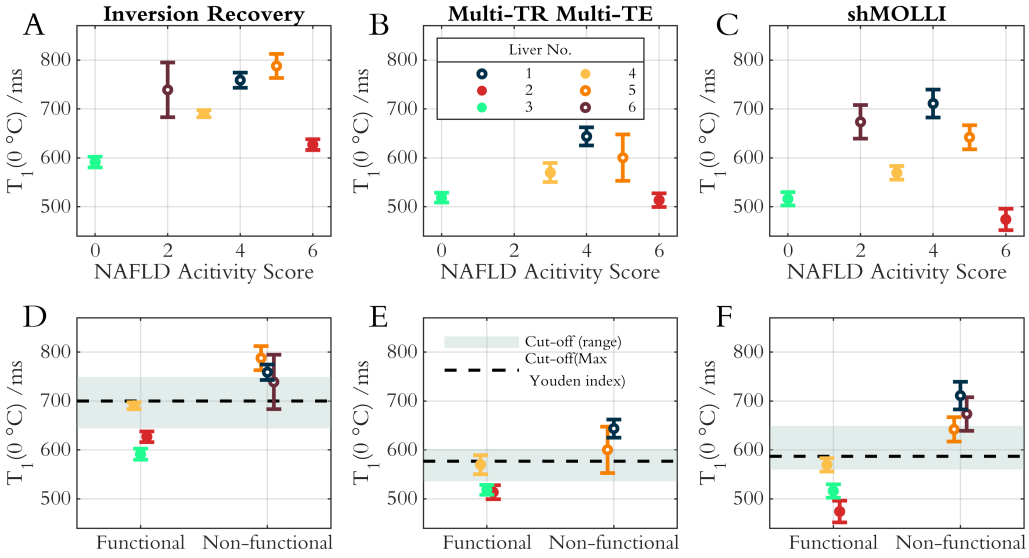


Figure 5.8: Correlations of three different measures of T_1 with histological and functional assessment biomarkers in ex vivo human livers. (A) A positive but non-significant correlation of spectroscopic inversion recovery T_1 with Non-alcoholic fatty liver disease (NAFLD) activity score. (B) and (C) show similar correlations of NAFLD activity score and T_1 measured using multi-TR multi-TE spectroscopy and shMOLLI respectively. (D-F) show differences in T_1, measured using the same three techniques, between livers deemed functional during normothermic machine perfusion using the viability criteria and those deemed non-functional. Significant differences were observed in both inversion recovery T_1 and shMOLLI T_1 values between functional and non-functional livers ($P < 0.002$). Possible cut-off values for diagnosing non-functional livers are presented at the maximum Yoden Index and as a range which all achieve >80% sensitivity and specificity. Differences in T_1 measured using multi-TR, multi-TE spectroscopy between functional and non-functional livers were not assessed for statistical significance due to the lack of data for Liver 6.

cold storage. Therefore, I propose a correction to enable the estimation of temperature independent values. Temperature-corrected values of T_1 were predictive of liver function during normothermic machine perfusion and fat fraction showed promise for non-invasive assessment of steatosis level, which may also be predictive of liver function.

The temperature changes of more than 9 °C are in-line with previous invasive temperature measurements of livers during static cold storage [94 217] and highlight the importance of accounting for any temperature effects in proposed biomarkers. The fat-water frequency offset provides a reliable non-invasive temperature measurement in ex vivo human livers livers with an average error of ±1.13 °C compared to the gold-standard fibre-optic temperature probe measurements. This error is only slightly larger than the reported ±0.8 °C uncertainty of the fibre optic temperature probes. [157] Some of the additional variation is likely due to

Table 5.5: Possible cut off values for temperature corrected T_1 and fat fraction measured in static cold stored ex vivo human livers for differentiating between functional and non-functional livers. The cut-off value which maximises the Youden index is presented, together with the range of cut-off values that achieve sensitivity and specificity >80%. Further work will be needed to recommend and validate a specific cut-off for clinical studies.

	Cut-off value range (ms)	*Cut-off value with maximum Youden index (ms)*	*Maximum Youden index*
IR spectroscopy T_1	644 - 749	700	0.96
Multi-TR multi-TE spectroscopy T_1	536 - 602	577	0.86
shMOLLI T_1	560 - 649	587	1.00
	Cut-off value range (%)	*Cut-off value with maximum Youden index (%)*	*Maximum Youden index*
FF_{MRS}	-	3.2	0.25
$PDFF_{MRS}$	-	4.4	0.71
$PDFF_{MRI}$	3.0 - 4.7	3.4	0.84

spatial variation in liver temperature and the differing effect this will have on the point measurement from the fibre optic temperature probe and global average calculated by the fat-water offset measurements. The temperature sensitivity of fat-water frequency offset in ex vivo human livers flushed with HTK preservation solution is very similar to reported values in phantoms[92] and a range of animal tissues.[172] This suggests that although the technique is only validated for ex vivo human livers in this study, it is likely applicable more widely to studies of other ex vivo human organs.

Making multiple measurements of the same organs over time and fitting the measured values to a linear mixed model enabled the background variation due to underlying pathological variability and differing donor histories to be removed. This provided tight estimates of the temperature sensitivity of the MR parameters studied. The three different T_1 quantification methods used all showed very similar sensitivities to temperature, which suggests that other confounding effects that influence shMOLLI T_1 measurements but have smaller effects on spectroscopic inversion recovery T_1 measurements (for example tissue iron concentrations[212]) are independent confounders whose influence may not itself be sensitive to temperature. Out of the three T_1 measurement techniques examined, shMOLLI

had the highest dispersion of measured T_1 values. This may be due to regional variation within the liver because shMOLLI was measured in four regions of interest compared to the single voxels for the spectroscopic techniques. Therefore, if there is spatial variation in the temperature of the liver the shMOLLI T_1 measurements may reflect this. Equally, shMOLLI T_1 is known to be confounded by the presence of fat within the liver and, given the distribution of liver fat may not be homogeneous, this could also be adding additional noise into the shMOLLI T_1 measurements.

The substitution of blood with HTK preservation solution and removing the liver from the body appear to have little effect on the temperature sensitivity of liver T_1 given the comparable values reported in this study and a study by Zech et al. who assessed the liver T_1 temperature sensitivity in human cadavers.[237] Zech et al. measured liver T_1 using an inversion recovery sequence during MR post-mortem examinations and reported a temperature sensitivity of 11.026 ms/°C.[237] Additionally, they noted very little or no temperature sensitivity of T_2 in cadaveric livers, which is consistent with this study's findings in ex vivo human livers.

Significant linear correlations were also seen for the variation of fat fraction and PDFF measurements with temperature ($\rho > 0.65$, $R^2 > 0.42$, $P < 0.001$). Unlike T_1 however, the different fat fraction and PDFF measurement techniques showed large differences in temperature sensitivity. The spectroscopic and imaging-based PDFF methods had similar sensitivities. However, the simple spectroscopic fat fraction was approximately twice as sensitive to temperature. This suggests that calculating PDFF, by performing a T_1 and T_2 correction to the spectroscopy data or frequency correction to the fat model used to reconstruct the GRE imaging data, substantially compensates for variation in the measurement due to temperature-induced changes in tissue relaxation parameters. Recovery of liver T_1 values to approximately their initial values upon re-warming of the tissue to 11 °C and the further increase with additional warming indicate that the trends observed in this study are a true function of temperature rather than preservation time.

I believe most of the remaining variation in measured PDFF or fat fraction could be due to a partial change of state in the fat. At cold temperatures, I suggest that some of the

hepatic macrovesicular fat droplets begin to solidify and then become 'MR invisible' due to the extremely short T_2 values seen in the semi-solid 'frozen droplet' state. This hypothesis would be consistent with results from food science where increased solid fat content has been observed at lower temperatures in a wide range of substances from lard to chocolate.[36] The slower recovery of the measured fat concentration during rewarming could support the hypothesis of a partial state change which could cause a delayed response on warming due to temperature hysteresis effects caused by the rapid re-warming that was performed.

Perfusing the livers before the MR examination enabled standardisation of the initiation of static cold storage and an opportunity to observe the livers during very short durations of static cold storage. This is not feasible during the initial retrieval because the liver sample needs to be transported from the donor hospital to the MR centre – a process which took a minimum of 9 hours in this study.

Additionally, the functional parameters measured during NMP provided a surrogate end-point to enabling a preliminary assessment of the potential of MRI and MRS biomarkers to predict a liver's viability for transplantation. I report the viability criteria defined by Mergental et al.. These criteria have been used to safely transplant 22 livers that had initially been deemed unsuitable for transplantation with 100% 90-day graft survival.[139] They are also used by the NAPLES programme which is transplanting 'high risk' donated livers following this viability assessment.[125] Therefore, these criteria act as a good surrogate marker for a liver's viability for transplantation. However, it is important to note that the negative predictive value of the current cut-offs is not known for human livers as the limits have been set conservatively to prevent post-transplant complications for patients. In this study perfusion was performed for 48 hours, which is not currently performed clinically. However, preclinical porcine studies have demonstrated that livers preserved using NMP for 48 hours can be safely transplanted.[218]

Using the viability criteria to determine a liver's function during NMP, I observed stark differences in T_1 between functional and non-functional livers (520 ± 48 ms versus 676 ± 34 ms, $P = 0.01$ for shMOLLI T_1).

However, this is a hypothesis generating study which is limited by the small number of

livers scanned and use of a surrogate endpoint. Therefore, larger scale prospective clinical trials will be needed to ascertain whether any of the MR biomarkers considered here are actually predictive of post-transplant outcome. Additionally, all of the livers in this study were scanned following NMP and therefore another study would be needed to determine if the MR biomarkers would be predictive in livers preserved solely by static cold storage. Of specific interest would be whether ischaemia reperfusion injury can be detected, or predicted, in livers only undergoing SCS, which have yet to undergo re-perfusion and encounter the damaging metabolic and inflammatory processes that occur. Livers undergoing normothermic machine perfusion after a period of static cold storage have already undergone re-perfusion and hence, although performed in a less inflammatory environment than in vivo, will have sustained most of the ischaemia reperfusion injury they are likely to receive. Therefore, it would be interesting to examine if the signal detected in this study is larger than what would be seen in liver undergoing solely static cold storage.

Previous work has highlighted additional confounding effects on shMOLLI T_1 measurements, such as fat and iron concentrations, and developed corrections for them.[147] These corrections were not performed in this study due to the unknown relationship between these additional confounding effects and temperature. However, the livers in this study showed a negligible temperature sensitivity in the measured T_2 and $T_2^\star$ values. Therefore, with a larger sample size it should be possible to update the model proposed by Mozes et al.[147] for ex vivo applications.

5.6 Conclusion

This chapter has characterised the temperature sensitivity of tissue relaxation parameters and measures of fat fraction in ex vivo cold stored human livers. I have then proposed a temperature correction for T_1, fat fraction and PDFF measurements that improves the coefficients of reproducibility of these techniques. Finally, I have demonstrated on the basis of 6 livers that metrics from MRI assessment during cold storage correlate with an established viability scoring system applied during NMP. Further study in a suitably powered prospective

clinical trial will be needed to test whether this correlation can be used to predict future viability on the basis of MRI assessment during cold storage.

6

Exploring metabolic and structural effects of normothermic machine perfusion in ex vivo porcine livers

6.1 Background

Static cold storage in UW solution has been the standard method of preserving donated livers for transplantation since the 1980s.[15] This has proven to be a cheap, easy and effective method for preserving healthy livers. However, as previously described in Section 2.1.3.3, a significant proportion of donated livers will not be viable candidates for transplantation following preservation by static cold storage and so are discarded. For example, livers from older donors or that are more steatotic or donated following circulatory arrest are commonly discarded.[73 130] This effect is being felt more acutely every year as the population becomes increasingly old and obese.[47 182]

Therefore, enhanced preservation techniques, such as normothermic machine perfusion (NMP), have recently been developed to better preserve these higher risk donated livers. Indeed, in 2018 the COPE consortium showed that continuous NMP could reduce post-transplant graft injury, measured by liver enzyme released, by 50%.[150] More recently,

Mergental et al. have shown that in up to 70% of cases it can be safe to transplant higher risk livers, deemed non-viable for transplantation by all UK transplant centres, when NMP is used for preservation and assessment of the organ.[139]

However, these extended criteria donor livers carry higher risk of post-transplant complications. There is not yet an agreement over the optimum assessment that should be used to determine which can be safely transplanted and which need to be discarded. As the study by Mergental et al. demonstrated, the traditional risk factors (for example: type of donation, donor age, level of hepatic steatosis, and warm or cold ischaemia duration)[228 57] are no longer enough to accurately predict viability. Indeed in a recent study, when a wide range of international transplant experts were all asked whether they would accept or decline the same set of livers for transplantation having been given all of the information that was available to the surgeons who were originally offered the livers, the Krippendorff's alpha coefficient was just 0.11 across all cases and dropped to -0.01 and 0.02 for older and steatotic donors respectively. For reference: Krippendorff's alpha coefficient varies between 1 and -1, where 1 would represent perfect agreement, -1 shows perfect disagreement and 0 reflects no agreement above random chance.[168] In the same study, 45% of the experts stated they would want to perform viability testing of the liver during NMP before deciding on the transplantability in >70% of the cases they were presented with. However, establishing a validated set of biomarkers that can assess liver function and tissue viability during NMP with sufficient sensitivity and specificity to predict both short- and long-term successful post-transplant outcomes has proven challenging. Hence, there remains much disagreement about which biomarkers should be included in the assessment and what the appropriate thresholds are to apply to each biomarker (Tables 2.2 and 2.3 show the range of biomarkers and cut-offs currently being used).

Many of the biomarkers currently considered are indirect assessments of liver function or physiology (eg. flow rates of blood or perfusate biochemistry) and many of the choices of biomarkers and thresholds have been derived through observations from relatively small numbers of cases that had particularly smooth or troublesome post-transplant outcomes. Therefore, one route for optimising the choice of biomarkers used to determine viability

is to better characterise physiological and metabolic changes that occur in livers during NMP, through direct non-invasive measurements of the liver tissue, which may help improve understanding of what changes in the indirect biomarkers mean for the liver. This improved understanding can then feed into an improved choice of biomarkers and cut-offs.

In Chapter 4, I demonstrated how a range of MR techniques could be used to non-invasively study changes in liver metabolism and physiology in two different porcine deceased liver donor models over time. In this chapter, I aim to undertake a similar assessment utilising MRI and MRS techniques to monitor physiological and metabolic changes in ex vivo porcine livers while they undergo an extended period of NMP.

In addition to aiming to increase understanding of existing biomarkers, I also aimed to examine the potential of MR biomarkers to assess viability for transplantation. In Chapter 5, I demonstrated that relaxometry and proton density fat fraction measurements may be useful in determining viability for transplantation in cold stored organs. Therefore, I hypothesised that these biomarkers may show similar potential for assessment of ex vivo livers during NMP. Additionally, as the livers should be more metabolically active during NMP than during SCS, extra assessments of oxidative metablism by ^{31}P MRS and glycolytic metablism using hyperpolarised ^{13}C MRS may also provide useful insight into organ viability.

This study also presented an additional opportunity to assess how well ex vivo normothermic machine perfusion replicates in vivo conditions. Many previous studies have claimed that NMP recreates or maintains a liver in a (near) physiological environment outside the body.[150 25 178] These claims are based predominantly on the livers being supplied with nutrients and oxygen in a blood-based perfusate at physiological temperature and flow rates, which has resulted in signs of normal aerobic metabolism being observed. However, comprehensive comparisons between livers during NMP and healthy in vivo livers have yet to be performed. This is especially true for measures of tissue perfusion where bulk flow through the liver is regularly measured but perfusion at the microvascular level has not been characterised. Given the non-invasive nature of MR measures and the normal ranges for MR parameters I established in Chapter 4, I also planned to examine how close to a normal physiological state NMP manages to achieve while preserving the donated livers.

In Chapter 4, I demonstrated significant changes occurring in the liver that were dependent on the type of donation. Therefore, to explore the impact of donor history on the biomarkers, I used two very different porcine models of organ donation. First, a whole-liver heart beating donor (HBD) model with minimal warm ischemia time and injury during retrieval but an extended, clinically relevant, cold ischaemia time. Then second, a more severe insult model of donation following circulatory arrest with 60 minutes of warm ischaemia and a short period of cold ischaemia afterwards. This second model would be deemed unsafe to transplant by traditional criteria.[26] It has been shown to be a non-survivable porcine model when the liver is only preserved by static cold storage.[190] However, Schön et al. have shown that with the addition of normothermic machine perfusion many livers can tolerate 60 minutes of warm ischaemia and can survive in a porcine transplant model with good post-operative outcomes.[190] Meanwhile, Reddy et al. have shown the sensitivity of porcine livers to periods of cold ischaemia prior to NMP.[179] Hence both of the models considered are livers that have sustained an insult but are potentially viable for transplantation following a period of NMP. The remaining challenge is identifying which specific livers are most likely to survive. This is the topic of this chapter.

6.2 Aims

I aimed to:

- Assess the structural and physiological changes occurring in ex vivo porcine livers during NMP in a variety of clinically relevant models of organ donation.
- Explore the promise of the MR biomarkers to assess liver viability and function during normothermic machine perfusion.
- Examine how effectively an MR-compatible NMP circuit can replicate in vivo conditions.

6.3 Methods

6.3.1 Study design and animal models

Livers were retrieved from nine female White Landrace pigs (55 - 65 kg). Liver procurement was performed using a standard technique under general anaesthesia.[27] During retrieval, all livers were flushed with ice cold preservation solution as per standard clinical practice.[15] Livers were then transported to the MRI department via static cold storage before either undergoing 30 hours of NMP or continued SCS while MR examinations were performed. Two donor models were used in this study: a heart beating donor (HBD) with minimal warm ischaemic time and a non-heart beating donor with 60 minutes of warm ischaemia (NHBD-60). A summary of the study protocol is presented in Figure 6.1.

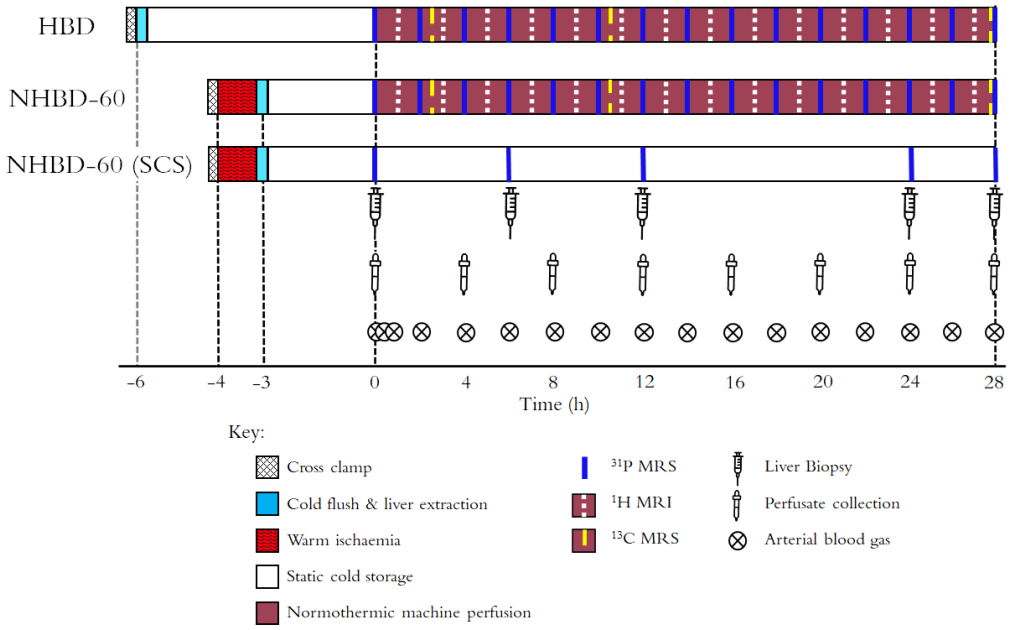


Figure 6.1: Summary of the study procedures. Abbreviations: *heart beating donor, HBD; non-heart beating donor, NHBD; static cold storage, SCS*

6.3.2 Donor procedure

Livers were retrieved under general anaesthesia according to standard clinical practice for an abdominal retrieval following brain-stem death.[27] 20,000 units of unfractionated heparin

were administered intravenously 10 minutes prior to aortic cross-clamping. Blood collection was performed immediately before cross-clamping the aorta by direct puncture of the abdominal aorta with the blood collection needle attached to the blood bag (Compoflex, Fresenius Kabi, Germany). A plasma expander (Gelospan, B Braun Medical Ltd, Sheffield, UK) was infused under gravity during blood collection to maximise the retrieved volume and ensure five bags of blood could be collected. Cold perfusion of the liver was performed down the portal vein and hepatic artery with 3 L of University of Wisconsin solution (UW, Bridge to Life, London, UK) for pigs in the groups scheduled to undergo NMP and histidine-tryptophan-keto gluterate (HTK, Custodiol, Pharmapal Ltd, Hertfordshire, UK) for pigs scheduled to undergo prolonged SCS. HTK solution was used in the SCS group as the high inorganic phosphate concentration of UW solution would not be flushed out and hence would corrupt the ^{31}P-MRS measurements. For the non-heart beating donor organs, the above procedure was followed but a 60 minute stand-off period was observed from the start of functional warm ischaemia and before the cold perfusion. A systolic blood pressure of below 50 mmHg was defined as functional warm-ischaemia and if not observed during blood collection was deemed to begin following cross clamping of the aorta.

6.3.3 Preservation phase

6.3.3.1 Liver preparation

All livers were stored in preservation solution and on ice for three (NHBD-60) or six (HBD) hours during transportation to the MRI department. Livers in the normothermic machine perfusion groups were prepared for NMP as previously described.[132] Briefly, the inferior vena cava (IVC), portal vein, hepatic artery, and bile duct were dissected free from surrounding tissue. Any remaining diaphragmatic tissue was removed and the suprahepatic IVC oversewn with 4:0 prolene sutures (Ethicon, Johnson & Johnson Medical Devices, Wokingham, UK). Haemostasis was meticulously carried out by ligating any small branches of the portal vein or hepatic artery and any lymphatic tissue. The IVC, portal vein, and hepatic artery were cannulated with 28 Fr, 20 Fr and 10 Fr cannulae (Infusion, Warsaw, Poland) respectively. The

common bile duct was cannulated with a 12 - 18 Fr T-tube (Summit Medical, Cheltenham, UK). After cannulation, the livers were primed with 0.5-1 L of Gelofusine (B Braun Medical Ltd, Sheffield, UK) initially down the portal and then arterial cannula. All pockets of air were carefully removed from the vessels and cannulae before perfusion commenced.

6.3.3.2 Normothermic machine perfusion

All livers were perfused using an adapted version of a CE-marked, commercial device which is clinically available for normothermic preservation of donor livers in the UK (*metra*, OrganOx Ltd, Oxford, UK). The device circulates a blood-based perfusate from a reservoir round a closed circuit using a centrifugal pump. A heater/oxygen concentrator warms and oxygenates the perfusate, while in-line Wheatsone bridge pressure sensors and ultrasonic flow sensors read out the fluid pressure and flow rates in the IVC and arterial cannualae. Arterial flow is pressure controlled by automated algorithms which maintain arterial pressure between 60 and 75 mmHg and is delivered continuously (i.e. non-pulsatile flow). The portal vein is gravity fed from the reservoir which is above the liver.

Under the standard conditions, this device is not MR compatible and hence adaptations were made. In previous work submitted as part of a Master of Chemistry "Part II" thesis, I demonstrated that by moving only the organ container into the scanner and keeping the rest of the perfusion device outside of the MR scanner's Faraday cage, which required a 6.5 m extension of the perfusion circuit, a porcine liver could be perfused for 6 h inside an MR scanner.[234] Additionally, I showed that by swapping the standard metal re-enforced cannulae from the CE-marked perfusion circuit to non-metallic alternatives it was possible to achieve homogeneous B_0 and B_1 fields and hence perform imaging and spectroscopic studies on the system. I applied these validated modifications in this study too.

However, the previous system suffered from severe interference between the MRI scanner and pressure sensors on the organ container, whose readings determine the flow rates down the arterial and IVC lines, and unstable perfusion characteristics which prevented an extended duration of perfusion. Therefore, I added an additional low-pass filter to block induced voltages from the imaging gradients ($\sim$50 kHz in frequency) and any induced

voltages from the RF excitation pulses (30 - 120 MHz). Additionally, significant variations in the rates of blood flow were observed depending on the relative position of the pipes, organ container, and perfusion system. Therefore, the perfusion lines were stabilised with supports and the height of the perfusion device adjusted to ensure that the height of the reservoir relative to the organ was exactly matched to the standard circuit while inside the scanner. Figure 6.2 shows the final MR-compatible perfusion system used for all experiments.

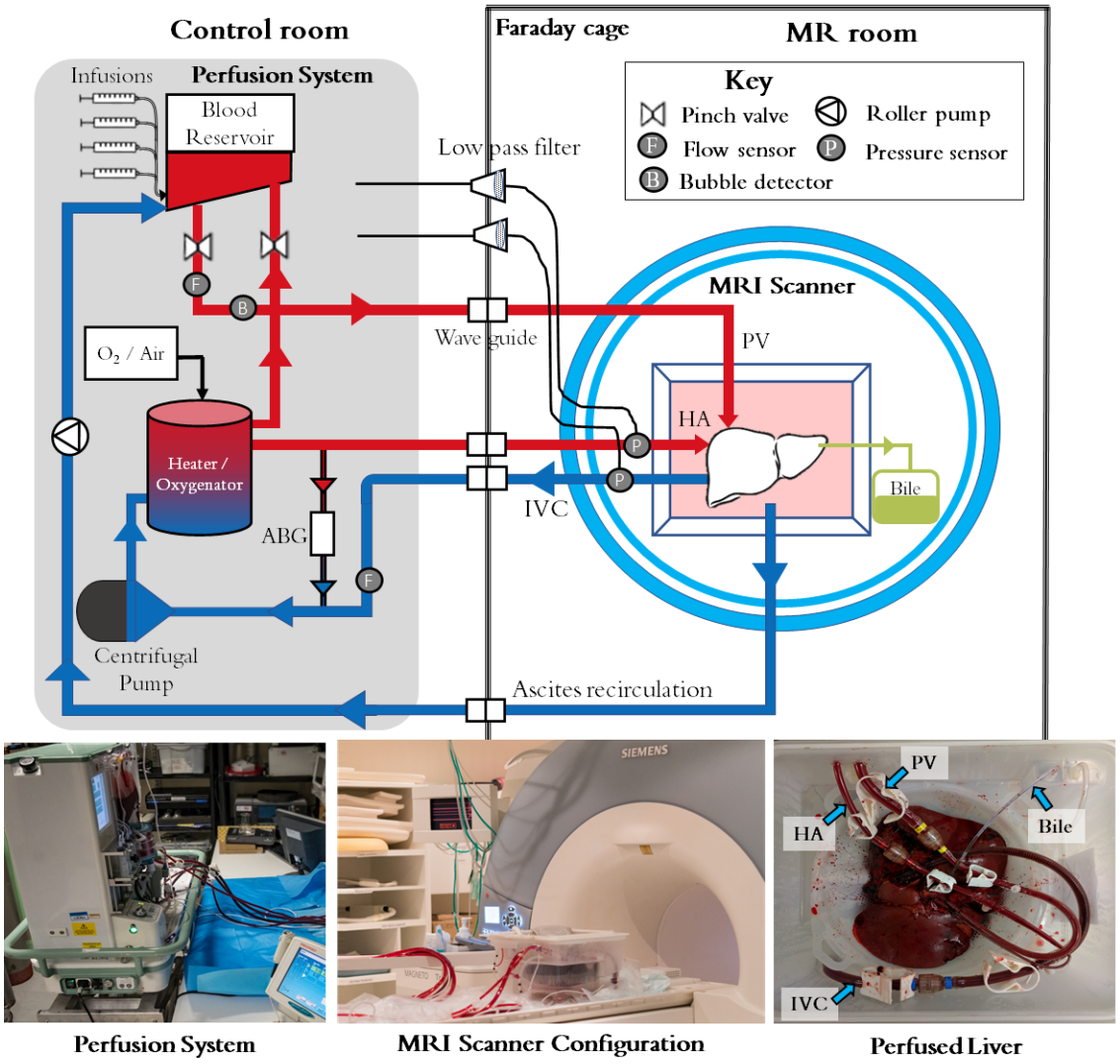


Figure 6.2: Schematic representation of the MR-compatible normothermic machine perfusion system with images of the experimental set-up and a liver undergoing NMP. Abbreviations: *hepatic artery, HA; inferior vena cava, IVC; portal vein, PV.*

Five units of autologous whole blood was combined with 1000 ml of Gelofusine (B Braun Medical Ltd, Sheffield, UK) to form the perfusate, where haemoglobin from the blood acts as the oxygen carrier and the colloid acts as a volume expander. To correct the

binding of citrate to calcium, prevent thrombosis, and protect from bacterial growth in the circuit, boluses of 10 mL 10% calcium gluconate (B Braun Medical Ltd, Sheffield, UK), 10,000 iU unfractionated heparin sodium (Wockhardt UK Ltd, Wrexham, UK), and 750 mg of cefuroxime (Flynn Pharma Ltd, Dublin, Ireland) were added to the reservoir prior to connection of the liver. Once the perfusate reached 37 °C, boluses of 8.4 % sodium bicarbonate (B Braun Medical Ltd, Sheffield, UK) were added to normalise the perfusate pH to physiological levels prior to connection of the liver. Four continuous infusions were performed during perfusion delivering:

- 25,000 IU unfractionated heparin sodium (Wockhardt UK Ltd, Wrexham, UK) to prevent thrombosis.
- 0.5 mg epoprostonol sodium (Flolan, GlaxoSmithKline, Middlesex, UK) to improve micro-perfusion.
- 4.5 g sodium taurocholate (OrganOx Ltd, Oxford, UK) to correct for the loss of entero-hepatic recycling of bile salts.
- 200 units insulin (Actrapid, NovoNordisk, West Sussex, UK) to assist glucose control.

The solutions were made up to 30 mL with 0.9 % sodium chloride solution (B Braun Medical Ltd, Sheffield, UK) and infused automatically at a rate of 1 mL/h. An additional infusion of total parenteral nutrition (TPN)(Nutriflex Special, B Braun Medical Ltd, Sheffield, UK) was performed at a rate of 4 mL/h when the perfusate glucose concentration fell below 10 mmol/L to provide additional glucose and amino acids for maintenance of the liver. Prior to connection of the liver, the device was allowed to reach optimal operating conditions for: temperature (37 °C), pO_2 (12-18 kPa), pCO_2 (4-6 kPa), pH (7.2 - 7.35 kPa).

Continuous monitoring of flow rates, pressures and perfusate parameters (including pO_2, pCO_2, pH, and temperature) were provided by in-line ultrasonic, Wheatstone bridge, and optical fluorescence sensors built into the clinical perfusion system. After 15 minutes of perfusion and then every 2 hrs, a perfusate sample was taken for arterial blood gas analysis on a clinical electrochemical analyser (ABL90 Flex, Radiometer Ltd, Sussex, UK). For the first two hours, additional boluses of 8.4% sodium bicarbonate were administered to

ensure all livers achieved a perfusate pH ≥7.20 according to the in-line sensor. Once a liver had reached a perfusate pH of ≥7.20 no further boluses were administered to allow the observation of the liver's ability to maintain acid-base homoeostasis.

6.3.4 MR assessment

6.3.4.1 ^{31}P-MRS acquisition and analysis

Non-localised pulse acquire spectroscopy was performed using a 10-cm loop ^{31}P coil (PulseTeq Ltd, Surrey, UK). Spectra were acquired every two hours with: TR = 3000 s, TE = 0.85 ms, FA = 90° flip angle, 4 kHz bandwidth, 2048 complex points, 20 averages and 50 measurements. When hyperpolarized ^{13}C-MRS acquisitions were performed (following 2.5, 12.5, and 28.5 hours of perfusion) only 30 ^{31}P-MRS measurements were acquired. All spectra were fitted with the OXSA and FID-A toolboxes in MATLAB (MathWorks, Natick, MA, USA).[193 175] Spectra were collated into hourly averages for processing following phase and frequency alignment.[154] The averaged spectra were then fit using AMARES.[216] A prior knowledge file for the perfusion was generated by first fitting a high SNR spectrum obtained from averaging all available spectra from the perfusion.

6.3.4.2 Hyperpolarised ^{13}C-pyruvate preparation, MR acquisition and analysis

A mixture of 650 mg [1-^{13}C]pyruvic acid (Sigma Aldrich, Gillingham, UK) and 15 mM electron paramagnetic agent (EPA)(AH111501, Syncom, Groningen, Netherlands) was hyperpolarised by dynamic nuclear polarisation (DNP) in a clinical 5T polariser (SpinLab, GE Healthcare, Chicago, USA). Samples were polarised for 3 h to achieve a net polarisation of 40%. A dissolution was performed by forcing 26.7 g of de-ionised water with 100 mg/L EDTA disodium dihydrate heated to 130 °C under 250 psi pressure through the pyruvate containing vessel into a receiver vessel containing 9.95 mL of dissolution media (720 mM NaOH, 400 mM Tris pH 7.6, and 100 mg/L EDTA disodium dihydrate). After mixing, 25 mL of the hyperpolarised, neutralised, 250 mM pyruvic acid solution was rapidly loaded into a 50 mL injection syringe (Bayer, Indianola, USA) and administered directly into the portal

vein of the liver before a 20 mL normal saline (0.9% NaCl, BBraun Ltd) flush. Injections were performed at a rate of 5 mL/s using a power injector system (MEDRAD, Bayer, Berlin, Germany).

A 10 cm loop ^{13}C coil (PulseTeq Ltd, Surrey, UK) was used to acquire non-localised pulse-acquire spectra during and following injection of the hyperpolarised substrate with: TR = 1 s, FA = 10°, bandwidth = 5 kHz, 2048 complex points, 240 measurements. 60 measurements were made prior to injection of pyruvate in order to allow subtraction of thermally polarised baseline signals. Following background subtraction, spectral peaks were quantified using the AMARES algorithm[216] in jMRUI.[199] Following this the resulting metabolic time course data was fit to Zierhut's metabolic model:[241]

$$S_{\mathrm{Pyr}}(t) = \begin{cases} 0 & t < t_{\mathrm{start}} \\ \frac{R_{\mathrm{i}}}{k_{\mathrm{Pyr}}}\left[1 - e^{-k_{\mathrm{Pyr}}(t-t_{\mathrm{arrival}})}\right] & t \in [t_{\mathrm{arrival}}, t_{\mathrm{end}}] \\ M_{\mathrm{Pyr}} e^{-k_{\mathrm{Pyr}}(t-t_{\mathrm{end}})} & t > t_{\mathrm{end}} \end{cases} \tag{6.1}$$

$$S_{\mathrm{x}}(t) = \begin{cases} 0 & t < t_{\mathrm{start}} \\ \frac{k_{\mathrm{Pyr}\to\mathrm{x}} R_{\mathrm{i}}}{k_{\mathrm{Pyr}} - k_{\mathrm{x}}}\left[\frac{1-e^{-k_{\mathrm{x}}(t-t_{\mathrm{arrival}})}}{k_{\mathrm{x}}} - \frac{1-e^{-k_{\mathrm{Pyr}}(t-t_{\mathrm{arrival}})}}{k_{\mathrm{Pyr}}}\right] & t \in [t_{\mathrm{arrival}}, t_{\mathrm{end}}] \\ \frac{M_{\mathrm{Pyr}} \cdot k_{\mathrm{Pyr}\to\mathrm{x}}}{k_{\mathrm{Pyr}} - k_{\mathrm{x}}}\left[e^{-k_{\mathrm{x}}(t-t_{\mathrm{end}})} - e^{-k_{\mathrm{Pyr}}(t-t_{\mathrm{end}})}\right] + M_{\mathrm{x}} e^{-k_{\mathrm{x}}(t-t_{\mathrm{e}})} & t > t_{\mathrm{end}} \end{cases} \tag{6.2}$$

where S_{x} is the signal from metabolite x at time t, R_{i} is the rate of injection, k_{x} is the decay rate of metabolite x, M_{Pyr} is the maximum pyruvate signal, t_{start} and t_{end} are the start and finish times of the injection, and $k_{\mathrm{Pyr}\to\mathrm{x}}$ is the pseudo first order chemical exchange rate constant for the conversion of pyruvic acid to metabolite x.

This model was fitted using a delayed rejection adaptive metropolis Markov chain Monte Carlo (DAM-MCMC) method.[142] DAM-MCMC was initialised with the output from 'lsqcurvefit' and used non-informative priors with a uniform distribution $[0, \infty]$ for all parameters except t_{arrival} and t_{end} which were constrained to fall within the experiment and have $t_{\mathrm{end}} > t_{\mathrm{start}}$. 6×10^3 iterations were performed.

To assess the localisation of the detected metabolic signals in one liver, a spectro-spatial acquisition was performed using a 3-D implementation of hybrid-shot spiral readout (HYSS).[119] A flyback spectral-spatial pulse with nominal flip angles of 6° on pyruvate and 30° on lactate was used to acquire 3 shots of pyruvate and lactate every 4.8 s at 5 mm isotropic resolution. Signal from all reconstructed images was summed to give total pyruvate and lactate signal.

6.3.4.3 ^{1}H-MRI and MRS acquisition and analysis

ShMOLLI T_1maps were acquired using the protocol detailed in Table 4.2. The shMOLLI conditional fitting algorithm was used to calculate T_1 values.[173] Three 15 mm diameter circular regions of interest (ROI) were positioned in the parenchyma of the right lobes of the liver away from any obvious vasculature.

Diffusion weighted images were acquired using a spin-echo echo planar imaging sequence. 10 b-values were acquired ranging from b = 0 to 800 s/mm^2. A complete list of acquisition parameters are given in Table 4.2.

To assess spatial variability, eight ROIs were drawn on the central b = 0 s/mm^2 image of the liver. Two ROIs were placed in each of the left lateral and medial lobes as well as their right equivalents. In each lobe one ROI was placed 1 cm in from the edge of the liver and a second was placed as close to the centre of the liver as possible while avoiding any obvious vasculature. The mean signal intensity from all ROIs at the edge of the liver was calculated for each b-value, before the process was repeated for all ROIs in the centre of the liver. All signal intensities were then normalised to the signal intensity at b = 0 s/mm^2. The variation in normalised signal intensity with increasing b-value was then fit to the tri-exponential model (Equation 3.22) using the segmented fitting method described in Section 4.3.6.2.

6.3.5 Histological assessment

Liver biopsies were acquired with a 18G Biopince™ Full Core Biopsy Instrument (Argon Medical Devices, Texas, USA) using a 33 mm throw length (resulting in a 29 mm specimen length). Biopsy specimens were fixed in 10% formalin solution and stored at 4 °C.

Formalin fixed samples were automatically embedded into paraffin blocks using the standard method.[203] The formalin-fixed paraffin-embedded (FFPE) samples were then sectioned at 4 μm thickness using a microtome prior to staining with Picrosirius red.[203]

6.3.5.1 Histological image analysis

Fibrosis was quantified as the relative area of positive stain to total section area for images of the serial Picrosirius Red-stained sections using an open-source image analysis software (QuPath)[12] using a protocol developed by Pavlides et al..[171] Briefly, the total area of the section was calculated by intensity thresholding, before the image was separated into red, green and blue colour channels. The green colour channel was then thresholded to obtain areas of positive stain. The same threshold for positive stain was used for all images. The positive stain area was calculated using any pixels with intensity less than the threshold value. Finally, the collagen proportionate area (CPA) was calculated as the ratio of positively stained tissue to total tissue area. A summary of the analysis pipeline is shown in Figure

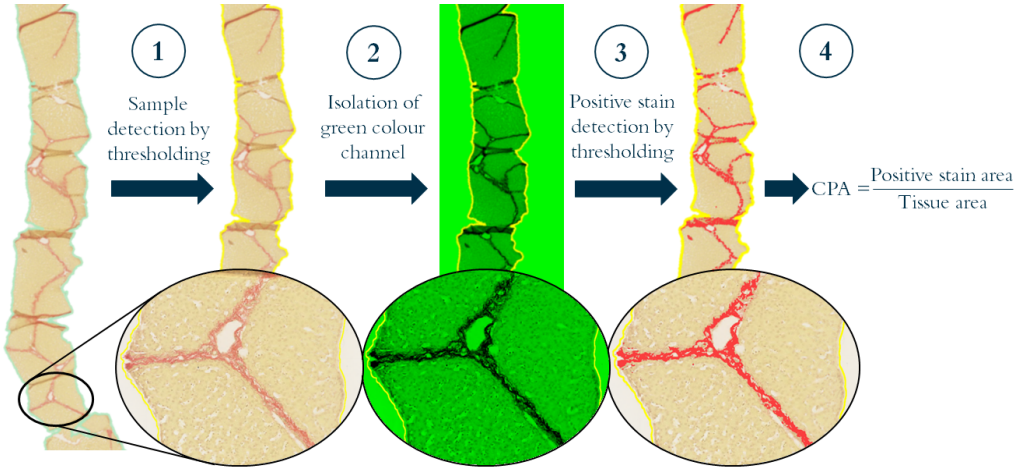


Figure 6.3: Summary of digital image analysis pipeline for calculation of collagen proportionate area (CPA) from Picosirius red stained histology sections.

6.3.6 Biochemical assessment

Perfusate samples were collected for analysis at the Department of Clinical Biochemistry at the John Radcliffe Hospital. Increased demand on the clinical biochemistry team due to the COVID-19 pandemic has delayed processing of the samples. However, samples will be

thawed, vortexed and analysed using spectrophotometry on a clinical biochemical analyser (Abbott Architect c8000, Abbott diagnostics, Illinois, USA) for all of the following:

- Alanine aminotransferase (ALT)
- Aspartate aminotransferase (AST)
- Gamma glutamyl transferase (GGT)
- Bilirubin
- Alkaline Phosphatase (ALP)
- Lactate Dehydrogenase (LDH)
- Haemolysis Index

6.3.7 Functional assessment of livers during NMP

During NMP, hemodynamic parameters were monitored continuously as described above and perfusate blood gas analysis (ALB90 Flex, Radiometer, UK) was performed every two hours throughout perfusion. From these parameters an assessment of viability for transplantation was performed according to the VITTAL criteria.[139] A liver was deemed viable for transplantation if it was able to meet the essential criterion:

1. Clear perfusate lactate to concentrations $\leq$2.5 mmol/L within 4 hrs of perfusion and maintain perfusate lactate $\leq$2.5 mmol/L.

and meet at least two of the following criteria:

2. Maintenance of a stable perfusate pH $\geq$7.30.
3. Evidence of glucose metabolism characterised by a spontaneous fall in perfusate glucose concentration.
4. Hepatic artery flow > 100 mL/min and portal venous flow > 500 mL/min
5. Evidence of bile production
6. Visibly homogeneous perfusion with soft consistency of the parenchyma.

6.3.8 Statistical analysis

Temporal variation of parameters was characterised by repeated measures correlation analysis using the 'rmcorr' package in R (R Foundation for Statistical Computing, Vienna, Austria).[10] This method uses a linear model, with Liver ID and NMP duration as factors, to determine a common regression slope while accounting for the non-independent nature of the observation and inter-liver effects. Previous studies have shown rapid changes in the initial period of perfusion, which do not appear linear in nature. Therefore, only data acquired at or after 6 h of NMP were included in this analysis. The impact of a liver's study group and functional status, as determined by the VITTAL criteria, were assessed using a two-sample Student's t-test to compare the mean of all measurements taken at or after 6 h of NMP.

Equivalence testing was performed, using the two one-sided tests (TOST) method,[191] in order to assess if the MR-compatible perfusion system replicated conditions to either previously published values for livers perfused on the clinical NMP system or the normal in vivo range determined in Chapter 4. For each parameter the upper and lower equivalence bounds were set to be the limits of the reference range, which was derived from the 95% prediction interval of the measured in vivo or reported standard NMP reference data as specified for each parameter.[87]

If the parameters were found to be not equivalent, the extent of any differences between NMP parameters and the reference ranges was characterised by the percentage difference between the closest limit of the reference range and the measurements from livers during NMP on the MR-compatible circuit.

All statistical hypothesis testing was performed at significance level $\alpha = 0.05$.

6.4 Results

6.4.1 Clinical assessment

A summary of the changes observed in the biochemical and haemodynamic parameters considered in the VITTAL criteria are presented for all perfusions in Figure 6.4. Four livers

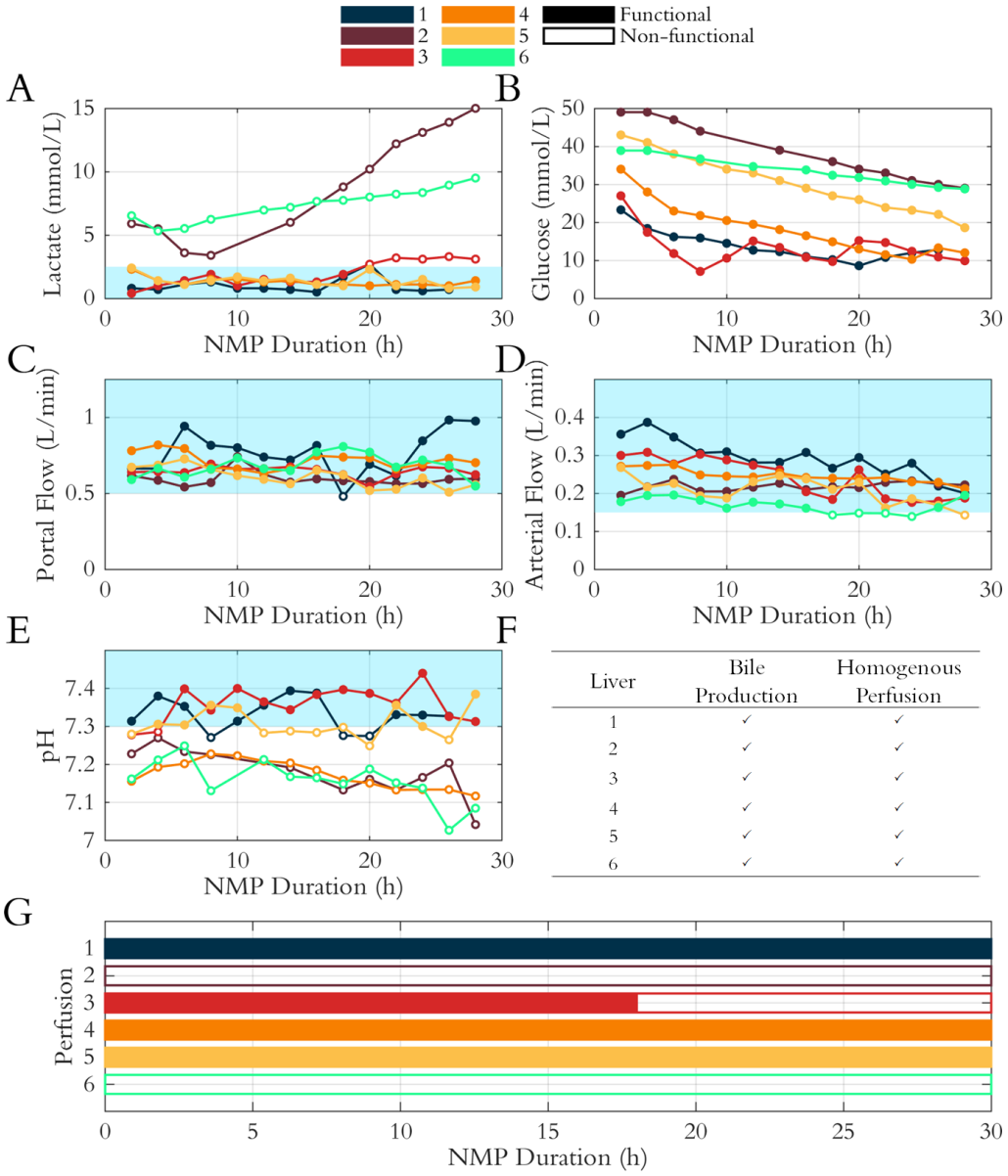
cleared perfusate lactate levels to below 2.5 mmol/L within the first four hours of perfusion and three of these livers maintained lactate concentrations below the VITTAL threshold for the duration of perfusion. The two remaining livers, numbers 2 and 6, showed evidence of some lactate clearance with maximum decreases of 0.95 and 0.61 mmol/L/hr respectively. However, both livers failed to reduce their lactate concentrations below the threshold defined in the VITTAL criteria at any point during perfusion. Liver 3 initially cleared perfusate lactate to a minimum concentration of 0.4 mmol/L following 2 hrs of perfusion but began to show increasing lactate levels following 8 hrs of perfusion reaching a peak of 4.1 mmol/L by the end of the experiment. Therefore, applying the lactate clearance requirement, Livers 2,3, and 6 were deemed non-functional by the VITTAL criteria.

In addition to meeting the lactate clearance criteria, Livers 1,4, and 5 also met at least two of the additional viable criteria, with all three showing good metabolism of glucose; stable and clinically acceptable flow rates down the hepatic artery and portal vein; production of bile within the first 4 hours of perfusion and visibly homogeneous perfusion. Livers 1 and 5 also maintained perfusate pH at >7.30. Liver 4 showed increasing acidosis of the perfusate in the later stages of the experiment with a decrease in pH from 7.23 following 8 hours of perfusion to 7.11 at the end. Nevertheless, this liver was deemed functional as it still met a sufficient number of the additional VITTAL criteria.

6.4.2 Haemodynamic and tissue perfusion assessment

6.4.2.1 Haemodynamic assessment

Table 6.2 shows that the mean arterial pressure was stable throughout perfusion and equivalent to the range of values seen in porcine livers perfused on the clinical perfusion system (65 ±4 mmHg, P_{diff} <0.001). Arterial pressure was also consistent between livers with no significant differences detected between the HBD and NHBD-60 groups (P = 0.93) or between livers deemed functional or non-functional by clinical criteria (P = 0.56). The mean arterial and portal flow rates for all livers across the whole of perfusion were 229 ±53 mL/min and 698 ±106 mL/min respectively, which are both greater than the minimum clinically acceptable



Liver	Bile Production	Homogenous Perfusion
1	✓	✓
2	✓	✓
3	✓	✓
4	✓	✓
5	✓	✓
6	✓	✓

Figure 6.4: A summary of the biochemical and haemodynamic parameters included in the VITTAL viability criteria during each perfusion (A-F). Summary of whether the liver would be deemed viable by the VITTAL criteria at each time (G). Liver 3 which initially met the VITTAL criteria but then failed the criteria at later stages of the experiment is considered non-viable in all subsequent analysis.

flow rates (150 mL/min and 500 mL/min for arterial and portal flow rates respectively)[139]. A slight decrease in arterial flow with increasing perfusion duration was observed (-2.5 ml/min/h, $P < 0.001$), decreasing from 262 ±66 mL/min to 194 ±28 mL/min from the second hour to the final hour of perfusion. Arterial flow was slightly decreased in the NHBD-60 group compared to the HBD livers and for livers deemed non-viable vs those deemed viable, although these trends were not statistically significant (203 ±38 mL/min for NHDB-60 vs 244 ±31 mL/min for HBD, $P = 0.22$ and 206 ±36 mL/min for non-viable livers vs 241 ±39 mL/min for livers deemed viable, $P = 0.31$). Regardless of group or functional status, all livers showed arterial flow rates on the MR-compatible system that were equivalent to previously reported values for porcine livers on the clinical perfusion system ($P_{diff} = 0.007$). In contrast, Figure 6.5 shows how portal flow was 10% lower for livers on the MR-compatible system than the limit of previously reported values from the clinical system and hence not equivalent ($P_{diff} = 0.93$). No significant differences were detected depending on donor type or functional status ($P > 0.46$).

The system also maintained a standard temperature with a perfusate temperature of 36.8 ±0.06 °C.[218]

6.4.2.2 Tissue perfusion and diffusion assessment

Perfusion and diffusion parameters derived from IVIM scans were compared between the inner portion and outer edges of the liver lobes. No significant differences were detected ($P > 0.42$). However in 11 measurements across the first 12 h in three livers, a tri-exponential fit resulted in no intermediate compartments and instead both D^*_1 and D^*_2 were the same very fast value. In these cases, the perfusion fraction fitted to these components was combined into the perfusion fraction of the fast compartment (f_2) and the perfusion fraction of the intermediate compartment (f_1) was set to zero, while the fitted diffusion coefficient of the intermediate compartment was excluded from further analysis as it did not represent the intermediate diffusion compartment.

The temporal changes of the IVIM-derived parameters are shown in Figure 6.6 and Table 6.2. The passive diffusion coefficient (D) in ex vivo perfused livers was equivalent

Table 6.1: Biochemical and MR biomarkers observed in ex vivo porcine livers following ≥6 h of normothermic machine perfusion on an MR-compatible perfusion system. The mean and standard deviation ($\bar{x} \pm \sigma$), results of a two one-sample equivalence test (P_{diff}) and where applicable percentage difference Δ from the normal reference range are shown. Parameters in which the reference range and the measured values were equivalent are shown by ⇔ and parameters which have a mean within the reference range but were not statistically equivalent are represented by a single dash.

Parameter	Reference Range	All livers			Donor type						Functional classification					
					HBD			NHBD-60			Functional			Non-functional		
		$\bar{x} \pm \sigma$	P_{diff}	Δ (%)	$\bar{x} \pm \sigma$	P_{diff}	Δ (%)	$\bar{x} \pm \sigma$	P_{diff}	Δ (%)	$\bar{x} \pm \sigma$	P_{diff}	Δ (%)	$\bar{x} \pm \sigma$	P_{diff}	Δ (%)
Perfusion parameters																
Arterial flow (mL/min)	51 - 451†	223 ±38	0.007	⇔	244 ±31	0.05	⇔	203 ±38	0.02	⇔	241 ±39	0.05	≡	206 ±36	0.02	⇔
Portal flow (mL/min)	744 - 1456†	669 ±73	0.93	-10	675 ±99	0.83	-9	662 ±59	0.89	-11	695 ±95	0.76	-7	644 ±48	0.93	-14
Arterial pressure (mmHg)	29 - 127†	65 ±3	<0.001	⇔	65 ±2	<0.001	⇔	65 ±4	0.001	⇔	64 ±4	0.001	⇔	66 ±2	<0.001	⇔
PaO_2 (kPa)	9.4 -56.6°	15.6 ±1.2	<0.001	⇔	15.5 ±0.4	0.002	⇔	15.7 ±1.0	0.002	⇔	15.4 ±0.6	0.003	⇔	15.9 ±0.7	0.002	⇔
$PaCO_2$ (kPa)	4.1 -7.0°	5.3 ±0.6	<0.001	⇔	5.4 ±0.4	0.003	⇔	5.2 ±0.2	0.003	⇔	5.4 ±0.2	0.003	⇔	5.2 ±0.3	0.006	⇔
Perfusate blood gas analysis																
Lactate (mmol/L)	0.38 - 3.13°	3.56 ±3.72	0.90	+23	4.29 ±4.62	0.92	+36	3.40 ±3.70	0.86	+8.5	1.19 ±0.13	0.02	⇔	6.49 ±3.82	1.00	+107
Glucose (mmol/L)	3.8 - 9.9°	21.9 ±10.4	0.99	+129	20.0 ±13.7	0.98	+101	25.6 ±8.3	1.00	+157	19.0 ±8.4	0.99	+91	26.6 ±12.9	1.00	+167
pH	7.37 - 7.61°	7.25 ±0.10	0.99	-1.7	7.29 ±0.11	0.95	-1.1	7.21 ±0.08	1.00	-2.2	7.27 ±0.08	0.98	-1.4	7.23 ±0.12	0.99	-1.9
Haematocrit (%)	27.1 - 34.6°	9.61 ±4.33	1.00	-65	7.8 ±3.4	1.00	-71	11.0 ±3.5	1.00	-59	10.9 ±3.6	1.00	-60	7.8 ±3.4	1.00	-71
Relaxometry and tissue characterisation																
T_1(ms)	649 - 940°	934 ±102	0.44	-	937 ±76	0.47	-	931 ±143	0.43	-	851 ±11	<0.001	⇔	1018 ±72	0.99	+8.3
Tissue perfusion and diffusion																
f_1 (%)	5.2 - 10.3°	3.98 ±0.97	0.97	-23	4.43 ±0.75	0.84	-14	3.52 ±1.08	0.98	-32	3.28 ±0.75	0.99	-36	4.67 ±0.58	0.76	-9
f_2 (%)	5.8 - 21.7°	7.78 ±1.99	<0.001	⇔	7.80 ±1.19	0.004	⇔	7.95 ±2.91	0.005	⇔	9.16 ±1.25	0.001	⇔	6.58 ±1.83	0.01	⇔
D ($\times 10^{-3}$ mm^2/s)	1.12 - 1.75°	1.53 ±0.15	0.006	⇔	1.42 ±0.13	0.004	⇔	1.65 ±0.05	0.11	⇔	1.57 ±0.15	0.04	⇔	1.50 ±0.18	0.01	⇔
$D^\star_1$ ($\times 10^{-3}$ mm^2/s)	8.38 – 18.91°	17.86 ±6.4	0.34	-	13.49 ±5.75	0.02	⇔	22.24 ±3.45	0.96	+18	16.86 ±7.74	0.24	-	18.86 ±6.29	0.49	-
$D^\star_2$ ($\times 10^{-3}$ mm^2/s)	157 - 380°	147 ±22	0.69	-6	156 ±27	0.52	-1	139 ±14	0.75	-12	161 ±23	0.46	-	134 ±11	0.80	-15

†Reference range derived from reported values of porcine livers on standard clinical NMP perfusion circuit.[218]

°Reference range for healthy in vivo porcine liver and blood, derived from anaesthetised pigs.

Abbreviations: *fat fraction, FF; pure molecular diffusion coefficient, D; psuedo-diffusion coefficient of fast compartment, $D^\star_1$; psuedo-diffusion coefficient of very fast compartment, $D^\star_2$*

Table 6.2: Summary of temporal changes in ex vivo porcine livers during NMP. Data from perfusion durations ≥6 h were considered in this analysis and a linear model applied which accounted for intra-liver variation but assumed a common trend.

Parameter	All livers			Donor type						Functional classification					
				HBD			NHBD-60			Functional			Non-functional		
	Slope	r	*P*	Slope	r	*P*	Slope	r	*P*	Slope	r	*P*	Slope	r	*P*
Haemodynamic analysis															
Arterial flow (mL/min/h)	-2.5 [-3.1, -1.9]	-0.59	<0.001	-1.5 [-2.2, -0.8]	-0.49	<0.001	-3.6 [-4.5, -2.6]	-0.68	<0.001	-2.9 [-3.7, -2.1]	-0.67	<0.001	-2.2 [-3.1, -1.3]	-0.51	<0.001
Portal flow (mL/min/h)	-2.5 [-4.8, -0.3]	-0.19	0.03	-4.4 [-6.9, -1.8]	-0.39	0.001	-0.6 [-4.4, 3.0]	-0.04	0.72	-4.1 [-8.1, -0.1]	-0.25	0.04	-0.9 [-3.0, 1.2]	-0.11	0.39
Arterial pressure (mmHg/h)	0.01 [-0.06, 0.07]	0.02	0.80	0.08 [0.00, 0.16]	0.24	0.05	-0.06 [-0.16, 0.04]	-0.16	0.20	0.08 [-0.01, 0.16]	0.21	0.09	-0.06 [-0.15, 0.03]	-0.16	0.19
PaO_2 (kPa/h)	0.05 [0.02, 0.09]	0.39	0.01	0.07 [0.02, 0.13]	0.42	0.01	0.04 [0.00, 0.08]	0.38	0.03	0.00 [-0.03, 0.03]	0	0.99	0.11 [0.06, 0.17]	0.61	<0.001
$PaCO_2$ (kPa/h)	0.00 [-0.02, 0.02]	-0.02	0.86	-0.01 [-0.04, 0.02]	-0.12	0.5	0.01 [-0.02, 0.03]	0.1	0.58	0.00 [-0.02, 0.03]	0.03	0.85	-0.01 [-0.04, 0.02]	-0.07	0.7
Perfusate blood gas analysis															
Lactate (mmol/L/h)	0.1 [0.1, 0.2]	0.52	<0.001	0.0 [0.0, 0.1]	0.41	0.02	0.2 [0.1, 0.3]	0.66	<0.001	0.0 [-0.1, 0.1]	-0.15	0.39	0.3 [0.2, 0.4]	0.78	<0.001
Glucose (mmol/L/h)	-0.5 [-0.6, -0.4]	-0.78	<0.001	-0.6 [-0.7, -0.5]	-0.95	<0.001	-0.3 [-0.5, -0.1]	-0.58	<0.001	-0.6 [-0.7, -0.5]	-0.89	<0.001	-0.4 [-0.5, -0.2]	-0.64	<0.001
pH (h^{-1})	-0.003 [-0.005, -0.001]	-0.47	<0.001	-0.004 [-0.006, -0.002]	-0.55	<0.001	-0.002 [-0.005, 0.000]	-0.37	0.04	-0.002 [-0.004, 0.000]	-0.35	0.05	-0.004 [-0.006, -0.002]	-0.58	<0.001
Haematocrit (%/h)	-0.2 [-0.3, -0.2]	-0.58	<0.001	-0.3 [-0.5, -0.2]	-0.73	<0.001	-0.1 [-0.3, 0.00]	-0.37	0.05	-0.1 [-0.3, -0.0]	-0.36	0.04	-0.4 [-0.5, -0.2]	-0.75	<0.001
Relaxometry and tissue characterisation															
T_1 (ms/h)	2.8 [1.3, 4.3]	0.44	<0.001	3.8 [1.5, 6.1]	0.52	0.002	1.82 [-0.12, 3.75]	0.33	0.07	0.4 [-1.5, 2.3]	0.08	0.67	5.3 [3.3, 7.3]	0.71	<0.001
Tissue perfusion and diffusion															
f_1 (%/h)	0.00 [-0.05, 0.05]	0.01	0.97	0.03 [-0.06, 0.11]	0.14	0.54	-0.02 [-0.08, 0.05]	-0.10	0.59	0.03 [-0.02, 0.08]	0.25	0.21	-0.03 [-0.12, 0.06]	-0.14	0.51
f_2 (%/h)	0.06 [-0.03, 0.15]	0.17	0.21	0.13 [-0.25, 0.29]	0.32	0.09	-0.02 [0.11, 0.08]	-0.06	0.74	0.12 [-0.02, 0.27]	0.32	0.09	-0.01 [-0.12, 0.11]	-0.02	0.91
D ($\times 10^{-3}$ $mm^2/s/h$)	0.00 [-0.01, 0.01]	-0.06	0.66	0.00 [-0.01, 0.01]	-0.11	0.57	0.00 [-0.01, 0.01]	0.01	0.97	0.00 [-0.01, 0.01]	-0.06	0.77	0.00 [-0.01, 0.01]	-0.06	0.74
D^*_1 ($\times 10^{-3}$ $mm^2/s/h$)	0.13 [-0.29, 0.56]	0.10	0.54	0.39 [-0.43, 1.21]	0.22	0.33	-0.08 [-0.48, 0.32]	-0.09	0.69	0.43 [-0.30, 1.16]	0.28	0.23	-0.2 [-0.7, 0.4]	-0.13	0.53
D^*_2 ($\times 10^{-3}$ $mm^2/s/h$)	0.8 [-0.9, 2.6]	0.13	0.35	-0.9 [-2.4, 0.6]	-0.24	0.21	2.6 [-0.7, 5.8]	0.3	0.12	1.8 [-1.7, 5.3]	0.20	0.29	-0.1 [-1.3, 1.1]	-0.04	0.84

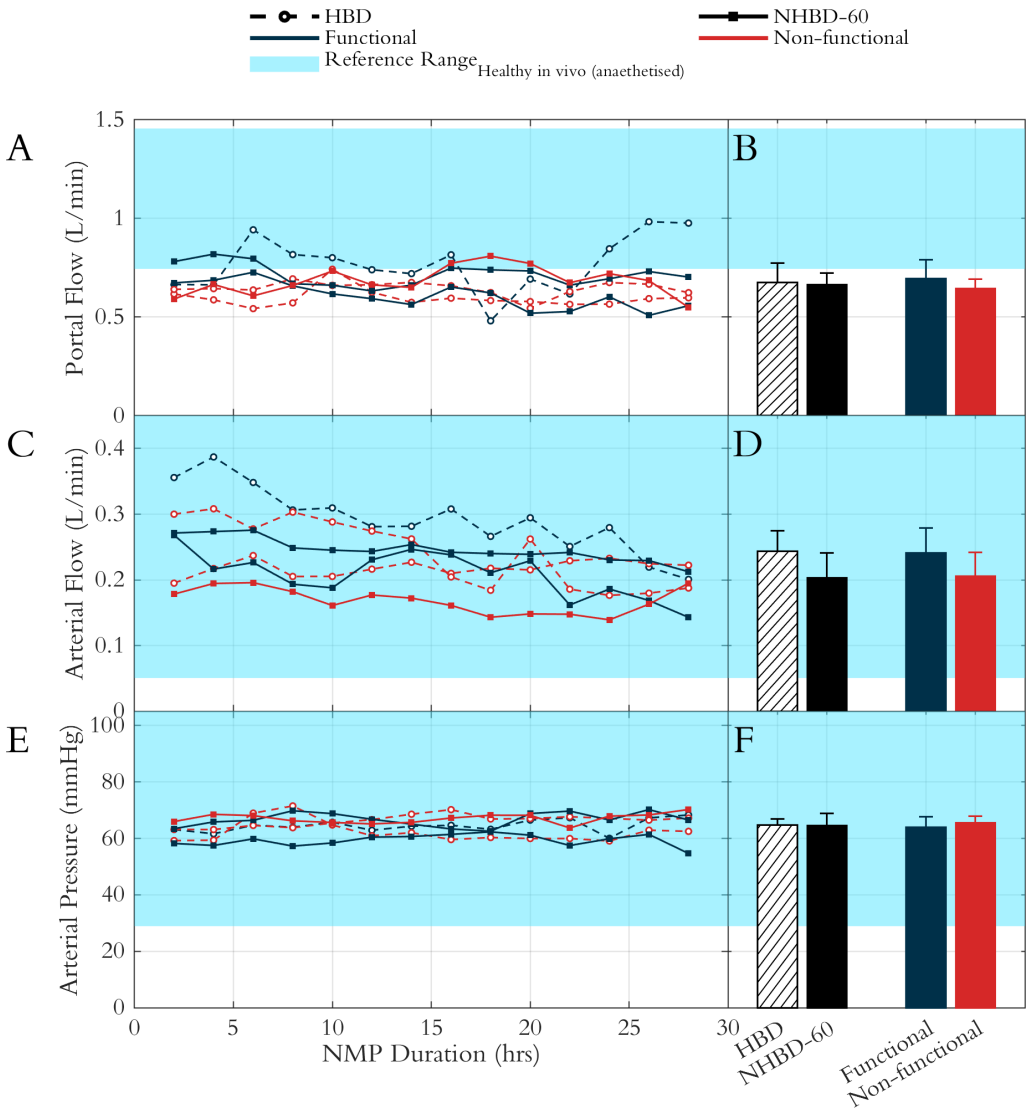


Figure 6.5: Portal flow (A), arterial flow (C) and arterial pressure (E) in porcine livers during NMP on the adapted MR-compatible version of a clinical NMP device. Panels B, D, and F show the mean and standard deviation of the data grouped by donation type (HBD vs NHBD-60) and the livers' functional status according to the VITTAL criteria.[117] The normal ranges for flow rates and pressures for porcine livers on the clinical perfusion system, as reported by Vogel et al., are also shaded pale blue.[218] Abbreviations: *heart beating donor, HBD; non-heart beating donor with 60 minutes warm ischaemia, NHBD-60, normothermic machine perfusion, NMP.*

to values obtained from in vivo porcine liver (P_{diff} = 0.006) and showed no significant variation with time ($P_{temporal\ correlation}$ = 0.66) or functional status ($P_{temporal\ correlation}$ = 0.63). D was increased in livers from non-heart beating donors compared to livers from HBD (1.67 ±0.05 ×10^{-3} mm^2/s vs 1.42 ±0.13 ×10^{-3} mm^2/s, P = 0.04) but both were still within the reference range for healthy in vivo liver (both $P_{diff} \leq 0.01$).

The perfusion fraction of the fast, microvascular perfusion, compartment (f_2) was also equivalent to in vivo values ($P_{diff} < 0.001$) and stable across donor type (P = 0.84). f_2 trended higher in livers deemed functional compared to those deemed non-functional, although this effect was not statistically significant (9.16 ±1.25% vs 6.58 ±1.83%, P = 0.16).

Looking at the linear model slopes in Table 6.2, a trend of increasing f_2 with perfusion duration was seen in livers from HBD and those classified as functional by the VITTAL criteria (+0.13 %/h, P = 0.09, and +0.12%/h, P = 0.09, respectively). No temporal change was detected in livers from NHBD-60 or those deemed non-functional. Although the fraction of signal from the compartment was equivalent to in vivo, a 6% reduction in D^*_2 in ex vivo perfused livers was observed compared to in vivo values and no significant dependence on donor type or functional classification was detected ($P > 0.16$).

In contrast, the intermediate perfusion fraction (f_1) decreased by 23% (P_{diff} = 0.97). The intermediate diffusion coefficient for perfused livers tended to be higher than the in vivo reference range (P_{diff} = 0.34). This effect was more pronounced in livers from NHBD-60, although still not significantly different (P = 0.08).

6.4.3 Perfusate biochemistry

6.4.3.1 Blood gas analysis

The adapted MR-compatible perfusion system was able to maintain stable regulation of blood gas supply to the ex vivo livers within the normal in vivo ranges measured in porcine livers for the duration of perfusion with PaO_2 = 15.6 ±1.2 kPa, $PaCO_2$ = 5.3 ±0.6 kPa respectively (both $P_{equivalence} \leq 0.001$) as shown in Figure 6.7. No significant effect of liver donor type or functional classification were observed ($P > 0.42$).

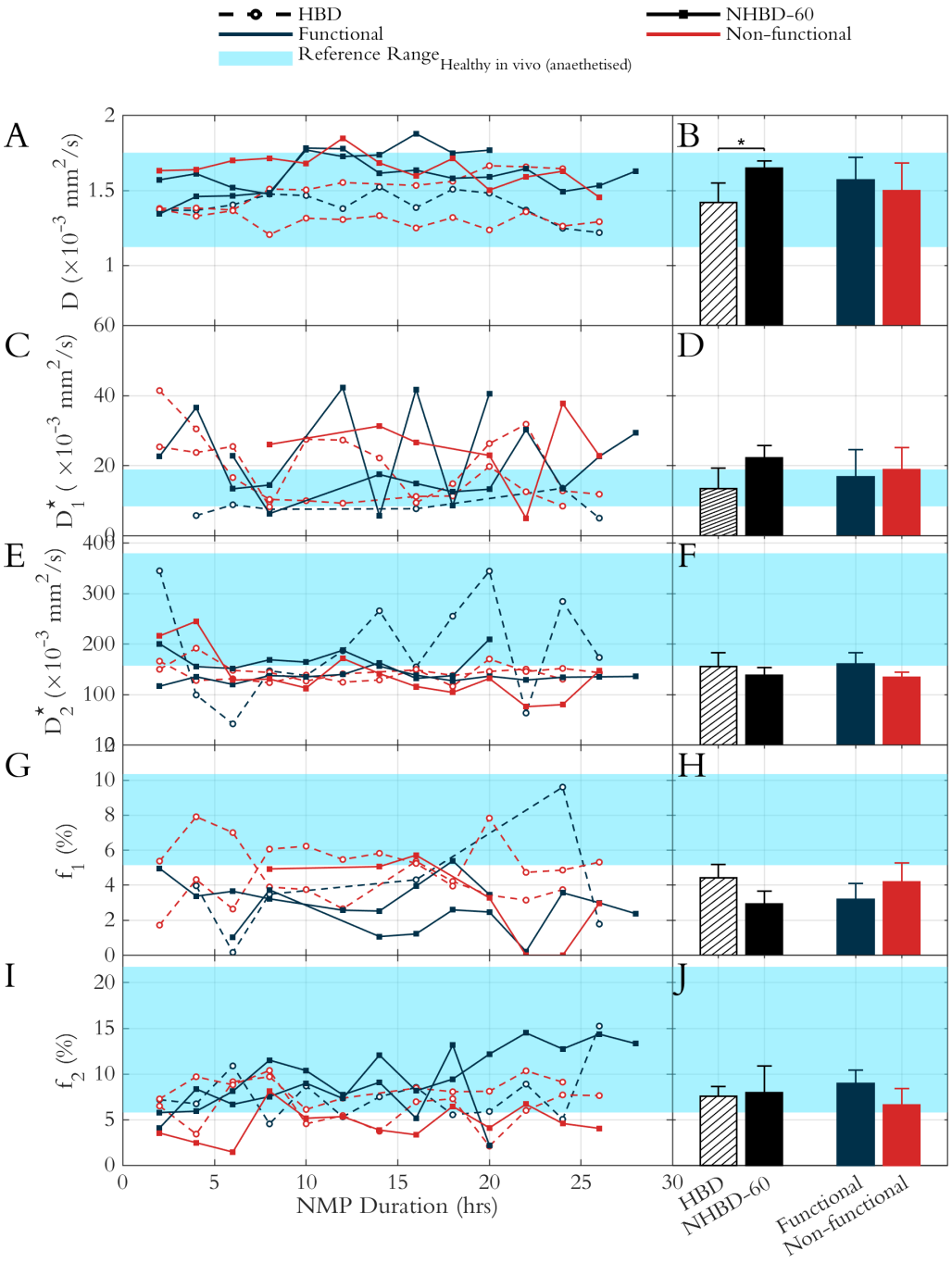


Figure 6.6: Diffusion and perfusion parameters measured using IVIM in ex vivo porcine livers during NMP. Diffusion coefficients for the passive, intermediate, and fast compartments are represented by D, $D^{\star}_1$ and $D^{\star}_2$ respectively. The perfusion fractions of the intermediate and fast compartment are quantified by f_1 and f_2. Panels B, D, F, H, and J show the mean and standard deviation of data grouped by study group (HBD vs NHBD-60) and by liver function according to the VITTAL criteria. The healthy in vivo reference range for each parameter is shown. Abbreviations: *heart beating donor, HBD; non-heart beating donor with 60 minutes warm ischaemia, NHBD-60.*

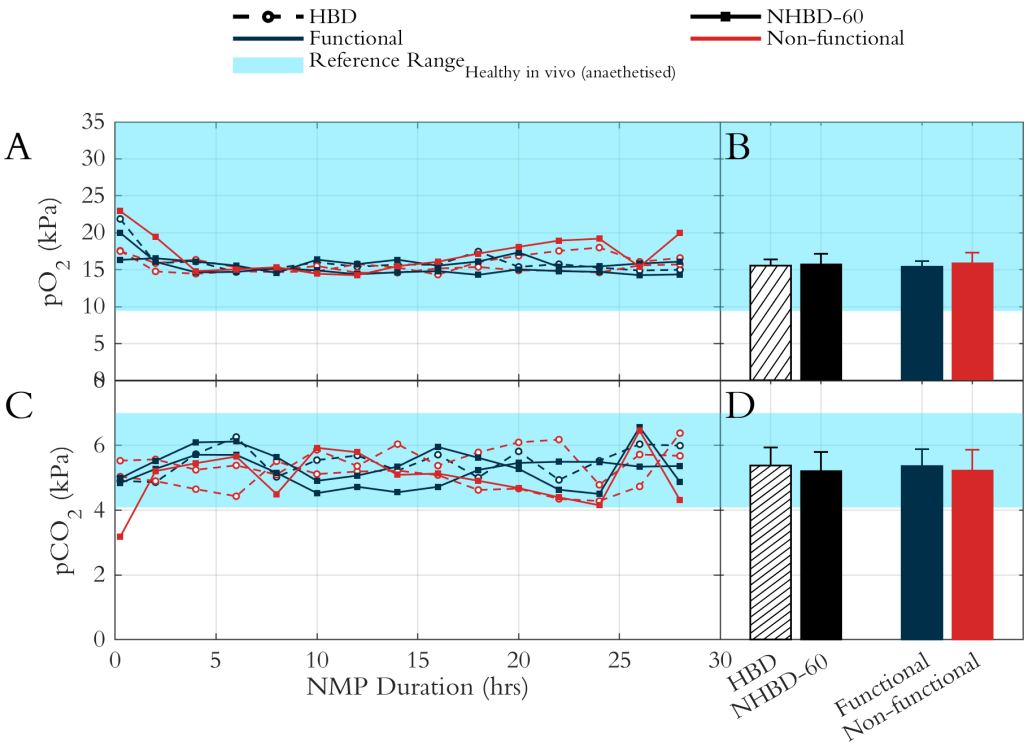


Figure 6.7: Changes in PaO_2 (A) and $PaCO_2$ in porcine livers during NMP on an adapted MR-compatible version of a clinical NMP device. Panels B and D show the mean and standard deviation of the data grouped by donation type (HBD vs NHBD-60) and the livers functional status according to the VITTAL criteria.[117] The reference ranges for in vivo porcine livers are also shown. Abbreviations: *heart beating donor, HBD; non-heart beating donor with 60 minutes warm ischaemia, NHBD-60, normothermic machine perfusion, NMP.*

6.4.3.2 Acid-Base Homeostasis

Aided by boluses of 8% sodium bicarbonate (10 - 40 mL in the first 2 hrs of perfusion) an increase of perfusate pH from 7.07 ±0.06 following 15 minutes of perfusion to physiological levels (7.29 ±0.08) was observed within 4 hours. Livers retrieved from non-heart beating donors had slightly lower perfusate pH than those retrieved from heart beating donors although this trend was not statistically significant (7.21 ±0.08 vs 7.29 ±0.11, $P = 0.33$). Livers deemed viable and non-viable by the VITTAL criteria also showed no significant difference in perfusate pH ($P = 0.69$).

6.4.3.3 Lactate Clearance

Figure 6.8 shows that although initially all livers reduced perfusate lactate concentrations, as perfusion was continued livers from NHBD and those deemed non-functional showed a

trend of increasing perfusate lactate (+0.02 and +0.03 mmol/L/h, $P < 0.001$, respectively). Meanwhile lactate concentration remained stable in livers from HBD and those deemed functional ($P = 0.39$). Only livers deemed functional had perfusate lactate levels equivalent to the in vivo reference range of blood lactate concentration until the end of the perfusion.

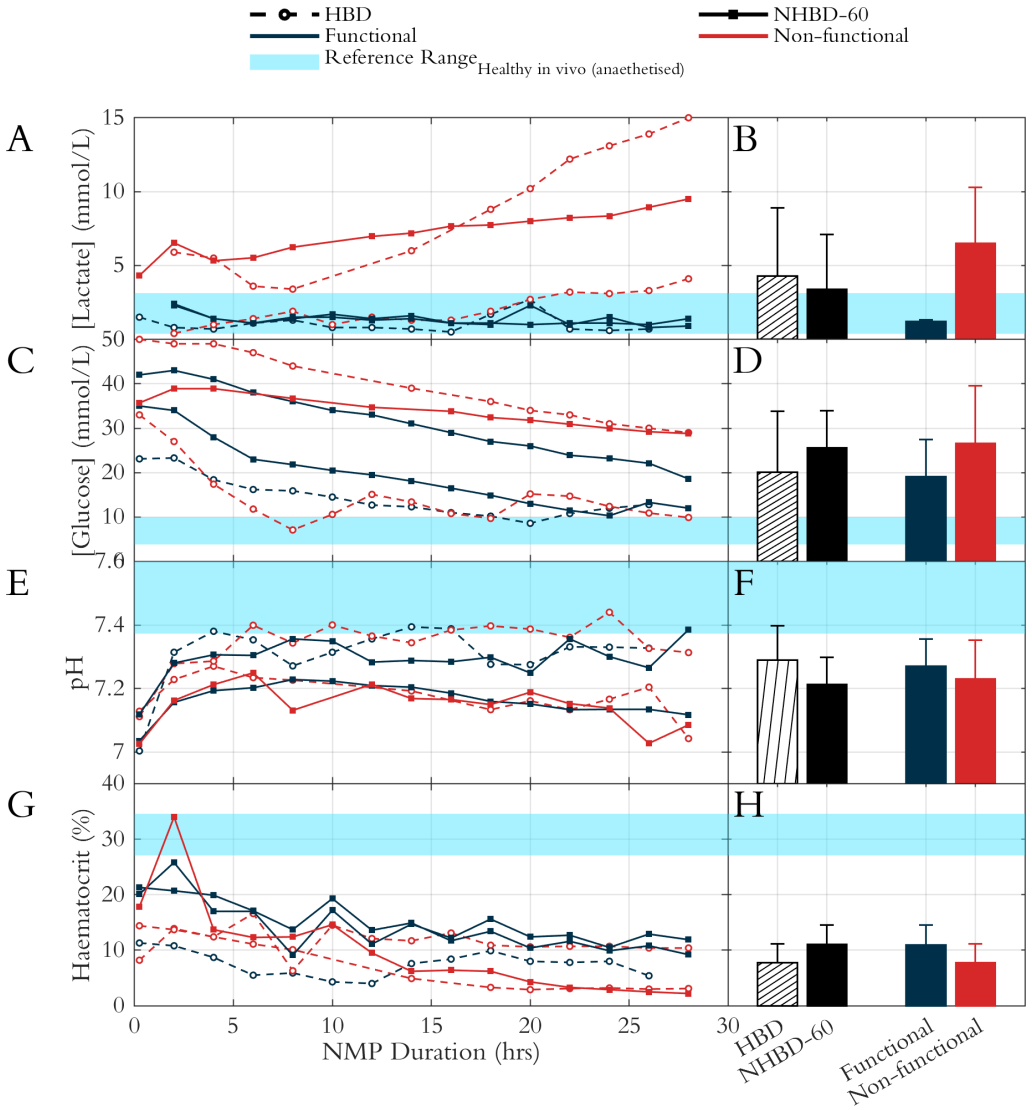


Figure 6.8: Changes in perfusate arterial blood gas parameters from ex vivo porcine livers during NMP. Panels B, D, F, and H show the mean and standard deviation of data grouped by study group (HBD vs NHBD-60) and the liver fuction according to the VITTAL criteria. The healthy in vivo reference range of each parameter are shown. Abbreviations: *heart beating donor, HBD; non-heart beating donor with 60 minutes warm ischaemia, NHBD-60.*

6.4.3.4 Glucose metabolism

Evidence of glucose metabolism was observed in all livers through a significant decrease in perfusate glucose concentration from 36.5 ±9.02 following 15 minutes of perfusion to 18.5 ±8.54 by the end of perfusion ($P < 0.01$). TPN infusions were performed for three livers to maintain perfusate glucose levels above 10 mmol/L to the end of perfusion. Livers 2, 5, and 6 did not require TPN infusion and they all had initial perfusate glucose concentrations > 35 mmol / L. Livers from HBD appeared to have quicker metabolism of glucose during the first four hours of perfusion than livers retrieved from NHBD, although this result was not statistically significant (1.35 ±1.18 mmol/L/h vs 0.28 ±0.89 mmol/L/h, $P = 0.27$). All perfused livers showed increased perfusate glucose compared to the reference range measured in vivo ($P_{diff} = 0.99$).

6.4.3.5 Haematocrit assessment

The perfusate, a mixture of whole blood and colloid volume expander, had a lower haematocrit than in vivo porcine blood (9.61 ±4.33 compared to in vivo reference range of 27.1 - 34.6%, $P_{diff} = 1.00$). Functional livers tended to have a higher haematocrit although this effect was not significant (10.9 ±3.6% vs 7.8 ±3.4%, $P = 0.34$). As perfusion duration increased, the haematocrit decreased (-0.2%/h, $P < 0.001$).

6.4.4 Tissue assessment

6.4.4.1 Fibrosis assessment

Overall, low levels of fibrosis were observed in the livers with an average collagen proportionate area (CPA) of 16.17 ±5.84 % and remained stable with no significant dependence on duration of perfusion observed ($P = 0.64$). Figure 6.9 shows that neither donor type nor functional status were significant predictors of CPA ($P = 0.98$ and $P = 0.41$ respectively).

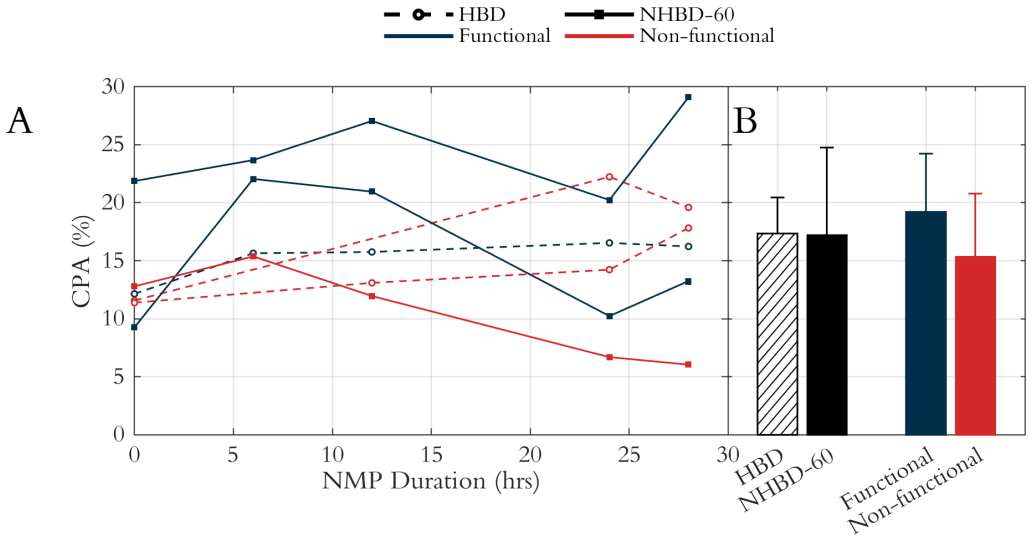


Figure 6.9: Collagen proportionate area (CPA) in ex vivo porcine livers during NMP.

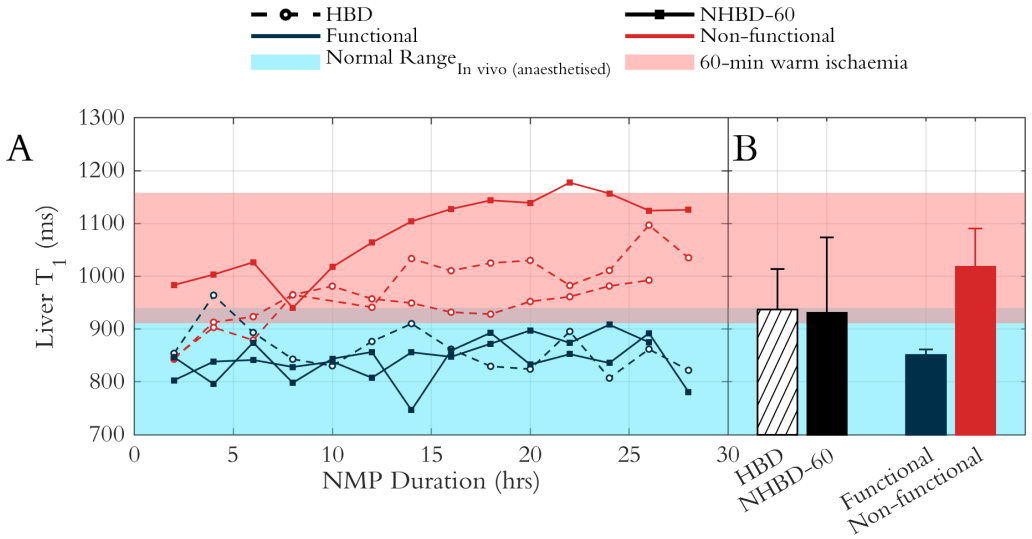


Figure 6.10: Liver T_1 in ex vivo porcine livers during NMP. Panel B shows the mean and standard deviation of data grouped by study group (HBD vs NHBD-60) and the liver function according to the VITTAL criteria. The reference range for liver T_1 in healthy in vivo porcine livers are shown as is the range of liver T_1 for four porcine livers following 1 h of warm ischaemia, which were reported in Chapter 4. Abbreviations: *heart beating donor, HBD; non-heart beating donor with 60 minutes warm ischaemia, NHBD-60.*

6.4.4.2 Relaxometry

Figure 6.10 shows how livers deemed functional by the VITTAL criteria had stable liver T_1 values that were equivalent to those of healthy in vivo tissue (851 ±11, $P_{\text{Temporal dependence}}$ = 0.67, P_{diff} <0.001). In comparison, livers deemed non-functional by the VITTAL criteria had higher T_1 which was above the reference range for in vivo liver and increased throughout perfusion (1018 ±72, P_{diff} = 0.99, rate of increase = 5.3 ms/h, P < 0.001). Liver T_1 showed no dependence on donor type (HBD or NHBD-60) (P = 0.95). Slight spatial variation within the T_1 maps can be observed in Figure 6.11. However, there is no consistent trend in the spatial variation seen and I suggest that this may be down to very slight differences in perfusion within the heavily vascularised porcine livers. Indeed the significant trend shown in Figure 6.11 is the increase in T_1 of livers deemed non-functional during prolonged NMP.

Figure 6.12 shows the strong correlation between liver T_1 and perfusate lactate concentration (r = 0.75, P < 0.001). When stratifying livers by whether they were still functional at the end of perfusion, ie. if they met the lactate requirement of the VITTAL criteria, T_1 varied significantly when considering all measurement time points (851 ±41 for functional livers compared to 1014 ±80 for non-functional livers, P <0.001).

Using the VITTAL criteria as a gold-standard, a range of T_1 cut-off values could achieve >80% sensitivity and specificity for determining function in these livers (877 - 941 ms). Applying a cut-off at the maximum Youden Index would give a threshold T_1 value of 912 ms and differentiated the livers that would be deemed functional until the end of perfusion from those that would not within 4 h of NMP. The lactate based criteria managed the same differentiation but after 20 h of perfusion instead of the 4 h of perfusion needed for discrimination by T_1.

6.4.5 Metabolic assessment

6.4.5.1 Oxidative metabolism

Figure 6.13 shows a sustained increase in ATP as a proportion of ^{31}P signal in all perfused livers for at least the first 4 h of preservation by NMP (6.4 ±3.7% to 9.7 ±3.3%, P = 0.003).

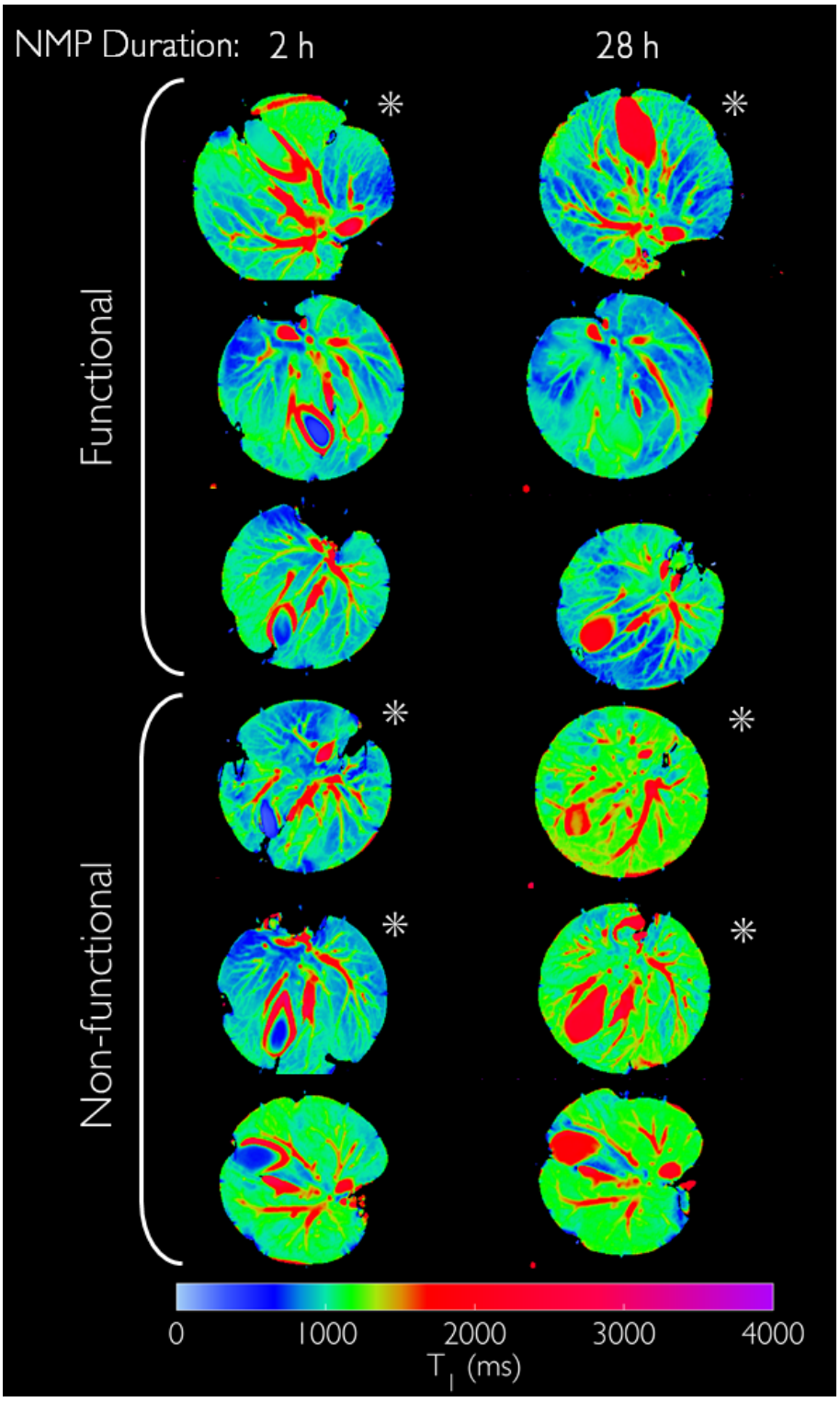


Figure 6.11: ShMOLLI T_1 maps for six porcine livers following 2 and 28 hours of NMP. All images are acquired in the horizontal plane which is approximately equivalent to a transverse section when in vivo. Livers marked with an asterisk were retrieved from heart beating donors while those without an asterisk were acquired from non-heart beating donors with 60 minutes of warm ischaemia prior to cold storage and NMP. The livers function during NMP was determined using the the VITTAL criteria. Abbreviations: *normothermic machine perfusion, NMP.*

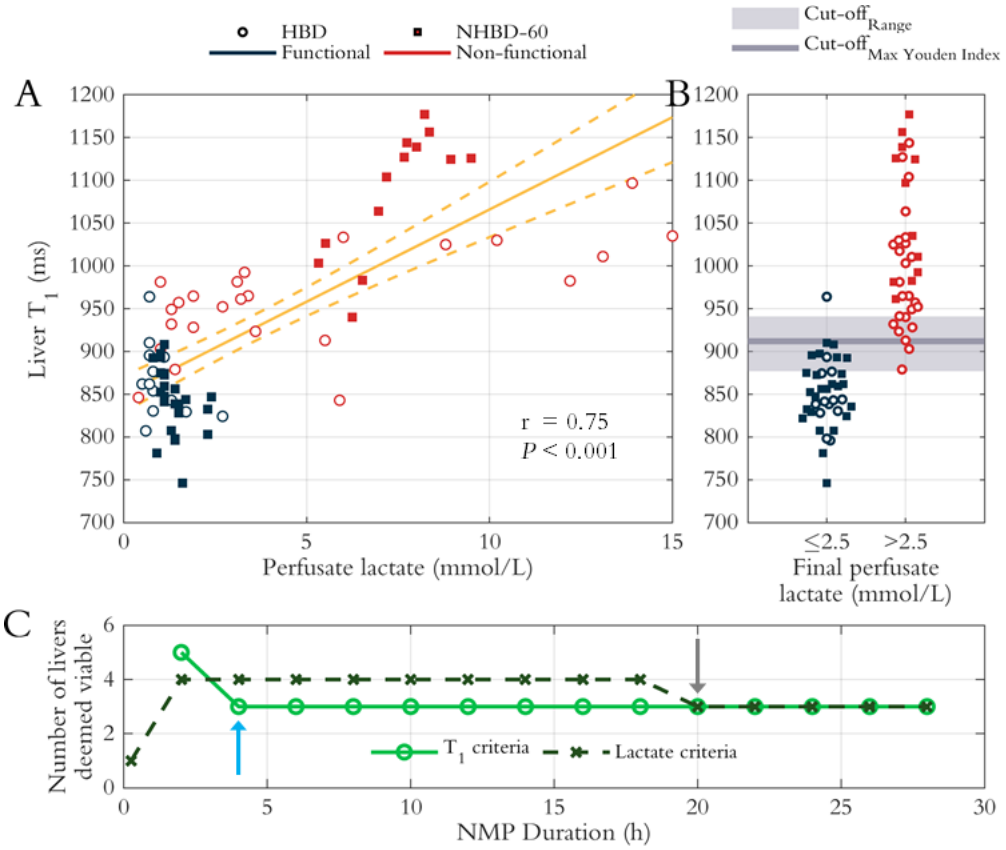


Figure 6.12: Comparison of perfusate lactate and liver T_1 for stratification of functional and non-functional livers. A significant correlation of liver T_1 with perfusate lactate concentration was seen (A). (B) Differences in liver T_1 between livers which are above and below the lactate threshold from the VITTAL criteria at the end of perfusion and a range of possible T_1 cut-off values that could achieve >80% sensitivity and specificity for the same categorisation. C shows how many livers would be deemed viable for transplantation applying either the lactate criteria from the VITTAL definition or the derived T_1 criteria with a threshold of 912 ms (which is the value that maximises the Youden Index in this study). Both methods reach the same conclusion but the T_1 criteria reach this conclusion after 4 h (blue arrow) while the lactate criteria take 20 h (grey arrow).

After the initial increase, ATP content remained stable in 4 livers. Livers 2 and 3 showed a slight decrease in ATP content from 6 h to 28 h perfusion. Both livers that showed a trend of decreasing ATP content were deemed non-functional by the biochemical criteria.

No significant differences were observed in ATP content between HBD and NHBD-60 livers ($P = 0.35$). However, livers preserved solely by SCS had significantly lower ATP content ($P = 0.005$), with no visible β- or γ-ATP peaks visible in the ^{31}P spectrum by the end of perfusion (Figure 6.14).

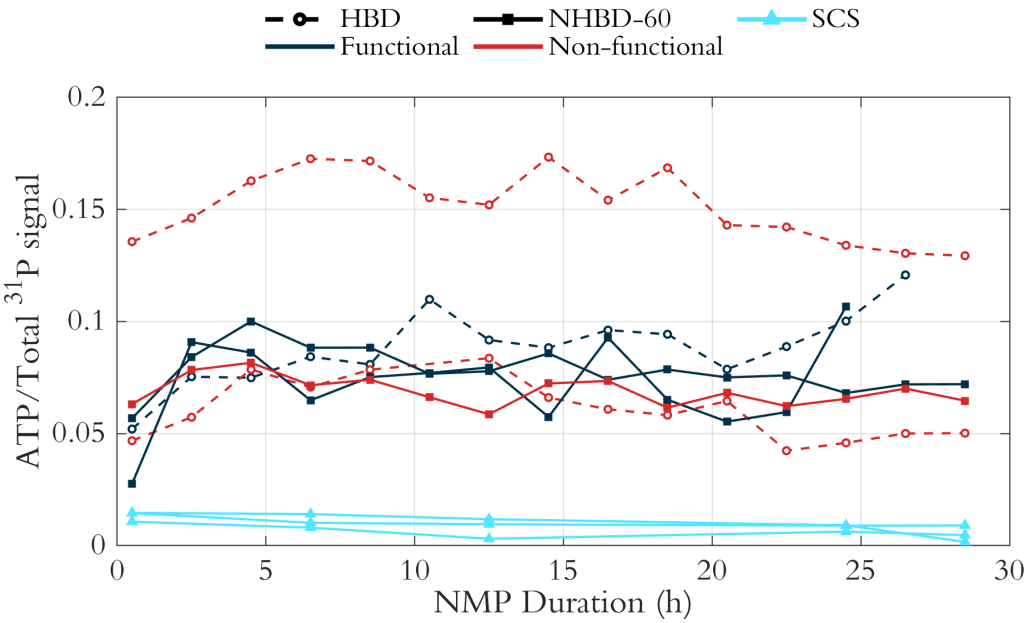


Figure 6.13: Changes in ATP as a proportion of total ^{31}P signal in ex vivo porcine livers during preservation by either static cold storage (SCS) or normothermic machine perfusion (NMP). Abbreviations: *heart beating donor, HBD; non-heart beating donor with 60 minutes warm ischaemia, NHBD-60.*

6.4.5.2 Glycolytic metabolism

Figure 6.15 shows that evidence of active glycolytic metabolism was detected in all livers where hyperpolarized ^{13}C spectra were acquired. No hyperpolarized acquisitions were possible for Liver 6 due to technical issues with the hyperpolarizer.

The conversion of pyruvate to lactate tended to be higher in livers deemed non-functional than functional, with $k_{Pyr \rightarrow Lac} = 7.7 \pm 2.8 \times 10^{-4}$ s^{-1} and $2.2 \pm 1.6 \times 10^{-4}$ s^{-1} respectively. $k_{Pyr \rightarrow Lac}$ peaked following 12 h of perfusion $6.4 \pm 4.7 \times 10^{-4}$ s^{-1} compared to 5.6 ± 3.9

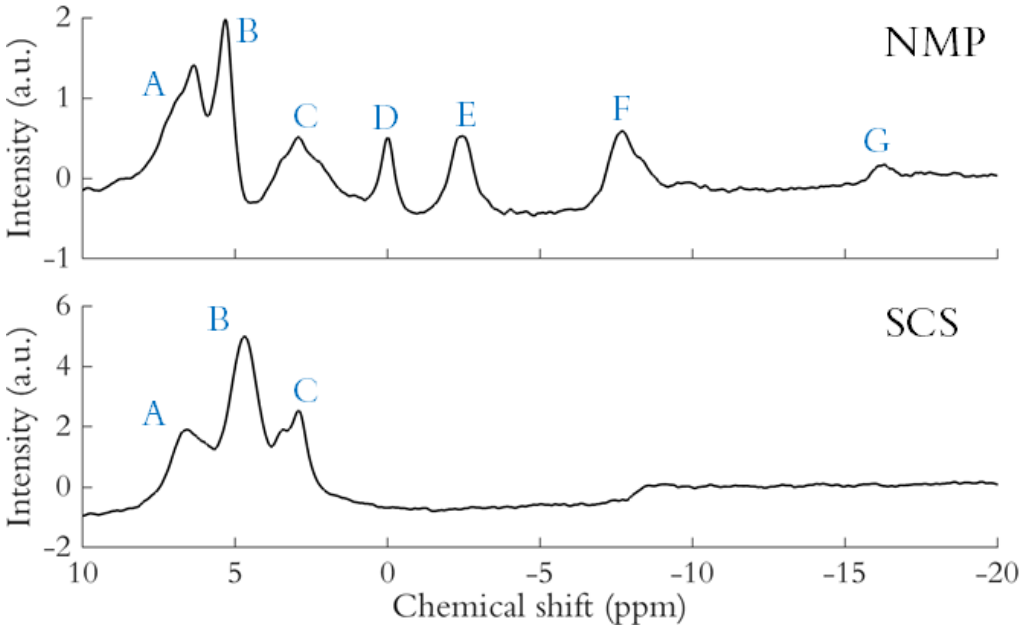


Figure 6.14: Representative ^{31}P spectra from ex vivo porcine livers at the end of 28 h of normothermic machine perfusion (A) and static cold storage (B). Both livers were retrieved from non-heart beating donors and were subjected to 60 minutes of warm ischaemia and 3 h of cold ischaemia prior to the 28 h assessment period. Peak assignments: A - phosphodiesters; B - inorganic phosphate; C - phosphomonesters; D - PCr; and E, F, and G - γ, α, and β-ATP.

$\times 10^{-4}$ s^{-1} and 4.5 $\pm$2.6 $\times 10^{-4}$ s^{-1} following 2 and 28 h of NMP respectively. However, these differences were not statistically significant. Moreover, the functional livers were consistently below the normal reference range and the non-functional livers sometimes fell within the reference range.

The peak rates of conversion of pyruvate to alanine, parametrised by $k_{Pyr \rightarrow Ala}$, and pyruvate to bicarbonate, characterised by $k_{Pyr \rightarrow Bic}$ also peaked following 12 h of perfusion but again these differences were not significant. The bicarbonate peak in the spectrum was very small at all time points in all livers and is reflected in a low fitted $k_{Pyr \rightarrow Bic}$ ($<2.4 \times 10^{-4}$ s^{-1}).

Figure 6.16 shows that the maximum pyruvate signal was obtained from the vasculature where the hyperpolarized substrate was injected into but that signal was also detected across the liver parenchyma indicating that the pyruvate had been perfused through the tissue. In contrast, the lactate signal was detected primarily in the liver parenchyma not the vasculature, indicating that the metabolism detected is hepatic metabolism and not glycolytic metabolism

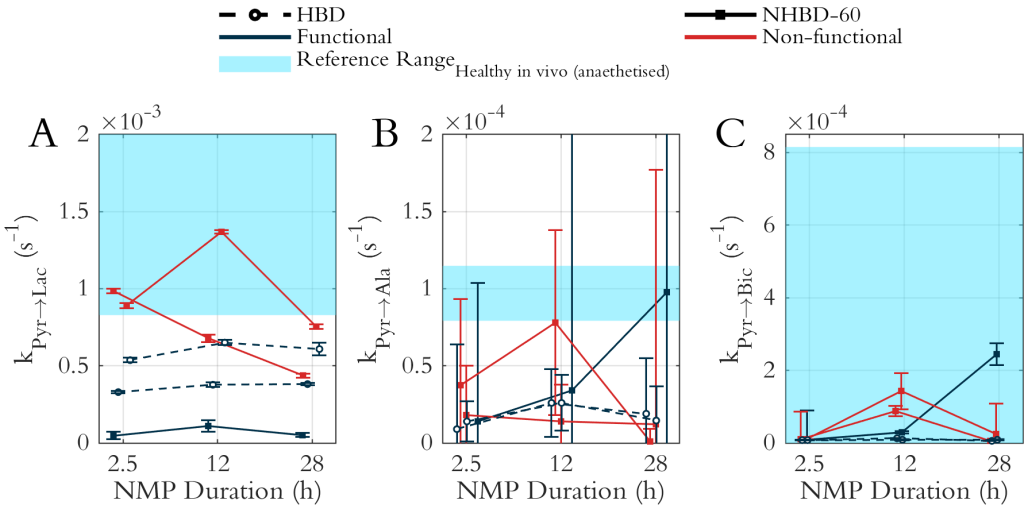


Figure 6.15: A summary of pseudo first-order chemical exchange rate constants for the conversion of pyruvate to lactate ($k_{Pyr\rightarrow Lac}$, A), alanine ($k_{Pyr\rightarrow Ala}$, B), and bicarbonate ($k_{Pyr\rightarrow Bic}$, C) observed in ex vivo porcine livers during NMP. Reference ranges were calculated using data provided by Prof Christoffer Laustsen, Aarhus University, who acquired ^{13}C-MRS of in vivo liver in four healthy pigs following the administration of hyperpolarized [1-^{13}C]pyruvate for a separate study.[109] All spectra were re-processed using the same analysis pipeline.

within the perfusate.

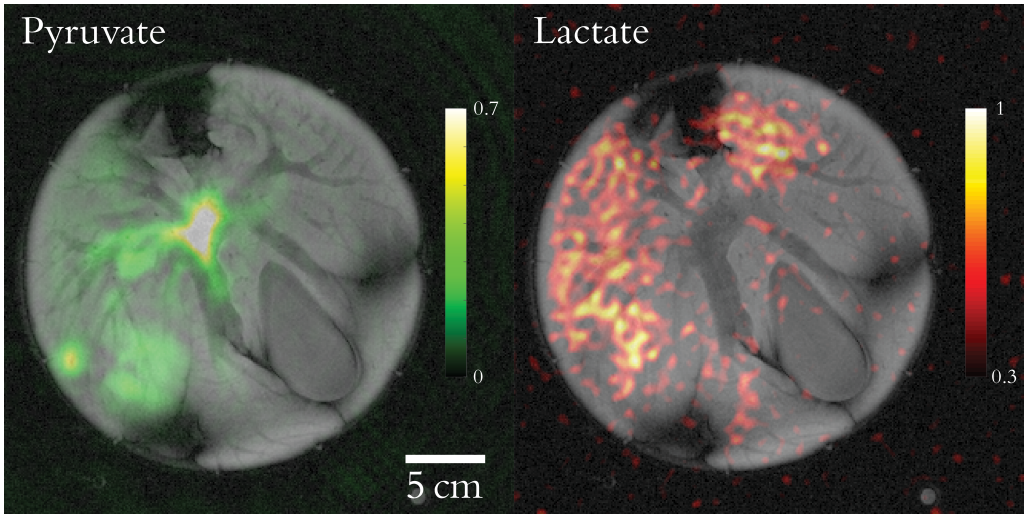


Figure 6.16: Images of pyruvate and lactate signal detected in a porcine liver after 28 h of normothermic machine perfusion. Images are overlaid on a GRE image for anatomical reference.

6.5 Discussion

Determining whether a donated liver is viable for transplantation is currently a difficult task as none of the biomarkers used to date have proven to be sufficiently sensitive and specific. Therefore, novel biomarkers are needed to provide accurate risk stratification of donor livers and hence aid the surgical team who must decide whether a donated organ is suitable for transplantation. In this chapter, I have demonstrated the feasibility of performing prolonged examinations of ex vivo livers while they are preserved using an MR-compatible NMP system. Combining the direct, non-invasive MR measurements of liver pathophysiology with the in-direct biochemical measures obtained through analysis of the perfusate provides an opportunity to perform comprehensive phenotyping of ex vivo livers. With refinement, this could enable the viability of each individual donated liver to be assessed rather than relying upon broad categories (such as donor type) as has been performed traditionally.

6.5.1 Impact of changes to clinical perfusion system

In order to enable the safe combination of the clinical NMP system and a 3T MRI scanner, a range of adaptations to the perfusion system were necessary. This study has demonstrated that the changes in the perfusion system have not reduced its ability to preserve livers for extended periods of time, with 4 out of 6 livers perfused meeting clinical viability criteria for transplantation within the first 4 h of perfusion and 3 of the livers remaining functional until the end of the experiment at 28 h. Both the flow rate and pressure within the hepatic artery while perfused using the MR-compatible system were statistically equivalent to the rates and pressures normally seen during perfusion on the standard clinical system ($P = 0.007$ and $P < 0.001$ respectively). However, the rate of portal flow in the MR-compatible perfusion system was 10% lower than the minimum of the normal range reported for porcine livers on the standard clinical system.[218] In the perfusion system, the arterial supply is driven by the centrifugal pump while the portal flow is provided purely by gravity. Therefore, the portal circuit will always be more sensitive to slight changes in resistance or relative height of the perfusate reservoir and organ than the arterial circuit. Hence the effect of the longer

perfusion lines, increased resistance, and mobile organ container are seen in the portal flow but not the arterial flow. Even with slightly reduced flow down the portal vein, the rates of blood flow into the liver during perfusion with the MR-compatible perfusion system were sufficient to meet VITTAL criteria for acceptable flow rates (150 mL/min and 500 mL/min for the hepatic artery and portal vein respectively)[139] in all livers. Additionally, the oxygenator and heat-exchanger were both able to maintain the livers in a state equivalent to those under-going NMP using the clinical system with average pO_2 and pCO_2 of 15.6 and 5.5 kPa respectively ($P_{Equivalent}$ <0.001 for both) and a perfusate temperature of 37 °C. Therefore, the changes performed to the clinical perfused system in order to allow the livers to go into an MRI scanner while undergoing NMP did not cause a significant deterioration of the quality of the perfusion.

6.5.2 Replication of physiological conditions

The non-invasive nature of MR measurements provides a good opportunity to compare how well the NMP circuit replicates in vivo conditions. The rates of flow into the liver are designed to be physiological but IVIM measurements have shown that these correspond to a level of microvascular perfusion which is slightly reduced but within the normal range for in vivo liver (f_2 = 7.78 ±1.99%, with the reference range = 5.8 - 21.7%). The diffusion coefficient for the microvascular compartment was also slightly reduced in comparison to in vivo, at 6% lower than the reference range, but remained stable for the duration of perfusion. The passive diffusion coefficient was also stable through out perfusion and equivalent to measurements made in vivo, indicating that ex vivo NMP replicated the very slow and very fast diffusion and perfusion within the liver well.

Slightly surprisingly, the compartment that appeared the most affected by the switch from in vivo conditions to ex vivo perfusion was the intermediate diffusion compartment. The diffusion coefficient of this compartment was more variable and slightly increased compared to in vivo liver (17.9 ±6.4 $\times 10^{-3}$ mm^2/s compared to a reference range of 8.4 - 18.1 $\times 10^{-3}$ mm^2/s). Additionally, the fraction of signal corresponding to this compartment was reduced by about 1/4 compared to in vivo liver and in some early time points of some

livers was not detectable at all. These observations may be explained if the intermediate compartment is considered to be predominantly representative of the portal system as proposed by Wurnig *et al.*[230] The reduced perfusion rates observed could then be linked to the slightly reduced portal flow rates in the MR-compatible perfusion system, while the greater instability of diffusion within this compartment could be associated with a form of post-reperfusion syndrome (PRS). PRS is typically observed following reperfusion of the portal vein during the transplant operation and is characterised by a period of haemodynamic instability.[194] The changes in the intermediate diffusion compartment could be a localised manifestation of these changes within the liver tissue. In future studies, arterial spin labelling (ASL) may assist a deeper investigation of this affect. By examining changes in liver perfusion through variations in the rate of in-flowing blood reaching the different areas of the liver, this may give additional information on the pathophysiological changes causing the altered perfusion detected by IVIM - a technique which relies on changes in local diffusion within the tissue.

For some parameters, whether in vivo conditions were replicated during perfusion appeared to depend more on the liver function than parameters provided by the system. For example, perfusate lactate concentrations returned to physiological levels in four of the livers initially and remained at physiological levels in three cases. Similarly, the liver T_1 - a measure sensitive to fibrosis, necrosis and inflammation - remained equivalent to healthy in vivo reference ranges in livers that were deemed functional by clinical criteria but increased significantly in those that were deemed non-functional.

Haematocrit was consistently non-physiological in this adapted perfusion system. This unfortunately was caused by the increased volume of the extended perfusion circuit requiring a slight dilution of the blood recovered from the pig. This did not appear to have a detrimental effect on the livers with perfusate pO_2 and pCO_2 equivalent to blood in vivo and evidence of good metabolic function detected in many of the livers.

Overall the MR-compatible NMP circuit replicated in vivo conditions well and provided an environment in which livers could function well providing they were not too injured to begin with. This was evidenced through regeneration of ATP, demonstrating a

restoration of oxidative energy metabolism, and production of bile, highlighting recovery of synthetic function. The significant improvement in ATP content of livers persevered by NMP compared to SCS (visible in Figures 6.13 and 6.14) highlights the stark improvement in metabolism that dynamic preservation by NMP offers over conventional static cold storage. The hyperpolarized imaging data (Figure 6.16) showed evidence of active metabolism across all of the parenchyma within the coil's sensitive region suggesting that the perfusion system managed to re-animate the entire liver rather than small sections.

6.5.3 Is donor history or functional assessment more valuable?

Determining whether a liver was too injured to be considered viable for transplantation appeared to depend on more factors than purely the type of donation, which also changed the relative warm and cold ischaemia durations in the animal models. This study started with healthy livers prior to retrieval, yet liver function on the system was mixed within each study group. Two livers from NHBD-60 group, which had experienced 60 minutes of warm ischaemia and hence by traditional criteria would be non-viable for transplantation, showed excellent function during perfusion, while two livers from the 'ideal' case of a whole liver heart beating donor showed evidence of poor liver function during perfusion. In fact, apart from the passive diffusion coefficient which was increased in livers from non-heart beating donors, none of the parameters considered varied significantly between the heart-beating donor and non-heart beating donor groups and instead varied much more consistently between 'functional' livers and 'non-functional' livers.

Previous studies have shown increased risk of post-transplant complications in livers from non-heart beating donors, so at first glance the results of the present study may be surprising. However, the current results merely highlight the need for organ specific viability assessment that not only considers historical risk factors but also accounts for the state of the liver currently being considered for transplantation. Many 'high-risk' livers from non-heart beating donors have excellent post-transplant outcomes, while some livers from 'ideal' healthy, heart-beating donors have very challenging outcomes. The difficulty currently is predicting what the outcome will be for each potential liver transplant.

In this study, a selection of MR biomarkers have been presented which provide additional information on the state of the liver and may be able to help determine if a liver is viable for transplantation. For example, Liver T_1 differentiated those livers which were deemed functional or non-functional by metabolic criteria within 4 h. Liver T_1 is a very quick measurement to make (~11 s for a single slice measured with shMOLLI) and with all major MRI scanner vendors now providing fast T_1 mapping methods, it is easy to see how this could be a rapid and widely available assessment technique. Therefore, liver T_1 would make a strong candidate biomarker to examine further as one can see how this could be included into a clinical work flow if the promising signal detected in this study persist in larger prospective clinical trials.

At the same time, more complex techniques, such as hyperpolarized ^{13}C-MRS, provided more in depth assessments of liver metabolism allowing the differentiation of instantaneous rates of chemical exchange through different glycolytic pathways. Up to 100-fold changes in the rates of chemical exchange of pyruvate and lactate, bicarbonate or alanine were seen between livers and also temporally within a given perfusion. In contrast, the rate of perfusate glucose clearance appeared fairly consistent between livers and constant throughout perfusion. Therefore, it may be important to use more advanced direct measurements of liver metabolism to properly characterised the metabolic milieu that is present rather than relying on in-direct secondary measurements from the perfusate.

6.5.4 Timing of viability assessment

Currently, there is little consensus over the duration of perfusion that should be performed for and when during perfusion any viability assessments should be made. One difficult case in this study, which is representative of cases that have been seen in previous studies, is a liver that initially clears perfusate lactate and looks very promising but gradually sees an increasing lactate concentration in the perfusate. In the VITTAL study, Mergental et al. highlight several of these cases with a comment that the clinical significance of this is uncertain.[139] Interestingly the one case with increasing perfusate lactate that was transplanted, suffered from a substantial period of early allograft dysfunction. Although we must exercise caution

in interpreting a single event. The results from my study suggest that even a slight increase in perfusate lactate may be a sign that a significant level of injury has already occurred to the liver parenchyma. In my study, one liver from a HBD saw the perfusate lactate began to creep up after meeting the lactate criteria within 2 h of perfusion. Because this liver was starting from very low concentrations (0.4 mmol/L), it only breached the VITTAL lactate viability threshold of 2.5 mmol/L following 20 h of NMP. However, the liver T_1 increased rapidly and after just 4 h of NMP the T_1 had already reached 965 ms - an increase of over 130 ms compared to its initial value. Therefore, by this point there was already significant amounts of inflammation, oedema, fibrosis, or necrosis, present in the parenchyma. Having a liver which initially appears to be viable for transplantation but later is determined to be non-viable is a dangerous situation as in a clinical setting, the transplant of the now non-viable organ may still need to be performed if the recipient's operation has gone too far. This would put the patient at high risk of post-transplant complications. Therefore, if direct assessment of liver parenchyma did provide an earlier signal of liver health than the in-direct measures, such as perfusate lactate, as was seen in this case, it could be a very beneficial biomarker.

Aside from possibly being helpful as an early predictor of graft health during NMP, these T_1 results also support Mergental et al. that extreme caution should be taken with grafts that show increasing perfusate lactate.[139] Overall, T_1 appeared to be a useful predictor of liver function in this study. Applying a cut-off value of 912 ms predicted liver function out to the end of perfusion from any measurement taken from 4 h of NMP onwards.

6.5.5 Limitations

This study was designed to demonstrate the feasibility of prolonged MR investigation of ex vivo livers preserved using NMP and so is not powered to compare how effective different biomarkers are at predicting liver function or viability for transplantation. Additionally, my study design necessitated reliance on a surrogate marker of viability for transplantation, the VITTAL criteria, rather than examining post-transplant outcomes which limits my ability to determine which biomarkers may be most predictive. However, the promising signals observed in MR biomarkers within this small study group can be used to shape future,

suitably powered, transplant studies to truly examine the effectiveness and optimum cut-off values for the biomarkers.

The comparisons to in vivo reference ranges performed in this study should also be treated as an initial assessment. The reference ranges were derived from small numbers of anaesthetised animals (n=8) and so contain a wide degree of uncertainty. Also, the reference ranges were derived from pigs reared in Aarhus, Denmark, while the perfused pig livers were reared in Oxfordshire, UK. It is possible that slight differences could be attributed to differences in feeding and environmental conditions. However, as shown by the previous study reported in Chapter 6, the difference between a healthy in vivo liver and a liver following an extended period of ischaemia are numerous and severe. These differences appear much larger than the differences previously observed between feeding status or rearing conditions.[121 52] Therefore although imperfect, my comparisons between in vivo livers and ex vivo livers undergoing NMP still provide to a useful indication of how physiological the state NMP creates in the liver is.

6.6 Conclusion

In this study, I have demonstrated the feasibility of performing prolonged MR examinations on ex vivo livers undergoing NMP and have demonstrated that the adaptations needed to make a clinical perfusion system MR-compatible do not prevent effective perfusion.

Through comparison to an in vivo porcine model, I have shown that NMP replicates in vivo perfusion conditions well. Although there may be slight variations in the intermediate diffusion compartment, which has been attributed to portal flow.

Overall, this study highlights the need for organ specific assessments of viability and has presented a range of new biomarkers that may assist in this cause. Changes in liver T_1 appear to be a very promising candidate for early prediction of liver function during NMP and hence may be useful for prediction of post-transplant outcomes. Further larger studies are now warranted to examine the predictive power of T_1 and other MR biomarkers for determining viability of an organ for transplantation.

7

Assessment of perfused human livers by MRI and MRS: a feasibility study

7.1 Background

In Chapter 5, I demonstrated that temperature corrected T_1 and PDFF show promise for distinguishing functional and non-functional livers during static cold storage (SCS). However as described in Section 2.2.1, the effect of static cold storage is to slow metabolism by 95% and reduce damage to the organ by holding livers in an approximately 'paused' state.[223] Under these conditions, metabolic assessment is unlikely to be representative as much of the damage that occurs to transplanted organs is as a consequence of ischaemia reperfusion injury, which takes place when an oxygenated blood supply is restarted and effects of the ischaemic metabolism that occurred during cold storage are felt. For healthy, low-risk livers, the damage due to the cold ischaemic period is survivable and a transplant can be safely performed. However, many studies have demonstrated that there is a significant risk to transplanting steatotic livers that have been preserved using static cold storage. For this reason, many steatotic livers are currently deemed unsuitable for transplantation and discarded.

The advent of normothermic machine perfusion has enabled livers to be maintained perfused ex situ and held in a metabolically active state with evidence of haemodynamic,

synthetic, and excretory function examined prior to transplantation. [150,178,139] These assessments have been used to demonstrate that steatotic livers are better preserved by NMP than SCS and that with enhanced preservation it is possible to safely transplant livers previously deemed non-viable for transplantation. [39,139]

However, as described in Section 2.2.3, there are many different criteria for suitability for transplantation being applied at different transplant centres with no clear consensus as to which parameters are most predictive or the thresholds that should be applied. This is due to the lack of any proven sensitive and specific techniques to identify livers which will have severe post-transplant complications and so should be discarded or those that will have smooth post-transplant outcomes. Therefore, it is important to keep exploring novel biomarkers which may aid the decision making process.

Identifying and validating additional biomarkers becomes increasingly important as more novel interventions are starting to be performed on ex situ livers, for example, to remove fat with a de-fatting cocktail of drugs, [38,21] or to modulate immune responses with infusions of anti-inflammatory agents and cellular therapies. [35,62] Therefore, there is much interest in performing more in-depth assessments of donated livers' viability for transplantation during ex situ normothermic machine perfusion in order to enable safe usage of more 'high-risk' extended donor criteria organs and assessment of whether an intervention has been successful.

In Chapter 6, I demonstrated that MR biomarkers could provide a non-invasive way to monitor liver metabolism and physiology during ex situ perfusion in a porcine model. However, the reality of clinical transplantation is quite different from these pre-clinical models with more severely steatotic and damaged organs considered, longer cold ischaemia times necessitated and greater unpredictability in the schedule of the examinations. Therefore, I set out to perform a feasibility study to prove that it is possible to use MR biomarkers to assess steatotic human livers during ex vivo normothermic machine perfusion.

7.2 Aims

In this chapter I aim to:

- Demonstrate the feasibility of MR assessment of ex vivo human livers during normothermic machine perfusion.
- Determine whether the adapted system is capable of providing a clinical standard of perfusion to the discarded livers for 12 hours.
- Investigate the suitability of a range of MR biomarkers to predict a liver's viability for transplantation.

7.3 Methods

7.3.1 Liver procurement and perfusion protocol

Three human livers were retrieved for transplantation as part of a standard multi-organ deceased donor organ retrieval.[27] During the back table work at either the donor or recipient hospital, all livers were deemed unsuitable for transplantation due to the presence of severe steatosis. The organs were cold flushed with UW solution (Bridge to Life, London, UK) before removal and then transported on ice per standard practice. Upon arrival at the Oxford Transplant Centre, the livers were prepared for perfusion and cannulated following normal protocols with the substitution of the cannulae for non-metallic alternatives as described previously (full details are provided in 6.3.3.1).[132] Livers were primed with 0.5 - 1 L of Gelofusine solution (B Braun Medical Ltd, Sheffield, UK) initially down the portal and then the arterial cannula. The livers were then transported on ice to the MRI scanner for perfusion and examination.

This study was approved by National Ethics Review Committee of the United Kingdom (REC reference 16/NE/0248).

Livers were perfused using an adapted MR-compatible version of a clinical perfusion device (*metra*, OrganOx, Oxford, UK) described in Section 6.3.3.2. The perfusate used for

human liver perfusions consisted of 5 units of recently expired group O packed red cells from the Oxford Blood Bank as an oxygen carrier and 1 L of Gelofusine (B Braun Medical Ltd, Sheffield, UK), which is a colloid added to normalise the haematocrit and osmolarity. Boluses of calcium gluconate, unfractionated heparin sodium, sodium bicarbonate and cefuroxime were added to the reservoir during priming of the circuit and constant infusions of unfractionated heparain sodium, insulin, taurocholate, and epoprostonol sodium were administered during perfusion of the liver as per the protocol described previously (Section 6.3.3.2).

7.3.2 MR examination

All livers underwent 12 h of perfusion and examination in a 3T MRI scanner (TIM-Trio, Siemens, Erlangen, Germany). The protocol consisted of alternating hours of non-localised ^{31}P MRS acquired using a 10-cm loop coil (PulseTeq Ltd, Surrey, UK) and ^{1}H MRI and MRS acquisitions using a 32-channel surface array (Rapid Biomedical GmbH, Rimpar, Germany). In two livers, 20 mL of hyperpolarized 1-^{13}C pyruvic acid was injected into the portal vein and non-localised ^{13}C spectra were acquired using a 10-cm loop coil (PulseTeq Ltd, Surrey, UK) following 2.5 h and 12 h of perfusion. The ^{1}H protocol consisted of:

- Relaxometry, including: ShMOLLI T_1 maps, $T_2^\star$ maps calculated from multi-echo GRE images, T_2 measured by multiple-TR multiple-TE STEAM spectroscopy.
- Perfusion assessment using IVIM parameters calculated from DWI data.
- Fat fraction calculated from STEAM spectra.

Full details of all acquisition parameters and data processing are presented in Section 6.3.4.

7.3.3 Haemodynamic and biochemical analysis of liver function

Rates of flow and pressures within the hepatic artery and IVC were continually measured using sensors integrated in the perfusion device (*metra*, OrganOx Ltd, Oxford, UK). Additionally,

perfusate pH, pO_2, and pCO_2 were continually measured using an in-line arterial sensor (CDI 550, Terumo UK Ltd, Surrey, UK).

Every four hours, arterial blood gas analysis was performed on perfusate samples to assess changes in lactate and glucose concentrations, perfusate pH, and haematocrit using a point of care test (iStat, Abbott Point of Care Inc., NJ, USA).

7.3.3.1 Histological analysis

Needle biopsy samples were collected from the right lobe of the livers prior to and every 6 h during NMP. Samples were fixed in formalin and embedded in paraffin as previously described (Section 6.3.5). Further processing has been delayed by the impact of the COVID-19 pandemic on the histopathology team. However, samples will be sectioned and stained with: Haematoxylin & Eosin to assess basic tissue structure; Picrosirius red to monitor fibrosis, and periodic acid-Schiff (PAS) stain to detect glycogen within the tissue.

7.3.4 Statistical analysis

Unless otherwise stated, all data are presented as mean ±standard deviation and any fitted parameters are presented as the predicted value followed by the 95% confidence interval in brackets. Spatial variability between regions within a liver was assessed through a paired Student's t-tests. Temporal and inter-liver variability was assessed using a linear mixed-effects regression analysis. All statistical hypothesis testing was performed at significance level $\alpha = 0.05$.

7.4 Results

7.4.1 Clinical data

Table 7.1 summaries the donor demographics for the three human livers included in this study. Livers B and C had much longer cold ischaemia time before perfusion commenced than Liver A because they were transported to the intended recipient's hospital prior to

being discarded while Liver A arrived directly from the retrieval hospital. All livers were discarded primarily for being deemed severely steatotic during macroscopic inspection. The retrieval surgeon also noted that there was patchy perfusion within the left lobe of Liver C during the in situ flush.

Table 7.1: Summary of donor demographics

Donor	A	B	C
Donation Type	DBD	DBD	DBD
Sex	M	F	M
Donor Age (yrs)	52	72	51
Cold ischaemia time (min)	608	1282	1592
Reason for discard	Severe steatosis	Severe steatosis	Severe steatosis

Abbreviations: *donation after brain-stem death, DBD; donation after circulatory death, DCD; female, F; male, M.*

7.4.2 Haemodynamic and perfusion characteristics

All livers had clinically acceptable flow rates of >150 mL/min down the hepatic artery and >500 mL/min into the portal vein during perfusion on the adapted circuit. Figure 7.1 shows changes in the flow rates over the course of the perfusion for Livers A and C. Unfortunately, a system crash deleted the flow rate data for Liver B and hence this is not reported. Liver A and C had average flow rates of 268 ±81 mL/min and 171 ±12 mL/min respectively into the hepatic artery and 613 ±62 mL/min and 668 ±53 mL/min respectively into the portal vein over the whole perfusion. The hepatic artery flow rates are comparable to values reported by Ceresa et al. for discarded steatotic human livers on the standard clinical perfusion system (reported normal range = 149 - 212 mL/min over 12 hrs of perfusion compared to an obsereved flow rate of 222 ±61 mL/min).[39] However, the observed portal flow was significantly reduced compared to the anticipated flows in the standard perfusion system (reported normal range = 977 - 1124 mL/min compared to an observed flow rate of 640 ±64 mL/min).[39]

Rates of perfusion and diffusion appeared to be stable throughout ex vivo perfusion

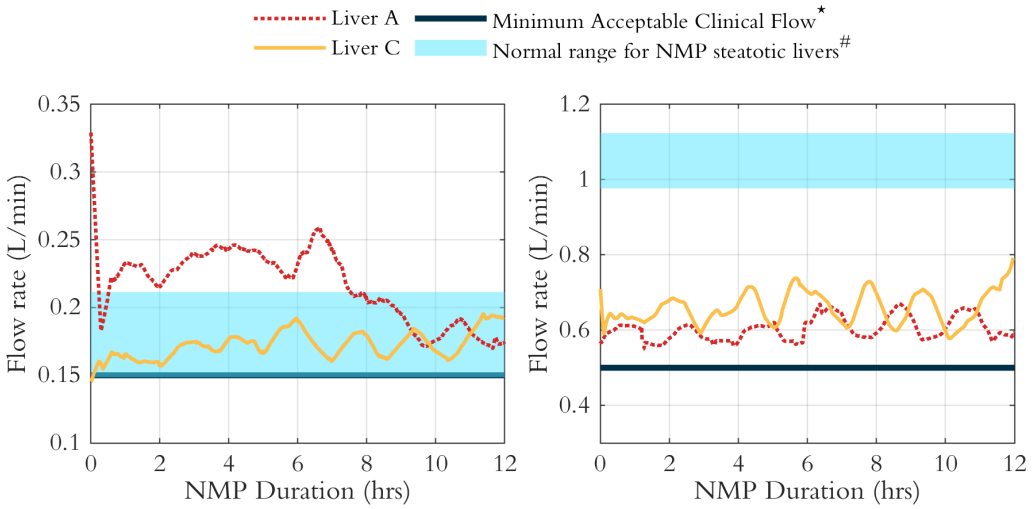


Figure 7.1: Changes in rates of flow down the hepatic artery (A) and portal vein (B) in two human livers during ex vivo normothermic machine perfusion. Data from Liver B are not presented since this data was lost in a system crash following perfusion. Previously reported ranges for perfusion flow rates in steatotic human livers on the clinical perfusion system are presented as well as the minimum acceptable flow rates defined by the VITTAL criteria.[39 117] Abbreviations: normothermic machine perfusion, NMP.

with no significant dependence on perfusion duration detected in any parameter (all $P > 0.28$). Figure 7.2 presents the changes in perfusion and diffusion observed in the perfused human livers. To place these parameters in context, the range of normal parameters reported for healthy human livers in vivo in previous studies that used a tri-exponential model to fit IVIM data is also presented.[37,113,230,45,187,186]

Although all livers showed comparable diffusion coefficients (D, $D^{\star}_1$, and $D^{\star}_2$), a significantly reduced perfusion fraction of the fast compartment was observed in Liver B which in turn caused a reduction in the total perfusion fraction (both $P < 0.001$). In Liver C, a reduction in both perfusion fractions associated with the intermediate and fast components was observed in the edge of the left lobe compared to the right lobe (5.7 $\pm$0.6% vs 2.0 $\pm$1.3%, $P = 0.01$, and 12.1 $\pm$2.4% vs 3.2 $\pm$1.0%, $P = 0.002$, for the intermediate and fast components respectively).

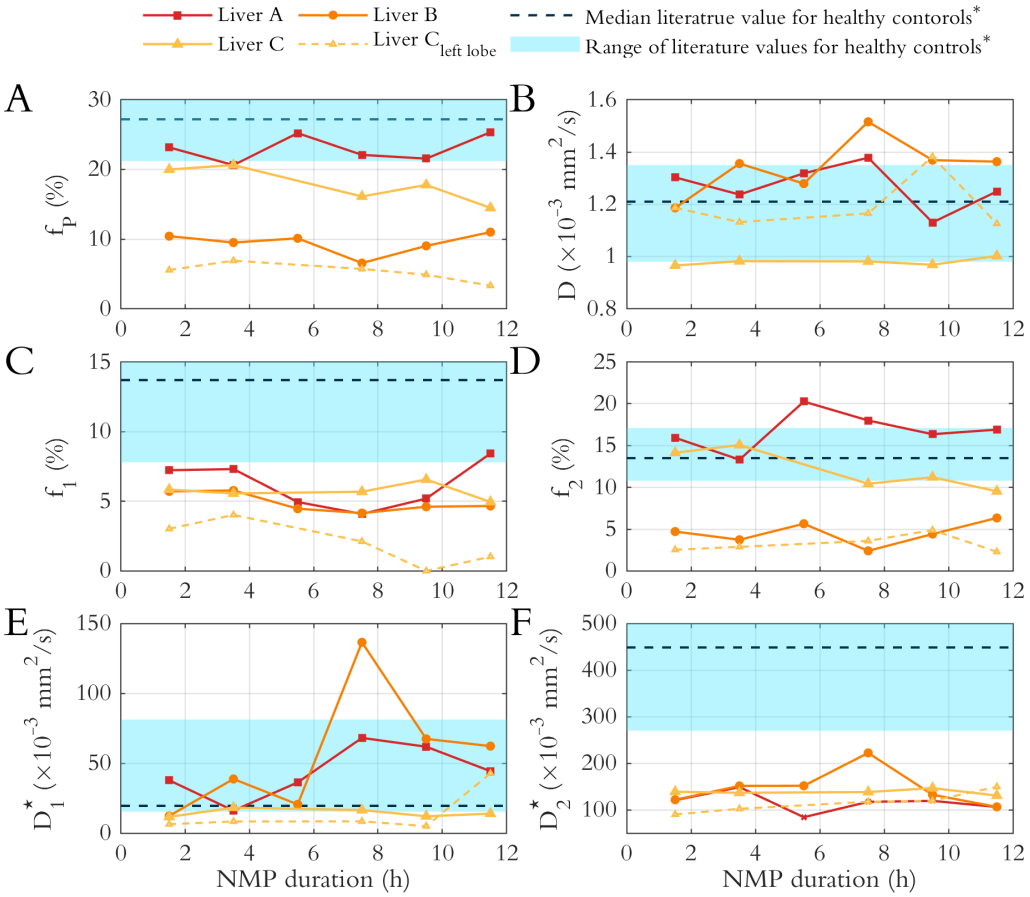


Figure 7.2: A summary of changes in tissue perfusion in three human livers during ex vivo normothermic machine perfusion measured by IVIM. For reference, a range of normal values for in vivo livers from healthy controls is also presented using reported values from studies applying a tri-exponential IVIM model.[37,113,230,45,187,186] Abbreviations: *pure diffusion coefficient for passive diffusion, D, pseudo-diffusion coefficients for intermediate and fast diffusion compartments, $D^\star_1$ and $D^\star_2$ respectively; perfusion fraction for intermediate and fast compartments, f_1 and f_2 respectively.*

7.4.3 Metabolic assessment

7.4.3.1 Blood gas and perfusate analysis

Figure 7.3 show the changes in perfusate composition observed during normothermic machine perfusion. Livers A and C rapidly cleared their perfusate lactate levels and had perfusate lactate below the VITTAL threshold of 2.5 mmol/L at 12 hrs. They also maintained a physiological perfusate pH averaging 7.41 ±0.05 and 7.38 ±0.03 from 4 h until the end of perfusion. In contrast, Liver B failed to clear the perfusate lactate and failed to maintain a physiological perfusate pH with an average of 7.10 ±0.06 from 4 h to the end of perfusion.

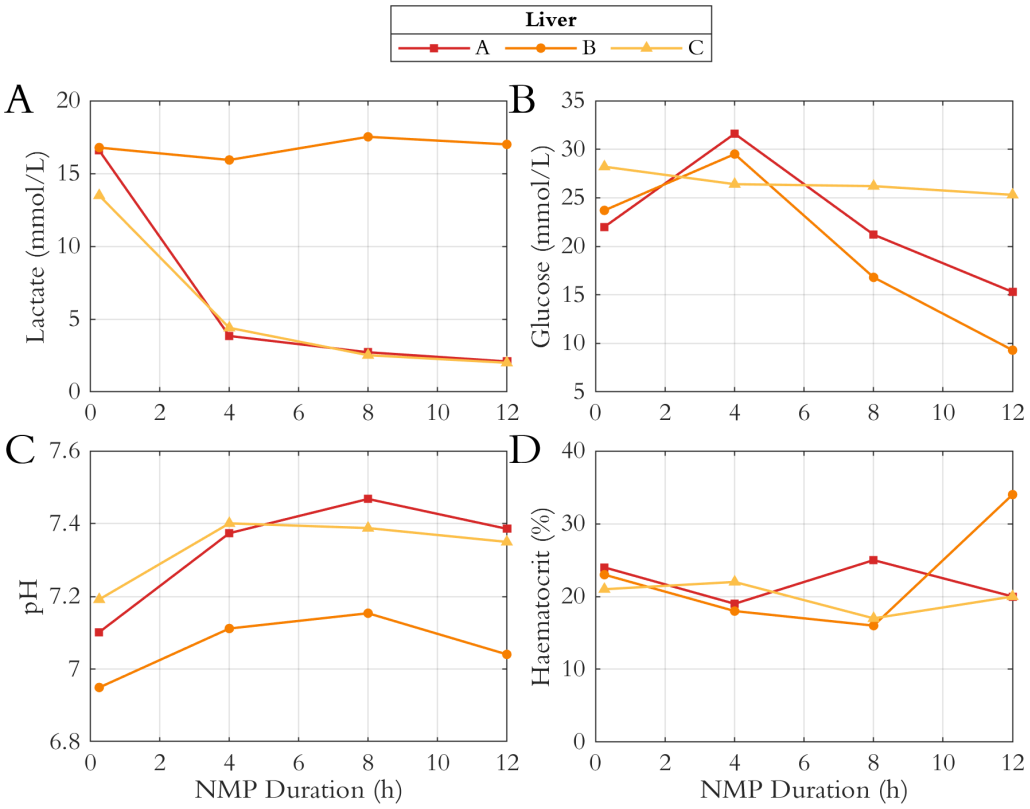


Figure 7.3: A summary of changes in perfusate composition with increasing duration of normothermic machine perfusion assessed using arterial blood gas analysis.

All livers showed evidence of glucose metabolism through decreasing perfusate glucose concentrations. However, Liver C showed a slower decline in glucose with a peak rate of -0.48 mmol/L/h compared to -2.6 mmol/L/h and -3.2 mmol/L/h for Livers A and B respectively.

7.4.3.2 Assessment of oxidative metabolism

The ATP:Pi ratio increased from 0.21 ±0.04 to 0.50 ±0.04 during 12 hrs of normothermic machine perfusion (P = 0.002). Figure 7.4 shows the non-linear rate at which this change occurred with greater increased observed during the early stages of perfusion. Assuming an exponential recovery model, gave a time constant for this recovery of 0.44 (-0.03, 0.91) h^{-1}.

However, Liver B consistently had a lower ATP:Pi ratio compared to Livers A and C (P = 0.01 and 0.04 respectively over all time points). This was echoed with a slower predicted rate constant for the increase in ATP:Pi ratio in Liver B compared to Livers A and C (0.19 [-0.89 - 1.28], 0.46 [0.03 - 0.87], 0.71 [-0.56 - 1.97] h^{-1} respectively), although

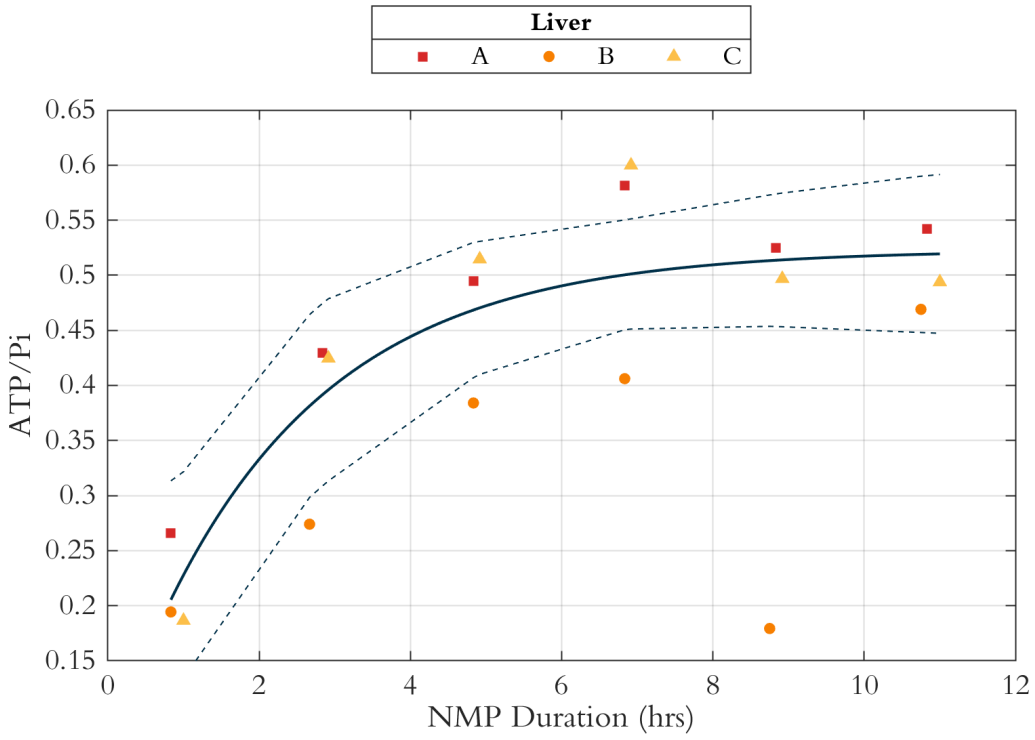


Figure 7.4: Changes in ATP/Pi ratio observed in three human livers during normothermic machine perfusion.

these differences were not significant.

7.4.3.3 Assessment of glycolytic metabolism

Hyperpolarized [1-^{13}C]pyruvate was successfully injected into the portal vein and MR spectra acquired on all attempts without any interference with perfusion of the liver. The conversion of pyruvate to lactate (characterised through $k_{Pyr\rightarrow Lac}$) was similar in both livers following 2.5 h of perfusion (6.46 $\times 10^{-3}$ and 5.08 $\times 10^{-3}$ s^{-1} for livers B and C respectively). However, by the end of perfusion Liver C saw a 5-fold decrease in $k_{Pyr\rightarrow Lac}$ to 1.02 $\times 10^{-3}$ s^{-1} while Liver B remained approximately constant at $\sim$6 $\times 10^{-3}$ s^{-1}. Both livers showed slower flux through ALT and PDH with rates of conversion to alanine and bicarbonate 100$\times$and 10$\times$slower than the flux through LDH. As shown in Figure 7.5, Liver C saw the rate of flux through both ALT and PDH fall from 2.5 h to 12 h of perfusion. In contrast, flux through ALT increased in Liver B with prolonged perfusion and only a small decrease in PDH flux was observed.

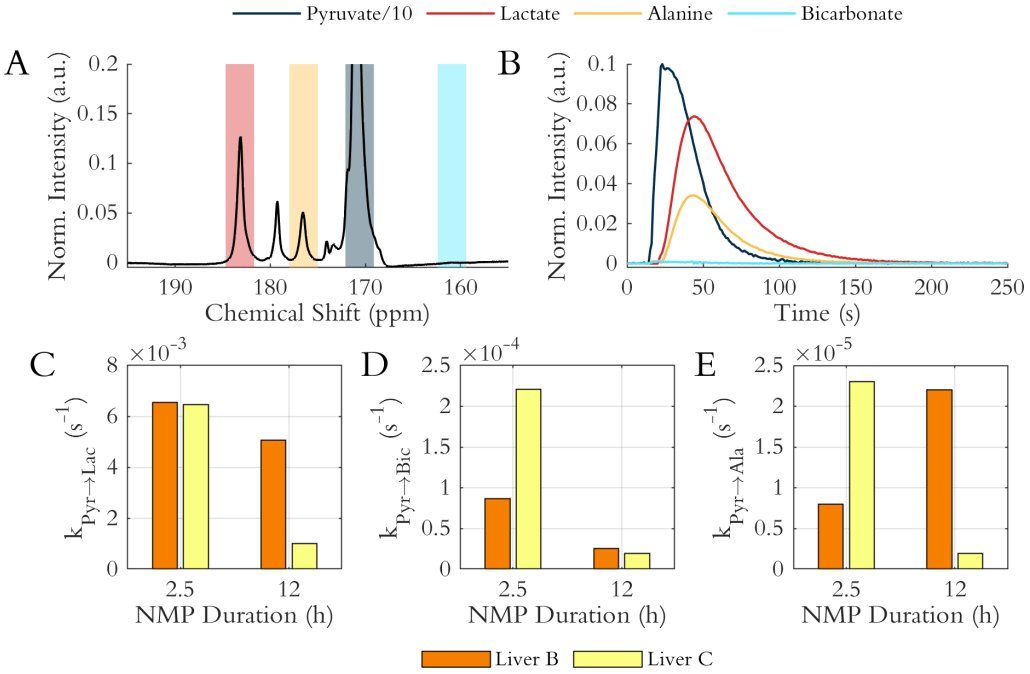


Figure 7.5: A summary of glycolitic metabolism assessed through hyperpolarised ^{13}C-MRS. An example spectrum and time course of peak integral changes are shown in A and B with conversion of pyruvate into lactate, alanine and bicarbonate visible. In C - E, the rate constants for conversion of pyruvate to lactate, bicarbonate and alanine in Livers B and C following 2.5 and 12 hrs of NMP are shown.

7.4.4 Tissue characterisation

Liver T_1 was stable throughout perfusion with no significant variation with NMP duration seen in the parenchyma of the right lobe in any liver (Figure 7.7,$P = 0.69$). However, actual T_1 varied greatly with Livers B and C having significantly higher liver T_1 values compared to Liver A ($P < 0.001$ from a linear mixed model fit of all measurements). Figure 7.6 shows a localised increase in T_1 in the lower section of the left lobe of Liver C, where reduced perfusion was also observed.

T_2 increased slightly with prolonged perfusion duration with a dependency of 0.20 (0.03 - 0.38) ms/h, $P = 0.03$. This effect was mirrored in the T_2^*-based predicted hepatic iron content, which showed a slight decrease over time of -0.14 (-0.04 - -0.24) mg/g/h, $P = 0.01$. However, as Figure 7.7 shows although these effects were statistically significant, the magnitude of these changes is very small.

Another very small change was observed in fat fraction with a slight decrease observed

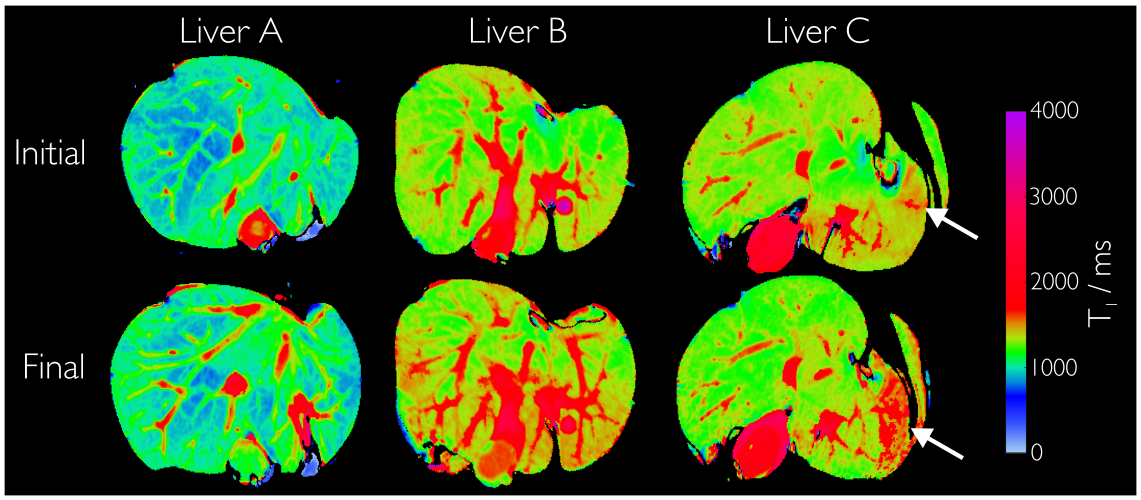


Figure 7.6: ShMOLLI T_1 maps for three human livers following 2 hrs and 12 hrs of normothermic machine perfusion. All images are acquired in the horizontal plane which is approximately equivalent to a transverse section when in vivo. The edge of the left lobe of Liver C, which was identified in the donor as poorly perfused, is identified by a white arrow.

with increasing perfusion duration of -0.47 (-0.01 - -0.93) %/h, $P = 0.05$.

7.5 Discussion

This study has demonstrated the feasibility of MRI assessment of ex vivo human livers during normothermic machine perfusion using a wide range of MRI and MRS techniques. Three human livers deemed too high risk to transplant by traditional clinical criteria were stably perfused for 12 hrs on an MR-compatible version of a clinical normothermic machine perfusion device (*metra*). Image and spectral quality was sufficient to enable assessment of the pathophysiology and metabolism non-invasively through MR biomarkers.

7.5.1 Perfusion quality

The adaptations performed to make the perfusion device MR-compatible did not reduce the quality of perfusion below clinically acceptable ranges with flow rates in the hepatic artery and portal vein consistently above the minimum thresholds set out in the VITTAL criteria of 150 mL/min and 500 mL/min respectively.[117] No changes were observed in the rate of flow down the hepatic artery with rates within previously reported ranges for steatotic livers

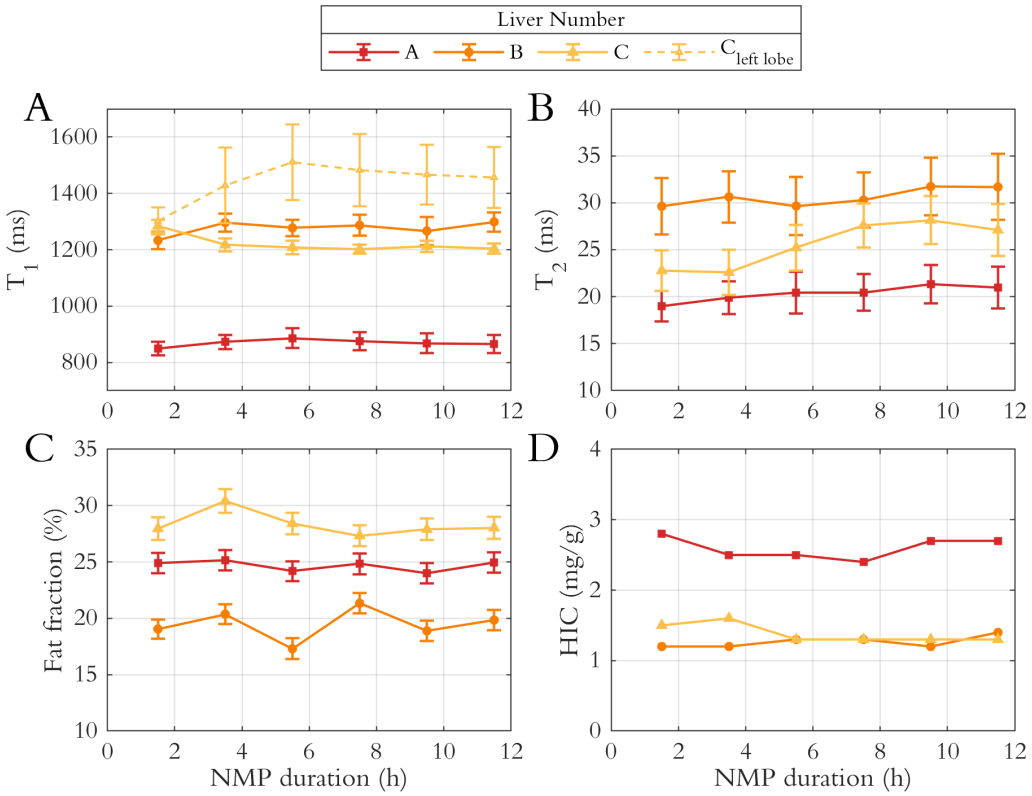


Figure 7.7: A summary of changes relaxometry and fat fraction parameters in three human livers during ex vivo normothermic machine perfusion.

on the standard clinical NMP circuit (222 ±61 mL/min for livers on the MR-compatible perfusion system and a reported normal range of 149 - 212 mL/min for steatotic livers perfused using the standard clinical perfusion system).[39] However, the adaptations did cause a slight reduction in the rate of portal flow observed in the MR-compatible circuit compared to previously reported values for steatotic livers on the standard clinical circuit (640 ±64 mL/min vs a reported normal range of 977 - 1124 mL/min).[39] This is likely due to the gravity-driven system for the portal vein being more sensitive to the increased resistance and greater variability in the relative heights of the reservoir and organ caused by moving the organ container away from the perfusion device and into the MRI scanner. Crucially even with the slight reduction in portal vein flows, all parameters remained above standard pre-defined minimum thresholds.[117]

7.5.2 Liver function

Two livers showed acceptable function during NMP by haemodynamic and biochemical VITTAL criteria that would have resulted in both being deemed suitable for transplantation.[139] The combination of the multiple risk factors, including severe steatosis and prolonged cold ischaemia time, appeared to be too extreme an insult for Liver B which demonstrated poor function on the device with no evidence of lactate clearance and increasing acidosis of the perfusate during perfusion.

A similar trend was observed in the perfusion fractions of the livers. Both livers deemed functional by the traditional criteria had total perfusion fractions (f_p) similar to those previously reported for healthy liver. Meanwhile, Liver B, which appeared non-functional by traditional criteria, and the edge of the left lobe of Liver C, which was identified as having patchy perfusion during retrieval, both showed reduced perfusion fractions for the duration of perfusion. Whether the poor perfusion causes the metabolic dysfunction or some localised insult causes tissue damage that reduces perfusion cannot be ascertained from this data but would be of interest to investigate in future studies. The slow passive diffusion coefficient (D) and intermediate pseudo-diffusion coefficient (D^*_1) were comparable in all livers to reported values for healthy human livers in vivo.[37,113,230,45,187,186] The rate of perfusion attributed to the intermediate compartment was slightly reduced in all livers compared to reported normal in vivo ranges (5.3 $\pm$1.8% for perfused livers vs a reported normal range of 13.7 [7.8 - 17.6]% for health liver in vivo, $P < 0.001$).[37,113,230,45,187,186] The pseudo-diffusion coefficient of the fast compartment (D^*_2) was much lower in perfused livers compared to reported in vivo values in health liver (126 $\pm$42 $\times 10^{-3}$ s/mm^2 in this study compared to 449 [270 - 2453] $\times 10^{-3}$ s/mm^2 for the median and range reported in previous in vivo studies, $P < 0.001$).[37,113,230,45,187,186] Reduced perfusion within the intermediate, possibly venous, compartment and diffusion within the fast microvascular compartment could be indicative of increased fibrosis, inflammation and steatosis within these perfused livers. This would align with previous studies that reported a reduction of both overall perfusion and diffusion within the fast microvascular compartment in vivo with increasing fibrosis and inflammation

within the liver,[2] as well as reduced diffusion coefficients in steatotic livers.[84] However, it is also possible that the slight reduction in liver perfusion observed is caused by imperfections in the perfusion being supplied by the adapted NMP device compared to what would occur in vivo.

Significant caution must be applied to any comparisons to the previously reported normal ranges. The choice of *b*-values, imaging technique used and method of respiratory control (e.g. breath-held or free-breathing) may all impact the results.[186 67] These differences are confounded by the fitting process as a tri-exponential model is incredibly sensitive to the fitting method chosen and any constraints placed upon the system. No standardised acquisition and fitting protocol has yet been agreed for IVIM data and hence each study will give different results. Additionally, for almost all of the studies included in the calculation of reference ranges the subjects were almost exclusively <30 years old and male compared to the livers perfused in this study which were from older male and female donors. Both age and gender have been shown to affect perfusion and diffusion parameters in a bi-exponential IVIM model[99] and hence are likely to also influence the parameters in the tri-exponential IVIM model used in this study.

The stable haematocrit and hepatic iron content, measured by arterial blood gas in the perfusate and $T_2^\star$ mapping respectively, demonstrate that the adaptations performed to the perfusion system have not led to increased mechanical insults or trauma for the red blood cells in the perfusate and hence do not cause a significant amount of haemolysis for at least 12 hrs of perfusion.

7.5.3 Tissue assessment by relaxometry

Large differences were observed between the initial liver T_1 values of Liver A and those of Livers B and C. This is likely due to a combination of an increased amount of oedema combining with greater ischaemia reperfusion injury and hence greater levels of inflammation in the livers which underwent prolonged static cold storage. The consistency of liver T_1 during NMP suggests that additional inflammation, oedema, fibrosis or necrosis is not building up during perfusion. In other words, the liver is being held in a stable state by NMP.

The importance of effective perfusion is highlighted by the edge of the left lobe of Liver C which had poor perfusion measured by IVIM and saw a significant increase in T_1 - a direct contrast to the well perfused areas of this liver. A similar but less significant trend was observed for the outer edges of Liver B where T_1 slightly increased during perfusion. This gave a more variable appearance to the later T_1 maps from Liver B and may indicate small pockets of poorly perfused tissue appearing throughout the graft. However, all biomarkers currently used to determine viability for transplant examine the net state of the liver and hence the significance of these spatial variation on the short- and long-term outcomes post-transplant is unknown. Whether spatial variation is predictive in whole liver transplant or not, these spatial variations would likely be very important when determining whether a donated liver is a candidate for a split liver transplant.

7.5.4 Hepatic steatosis

Reducing the level of steatosis in livers prior to transplantation has been hypothesised as a method to further expanding the donor pool by converting a previously non-viable liver into a viable candidate for transplantation.[149] Jamieson et al. showed a reduction in hepatic steatosis could be achieved with a prolonged period of NMP in a porcine model.[103] However, in my study very little change in hepatic fat fraction was observed in human livers during 12 h of NMP. Therefore, to achieve a significant reduction in hepatic steatosis during a clinically realistic duration of NMP additional interventions which have been shown to decrease hepatic steatosis, such as lipoprotein apheresis filtration of the perfusate and pharmacological intervention to promote fatty acid transport and β-oxidation, may be necessary.[21 38]

7.5.5 Energy metabolism

All livers examined in this study showed evidence of ATP regeneration through an increased ATP/Pi ratio. Interestingly, the rate of recovery seen is comparable to that reported by Xu et al. who performed invasive measurements of ATP from biopsies in a pre-clinical

porcine liver perfusion model (85% recovery following 4 h of NMP in the porcine livers and a calculated 84% recovery in the human livers from the present study).[231] As well as the species difference, the two transplant models studied are very different with Xu et al. studying a previously healthy DCD model with 60 minutes of warm ischaemia before a short 2 h period of cold ischaemia and 4 h of NMP while the present study focused on steatotic DBD donors and had very long periods of cold ischaemia (up to 26 h) before NMP. That both models show similar rates of ATP recovery may indicate that there is a near universal rate of ATP recovery during NMP and it is only the absolute concentration of ATP that is different in different cases. Alternatively, it may be that in this instance the damage caused by prolonged cold ischaemia on the steatotic livers, which are known to be more sensitive to cold ischaemia,[196] has by chance equalled the warm ischaemic damage in previously healthy DCD livers.

7.5.6 Clinical implications

Both the previous pre-clinical study and this present human liver work suggest that the current guidance to perfuse a liver for at least 4 h may not be long enough to ensure full ATP recovery. In this study, livers would need to be perfused for at least 6.5 h to achieve 95% recovery of ATP or 10 h to reach 99% recovery, assuming an exponential recovery model. The minimum level of ATP recovery needed to obtain an optimum post-transplant outcome is currently unknown. However given that even in severely damaged tissue, such as cardiac muscle during heart failure, decreases in ATP content are <10%, it is reasonable to assume that a very high level of recovery would be necessary.[224]

Extended durations of perfusion may be increasingly necessary as transplant units move to a predominantly 'back-to-base' model, where the liver is transported on ice to the recipient hospital before undergoing end-ischaemic normothermic perfusion (i.e. NMP after static cold storage) as was performed in this study. Recent trials have shown this approach to be safe and that is has non-inferior post-transplant outcomes when compared to continuous NMP where the liver is placed on the perfusion device at the donor hospital and perfused during transportation.[25 40] This technique therefore makes an enticing alternative with simplified

logistics and reduced cost as compared to continuous NMP. However, having an extended ischaemic period may necessitate a longer recovery period during NMP as has been observed in this study. Alternatively, this back-to-base model may give a window of opportunity for MRI assessment of T_1 by clinical MRI or perhaps even using a point of care portable MRI machine.

During NMP, one of the standard criteria used to assess the viability of a donated liver is its ability to metabolise glucose.[117] However, even applying the Cambridge criteria which require a peak fall in glucose concentration of > 4.4 mmol/L/h/kg there is little information of how the liver is metabolising the glucose and what type of glycolytic metabolism is occurring.[222] Hyperpolarized ^{13}C-MRS provides a view into this metabolism by monitoring the flux of pyruvate through PDH, ALT and LDH via the conversion of a labelled pyruvate substrate into bicarbonate, alanine and lactate respectively.[220] This tracks the relative rates of fatty acid oxidation, protein synthesis and anaerobic glycolysis. In the livers examined in this study, the rate of conversion of pyruvate to lactate shadowed the perfusate lactate concentration, remaining high in Liver B and falling in Liver C over the time of the perfusion. Interestingly, previous cellular studies have shown that LDH activity and hence $k_{Pyr \rightarrow Lac}$ are not correlated to intra-cellular lactate concentration but instead are more dependent on the rate of transportation into the cell through monocarboxylate transporter-1 (MCT1).[177] Therefore, although the results correlated in this small sample, there may be additional information in the metabolic state of the liver through assessment of both perfusate lactate concentration and the rate of intra-cellular lactate production. The flux through PDH and ALT was much lower in both livers but appeared to show diverging trends, especially in ALT flux. Further experiments are needed to examine if these effects persist in a wide range of livers. The current results suggest that there may be more interesting changes occurring in glycolytic metabolism within the livers than are captured by blood glucose measurements.

7.5.7 Limitations

This study was designed to prove feasibility of perfusing ex vivo human livers inside an MRI scanner and perform a non-invasive assessment of the organ while it is being perfused. Therefore, it is inherently limited by the small number of organs perfused and not powered to make any firm judgements on the predictive power of the MR biomarkers considered. The lack of a post-transplant end-point also limits the capacity of the study to define useful MR biomarkers to predict viability. Therefore, the study should be viewed as hypothesis generating for possible MR biomarkers to be assessed in a future prospective clinical trial. In any future clinical trial, the impact of fat on the shMOLLI T_1 values should also be considered. Liver fat is a known confounder of shMOLLI T_1 values and in this study this effect was not accounted for. However, with a larger sample size, one could validate one of the in vivo correction algorithms to enable correction of the ex vivo shMOLLI T_1 values for the effect of severe steatosis. Additionally, although this study has demonstrated that it is possible to perform MR assessments on perfused livers the current experimental set-up is very delicate and labour intensive requiring an on-call team of surgeons, engineers, MR physicists and chemists. It also took a significant amount of time to prime the perfusion system within the MR scanner and to clean the scanner after a perfusion. With each task taking over 90 minutes, large amounts of time on the MRI scanner was required even excluding any time taken to perform the measurements. All of these factors mean the current system is not well suited to application into a clinical work-flow. Therefore, in future studies it may be beneficial to consider adapting the system to function on smaller scanners, eg. neo-natal or emergency portable MRI scanners, which have much smaller fringe fields and would require much more minimal adaptations to the perfusion system. This may allow the system to be integrated into a clinical pipeline better and hence allow the assessment of which, if any, of the MR biomarkers discussed here are predictive of post-transplant outcomes.

7.6 Conclusion

In summary, I have demonstrated the feasibility of MRI and MRS assessment of liver physiology and metabolism during normothermic machine perfusion without compromising the quality of either the perfusion system and without introducing artefacts into the MR images and spectra. This study has shown it is possible to examine glycolytic and oxidative metabolism in ex vivo livers using ^{13}C and ^{31}P MRS respectively, as well as tissue perfusion and underlying tissue structure through IVIM and relaxometry assessments.

Given the large temporal, and sometimes even spatial, variations observed in a range of the MR biomarkers, further studies are warranted to identify which of the trends persist and hence which biomarkers, if any, are predictive of an organ's viability for transplant.

8

Summary and outlook

8.1 Conclusions

The addition of machine perfusion techniques in deceased donor liver transplantation has redefined what makes a donated liver viable for transplantation and made many non transplantable organs transplantable.[139] However, to date no biomarkers have been identified with sufficiently high sensitivity and specificity to predict the transplantability of a donated liver. The lack of a predictive test, combined with a need for caution in the case of uncertainty, is limiting the expansion of the donor pool and hence reducing the number of liver transplants that can be safely performed. Therefore, novel biomarkers are needed to enable the viability of each specific donor liver to be assessed.

In this thesis I explored the utility of MRI and MRS biomarkers to non-invasively monitor the metabolic and physiological state of ex vivo livers. By correlating the MR biomarkers with current clinical viability criteria, I performed preliminary assessments of the potential of MR to predict liver viability and hence fulfil a major unmet clinical need in liver transplantation.

In order to understand the characteristics of a liver during ex vivo preservation, it is first important to consider the insults that have occurred during the donation process. Therefore, Chapter 4 characterised baseline in vivo conditions in a porcine model. Then the chapter

continued to presented deleterious effect of death, whether determined by circulatory or neurological criteria, on on the energetic and physiological state of the liver in the same animals thus tracking a model of human organ donation. The effect was considerably more profound in livers following circulatory arrest than following brain-stem death. However, this work demonstrated that in deceased donor transplantation all livers have been subjected to a significant insult before even being considered for transplantation. Hence this chapter emphasised the need to perform a viability assessment on a liver once it has been retrieved and has sustained that insult, rather than rely on donor history alone which will not properly account for this.

The obvious next point when a donor liver could be assessed is during static cold storage. This provided an added challenge for MR metrics, which are inherently temperature sensitive. However, as Chapter 5 demonstrated, it is possible to correct for the confounding effect of temperature and that temperature corrected T_1 shows significant potential for the differentiation of human livers deemed functional and non-functional by clinical criteria during NMP. This work was summarised in a paper published in Magnetic Resonance in Medicine.[235]

During static cold storage, a liver's metabolism is slowed to <10% of the normal rate and the lack of an oxygen supply causes a switch to anaerobic metabolism. This means that metabolic assessment in this state is difficult to interpret and will not account for the insult that awaits the liver during reperfusion when metabolism re-starts at pace. Therefore, in Chapter 6 I used MR to assess the metabolic and physiological state of pig livers during normothermic machine perfusion. I showed evidence of recovery in energetic metabolism with increased ATP/Pi ratios and identified liver T_1 as a promising biomarker for predicting liver function, even before biochemical biomarkers in one case.

Finally, I demonstrated the feasibility of assessing human livers using MRI and MRS techniques during ex vivo NMP in Chapter 7. Again, a recovery of energetic metabolism was observed in all livers using ^{31}P-MRS. However, this study highlighted the benefit of using imaging to provide a regional assessment of the liver rather than net averages provided through either perfusate biochemistry or non-localised spectroscopy. Indeed in one case,

excellent net biochemical function was observed but MRI-based perfusion and T_1 maps demonstrated an area that was poorly perfused and increasingly damaged during perfusion.

Throughout this thesis a range of MR biomarkers have been utilised to assess the metabolic or physiological state of the liver under the hypothesis that they may provide a useful metric to assess viability. For some of the biomarkers, a lot of potential has been seen for prediction of liver viability, while others may provide information more about the perfusion system or simply be to complex to interpret.

- *IVIM diffusion weighted imaging*

  Perfusion was seen to significantly decrease following the cessation of circulation in a porcine DCD model. However in ex vivo perfused livers, perfusion and diffusion metrics appeared to reflect the performance of the perfusion system more than the function of the liver. Indeed, no significant difference was observed between livers deemed functional and non-functional. A reduced intermediate perfusion compartment (representative of the portal system)[230] was seen in all livers on the MR-compatible NMP system. A corresponding reduction in the portal flow rate was observed in perfused liver, implying that the IVIM metrics may be more sensitive to changes in bulk flow generated by the perfusion system than liver function. These results suggest that IVIM may provide a useful metric to optimise a perfusion system, for example examining the effect of pulsatile or non-pulsatile flow. However from the data presented in this thesis, IVIM metrics are not strong candidate biomarkers to assess viability.

- *Hyperpolarized ^{13}C-MRS*

  As Figure 3.8 demonstrated, the balance of glycolytic and fatty acid metabolism within the liver is very carefully balanced and dependent on intra- and extra-cellular concentration of a range of metabolites including glucose, lactate, and fatty acids. This makes the interpretation of hyperpolarized ^{13}C-MRS results challenging to interpret in ex vivo livers where homoeostasis of many metabolites cannot be assumed. Although, the data in this thesis demonstrate that glycolytic metabolism was occurring

in livers during NMP, no clear trends were observed. Therefore, hyperpolarized ^{13}C-MRS biomarkers may be best suited to examine the impact of pharmacological interventions in metabolic studies rather than being useful for a broad assessment of transplant viability. For example, they may provide a non-invasive method for monitoring the changes in fatty acid oxidation when applying an intervention to reduce liver fat.

- *^{31}P-MRS*

  Increased ATP content within the liver immediately prior to transplantation is known to lead to improved post-transplant outcomes and ^{31}P-MRS provides a non-invasive method of assessing hepatic ATP content. This thesis has demonstrated that NMP can regenerated hepatic ATP content following a period of ischaemia. I have also suggested that a slightly longer duration of perfusion, above the minimum 4 h that is currently recommended, may enable a further improvement in ATP content which might improve post-transplant outcomes. Additionally, different rates of recovery of ATP were observed in different livers with some recovering ATP very rapidly and others taking several hours. Therefore, assessment of ATP content by ^{31}P-MRS could provide a useful biomarker to know when a liver has been perfused for long enough or whether additional metabolic (ATP) recovery could be obtained prior to transplantation. However, the low SNR of ^{31}P-MRS necessitates a long acquisition time and sufficiently high magnetic field to obtain analysable data. This combined with the technical complexity of ^{31}P-MRS experiments means that although the technique shows promise for monitoring liver viability, the clinical utility of the measurements may be impaired by the logistical challenges integrating the measurements into a clinical trial or in the future a clinical pipeline.

- *Proton density fat fraction (PDFF)*

  PDFF has been shown to provide a rapid, repeatable, and controlled assessment of liver steatosis in vivo. In this thesis, I have demonstrated that PDFF can also be measured in ex vivo livers and that these measurements are repeatable (with appropriate

correction for temperature effects). It is known that steatotic livers carry a higher risk of post-transplant complication than lean livers when preserved by static cold storage. However, recent evidence suggests that the impact of steatosis may be reduced or even removed when livers are preserved by NMP. Therefore, PDFF may make a good biomarker for screening livers to assess whether they are low risk and should be directly transplanted following static cold storage or are high risk and would benefit from a period of machine perfusion prior to transplantation. The measurement takes <20 s to make and can be performed on any clinical MRI scanner. Therefore, integration of this measurement into a clinical work flow is much more reasonable and supports further study of this biomarker. It could perhaps even be performed using the new generation of dedicated point-of-care MRI systems.

- *T_1*

  The most promising biomarker studied in this thesis is liver T_1. Significant differences were observed between functional and non-functional livers measured both during NMP and SCS. A large increase in liver T_1 was also seen following an hour of warm ischaemia in a model of DCD. These trends, combined with the early changes seen in one liver relative to perfusate lactate, suggest that liver T_1 may be a useful biomarker for predicting transplantability. This warrants further examination in a larger-scale study to confirm whether it is generalisable.

8.2 Future outlook

The preliminary studies performed in this thesis have demonstrated the feasibility and promise of performing MR examination of ex vivo livers during both static and dynamic organ preservation. The next study should perform the most promising candidate assessments, T_1 and PDFF, prior to transplantation and then assess whether they are predictive of clinical outcomes.

In order to achieve this and improve the likelihood of clinical adoption, an adaptation to the MR-compatible perfusion system would need to be made. The experiments detailed in

this thesis were only possible with a large inter-disciplinary team of surgeons, engineers, MR physicists, biochemists, and chemists constantly on-call and able to attend each experiment at the time that they were required. Additionally, the changes to the perfusion system meant that it required constant monitoring and this combined with controlling the MR scanner and collection of biochemical samples meant that at least 3 members of the study team were required to constantly intervene for the entire duration of any perfusions. This huge undertaking would not be feasible in a clinical work-flow where the demands on personnel and equipment would be too great. However, novel MRI technologies such as neonatal MRI scanners with zero fringe fields or low-field portable MRI scanners capable of scanning ventilated patients in intensive case, such as the HyperMag, may offer an alternative to a high-field clinical MRI scanner and hence remove the need for a heavily adapted perfusion system. If these scanners could be used, the feasibility of perfusing a liver on a standard perfusion system before quickly sliding the organ container into a magnet for a 2 minute MR scan to measure PDFF and liver T_1 can clearly be seen.

8.2.1 Other impacts

The potential benefit of MR assessment of donor organs in transplantation is not limited to livers. Indeed, the work contained in this thesis has contributed to the design of several further studies which are using MR biomarker to assess a range of organs including hearts, kidneys and pancreata during static cold storage, hypothermic machine perfusion and normothermic machine perfusion. The outcomes from these studies are eagerly awaited.

Outside of clinical transplantation, the ability to perform whole organ imaging on a clinical MRI scanner while the organ is held in a stable metabolically active state by NMP provides many opportunities in experimental medicine. Whether elucidating the biophysical underpinnings of changes in MR signal by comparison to histological samples, enabling repeated non-invasive assessments of metabolism to examine the pharmacokinetics of novel therapeutics in human organs or providing an assessment of perfusion systems to enable refinement of perfusion protocols, the MR-compatible NMP system that has been validated in this thesis holds potential to support a range of basic scientific studies.

Overall, ex vivo MR biomarkers hold significant promise in the non-invasive assessment of transplant organs and are deserving of further clinical investigations.

Bibliography

[1] Non-invasive rapid assessment of patients with liver transplants using magnetic resonance imaging with livermultiscan (RADIcAL2). Identifier: NCT03165201, 2017. URL `https://clinicaltrials.gov/ct2/show/NCT03165201`.

[2] T. M. A, W. J. J., van Dijk Anne-Marieke, M. A. Linde, R. J. H, V. Joanne, Nieuwdorp, H. A. G, N. A. J, and G.-C. O. J. Physics-informed deep neural network for tri-exponential intravoxel incoherent motion fitting in non-alcoholic fatty liver disease. In *Proc. ISMRM*, number 0312, 2021.

[3] Y. N. Abdul Manaf, J. M. Nazrim Marikkar, S. Musthafa, and M. M. Saari. Composition and thermal analysis of binary mixtures of mee fat and palm stearin. *J Oleo Sci*, 63(4): 325–332, 2014. doi: 10.5650/jos.ess13193.

[4] A. Abragam and M. Goldman. Principles of dynamic nuclear polarisation. *Rep Prog Phys*, 41(3):395–467, 1978. doi: 10.1088/0034-4885/41/3/002.

[5] L. C. Adams, K. K. Bressem, S. Scheibl, M. Nunninger, A. Gentsch, U. L. Fahlenkamp, K.-U. Eckardt, B. Hamm, and M. R. Makowski. Multiparametric assessment of changes in renal tissue after kidney transplantation with quantitative MR relaxometry and diffusion-tensor imaging at 3 T. *J Clin Med*, 9(32455558):1551, May 2020. doi: 10.3390/jcm9051551.

[6] A. Ali, J. Selamat, Y. B. Che Man, and A. M. Suria. Effect of storage temperature on texture, polymorphic structure, bloom formation and sensory attributes of filled dark chocolate. *Food Chem.*, 72(4):491–497, 2001. doi: 10.1016/S0308-8146(00)00271-5.

[7] A. Andreou, D. M. Koh, D. J. Collins, M. Blackledge, T. Wallace, M. O. Leach, and M. R. Orton. Measurement reproducibility of perfusion fraction and pseudodiffusion coefficient derived by intravoxel incoherent motion diffusion-weighted MR imaging in normal liver and metastases. *Eur Radiol*, 23(2):428–434, 2013. doi: 10.1007/s00330-012-2604-1.

[8] A. Apps, J. Y. C. Lau, J. J. J. J. Miller, A. Tyler, L. A. J. Young, A. J. M. Lewis, G. Barnes, C. Trumper, S. Neubauer, O. J. Rider, and D. J. Tyler. Proof-of-principle demonstration of direct metabolic imaging following myocardial infarction using hyperpolarized 13C CMR. *JACC: Cardiovasc Imaging*, 14(6):1285–1288, 2021. doi: 10.1016/j.jcmg.2020.12.023.

[9] J. H. Ardenkjaer-Larsen, B. Fridlund, A. Gram, G. Hansson, L. Hansson, M. H. Lerche, R. Servin, M. Thaning, and K. Golman. Increase in signal-to-noise ratio of > 10,000 times in liquid-state NMR. *Proc Nat Acad Sci USA*, 100:10158–63, Sep 2003. doi: 10.1073/pnas.1733835100.

[10] J. Z. Bakdash and L. R. Marusich. Repeated measures correlation. *Frontiers in Psychol*, 8:456, 2017. doi: 10.3389/fpsyg.2017.00456.

[11] R. Banerjee, M. Pavlides, E. M. Tunnicliffe, S. K. Piechnik, N. Sarania, R. Philips, J. D. Collier, J. C. Booth, J. E. Schneider, L. M. Wang, D. W. Delaney, K. A. Fleming, M. D. Robson, E. Barnes, and S. Neubauer. Multiparametric magnetic resonance for the non-invasive diagnosis of liver disease. *J Hepatol*, 60:69–77, Jan 2014. doi: 10.1016/j.jhep.2013.09.002.

[12] P. Bankhead, M. B. Loughrey, J. A. Fernández, Y. Dombrowski, D. G. McArt, P. D. Dunne, S. McQuaid, R. T. Gray, L. J. Murray, H. G. Coleman, J. A. James, M. Salto-Tellez, and P. W. Hamilton. QuPath: Open source software for digital pathology image analysis. *Sci Rep*, 7(1):16878, 2017. doi: 10.1038/s41598-017-17204-5.

[13] P. Bannas, H. Kramer, D. Hernando, R. Agni, A. M. Cunningham, R. Mandal, U. Motosugi, S. D. Sharma, A. M. del Rio, L. Fernandez, and S. B. Reeder. Quantitative magnetic resonance imaging of hepatic steatosis: Validation in ex vivo human livers. *Hepatology*, 62(5):1444–1455, 2015. doi: 10.1002/hep.28012.

[14] R. Barthwal, M. Höhn-berlage, and K. Gersonde. In vitro proton T1 and T2 studies on rat liver: analysis of multiexponential relaxation processes. *Magn Reson Med*, 3(6):863–875, 1986. doi: 10.1002/mrm.1910030607.

[15] F. O. Belzer and J. H. Southard. Principles of solid-organ preservation by cold storage. *Transplantation*, 45(4), 1988.

[16] V. Bewick, L. Cheek, and J. Ball. Statistics review 13: Receiver operating characteristic curves. *Crit Care*, 8(6):508, 2004. doi: 10.1186/cc3000.

[17] S. W. Biggins, H. J. Rodriguez, P. Bacchetti, N. M. Bass, J. P. Roberts, and N. A. Terrault. Serum sodium predicts mortality in patients listed for liver transplantation. *Hepatology*, 41(1):32–39, Jan. 2005. doi: 10.1002/hep.20517.

[18] J. M. Bland and D. G. Altman. Statistics notes: Measurement error. *BMJ*, 313(7059):744, 1996. doi: 10.1136/bmj.313.7059.744.

[19] J. M. Bland and D. G. Altman. Statistics notes: Measurement error proportional to the mean. *BMJ*, 313(7049):106, 1996. doi: 10.1136/bmj.313.7049.106.

[20] N. Bloembergen. Spin relaxation processes in a two-proton system. *Phys Res*, 104(6):1542–1547, Dec. 1956. doi: 10.1103/PhysRev.104.1542.

[21] Y. L. Boteon, J. Attard, A. P. C. S. Boteon, L. Wallace, G. Reynolds, S. Hubscher, D. F. Mirza, H. Mergental, R. H. Bhogal, and S. C. Afford. Manipulation of lipid metabolism during normothermic machine perfusion: Effect of defatting therapies on donor liver functional recovery. *Liver Transpl*, 25:1007–1022, Jul 2019. doi: 10.1002/lt.25439.

[22] P. A. Bottomley. Spatial localization in NMR spectroscopy in vivo. *Ann NY Acad Sci*, 508(1):333–348, 1987.

[23] P. A. Bottomley. *NMR spectroscopy of the human heart*. 2009. ISBN 9780470034590. doi: https://doi.org/10.1002/9780470034590.emrstm0345.pub2.

[24] A. E. Braat, J. J. Blok, H. Putter, R. Adam, A. K. Burroughs, A. O. Rahmel, R. J. Porte, X. Rogiers, J. Ringers, for the European Liver, I. T. A. (ELITA), and E. L. I. A. C. (ELIAC). The eurotransplant donor risk index in liver transplantation: ET-DRI. *Am J Transplant*, 12(10):2789–2796, Oct. 2012. doi: 10.1111/j.1600-6143.2012.04195.x.

[25] M. Bral, K. Dajani, D. Leon Izquierdo, D. Bigam, N. Kneteman, C. D. L. Ceresa, P. J. Friend, and A. M. J. Shapiro. A back-to-base experience of human normothermic ex situ liver perfusion: Does the chill kill? *Liver Transpl*, 25(6):848–858, 2019. doi: 10.1002/lt.25464.

[26] British Transplant Society (with NHS Blood and Transplant). Transplantationfrom deceased donors after circulatory death, 2013. URL `https://bts.org.uk/wp-content/uploads/2016/09/15_BTS_Donors_DCD-1.pdf`.

[27] J. G. Brockmann, A. Vaidya, S. Reddy, and P. J. Friend. Retrieval of abdominal organs for transplantation. *Br J Surg*, 93(2):133–146, 2006. doi: 10.1002/bjs.5228.

[28] R. A. Brooks and G. Di Chiro. Magnetic resonance imaging of stationary blood: A review. *Med Phys*, 14(6):903–913, 1987. doi: 10.1118/1.595994.

[29] R. W. Brown, Y.-C. N. Cheng, E. M. Haake, M. R. Thompson, and R. Venkatesan. *Magnetic Resonance Imaging*. 2014.

[30] R. G. Bryant. NMR relaxation studies of solute-solvent interactions. *Annu Rev Phys Chem*, 29(1):167–188, Oct. 1978. doi: 10.1146/annurev.pc.29.100178.001123.

[31] K. P. Burnham and D. R. Anderson. Multimodel inference: understanding AIC and BIC in model selection. *Sociol Methods Res*, 33(2):261–304, Nov. 2004. doi: 10.1177/0049124104268644.

[32] C. J. Callaghan, S. C. Charman, P. Muiesan, J. J. Powell, A. E. Gimson, J. H. P. van der Meulen, and on behalf of the UK Liver Transplant Audit. Outcomes of transplantation of livers from donation after circulatory death donors in the UK: a cohort study. *BMJ Open*, 3(9), 2013. doi: 10.1136/bmjopen-2013-003287.

[33] B. Cardini, R. Oberhuber, M. Fodor, T. Hautz, C. Margreiter, T. Resch, S. Scheidl, M. Maglione, C. Bösmüller, H. Mair, M. Frank, F. Augustin, A. Griesmacher, H. Schennach, J. Martini, R. Breitkopf, S. Eschertzhuber, W. Pajk, A. Obwegeser, H. Tilg, C. Watson, D. Öfner, A. Weissenbacher, and S. Schneeberger. Clinical implementation of prolonged liver preservation and monitoring through normothermic machine perfusion in liver transplantation. *Transplantation*, 104(9), 2020.

[34] R. Carini, R. Autelli, G. Bellomo, and E. Albano. Alterations of cell volume regulation in the development of hepatocyte necrosis. *Exp Cell Res*, 248:280–93, Apr 1999. doi: 10.1006/excr.1999.4408.

[35] K. Carlson, A. Barbas, N. Goldaracena, L. Fernandez, and D. P. Al-Adra. Immunological organ modification during ex vivo machine perfusion: The future of organ acceptance. *Transplant Rev*, 35(2):100586, 2021. doi: 10.1016/j.trre.2020.100586.

[36] A. Carrel and C. A. Lindbergh. The culture of whole organs. *Science*, 81:621–3, Jun 1935. doi: 10.1126/science.81.2112.621.

[37] J.-P. Cercueil, J.-M. Petit, S. Nougaret, P. Soyer, A. Fohlen, M.-A. Pierredon-Foulongne, V. Schembri, E. Delhom, S. Schmidt, A. Denys, S. Aho, and B. Guiu. Intravoxel incoherent motion diffusion-weighted imaging in the liver: comparison of mono-, bi- and tri-exponential modelling at 3.0-T. *Eur Radiol*, 25(6):1541–1550, 2015. doi: 10.1007/s00330-014-3554-6.

[38] C. Ceresa, D. Nasralla, T. Cornfield, A. Clark, P. Hook, L. Young, C. Coussios, L. Hodson, and P. J. Friend. Exploring the structural and functional effects of normothermic machine perfusion and defatting interventions on human steatotic livers. *Hepatology*, 68:2A–2A, 2018.

[39] C. D. L. Ceresa. *Novel approaches in optimising steatotic livers for transplantation*. Dphil thesis, University of Oxford, 2018.

[40] C. D. L. Ceresa, D. Nasralla, C. J. E. Watson, A. J. Butler, C. C. Coussios, K. Crick, L. Hodson, C. Imber, W. Jassem, S. R. Knight, H. Mergental, R. J. Ploeg, J. M. Pollok, A. Quaglia, A. M. J. Shapiro, A. Weissenbacher, and P. J. Friend. Transient cold storage prior to normothermic liver perfusion may facilitate adoption of a novel technology. *Liver Transpl*, 25(10):1503–1513, 2019. doi: 10.1002/lt.25584.

[41] R. Cervelli, M. Cencini, G. Buonincontri, F. Campana, A. Cacciato Insilla, G. Aringhieri, P. De Simone, U. Boggi, D. Campani, M. Tosetti, and L. Crocetti. 7-T MRI of explanted liver and ex-vivo pancreatic specimens: prospective study protocol

of radiological-pathological correlation feasibility (the EXLIPSE project). *Eur Radiol Exp*, 4(1):58, 2020. doi: 10.1186/s41747-020-00185-y.

[42] K. K. Changani, B. J. Fuller, J. D. Bell, D. J. Bryant, D. P. Moore, S. D. Taylor-Robinson, and B. R. Davidson. Hepatic nucleotide triphosphate regeneration after hypothermic reperfusion in the pig model: An in vitro: 31P-NMR study. *Transplantation*, 62(6), 1996.

[43] K. K. Changani, R. Jalan, I. J. Cox, M. Ala-Korpela, K. Bhakoo, S. D. Taylor-Robinson, and J. D. Bell. Evidence for altered hepatic gluconeogenesis in patients with cirrhosis using in vivo 31-phosphorus magnetic resonance spectroscopy. *Gut*, 49(4):557, Oct. 2001. doi: 10.1136/gut.49.4.557.

[44] H.-Y. Chen, R. Aggarwal, R. A. Bok, M. A. Ohliger, Z. Zhu, P. Lee, J. W. Gordon, M. van Criekinge, L. Carvajal, J. B. Slater, P. E. Z. Larson, E. J. Small, J. Kurhanewicz, and D. B. Vigneron. Hyperpolarized 13C-pyruvate MRI detects real-time metabolic flux in prostate cancer metastases to bone and liver: a clinical feasibility study. *Prostate Cancer Prostatic Dis*, 23(2):269–276, 2020. doi: 10.1038/s41391-019-0180-z.

[45] O. Chevallier, N. Zhou, J.-P. Cercueil, J. He, R. Loffroy, and Y. X. J. Wáng. Comparison of tri-exponential decay versus bi-exponential decay and full fitting versus segmented fitting for modeling liver intravoxel incoherent motion diffusion MRI. *NMR in Biomed*, 32(11):e4155, 2019. doi: 10.1002/nbm.4155. e4155 NBM-18-0260.R1.

[46] Y. J. Cho, W. S. Kim, Y. H. Choi, S. B. Lee, S. Lee, J.-E. Cheon, M. Paek, and S. Woo. Validation and feasibility of liver T1 mapping using free breathing MOLLI sequence in children and young adults. *Sci Rep*, 10(1):18390, 2020. doi: 10.1038/s41598-020-74717-2.

[47] K. Christensen, G. Doblhammer, R. Rau, and J. W. Vaupel. Ageing populations: the challenges ahead. *Lancet*, 374(19801098):1196–1208, Oct. 2009. doi: 10.1016/S0140-6736(09)61460-4.

[48] S. R. Chung, S. S. Lee, N. Kim, E. S. Yu, E. Kim, B. Kühn, and I. S. Kim. Intravoxel incoherent motion MRI for liver fibrosis assessment: a pilot study. *Acta Radiol*, 56: 1428–36, Dec 2015. doi: 10.1177/0284185114559763.

[49] R. Ciria, M. D. Ayllon-Teran, S. González-Rubio, I. Gómez-Luque, G. Ferrín, A. Moreno, M. Sánchez-Frías, F. Alconchel, C. Herrera, V. Martín, J. M. Sánchez-Hidalgo, . Arjona-Sánchez, Y. Okuda, I. Cabrera, B. Benavente, M. J. Rodriguez, I. Jurado-Martínez, J. M. Dueñas-Jurado, J. C. Robles-Arista, M. Rodriguez-Perálvarez, M. de La Mata García, P. López-Cillero, and J. Briceño. Rescue of discarded grafts for liver transplantation by ex vivo subnormothermic and normothermic oxygenated machine perfusion: First experience in spain. *Transplant Proc*, 51(1):20–24, 2019. doi: 10.1016/j.transproceed.2018.04.092.

[50] P. A. Clavien, P. R. Harvey, and S. M. Strasberg. Preservation and reperfusion injuries in liver allografts. an overview and synthesis of current studies. *Transplantation*, 53: 957–78, May 1992. doi: 10.1097/00007890-199205000-00001.

[51] D. Collett, P. J. Friend, and C. J. E. Watson. Factors associated with short- and long-term liver graft survival in the united kingdom: Development of a UK donor liver index. *Transplantation*, 101:786–792, Apr 2017. doi: 10.1097/TP.0000000000001576.

[52] A. Collin, J. van Milgen, S. Dubois, and J. Noblet. Effect of high temperature and feeding level on energy utilization in piglets. *J Anim Sci*, 79(7):1849–1857, July 2001. doi: 10.2527/2001.7971849x.

[53] K. P. Croome, D. D. Lee, D. K. Perry, J. M. Burns, J. H. Nguyen, A. P. Keaveny, and C. B. Taner. Comparison of longterm outcomes and quality of life in recipients of donation after cardiac death liver grafts with a propensity-matched cohort. *Liver Transpl*, 23:342–351, Mar 2017. doi: 10.1002/lt.24713.

[54] Y. Cui, H. Dyvorne, C. Besa, N. Cooper, and B. Taouli. IVIM diffusion-weighted imaging of the liver at 3.0 T: Comparison with 1.5 T. *Eur J Radiol Open*, 2:123–128, Jan. 2015. doi: 10.1016/j.ejro.2015.08.001.

[55] G. d'Assignies, A. Paisant, E. Bardou-Jacquet, A. Boulic, E. Bannier, F. Lainé, M. Ropert, J. Morcet, H. Saint-Jalmes, and Y. Gandon. Non-invasive measurement of liver iron concentration using 3-Tesla magnetic resonance imaging: validation against biopsy. *Eur Radiol*, 28(5):2022–2030, 2018. doi: 10.1007/s00330-017-5106-3.

[56] B. R. Davidson, M. L. Barnard, K. K. Changani, and S. D. Taylor Robinson. Liver transplantation: current and potential applications of magnetic resonance spectroscopy. *Liver Transpl Surg*, 3(5):481–493, 1997.

[57] E. L. de Graaf, J. Kench, P. Dilworth, N. A. Shackel, S. I. Strasser, D. Joseph, H. Pleass, M. Crawford, G. W. McCaughan, and D. J. Verran. Grade of deceased donor liver macrovesicular steatosis impacts graft and recipient outcomes more than the donor risk index. *J Gastroenterol Hepatol*, 27(3):540–546, Mar. 2012. doi: 10.1111/j.1440-1746.2011.06844.x.

[58] R. A. de Graaf. *In vivo NMR Spectroscopy*. 2014.

[59] M. E. de Vera, R. Lopez-Solis, I. Dvorchik, S. Campos, W. Morris, A. J. Demetris, P. Fontes, and J. W. Marsh. Liver transplantation using donation after cardiac death donors: long-term follow-up from a single center. *Am J Transplant*, 9:773–81, Apr 2009. doi: 10.1111/j.1600-6143.2009.02560.x.

[60] Y. de Vries, A. P. M. Matton, M. W. N. Nijsten, M. J. M. Werner, A. P. van den Berg, M. T. de Boer, C. I. Buis, M. Fujiyoshi, R. H. J. de Kleine, O. B. van Leeuwen, P. Meyer, M. C. van den Heuvel, V. E. de Meijer, and R. J. Porte. Pretransplant sequential hypo- and normothermic machine perfusion of suboptimal livers donated after circulatory death using a hemoglobin-based oxygen carrier perfusion solution. *Am J Transplant*, 19(4):1202–1211, Apr. 2019. doi: 10.1111/ajt.15228.

[61] R. Deichmann and A. Haase. Quantification of T1 values by SNAPSHOT-FLASH NMR imaging. *J Magn Reson*, 96(3):608–612, 1992. doi: 10.1016/0022-2364(92)90347-A.

[62] F. Dengu, S. H. Abbas, G. Ebeling, and D. Nasralla. Normothermic machine perfusion (NMP) of the liver as a platform for therapeutic interventions during ex-vivo liver preservation: A review. *J Clin Med*, 9(32272760):1046, Apr 2020. doi: 10.3390/jcm9041046.

[63] S. C. Deoni, B. K. Rutt, and T. M. Peters. Rapid combined T1 and T2 mapping using gradient recalled acquisition in the steady state. *Magn Reson Med*, 49(3):515–526, 2003. doi: 10.1002/mrm.10407.

[64] W. T. Dixon. Simple proton spectroscopic imaging. *Radiology*, 153(1):189–194, 1984. doi: 10.1148/radiology.153.1.6089263. URL `https://doi.org/10.1148/radiology.153.1.6089263`. PMID: 6089263.

[65] F. Durand, J. Levitsky, F. Cauchy, H. Gilgenkrantz, O. Soubrane, and C. Francoz. Age and liver transplantation. *J Hepatol*, 70(4):745–758, Apr. 2019. doi: 10.1016/j.jhep.2018.12.009.

[66] P. Dutkowski, C. E. Oberkofler, K. Slankamenac, M. A. Puhan, E. Schadde, B. Müllhaupt, A. Geier, and P. A. Clavien. Are there better guidelines for allocation in liver transplantation?: A novel score targeting justice and utility in the model for end-stage liver disease era. *Ann Surg*, 254(5), 2011.

[67] H. A. Dyvorne, N. Galea, T. Nevers, M. I. Fiel, D. Carpenter, E. Wong, M. Orton, A. de Oliveira, T. Feiweier, M.-L. Vachon, J. S. Babb, and B. Taouli. Diffusion-weighted imaging of the liver with multiple b values: effect of diffusion gradient polarity and breathing acquisition on image quality and intravoxel incoherent motion parameters–a pilot study. *Radiology*, 266:920–9, Mar 2013. doi: 10.1148/radiol.12120686.

[68] A. M. El-Badry, S. Breitenstein, W. Jochum, K. Washington, V. Paradis, L. Rubbia-Brandt, M. A. Puhan, K. Slankamenac, R. Graf, and P. A. Clavien. Assessment of hepatic steatosis by expert pathologists: the end of a gold standard. *Ann Surg*, 250(5):691–7, 2009. doi: 10.1097/SLA.0b013e3181bcd6dd.

[69] J. Ellis, M. Hundertmark, M. Spartera, W. Watson, C. T. Rodgers, and L. Valkovic. Comparison of human cardiac 31P-MRS on 3 T Trio and Prisma scanners. In *Proc. ISMRM*, 2019.

[70] D. Eshmuminov, D. Becker, L. Bautista Borrego, M. Hefti, M. J. Schuler, C. Hagedorn, X. Muller, M. Mueller, C. Onder, R. Graf, A. Weber, P. Dutkowski, P. Rudolf von Rohr, and P.-A. Clavien. An integrated perfusion machine preserves injured human livers for 1 week. *Nat Biotechnol*, 38(2):189–198, 2020. doi: 10.1038/s41587-019-0374-x.

[71] European Association for the Study of the Liver. EASL clinical practice guidelines: Liver transplantation. *J Hepatol*, 64(2):433–485, 2016. doi: 10.1016/j.jhep.2015.10.006.

[72] European Liver Transplant Registry. URL `http://www.eltr.org/`.

[73] S. Feng and J. C. Lai. Expanded criteria donors. *Clin Liver Dis*, 18(3):633–649, 2014. doi: 10.1016/j.cld.2014.05.005.

[74] S. Feng, N. P. Goodrich, J. L. Bragg-Gresham, D. M. Dykstra, J. D. Punch, M. A. DebRoy, S. M. Greenstein, and R. M. Merion. Characteristics associated with liver graft failure: The concept of a donor risk index. *Am J Transplant*, 6(4):783–790, Apr. 2006. doi: 10.1111/j.1600-6143.2006.01242.x.

[75] V. M. Ferreira, S. K. Piechnik, E. Dall'Armellina, T. D. Karamitsos, J. M. Francis, R. P. Choudhury, M. G. Friedrich, M. D. Robson, and S. Neubauer. Non-contrast T1-mapping detects acute myocardial edema with high diagnostic accuracy: a comparison to T2-weighted cardiovascular magnetic resonance. *J Cardiovasc Magn Reson*, 14(1):42, 2012. doi: 10.1186/1532-429X-14-42.

[76] D. P. Foley, L. A. Fernandez, G. Leverson, M. Anderson, J. Mezrich, H. W. Sollinger, and A. D'Alessandro. Biliary complications after liver transplantation from donation after cardiac death donors: an analysis of risk factors and long-term outcomes from a single center. *Ann Surg*, 253:817–25, Apr 2011. doi: 10.1097/SLA.0b013e3182104784.

[77] C. Fondevila, A. J. Hessheimer, M.-H. J. Maathuis, J. Muñoz, P. Taurá, D. Calatayud, H. Leuvenink, A. Rimola, R. J. Ploeg, and J. C. García-Valdecasas. Superior preservation of DCD livers with continuous normothermic perfusion. *Ann Surg*, 254 (6), 2011.

[78] J. Frahm, K. D. Merboldt, and W. Hanicke. Localized proton spectroscopy using stimulated echoes. *J Magn Reson*, 72(3):502–508, 1987. doi: 10.1016/0022-2364(87)90154-5.

[79] K. N. Frayn. *Matbolic Regulation: A human perspective*. 3rd edition, 2010.

[80] N. R. Ghugre, T. D. Coates, M. D. Nelson, and J. C. Wood. Mechanisms of tissue-iron relaxivity: nuclear magnetic resonance studies of human liver biopsy specimens. *Magn Reson Med*, 54:1185–93, Nov 2005. doi: 10.1002/mrm.20697.

[81] A. Gimson. Development of a UK liver transplantation selection and allocation scheme. *Curr Opin Organ Transplant*, 25(2), 2020.

[82] J. K. Gordon and J. McKinlay. Physiological changes after brain stem death and management of the heart-beating donor. *Continuing Education in Anaesth Crit Care Pain*, 12(5):225–229, Oct. 2012. doi: 10.1093/bjaceaccp/mks026.

[83] M. E. Guicciardi, H. Malhi, J. L. Mott, and G. J. Gores. *Apoptosis and Necrosis in the Liver*, pages 977–1010. American Cancer Society, 2013. ISBN 9780470650714. doi: 10.1002/cphy.c120020.

[84] B. Guiu, J.-M. Petit, V. Capitan, S. Aho, D. Masson, P.-H. Lefevre, S. Favelier, R. Loffroy, B. Vergès, P. Hillon, D. Krausé, and J.-P. Cercueil. Intravoxel incoherent motion diffusion-weighted imaging in nonalcoholic fatty liver disease: a 3.0-T MR study. *Radiology*, 265(1):96–103, 2012. doi: 10.1148/radiol.12112478.

[85] G. Hamilton, T. Yokoo, M. Bydder, I. Cruite, M. E. Schroeder, C. B. Sirlin, and M. S. Middleton. In vivo characterization of the liver fat 1H MR spectrum. *NMR in Biomed*, 24(7):784–790, 2011. doi: 10.1002/nbm.1622.

[86] G. Hamilton, M. S. Middleton, J. C. Hooker, W. M. Haufe, N. I. Forbang, M. A. Allison, R. Loomba, and C. B. Sirlin. In vivo breath-hold 1H MRS simultaneous estimation of liver proton density fat fraction, and T1 and T2 of water and fat, with a multi-TR, multi-TE sequence. *J Magn Reson Imaging*, 42(6):1538–1543, 2015. doi: 10.1002/jmri.24946.

[87] E. Harris and J. Boyd. Statistical bases of reference values in laboratory medicine. Book, 1995.

[88] T. Hayashi, T. Miyati, J. Takahashi, K. Fukuzawa, H. Sakai, M. Tano, and S. Saitoh. Diffusion analysis with triexponential function in liver cirrhosis. *J Magn Reson Imaging*, 38(1):148–153, 2013. doi: 10.1002/jmri.23966.

[89] B. Henninger, J. Alustiza, M. Garbowski, and Y. Gandon. Practical guide to quantification of hepatic iron with MRI. *Eur Radiol*, 30(1):383–393, 2020. doi: 10.1007/s00330-019-06380-9.

[90] D. Hernando, P. Kellman, J. P. Haldar, and Z.-P. Liang. Robust water/fat separation in the presence of large field inhomogeneities using a graph cut algorithm. *Magn Reson Med*, 63(1):79–90, 2010. doi: 10.1002/mrm.22177.

[91] D. Hernando, C. D. G. Hines, H. Yu, and S. Reeder. Addressing phase errors in fat-water imaging using a mixed magnitude/complex fitting method. *Magn Reson Med*, 67(3):638–644, 2012. doi: 10.1002/mrm.23044.

[92] D. Hernando, S. D. Sharma, H. Kramer, and S. B. Reeder. On the confounding effect of temperature on chemical shift-encoded fat quantification. *Magn Reson Med*, 72(2): 464–470, 2014. doi: 10.1002/mrm.24951.

[93] D. Hernando, S. D. Sharma, M. Aliyari Ghasabeh, B. D. Alvis, S. S. Arora, G. Hamilton, L. Pan, J. M. Shaffer, K. Sofue, N. M. Szeverenyi, E. B. Welch, Q. Yuan, M. R. Bashir, I. R. Kamel, M. J. Rice, C. B. Sirlin, T. Yokoo, and S. B. Reeder. Multisite, multivendor validation of the accuracy and reproducibility of proton-density fat-fraction quantification at 1.5T and 3T using a fat–water phantom. *Magn Reson Med*, 77(4):1516–1524, 2017. doi: 10.1002/mrm.26228.

[94] M. Hertl, T. K. Howard, J. A. Lowell, S. Shenoy, P. Robert, C. Harvey, and S. M. Strasberg. Changes in liver core temperature during preservation and rewarming in human and porcine liver allografts. *Liver Transpl Surg*, 2(2):111–7, 1996. doi: 10.1002/lt.500020205.

[95] J. M. Homer and M. S. Beevers. Driven-equilibrium single-pulse observation of t1 relaxation. a reevaluation of a rapid method for determining nmr spin-lattice relaxation times. *J Magn Reson*, 63:287–297, 1985.

[96] P. J. Hore. *Nuclear Magnetic Resonance*. Oxford University Press, 2015.

[97] D. P. Hoyer, A. Paul, A. Gallinat, E. P. Molmenti, R. Reinhardt, T. Minor, F. H. Saner, A. Canbay, J. W. Treckmann, G. C. Sotiropoulos, and Z. Mathé. Donor information based prediction of early allograft dysfunction and outcome in liver transplantation. *Liver Int*, 35(1):156–163, Jan. 2015. doi: 10.1111/liv.12443.

[98] H. H. Hu, P. Börnert, D. Hernando, P. Kellman, J. Ma, S. Reeder, and C. Sirlin. ISMRM workshop on fat–water separation: Insights, applications and progress in MRI. *Magn Reson Med*, 68(2):378–388, 2012. doi: 10.1002/mrm.24369.

[99] H. Huang, C.-J. Zheng, L.-F. Wang, N. Che-Nordin, and Y. X. J. Wáng. Age and gender dependence of liver diffusion parameters and the possibility that intravoxel incoherent motion modeling of the perfusion component is constrained by the diffusion component. *NMR in Biomed*, 34(3):e4449, 2021. doi: 10.1002/nbm.4449.

[100] I. S. Idilman, H. Aniktar, R. Idilman, G. Kabacam, B. Savas, A. Elhan, A. Celik, K. Bahar, and M. Karcaaltincaba. Hepatic steatosis: quantification by proton density fat fraction with MR Imaging versus Liver Biopsy. *Radiology*, 267(3):767–775, 2013. doi: 10.1148/radiol.13121360.

[101] M. Imran, L. Wang, J. McCrohon, C. Yu, C. Holloway, J. Otton, J. Huang, C. Stehning, K. J. Moffat, J. Ross, V. O. Puntmann, V. S. Vassiliou, S. Prasad, E. Kotlyar, A. Keogh, C. Hayward, P. Macdonald, and A. Jabbour. Native T1 mapping in the diagnosis of cardiac allograft rejection: A prospective histologically validated study. *JACC. Cardiovasc Imaging*, 12:1618–1628, Aug 2019. doi: 10.1016/j.jcmg.2018.10.027.

[102] E. Insko and L. Bolinger. Mapping of the radiofrequency field. *J Magn Reson*, 103(1):82–85, 1993. ISSN 1064-1858. doi: https://doi.org/10.1006/jmra.1993.1133. URL `https://www.sciencedirect.com/science/article/pii/S1064185883711332`.

[103] R. W. Jamieson, M. Zilvetti, D. Roy, D. Hughes, A. Morovat, C. C. Coussios, and P. J. Friend. Hepatic steatosis and normothermic perfusion–preliminary experiments in a porcine model. *Transplantation*, 92(3), 2011.

[104] O. K. Jawitz, V. Raman, Y. Barac, M. S. Mulvihill, C. Moore, A. Y. Choi, M. Hartwig, and J. Klapper. Impact of donor brain death duration on outcomes after lung transplantation. *Ann Thorac Surg*, 108:1519–1526, Nov 2019. doi: 10.1016/j.athoracsur.2019.05.026.

[105] O. K. Jawitz, V. Raman, Y. D. Barac, J. Anand, C. B. Patel, R. J. Mentz, A. D. DeVore, and C. Milano. Influence of donor brain death duration on outcomes following heart transplantation: A united network for organ sharing registry analysis. *J Thorac Cardiovasc Surg*, 159:1345–1353.e2, Apr 2020. doi: 10.1016/j.jtcvs.2019.04.060.

[106] A. N. A. Jayaswal, C. Levick, E. A. Selvaraj, A. Dennis, J. C. Booth, J. Collier, J. Cobbold, E. M. Tunnicliffe, M. Kelly, E. Barnes, S. Neubauer, R. Banerjee, and M. Pavlides. Prognostic value of multiparametric magnetic resonance imaging,

transient elastography and blood-based fibrosis markers in patients with chronic liver disease. *Liver Int*, 2020. doi: 10.1111/liv.14625.

[107] P. S. Kamath, R. H. Wiesner, M. Malinchoc, W. Kremers, T. M. Therneau, C. L. Kosberg, G. D'Amico, E. R. Dickson, and W. R. Kim. A model to predict survival in patients with end-stage liver disease. *Hepatology*, 33:464–70, Feb 2001. doi: 10.1053/jhep.2001.22172.

[108] I. H. Kim, T. Kisseleva, and D. A. Brenner. Aging and liver disease. *Curr Opin Gastroenterol*, 31(3), 2015.

[109] U. Kjaergaard, C. Laustsen, T. Nørlinger, R. S. Tougaard, E. Mikkelsen, H. Qi, L. B. Bertelsen, N. Jessen, and H. Stødkilde-Jørgensen. Hyperpolarized [1-13C] pyruvate as a possible diagnostic tool in liver disease. *Physiol Rep*, 6(30548433):e13943–e13943, Dec. 2018. doi: 10.14814/phy2.13943.

[110] D. E. Kleiner, E. M. Brunt, M. Van Natta, C. Behling, M. J. Contos, O. W. Cummings, L. D. Ferrell, Y. C. Liu, M. S. Torbenson, A. Unalp-Arida, M. Yeh, A. J. McCullough, A. J. Sanyal, and C. Nonalcoholic Steatohepatitis. Design and validation of a histological scoring system for nonalcoholic fatty liver disease. *Hepatology*, 41(6):1313–1321, 2005. doi: 10.1002/hep.20701.

[111] G. Kootstra, J. H. Daemen, and A. P. Oomen. Categories of non-heart-beating donors. *Transplant Proc*, 27:2893–4, Oct 1995.

[112] M. Krssak, A. Brehm, E. Bernroider, C. Anderwald, P. Nowotny, C. D. Man, C. Cobelli, G. W. Cline, G. I. Shulman, W. Waldhäusl, and M. Roden. Alterations in postprandial hepatic glycogen metabolism in type 2 diabetes. *Diabetes*, 53(12):3048, Dec. 2004. doi: 10.2337/diabetes.53.12.3048.

[113] Z.-X. Kuai, W.-Y. Liu, and Y.-M. Zhu. Effect of multiple perfusion components on pseudo-diffusion coefficient in intravoxel incoherent motion imaging. *Phys Med Biol*, 62:8197–8209, Oct 2017. doi: 10.1088/1361-6560/aa8d0c.

[114] K. Kumar Changani, B. J. Fuller, D. J. Bryant, J. D. Bell, M. Ala-Korpela, S. D. Taylor-Robinson, D. P. Moore, and B. R. Davidson. Non-invasive assessment of ATP regeneration potential of the preserved donor liver: A 31P MRS study in pig liver. *J Hepatol*, 26(2):336–342, Feb. 1997. doi: 10.1016/S0168-8278(97)80050-5.

[115] A. J. Kwong, W. R. Kim, J. R. Lake, J. M. Smith, D. P. Schladt, M. A. Skeans, S. M. Noreen, J. Foutz, S. E. Booker, M. Cafarella, J. J. Snyder, A. K. Israni, and B. L. Kasiske. OPTN/SRTR 2019 annual data report: Liver. *Am J Transplant*, 21(S2):208–315, Feb. 2021. doi: 10.1111/ajt.16494.

[116] R. W. Laing, R. H. Bhogal, L. Wallace, Y. Boteon, D. A. H. Neil, A. Smith, B. T. F. Stephenson, A. Schlegel, S. G. Hübscher, D. F. Mirza, S. C. Afford, and H. Mergental. The use of an acellular oxygen carrier in a human liver model of normothermic machine perfusion. *Transplantation*, 101(11), 2017.

[117] R. W. Laing, H. Mergental, C. Yap, A. Kirkham, M. Whilku, D. Barton, S. Curbishley, Y. L. Boteon, D. A. Neil, S. G. Hübscher, M. T. P. R. Perera, P. Muiesan, J. Isaac, K. J. Roberts, H. Cilliers, S. C. Afford, and D. F. Mirza. Viability testing and transplantation of marginal livers (VITTAL) using normothermic machine perfusion: study protocol for an open-label, non-randomised, prospective, single-arm trial. *BMJ Open*, 7(11), 2017. doi: 10.1136/bmjopen-2017-017733.

[118] A. Lanir, R. L. Jenkins, C. Caldwell, R. G. Lee, U. Khettry, and M. E. Clouse. Hepatic transplantation survival: correlation with adenine nucleotide level in donor liver. *Hepatology*, 8:471–5, May-Jun 1988. doi: 10.1002/hep.1840080306.

[119] J. Y. Lau, A. Apps, J. J. Miller, A. Tyler, L. A. Young, A. J. Lewis, G. Barnes, C. Trumper, S. Neubauer, O. J. Rider, and D. J. Tyler. Human 13C hybrid-shot spiral (HYSS) imaging of pathological cardiac metabolism following myocardial infarction. In *Proc. ISMRM*, 2020.

[120] D. Le Bihan, E. Breton, D. Lallemand, M. L. Aubin, J. Vignaud, and M. Laval-Jeantet. Separation of diffusion and perfusion in intravoxel incoherent motion MR imaging. *Radiology*, 168(2):497–505, Aug. 1988. doi: 10.1148/radiology.168.2.3393671.

[121] T. Le Naou, N. Le Floc'h, I. Louveau, H. Gilbert, and F. Gondret. Metabolic changes and tissue responses to selection on residual feed intake in growing pigs. *J Anim Sci*, 90(13):4771–4780, Dec. 2012. doi: 10.2527/jas.2012-5226.

[122] Y. Lee, M. F. Callaghan, and Z. Nagy. Analysis of the precision of variable flip angle t1 mapping with emphasis on the noise propagated from rf transmit field maps. *Front Neurosci*, 11, 2017. ISSN 1662-453X. doi: 10.3389/fnins.2017.00106. URL `https://www.frontiersin.org/article/10.3389/fnins.2017.00106`.

[123] H. Lei, K. Ugurbil, and W. Chen. Measurement of unidirectional Pi to ATP flux in human visual cortex at 7 T by using in vivo 31P magnetic resonance spectroscopy. *Proc Nat Acad Sci USA*, 100(14612566):14409–14414, Nov. 2003. doi: 10.1073/pnas.2332656100.

[124] H. S. Leitão, S. Doblas, G. d'Assignies, P. Garteiser, J.-L. Daire, V. Paradis, C. F. G. C. Geraldes, V. Vilgrain, and B. E. Van Beers. Fat deposition decreases diffusion parameters at MRI: a study in phantoms and patients with liver steatosis. *Eur Radiol*, 23(2): 461–467, 2013. doi: 10.1007/s00330-012-2626-8.

[125] H. Lembach, S. Mckay, A. Hann, A. Carvalheiro, Y. Boteon, M. Alzoubi, P. Kadam, B. Dissanayake, D. Bartlett, M. Armstrong, N. Rajoriya, D. Neil, R. Brown, N. Murphy, M. Abradelo, K. Roberts, A. Schlegel, H. Mergental, D. Mirza, P. Muiesan, J. Isaac, and T. Perera. NAPLES study (normothermic machine perfusion of the liver to enable the sickest first): preliminary results. *Transplantation*, 104(S3), 2020.

[126] J. Li, S. Chang, T. Liu, H. Jiang, F. Dong, M. Pei, Q. Wang, and Y. Wang. Phase-corrected bipolar gradients in multi-echo gradient-echo sequences for quantitative susceptibility mapping. *Magma*, 28:347–55, Aug 2015. doi: 10.1007/s10334-014-0470-3.

[127] W. Li, K. Grgac, A. Huang, N. Yadav, Q. Qin, and P. C. van Zijl. Quantitative theory for the longitudinal relaxation time of blood water. *Magn Reson Med*, 76(1):270–281, 2016. doi: 10.1002/mrm.25875.

[128] T. F. Lindsay, S. Liauw, A. D. Romaschin, and P. M. Walker. The effect of ischemia/reperfusion on adenine nucleotide metabolism and xanthine oxidase production in skeletal muscle. *J Vasc Surg*, 12:8–15, Jul 1990. doi: 10.1067/mva.1990.19946.

[129] C.-M. Lo. Complications and long-term outcome of living liver donors: a survey of 1,508 cases in five asian centers. *Transplantation*, 75:S12–5, Feb 2003. doi: 10.1097/01.TP.0000046534.45645.47.

[130] V. J. Lozanovski, E. Khajeh, H. Fonouni, J. Pfeiffenberger, R. von Haken, T. Brenner, M. Mieth, P. Schirmacher, C. W. Michalski, K. H. Weiss, M. W. Büchler, and A. Mehrabi. The impact of major extended donor criteria on graft failure and patient mortality after liver transplantation. *Langenbeck's Arch Surg*, 403(6):719–731, 2018. doi: 10.1007/s00423-018-1704-z.

[131] C. Lussey-Lepoutre, A. Bellucci, N. Burnichon, L. Amar, A. Buffet, T. Drossart, S. Fontaine, O. Clement, P. Benit, P. Rustin, L. Groussin, T. Meatchi, A.-P. Gimenez-Roqueplo, B. Tavitian, and J. Favier. Succinate detection using in vivo 1H-MR spectroscopy identifies germline and somatic SDHx mutations in paragangliomas. *Eur J Nucl Med Mol Imaging*, 47:1510–1517, Jun 2020. doi: 10.1007/s00259-019-04633-9.

[132] L. Makowka, A. C. Stieber, L. Sher, D. Kahn, L. Mieles, J. Bowman, J. W. Marsh, and T. E. Starzl. Surgical technique of orthotopic liver transplantation. *Gastroenterol Clin North Am*, 17(3292430):33–51, Mar. 1988.

[133] C. s. Mariager, E. S. S. Hansen, S. K. Bech, A. Munk, U. Kjærgaard, M. D. Lyhne, K. Søberg, P. F. Nielsen, S. Ringgaard, and C. Laustsen. Graft assessment of the ex vivo perfused porcine kidney using hyperpolarized [1-13C]pyruvate. *Magn Reson Med*, 84(5):2645–2655, Nov. 2020. ISSN 0740-3194. doi: 10.1002/mrm.28363.

[134] A. P. M. Matton, Y. de Vries, L. C. Burlage, R. van Rijn, M. Fujiyoshi, V. E. de Meijer, M. T. de Boer, R. H. J. de Kleine, H. J. Verkade, A. S. H. Gouw, T. Lisman, and R. J. Porte. Biliary bicarbonate, ph, and glucose are suitable biomarkers of biliary viability during ex situ normothermic machine perfusion of human donor livers. *Transplantation*, 103(7), 2019.

[135] D. McKeown, R. Bonser, and J. Kellum. Management of the heartbeating brain-dead organ donor. *Br J Anaesth*, 108:i96–i107, 2012. doi: 10.1093/bja/aer351.

[136] D. K. Menon, J. Sargentoni, S. D. Taylor-Robinson, J. D. Bell, I. J. Cox, D. J. Bryant, G. A. Coutts, K. Rolles, A. K. Burroughs, and M. Y. Morgan. Effect of functional grade and etiology on in vivo hepatic phosphorus-31 magnetic resonance spectroscopy in cirrhosis: biochemical basis of spectral appearances. *Hepatology*, 21(2):417–427, 1995.

[137] H. Mergental, M. T. P. R. Perera, R. W. Laing, P. Muiesan, J. R. Isaac, A. Smith, B. T. F. Stephenson, H. Cilliers, D. A. H. Neil, S. G. Hübscher, S. C. Afford, and D. F. Mirza. Transplantation of declined liver allografts following normothermic ex-situ evaluation. *Am J Transplant*, 16(11):3235–3245, Nov. 2016. doi: 10.1111/ajt.13875.

[138] H. Mergental, B. T. F. Stephenson, R. W. Laing, A. J. Kirkham, D. A. H. Neil, L. L. Wallace, Y. L. Boteon, J. Widmer, R. H. Bhogal, M. T. P. R. Perera, A. Smith, G. M. Reynolds, C. Yap, S. G. Hübscher, D. F. Mirza, and S. C. Afford. Development of clinical criteria for functional assessment to predict primary nonfunction of high-risk livers using normothermic machine perfusion. *Liver Transpl*, 24(10):1453–1469, Oct. 2018. doi: 10.1002/lt.25291.

[139] H. Mergental, R. W. Laing, A. J. Kirkham, M. T. P. R. Perera, Y. L. Boteon, J. Attard, D. Barton, S. Curbishley, M. Wilkhu, D. A. H. Neil, S. G. Hübscher, P. Muiesan, J. R. Isaac, K. J. Roberts, M. Abradelo, A. Schlegel, J. Ferguson, H. Cilliers, J. Bion, D. H. Adams, C. Morris, P. J. Friend, C. Yap, S. C. Afford, and D. F. Mirza. Transplantation of discarded livers following viability testing with normothermic machine perfusion. *Nat Commun*, 11(1):2939, 2020. doi: 10.1038/s41467-020-16251-3.

[140] R. M. Merion, N. P. Goodrich, and S. Feng. How can we define expanded criteria for liver donors? *J Hepatol*, 45(4):484–488, Oct. 2006. doi: 10.1016/j.jhep.2006.07.016.

[141] D. R. Messroghli, A. Radjenovic, S. Kozerke, D. M. Higgins, M. U. Sivananthan, and J. P. Ridgway. Modified Look-Locker inversion recovery (MOLLI) for high-resolution T1 mapping of the heart. *Magn Reson Med*, 52:141–6, Jul 2004. doi: 10.1002/mrm.20110.

[142] J. J. J. J. Miller, A. Z. Lau, and D. J. Tyler. Bounded rate constant estimation in hyperpolarised [1-13C]pyruvate Bounded rate constant estimation in hyperpolarised [1-13C]pyruvateexperiments by a delayed-rejection adaptive Metropolis Markov-chain monte experiments by a delayed-rejection adaptive Metropolis Markov-chain Monte Carlo (DAM-MCMC) method. In *Proc. ISMRM*, 2017.

[143] M. Mio, Y. Fujiwara, K. Tani, T. Toyofuku, T. Maeda, and T. Inoue. Quantitative evaluation of focal liver lesions with T1 mapping using a phase-sensitive inversion recovery sequence on gadoxetic acid-enhanced MRI. *Eur J Radiol Open*, 8:100312, 2021. doi: 10.1016/j.ejro.2020.100312.

[144] H. Motulsky and A. Christopoulos. *Fitting Models to Biological Data Using Linear and Nonlinear Regression: A Practical Guide to Curve Fitting*. Oxford University Press, 2004. ISBN 9780198038344. URL `https://books.google.co.uk/books?id=g1F09pquF3kC`.

[145] F. Mozes. *Magnetic resonance imaging of the liver. T1 dynamics: confounders and modelling*. Dphil thesis, University of Oxford, 2018.

[146] F. E. Mozes, E. M. Tunnicliffe, M. Pavlides, and M. D. Robson. Influence of fat on liver T1 measurements using modified Look-Locker inversion recovery (MOLLI) methods at 3T. *J Magn Reson Imaging*, 44(1):105–111, July 2016. doi: 10.1002/jmri.25146.

[147] F. E. Mozes, E. M. Tunnicliffe, A. Moolla, T. Marjot, C. K. Levick, M. Pavlides, and M. D. Robson. Mapping tissue water T1 in the liver using the MOLLI T1 method in the presence of fat, iron and B0 inhomogeneity. *NMR Biomed*, 32(2):e4030, 2019. doi: 10.1002/nbm.4030.

[148] C. Muscari, C. Finelli, C. Stefanelli, F. Flamigni, C. Guarnieri, and C. M. Caldarera. Age-dependent differences of ATP breakdown and ATP-catabolite release in ischemic and reperfused hearts. *Mech Ageing Dev*, 67(1):1–11, 1993. doi: 10.1016/0047-6374(93)90107-3.

[149] D. Nagrath, H. Xu, Y. Tanimura, R. Zuo, F. Berthiaume, M. Avila, R. Yarmush, and M. L. Yarmush. Metabolic preconditioning of donor organs: defatting fatty livers by normothermic perfusion ex vivo. *Metab Eng*, 11(19508897):274–283, 2009. doi: 10.1016/j.ymben.2009.05.005.

[150] D. Nasralla, C. C. Coussios, H. Mergental, M. Z. Akhtar, A. J. Butler, C. D. L. Ceresa, V. Chiocchia, S. J. Dutton, J. C. García-Valdecasas, N. Heaton, C. Imber, W. Jassem, I. Jochmans, J. Karani, S. R. Knight, P. Kocabayoglu, M. Malagò, D. Mirza, P. J. Morris, A. Pallan, A. Paul, M. Pavel, M. T. P. R. Perera, J. Pirenne, R. Ravikumar, L. Russell, S. Upponi, C. J. E. Watson, A. Weissenbacher, R. J. Ploeg, and P. J. Friend. A randomized trial of normothermic preservation in liver transplantation. *Nature*, 557:50–56, May 2018. doi: 10.1038/s41586-018-0047-9.

[151] National Institue for Health and Care Excellence. Ex-situ machine perfusion for extracorporeal preservation of livers for transplantation, 2019. URL `https://www.nice.org.uk/guidance/ipg636/resources/exsitu-machine-perfusion-for-extracorporeal-preservation-of-livers-for-transp`

[152] National Organ Retrieval Service. Annual report on the national organ retrieval service, 2021. URL `https://nhsbtdbe.blob.core.windows.net/umbraco-assets-corp/24643/annual-report-on-the-national-organ-retrieval-service-202021.pdf`.

[153] N. I. Nativ, T. J. Maguire, G. Yarmush, D. L. Brasaemle, S. D. Henry, J. V. Guarrera, F. Berthiaume, and M. L. Yarmush. Liver defatting: an alternative approach to enable steatotic liver transplantation. *Am J Transplant*, 12:3176–83, Dec 2012. doi: 10.1111/j.1600-6143.2012.04288.x.

[154] J. Near, R. Edden, C. J. Evans, R. Paquin, A. Harris, and P. Jezzard. Frequency and phase drift correction of magnetic resonance spectroscopy data by spectral registration in the time domain. *Magn Reson Med*, 73(1):44–50, 2015. doi: 10.1002/mrm.25094.

[155] K. Nehrke and P. Börnert. Dream—a novel approach for robust, ultrafast, multislice b1 mapping. *Magn Reson Med*, 68(5):1517–1526, 2012. doi: https://doi.org/10.1002/mrm.24158. URL `https://onlinelibrary.wiley.com/doi/abs/10.1002/mrm.24158`.

[156] E. Nemati, B. Einollahi, M. Lesan Pezeshki, V. Porfarziani, and M. R. Fattahi. Does kidney transplantation with deceased or living donor affect graft survival? *Nephro-urology monthly*, 6(25695017):e12182–e12182, July 2014. doi: 10.5812/numonthly.12182.

[157] Neoptix LP. T1 fiber optic temperature probe data sheet, 2013. URL `http://www.neoptix.com/literature/v1002_Datasheet_t1.pdf`.

[158] S. Neubauer. The failing heart–an engine out of fuel. *N Engl J Med*, 356:1140–51, Mar 2007. doi: 10.1056/NEJMra063052.

[159] NHS Blood and Transplant. Guidance around selecting potential DBD donors. https://www.odt.nhs.uk/deceased-donation/best-practice-guidance/donor-optimisation/, 2012. URL `https://www.odt.nhs.uk/deceased-donation/best-practice-guidance/donor-optimisation/`. Accessed: 10/08/2021.

[160] NHS Blood and Transplant. *Annual Report on Liver Transplantation*, 2021. URL `https://nhsbtdbe.blob.core.windows.net/umbraco-assets-corp/19867/nhsbt-liver-transplant-report-1920.pdf`.

[161] NHS Blood and Transplant. Organ and tissue donation and transplantation activity report 2020/21, 2021. URL `https://nhsbtdbe.blob.core.windows.net/umbraco-assets-corp/24053/activity-report-2020-2021.pdf`.

[162] W. N. Nijboer, C. Moers, H. G. D. Leuvenink, and R. J. Ploeg. How important is the duration of the brain death period for the outcome in kidney transplantation? *Transpl Int*, 24(1):14–20, 2011. doi: 10.1111/j.1432-2277.2010.01150.x.

[163] P. G. Northup, T. L. Pruett, D. M. Kashmer, C. K. Argo, C. L. Berg, and T. M. Schmitt. Donor factors predicting recipient survival after liver retransplantation: The retransplant donor risk index. *Am J Transplant*, 7(8):1984–1988, Aug. 2007. doi: 10.1111/j.1600-6143.2007.01887.x.

[164] J. M. O□Callaghan, R. D. Morgan, S. R. Knight, and P. J. Morris. The effect of preservation solutions for storage of liver allografts on transplant outcomes: a systematic review and meta-analysis. *Ann Surg*, 260:46–55, Jul 2014. doi: 10.1097/SLA.0000000000000402.

[165] S. op den Dries, N. Karimian, M. E. Sutton, A. C. Westerkamp, M. W. N. Nijsten, A. S. H. Gouw, J. Wiersema-Buist, T. Lisman, H. G. D. Leuvenink, and R. J. Porte. Ex vivo normothermic machine perfusion and viability testing of discarded human donor livers. *Am J Transplant*, 13(5):1327–1335, May 2013. doi: 10.1111/ajt.12187.

[166] N. Palaniyappan, E. Cox, C. Bradley, R. Scott, A. Austin, R. O'Neill, G. Ramjas, S. Travis, H. White, R. Singh, P. Thurley, I. N. Guha, S. Francis, and G. P. Aithal. Non-invasive assessment of portal hypertension using quantitative magnetic resonance

imaging. *J Hepatol*, 65(27475617):1131–1139, Dec. 2016. doi: 10.1016/j.jhep.2016.07.021.

[167] J. Patel, E. E. Sigmund, H. Rusinek, M. Oei, J. S. Babb, and B. Taouli. Diagnosis of cirrhosis with intravoxel incoherent motion diffusion MRI and dynamic contrast-enhanced MRI alone and in combination: preliminary experience. *J Magn Reson Imaging*, 31(20187201):589–600, Mar. 2010. doi: 10.1002/jmri.22081.

[168] D. Patrono, D. Cussa, F. Rigo, R. Romagnoli, and T. L. M. P. S. Group. Heterogeneous indications and the need for viability assessment: an international survey on the use of machine perfusion in liver transplantation. *Artificial Organs*, 2021. doi: 10.1111/aor.14061.

[169] M.-C. Pavel, E. Reyner, V. Molina, R. Garcia, A. Ruiz, R. Roque, A. Diaz, J. Fuster, and J. C. Garcia-Valdecasas. Evolution under normothermic machine perfusion of type 2 donation after cardiac death livers discarded as nontransplantable. *J Surg Res*, 235:383–394, Mar. 2019. doi: 10.1016/j.jss.2018.09.066.

[170] M. Pavlides, R. Banerjee, J. Sellwood, C. J. Kelly, M. D. Robson, J. C. Booth, J. Collier, S. Neubauer, and E. Barnes. Multiparametric magnetic resonance imaging predicts clinical outcomes in patients with chronic liver disease. *J Hepatol*, 64(2):308–315, 2016. doi: 10.1016/j.jhep.2015.10.009.

[171] M. Pavlides, J. Birks, E. Fryer, D. Delaney, N. Sarania, R. Banerjee, S. Neubauer, E. Barnes, K. A. Fleming, and L. M. Wang. Interobserver variability in histologic evaluation of liver fibrosis using categorical and quantitative scores. *Am J Clin Pathol*, 147(4):364–369, Apr. 2017. doi: 10.1093/ajcp/aqx011.

[172] R. T. D. Peters, R. S. Hinks, and R. M. Henkelman. Ex vivo tissue-type independence in proton-resonance frequency shift MR thermometry. *Magn Reson Med*, 40(3):454–459, 1998. doi: 10.1002/mrm.1910400316.

[173] S. K. Piechnik, V. M. Ferreira, E. Dall'Armellina, L. E. Cochlin, A. Greiser, S. Neubauer, and M. D. Robson. Shortened modified Look-Locker inversion recovery (ShMOLLI) for clinical myocardial T1-mapping at 1.5 and 3 T within a 9 heartbeat breathhold. *J Cardiovasc Magn Reson*, 12(1):69, 2010. doi: 10.1186/1532-429X-12-69.

[174] S. W. Provencher. Estimation of metabolite concentrations from localized in vivo proton nmr spectra. *Magn Reson Med*, 30:672–9, Dec 1993.

[175] L. A. B. Purvis, W. T. Clarke, L. Biasiolli, L. Valkovi, M. D. Robson, and C. T. Rodgers. OXSA: An open-source magnetic resonance spectroscopy analysis toolbox in MATLAB. *PLOS ONE*, 12(9):e0185356, 2017. doi: 10.1371/journal.pone.0185356.

[176] C. Quintini, P. Muiesan, O. Detry, M. Gastaca, J. de Jonge, P.-A. Clavien, L. Del Prete, and C. Fondevila. Early allograft dysfunction and complications in DCD liver transplantation: expert consensus statements from the international liver transplantation society. *Transplantation*, 105(8), 2021.

[177] Y. Rao, S. Gammon, N. M. Zacharias, T. Liu, T. Salzillo, Y. Xi, J. Wang, P. Bhattacharya, and D. Piwnica-Worms. Hyperpolarized [1-13C]pyruvate-to-[1-13C]lactate conversion is rate-limited by monocarboxylate transporter-1 in the plasma membrane. *Proc Nat Acad Sci USA*, 117(36):22378–22389, 2020. doi: 10.1073/pnas.2003537117.

[178] R. Ravikumar, W. Jassem, H. Mergental, N. Heaton, D. Mirza, M. T. P. R. Perera, A. Quaglia, D. Holroyd, T. Vogel, C. C. Coussios, and P. J. Friend. Liver transplantation after ex vivo normothermic machine preservation: A phase 1 (first-in-man) clinical trial. *Am J Transplant*, 16(6):1779–1787, 2016. doi: 10.1111/ajt.13708.

[179] S. P. Reddy, S. Bhattacharjya, N. Maniakin, J. Greenwood, D. Guerreiro, D. Hughes, C. J. Imber, D. W. Pigott, S. Fuggle, R. Taylor, and P. J. Friend. Preservation of porcine non-heart-beating donor livers by sequential cold storage and warm perfusion. *Transplantation*, 77(9), 2004.

[180] S. B. Reeder, A. R. Pineda, Z. Wen, A. Shimakawa, H. Yu, J. H. Brittain, G. E. Gold, C. H. Beaulieu, and N. J. Pelc. Iterative decomposition of water and fat with echo asymmetry and least-squares estimation (IDEAL): application with fast spin-echo imaging. *Magn Reson Med*, 54:636–44, Sep 2005. doi: 10.1002/mrm.20624.

[181] J. Reiling, N. Butler, A. Simpson, P. Hodgkinson, C. Campbell, D. Lockwood, K. Bridle, N. Santrampurwala, L. Britton, D. Crawford, C. H. C. Dejong, and J. Fawcett. Assessment and transplantation of orphan donor livers: A back-to-base approach to normothermic machine perfusion. *Liver Transpl*, 26(12):1618–1628, Dec. 2020. doi: 10.1002/lt.25850.

[182] J. J. Reilly, A. El-Hamdouchi, A. Diouf, A. Monyeki, and S. A. Somda. Determining the worldwide prevalence of obesity. *Lancet*, 391(10132):1773–1774, May 2018. doi: 10.1016/S0140-6736(18)30794-3.

[183] J. W. Rey, U. Wirges, H. P. Dienes, and J. W. U. Fries. Hepatic steatosis in organ donors: disparity between surgery and histology? *Transplant Proc*, 41:2557–60, Jul-Aug 2009. doi: 10.1016/j.transproceed.2009.06.121.

[184] J. Y. Rhee, J. Alroy, and R. B. Freeman. Characterization of the withdrawal phase in a porcine donation after the cardiac death model. *Am J Transplant*, 11(6):1169–1175, 2011. doi: 10.1111/j.1600-6143.2011.03567.x.

[185] B. Rial, M. D. Robson, S. Neubauer, and J. E. Schneider. Rapid quantification of myocardial lipid content in humans using single breath-hold 1H MRS at 3 Tesla. *Magn Reson Med*, 66(3):619–624, 2011. doi: 10.1002/mrm.23011.

[186] A. Riexinger, J. Martin, A. Wetscherek, T. A. Kuder, M. Uder, B. Hensel, and F. B. Laun. An optimized b-value distribution for triexponential intravoxel incoherent motion (IVIM) in the liver. *Magn Reson Med*, 85(4):2095–2108, 2021. doi: 10.1002/mrm.28582.

[187] A. J. Riexinger, J. Martin, S. Rauh, A. Wetscherek, M. Pistel, T. A. Kuder, A. M. Nagel, M. Uder, B. Hensel, L. Müller, and F. B. Laun. On the field strength dependence of bi- and triexponential intravoxel incoherent motion (IVIM) parameters in the liver. *J Magn Reson Imaging*, 50(6):1883–1892, 2019. doi: 10.1002/jmri.26730.

[188] C. Robinson. Policy POL196/8 – deceased donor liver distribution and allocation. https://nhsbtdbe.blob.core.windows.net/umbraco-assets-corp/22848/pol196.pdf, 2021. URL `https://nhsbtdbe.blob.core.windows.net/umbraco-assets-corp/22848/pol196.pdf`.

[189] L. I. Sacolick, F. Wiesinger, I. Hancu, and M. W. Vogel. B1 mapping by bloch-siegert shift. *Magn Reson Med*, 63(5):1315–1322, 2010. doi: https://doi.org/10.1002/mrm.22357. URL `https://onlinelibrary.wiley.com/doi/abs/10.1002/mrm.22357`.

[190] M. R. Schön, O. Kollmar, S. Wolf, H. Schrem, M. Matthes, N. Akkoc, N. C. Schnoy, Neuhaus, and Peter. Liver transplantation after organ preservation with normothermic extracorporeal perfusion. *Ann Surg*, 233(1), 2001.

[191] D. J. Schuirmann. A comparison of the two one-sided tests procedure and the power approach for assessing the equivalence of average bioavailability. *J Pharmacokinet Biopharm*, 15:657–80, Dec 1987. doi: 10.1007/BF01068419.

[192] A. Sgroi,V. Serre-Beinier, P. Morel, and L. Bühler. What clinical alternatives to whole liver transplantation? current status of artificial devices and hepatocyte transplantation. *Transplantation*, 87(4), 2009.

[193] R. Simpson, G. A. Devenyi, P. Jezzard, T. J. Hennessy, and J. Near. Advanced processing and simulation of MRS data using the FID appliance (FID-A)—An open source, MATLAB-based toolkit. *Magn Reson Med*, 77(1):23–33, 2017. doi: 10.1002/mrm.26091.

[194] A. Siniscalchi, L. Gamberini, C. Laici, T. Bardi, G. Ercolani, L. Lorenzini, and S. Faenza. Post reperfusion syndrome during liver transplantation: From pathophysiology to therapy and preventive strategies. *World J Gastroenterol*, 22(26819522):1551–1569, Jan. 2016. doi: 10.3748/wjg.v22.i4.1551.

[195] I. Solomon and N. Bloembergen. Nuclear magnetic interactions in the HF molecule. *J Chem Phys*, 25(2):261–266, Aug. 1956. doi: 10.1063/1.1742867.

[196] A. L. Spitzer, O. B. Lao, A. A. S. Dick, R. Bakthavatsalam, J. B. Halldorson, M. M. Yeh, M. P. Upton, J. D. Reyes, and J. D. Perkins. The biopsied donor liver: Incorporating macrosteatosis into high-risk donor assessment. *Liver Transpl*, 16(7):874–884, 2010. doi: 10.1002/lt.22085.

[197] T. G. St Pierre, P. R. Clark, W. Chua-anusorn, A. J. Fleming, G. P. Jeffrey, J. K. Olynyk, P. Pootrakul, E. Robins, and R. Lindeman. Noninvasive measurement and imaging of liver iron concentrations using proton magnetic resonance. *Blood*, 105:855–61, Jan 2005. doi: 10.1182/blood-2004-01-0177.

[198] T. E. Starzl, C. G. Groth, L. Brettschneider, I. Penn, V. A. Fulginiti, J. B. Moon, H. Blanchard, J. Martin, A J, and K. A. Porter. Orthotopic homotransplantation of the human liver. *Ann Surg*, 168(4877589):392–415, Sept. 1968. doi: 10.1097/00000658-196809000-00009.

[199] D. Stefan, F. D. Cesare, A. Andrasescu, E. Popa, A. Lazariev, E. Vescovo, O. Strbak, S. Williams, Z. Starcuk, M. Cabanas, D. van Ormondt, and D. Graveron-Demilly. Quantitation of magnetic resonance spectroscopy signals: the jMRUI software package. *Meas Sci Tech*, 20(10):104035, 2009. doi: 10.1088/0957-0233/20/10/104035.

[200] S. Stender, V. G. Zaha, C. R. Malloy, J. Sudderth, R. J. DeBerardinis, and J. M. Park. Assessment of rapid hepatic glycogen synthesis in humans using dynamic 13C magnetic resonance spectroscopy. *Hepatol Commun*, 4(3):425–433, Mar. 2020. doi: 10.1002/hep4.1458.

[201] C. Suntharalingam, L. Sharples, C. Dudley, J. A. Bradley, and C. J. E. Watson. Time to cardiac death after withdrawal of life-sustaining treatment in potential organ donors. *Am J Transplant*, 9:2157–65, Sep 2009. doi: 10.1111/j.1600-6143.2009.02758.x.

[202] M. E. Sutton, S. op den Dries, N. Karimian, P. D. Weeder, M. T. de Boer, J. Wiersema-Buist, A. S. H. Gouw, H. G. D. Leuvenink, T. Lisman, and R. J. Porte. Criteria for viability assessment of discarded human donor livers during ex vivo normothermic machine perfusion. *PLOS ONE*, 9(11):e110642, Nov. 2014. doi: 10.1371/journal.pone.0110642.

[203] K. S. Suvarna, C. Layton, and J. D. Bancroft. *Bancroft's theory and practice of histological techniques E-Book*. Elsevier Health Sciences, 2018.

[204] L. S. Szczepaniak, P. Nurenberg, D. Leonard, J. D. Browning, J. S. Reingold, S. Grundy, H. H. Hobbs, and R. L. Dobbins. Magnetic resonance spectroscopy to measure hepatic triglyceride content: prevalence of hepatic steatosis in the general population. *Am J Physiol Endocrinol Metab*, 288:E462–8, Feb 2005. doi: 10.1152/ajpendo.00064.2004.

[205] C. B. Taner, I. G. Bulatao, D. K. Perry, L. Sibulesky, D. L. Willingham, D. J. Kramer, and J. H. Nguyen. Asystole to cross-clamp period predicts development of biliary complications in liver transplantation using donation after cardiac death donors. *Transpl Int*, 25(8):838–846, 2012. doi: 10.1111/j.1432-2277.2012.01508.x.

[206] C. B. Taner, I. G. Bulatao, D. L. Willingham, D. K. Perry, L. Sibulesky, S. Pungpapong, J. Aranda-Michel, A. P. Keaveny, D. J. Kramer, and J. H. Nguyen. Events in procurement as risk factors for ischemic cholangiopathy in liver transplantation using donation after cardiac death donors. *Liver Transpl*, 18:100–11, Jan 2012. doi: 10.1002/lt.22404.

[207] M. A. Tanner, T. He, M. A. Westwood, D. N. Firmin, and D. J. Pennell. Multi-center validation of the transferability of the magnetic resonance T2* technique for the quantification of tissue iron. *Haematologica*, 91:1388–91, Oct 2006.

[208] M. Thuong, A. Ruiz, P. Evrard, M. Kuiper, C. Boffa, M. Z. Akhtar, J. Neuberger, and R. Ploeg. New classification of donation after circulatory death donors definitions and terminology. *Transpl Int*, 29(7):749–759, 2016. doi: 10.1111/tri.12776.

[209] T. Tirkes, X. Zhao, C. Lin, A. J. Stuckey, L. Li, S. Giri, and D. Nickel. Evaluation of variable flip angle, MOLLI, SASHA, and IR-SNAPSHOT pulse sequences for T1 relaxometry and extracellular volume imaging of the pancreas and liver. *Magma*, 32 (31165353):559–566, Oct. 2019. doi: 10.1007/s10334-019-00762-2.

[210] G. Tisone, T. M. Manzia, S. Zazza, N. De Liguori Carino, C. Ciceroni, I. De Luca, L. Toti, and C. U. Casciani. Marginal donors in liver transplantation. *Transplant Proc*, 36:525–6, Apr 2004. doi: 10.1016/j.transproceed.2004.02.022.

[211] J. F. Trotter, R. Adam, C. M. Lo, and J. Kenison. Documented deaths of hepatic lobe donors for living donor liver transplantation. *Liver Transpl*, 12:1485–8, Oct 2006. doi: 10.1002/lt.20875.

[212] E. M. Tunnicliffe, R. Banerjee, M. Pavlides, S. Neubauer, and M. D. Robson. A model for hepatic fibrosis: the competing effects of cell loss and iron on shortened modified Look-Locker inversion recovery T1 (shMOLLI-T1) in the liver. *J Magn Reson Imaging*, 45(2):450–462, 2017. doi: 10.1002/jmri.25392.

[213] A. C. Van Erp, R. A. Rebolledo, D. Hoeksma, N. R. Jespersen, P. J. Ottens, R. Nørregaard, M. Pedersen, C. Laustsen, J. G. M. Burgerhof, J. C. Wolters, J. Ciapaite, H. E. Bøtker, H. G. D. Leuvenink, and B. Jespersen. Organ-specific responses during brain death: increased aerobic metabolism in the liver and anaerobic metabolism with decreased perfusion in the kidneys. *Sci Rep*, 8:4405, Mar 2018. doi: 10.1038/s41598-018-22689-9.

[214] A. C. van Erp, H. Qi, N. R. Jespersen, M. V. Hjortbak, P. J. Ottens, J. Wiersema-Buist, R. Nørregaard, M. Pedersen, C. Laustsen, H. G. D. Leuvenink, and B. Jespersen. Organ-specific metabolic profiles of the liver and kidney during brain death and afterwards during normothermic machine perfusion of the kidney. *Am J Transplant*, 20:2425–2436, Sep 2020. doi: 10.1111/ajt.15885.

[215] O. B. van Leeuwen, Y. de Vries, M. Fujiyoshi, M. W. N. Nijsten, R. Ubbink, G. J. Pelgrim, M. J. M. Werner, K. M. E. M. Reyntjens, A. P. van den Berg, M. T. de Boer, R. H. J. de Kleine, T. Lisman, V. E. de Meijer, and R. J. Porte. Transplantation of high-risk donor livers after ex situ resuscitation and assessment using combined hypo- and normothermic machine perfusion: A prospective clinical trial. *Ann Surg*, 270: 906–914, Nov 2019. doi: 10.1097/SLA.0000000000003540.

[216] L. Vanhamme, van den Boogaart A, and S. Van Huffel. Improved method for accurate and efficient quantification of MRS data with use of prior knowledge. *J Magn Reson*, 129:35–43, Nov 1997. doi: 10.1006/jmre.1997.1244.

[217] R. Villa, C. Fondevila, I. Erill, A. Guimerà, E. Bombuy, C. Gómez-Suárez, J. C. Sacristán, and J. C. García-Valdecasas. Real-time direct measurement of human liver allograft temperature from recovery to transplantation. *Transplantation*, 81(3):483–6, 2006. doi: 10.1097/01.tp.0000195903.12999.bc.

[218] T. Vogel, J. G. Brockmann, D. Pigott, D. A. H. Neil, A. S. R. Muthusamy, C. C. Coussios, and P. J. Friend. Successful transplantation of porcine liver grafts following 48-hour normothermic preservation. *PLOS ONE*, 12(11):e0188494, 2017. doi: 10.1371/journal.pone.0188494.

[219] H. Z. Wang, S. J. Riederer, and J. N. Lee. Optimizing the precision in T1 relaxation estimation using limited flip angles. *Magn Reson Med*, 5(5):399–416, 1987. doi: 10.1002/mrm.1910050502.

[220] Z. J. Wang, M. A. Ohliger, P. E. Z. Larson, J. W. Gordon, R. A. Bok, J. Slater, J. E. Villanueva-Meyer, C. P. Hess, J. Kurhanewicz, and D. B. Vigneron. Hyperpolarized 13C MRI: State of the art and future directions. *Radiology*, 291(2):273–284, 2019. doi: 10.1148/radiol.2019182391.

[221] C. J. E. Watson, V. Kosmoliaptsis, L. V. Randle, A. E. Gimson, R. Brais, J. R. Klinck, M. Hamed, A. Tsyben, and A. J. Butler. Normothermic perfusion in the assessment and preservation of declined livers before transplantation: Hyperoxia and vasoplegia–important lessons from the first 12 cases. *Transplantation*, 101(5), 2017. ISSN 0041-1337.

[222] C. J. E. Watson, V. Kosmoliaptsis, C. Pley, L. Randle, C. Fear, K. Crick, A. E. Gimson, M. Allison, S. Upponi, R. Brais, I. Jochmans, and A. J. Butler. Observations on the ex situ perfusion of livers for transplantation. *Am J Transplant*, 18(8):2005–2020, 2018. doi: 10.1111/ajt.14687.

[223] P. D. Weeder, R. van Rijn, and R. J. Porte. Machine perfusion in liver transplantation as a tool to prevent non-anastomotic biliary strictures: Rationale, current evidence and future directions. *J Hepatol*, 63(1):265–275, July 2015. doi: 10.1016/j.jhep.2015.03.008.

[224] R. G. Weiss, G. Gerstenblith, and P. A. Bottomley. ATP flux through creatine kinase in the normal, stressed, and failing human heart. *Proc Natl Acad Sci USA*, 102:808–13, Jan 2005. doi: 10.1073/pnas.0408962102.

[225] C. W. White, R. Lillico, J. Sandha, D. Hasanally, F. Wang, E. Ambrose, A. Müller, O. Rachid, Y. Li, B. Xiang, H. Le, S. Messer, A. Ali, S. R. Large, T. W. Lee, I. M. C. Dixon, T. M. Lakowski, K. Simons, R. C. Arora, G. Tian, J. Nagendran, L. V. Hryshko, and D. H. Freed. Physiologic changes in the heart following cessation of mechanical ventilation in a porcine model of donation after circulatory death: Implications for cardiac transplantation. *Am J Transplant*, 16(3):783–793, 2016. doi: 10.1111/ajt.13543.

[226] E. F. Wijdicks. The diagnosis of brain death. *N Engl J Med*, 344(16):1215–1221, 2001. doi: 10.1056/NEJM200104193441606.

[227] H. R. Wilman, M. Kelly, S. Garratt, P. M. Matthews, M. Milanesi, A. Herlihy, M. Gyngell, S. Neubauer, J. D. Bell, R. Banerjee, and E. L. Thomas. Characterisation of liver fat in the UK biobank cohort. *PLOS ONE*, 12(2):e0172921, Feb. 2017. doi: 10.1371/journal.pone.0172921.

[228] A. Winter, C. Féray, E. Audureau, D. Azoulay, C. Antoine, J.-P. Daurès, and P. Landais. A donor quality index for liver transplantation: development, internal and external validation. *Sci Rep*, 8(29959344):9871–9871, June 2018. doi: 10.1038/s41598-018-27960-7.

[229] R. F. Wolf, R. L. Kamman, E. L. Mooyaart, E. B. Haagsma, R. P. Bleichrodt, and M. J. Slooff. 31P magnetic resonance spectroscopy of the isolated human donor liver-feasibility in routine clinical practice and preliminary findings. *Transplantation*, 55:949–51, Apr 1993.

[230] M. C. Wurnig, M. Germann, and A. Boss. Is there evidence for more than two diffusion components in abdominal organs? – a magnetic resonance imaging study in healthy volunteers. *NMR in Biomed*, 31(1):e3852, 2018. doi: 10.1002/nbm.3852. e3852 NBM-17-0016.R4.

[231] H. Xu, T. Berendsen, K. Kim, A. Soto-Gutiérrez, F. Bertheium, M. L. Yarmush, and M. Hertl. Excorporeal normothermic machine perfusion resuscitates pig DCD livers with extended warm ischemia. *J Surg Res*, 173(2):e83–e88, 2012. doi: 10.1016/j.jss.2011.09.057.

[232] H. Yersiz, C. Lee, F. M. Kaldas, J. C. Hong, A. Rana, G. T. Schnickel, J. A. Wertheim, A. Zarrinpar, V. G. Agopian, J. Gornbein, B. V. Naini, C. R. Lassman, R. W. Busuttil, and H. Petrowsky. Assessment of hepatic steatosis by transplant surgeon and expert pathologist: A prospective, double-blind evaluation of 201 donor livers. *Liver Transpl*, 19(4):437–449, Apr. 2013. doi: 10.1002/lt.23615.

[233] T. Yoshikawa, Y. Suzuki, M. Kanashiro, S. Li, T. Goto, T. Tanaka, K. Kakinoki, T. Sakai, Y. Tanioka, and Y. Fujino. Objective and rapid assessment of pancreas graft viability using 31P-nuclear magnetic resonance spectroscopy combined with two-layer cold storage method. *Transplantation*, 78(1):78–82, 2004.

[234] L. A. Young, C. D. Ceresa, J. J. Miller, L. Valkovic, D. Voyce, E. M. Tunnicliffe, J. Ellis, D. J. Tyler, P. J. Friend, C. C. Coussios, and C. T. Rodgers. Assessing metabolism and function of normothermically perfused ex vivo livers by multinuclear MR imaging and spectroscopy. In *Proc. ISMRM*, page 440, 2018.

[235] L. A. J. Young, C. D. L. Ceresa, F. E. Mózes, J. Ellis, L. Valkovic, R. Colling, C.-C. Coussios, P. J. Friend, and C. T. Rodgers. Noninvasive assessment of steatosis and viability of cold-stored human liver grafts by MRI. *Magn Reson Med*, July 2021. doi: 10.1002/mrm.28930.

[236] H. Yu, C. A. McKenzie, A. Shimakawa, A. T. Vu, A. C. S. Brau, P. J. Beatty, A. R. Pineda, J. H. Brittain, and S. B. Reeder. Multiecho reconstruction for simultaneous water-fat decomposition and T2* estimation. *J Magn Reson Imaging*, 26:1153–61, Oct 2007. doi: 10.1002/jmri.21090.

[237] W.-D. Zech, N. Schwendener, A. Persson, M. J. Warntjes, and C. Jackowski. Temperature dependence of postmortem MR quantification for soft tissue discrimination. *Eur Radiol*, 25(8):2381–2389, 2015. doi: 10.1007/s00330-015-3588-4.

[238] Y. Zhai, H. Petrowsky, J. C. Hong, R. W. Busuttil, and J. W. Kupiec-Weglinski. Ischaemia-reperfusion injury in liver transplantation–from bench to bedside. *Nat Rev Gastroenterol Hepatol*, 10(23229329):79–89, Feb. 2013. doi: 10.1038/nrgastro.2012.225.

[239] Q. Zhang, K. Werys, I. A. Popescu, L. Biasiolli, N. A. B. Ntusi, M. Desai, S. L. Zimmerman, D. J. Shah, K. Autry, B. Kim, H. W. Kim, E. R. Jenista, S. Huber, J. A. White, G. P. McCann, S. A. Mohiddin, R. Boubertakh, A. Chiribiri, D. Newby, S. Prasad,

A. Radjenovic, D. Dawson, J. Schulz-Menger, H. Mahrholdt, I. Carbone, O. Rimoldi, S. Colagrande, L. Calistri, M. Michels, M. B. M. Hofman, L. Anderson, C. Broberg, F. Andrew, J. Sanz, C. Bucciarelli-Ducci, K. Chow, D. Higgins, D. A. Broadbent, S. Semple, T. Hafyane, J. Wormleighton, M. Salerno, T. He, S. Plein, R. Y. Kwong, M. Jerosch-Herold, C. M. Kramer, S. Neubauer, V. M. Ferreira, and S. K. Piechnik. Quality assurance of quantitative cardiac T1-mapping in multicenter clinical trials - a T1 phantom program from the hypertrophic cardiomyopathy registry (HCMR) study. *Int J Cardiol*, 330:251–258, May 2021. doi: 10.1016/j.ijcard.2021.01.026.

[240] Z. Zhang, W. Ju, Y. Tang, L. Wang, C. Zhu, N. Gao, Q. Zhao, S. Huang, D. Wang, L. Yang, M. Han, W. Xiong, L. Wu, M. Chen, Y. Zhang, Y. Zhu, C. Sun, X. Zhu, Z. Guo, and X. He. First preliminary experience with preservation of liver grafts from extended-criteria donors by normothermic machine perfusion in asia. *Ann Transplant*, 25:e921529, Apr 2020. doi: 10.12659/AOT.921529.

[241] M. L. Zierhut, Y.-F. Yen, A. P. Chen, R. Bok, M. J. Albers, V. Zhang, J. Tropp, I. Park, D. B. Vigneron, J. Kurhanewicz, R. E. Hurd, and S. J. Nelson. Kinetic modeling of hyperpolarized [1-13C]-pyruvate metabolism in normal rats and TRAMP mice. *J Magn Reson*, 202(19884027):85–92, Jan 2010. doi: 10.1016/j.jmr.2009.10.003.